TECHNISCHE UNIVERSITÄT MÜNCHEN

Fakultät für Chemie

Lehrstuhl für Biotechnologie

Bi- and Multi-specific Antibodies

Christian Panke

Vollständiger Abdruck der von der Fakultät für Chemie
der Technischen Universität München zur Erlangung des akademischen Grades eines

Doktors der Naturwissenschaften (Dr. rer. nat.)

genehmigten Dissertation.

Vorsitzende:	Univ.-Prof. Dr. K. Lang
Prüfer der Dissertation:	1. Univ.-Prof. Dr. J. Buchner
	2. Univ.-Prof. Dr. M. J. Feige

Die Dissertation wurde am 18.08.2015 bei der Technischen Universität München
eingereicht und durch die Fakultät für Chemie
am 28.09.2015 angenommen.

List of publications

Panke, C., Weininger, D., Haas, A., Schelter, F., Schlothauer, T., Bader, S. et al. (2013). Quantification of cell surface proteins with bispecific antibodies. Protein Eng Des Sel, 26, 645-654.

Metz, S., Panke, C., Haas, A. K., Schanzer, J., Lau, W., Croasdale, R. et al. (2012). Bispecific antibody derivatives with restricted binding functionalities that are activated by proteolytic processing. Protein Eng Des Sel, 25, 571-580.

R. Castoldi, C. Panke, U. Jucknischke1, N. Neubert, J. Schanzer, R. Croasdale, et al. (2015). TetraMabs: Simultaneous targeting of four oncogenic receptor tyrosine kinases for tumor growth inhibition. *In preparation.*

Naumer M, Sonntag F, Schmidt K, Nieto K, Panke C. et al (2012). Properties of the adeno-associated virus assembly-activating protein. J Virol. 86 (23), 13038-48.

Abbreviations

A	
Ab	antibody
ABC	antibody binding capacity
ADC	antibody drug conjugates
ADCC	antibody-dependent cell mediated-cytotoxicity
B	
BiTEs	bispecific T-cell engagers or short
BSA	bovine serum albumin
BsAbs	bispecific antibodies
B-CLL	B-cell chronic lymphocytic leukemia
C	
C domain	constant domain
CDC	complement-dependent cytotoxicity
cDNA	complementary DNA
CDR	complement determining region
CI	cell index
CLL	chronic lymphocytic leukemia
CPRG	chlorophenol-red-β-D-galacto-pyranoside
CS	coding sequence
CS&T	cytometer setup & tracking
Ct value	cross-threshold value
CTG	Cell Titer Glo
C1q	complement 1q
D	
dAb	single domain antibodies
DAF	dual-acting-fragment antigen binding
dbs	diabodies
Dig	digoxigenin
DNA	deoxyribonucleic acid
dsFv	disulfide stabilized variable region fragment
dsscFv	disulfide stabilized single chain variable region fragment
DVD	dual variable domain antibody
E	
ECM	extracellular matrix
EGFR/HER1/ErbB-1	epidermal growth factor receptor
EMT	epithelial–mesenchymal transition
EpCAM	epithelial cell adhesion molecules
F	
Fab	fragment antigen binding
Fc	fragment crystallizable
FcRn	neonatal Fc receptor

FCS	fetal calf serum
FITC	fluorescein isothiocyanate
FSC	forward-side scatter
Fv	variable region fragment
F/P	fluorophore to protein ratio
G	
G4S	glycine serine motif
GOI	gene of interest
H	
HA	hemaglutinin
HC	heavy chain
HCC	hepatocellular carcinoma
HEMA	hydroxyethylmethacrylate
HER2	human epidermal growth factor receptor 2
HER3	human epidermal growth factor receptor 3
HGF	hepatocyte growth factor
HKG	housekeeping genes
HPLC	High-Performance Liquid Chromatography
HyD	hybrid detectors
I	
ICK	intestinal cell kinase
Ig	immunoglobulins
IGF-1R	insulin-like growth factor 1 receptor
K	
K_a	association constant
K_d	dissociation constant
KEX	kinetic extrapolation
kih	knobs-into-holes
L	
LB agar	Luria Bertani agar
LC	light chain
LEL/EC2	large extracellular loop
M	
mAb	monoclonal antibody
MESF	molecules of equivalent soluble fluorophore
MFI	mean fluorescence intensity
MHC	major histocompatibility complex
M	molar
MMP	matrix metalloproteases
N	
NEA	non essential amino acids
NHS	N-hydroxysuccinimide

NHS-ES	N-hydroxysuccinimide esters
NIST	National Institute of Standards and Technology
NK cells	natural killer cells
NR conditions	non-reducing conditions
NTC	non-template control
nd	not determined

P

PCR	polymerase chain reaction
PE	phycoerythrin
PEG	polyethylene glycol
PEGylation	polyethylene glycolylation
PI3K	phosphatidylinositol-4,5-bisphosphate 3-kinase
PI4K	phosphatidylinositol-4 kinase
PK	pharmacokinetics
PKC	protein kinase C
PLK-1	polo-like kinases 1
PMT	photomultiplier tube
PS	penicillin,streptomycin

Q

QFCM	quantitative flow cytometry

R

R conditions	reduced conditions
Rac1	ras-related C3 botulinum toxin substrate 1
RNAi	RNA interference
RT-PCR	reverse transcription polymerase chain reaction
RTCA	Real-Time Label-Free Cellular Analysis
RTK	receptor tyrosine kinase

S

SCB	simple cellular beads
scDbs	single chain diabodies
SCNAs	somatic copy-number alterations
scFab	single chain fragment antigen binding
scFv	single chain variable region fragment
SEL/EC1	small extracellular loop
SPR	surface plasmon resonance
STD	standard deviation

T

taFvs/scFv2	tandem single chain variable region fragment
TEMs	tetraspanin enriched microdomains
TM	transmembrane
Tspans	tetraspanins

U

uPA	urokinase-type plasminogen activation
UWA	unified window of analysis

V

V domain	variable domain
VCAM-1	vascular cell adhesion molecule 1
VEGF	vascular endothelial growth factor
VH domain	variable heavy domain
VL domain	variable light domain

Contents

1 Summary

1.1 FACS based quantitation of cell surface receptors and Tetraspanin screening

Flow cytometry is an established method for fast and accurate quantitation of cellular protein levels and requires fluorescently labeled antibodies as well as calibration standards. A critical step for quantitation remains the production of suitable detection antibodies with a precisely defined ratio of antigen-binding sites to fluorophores. Problems often arise as a consequence of inefficient and unspecific labeling which can influence antibody properties. In addition, the number of incorporated fluorophores requires a special normalization step for quantitation. To address these problems, we constructed different mono- and bivalent bispecific antibodies with binding site(s) for the tumor relevant cell surface antigens, cMET, EGFR1/HER1, ErbB2/HER2 and ErbB3/HER3 with an additional digoxigenin-binding single-chain Fv fusion. The fluorophore Cy5 was covalently coupled to digoxigenin and quantitatively bound by the bispecific antibody. A panel of tumor cell lines was assessed under different culture conditions for absolute receptor expression levels of the indicated antigens and the results were set in relation to mRNA, gene count and immunoblot data. I thereby sought to determine if a Fab-scFv format is an appropriate tool antibody for standardized flow cytometric receptor quantitation.

Overall, I could reproducibly quantify these receptors, omit the otherwise required normalization step and demonstrate the superiority of a 1 + 1 bispecific antibody format. By comparison of EGFR/Her1 levels in the epidermoid carcinoma cell line A431 to existing technologies such as lysine-linker chemistry and QuantiBRITE but also to literature data of non FACS based methods such as the radio ligand binding assay our conclusions were confirmed. The engineered bispecific antibodies showed highest reproducibility and sensitivity among the different technologies. It was possible to use the same antibodies to quantify the number of proteins in intracellular vesicles in confocal microscopy. It can be expected that this concept has broad applicability and could also be expanded for analysis of antigen internalization or for modeling and stimulation studies.

In the second part of this work a screening study was performed which investigated a set of transmembrane proteins called Tetraspanins. Out of 33 Tetraspanins family members only approximately half have been described and nine show implications in cancer cell biology. These

proteins play a role in tumor progression, metastasis formation and their expression patterns correlate with tumor prognosis of patients. Although their therapeutic relevance in cancer therapy is starting to emerge, single targeting is rather difficult since Tetraspanins are expressed in a variety of tissues. In addition, a key feature of Tetraspanins is their ability to form massive complexes with other molecules and to interact with growth factor receptors. I sought to determine proliferation promoting Tetraspanins in a panel of different tumor derived cell lines to provide a set of promising targets for bispecific antibodies generation.

An siRNA library screen was conducted consisting of Tetraspanin-specific siRNAs against all 33 known Tetraspanins in various tumor cell lines and in combination with RTK targeting. 2D and 3D proliferation assays were established and performed to screen for potential targets. Together with RT-PCR and western blot analysis the screen evaluated significant anti-proliferative effects upon mRNA silencing. According to our data I determined four Tetraspanins (Tspan4, Tspan8, Tspan13 and Tspan15) as promising targets. Even though Tspan4 and Tspan15 have poorly been described, literature examples of Tspan8 and Tspan13 underline the positive outcome of the performed Tetraspanin siRNA screen as reasonable tumor targets. Because Tetraspanins are expressed in nearly all cell and tissue types, a co-targeting approach by the development of a bispecific Ab is feasible and necessary. I hereby suggest to further investigate Tspan4, Tspan8, Tspan13 and Tspan15 as interesting and highly potential targets.

2 Introduction

2.1 From monoclonal to multi-specific antibody formats

The advent of the concept and technology to generate recombinant bispecific antibodies (BsAbs) was more than twenty years ago and firstly described by Morrison and colleagues (Coloma & Morrison, 1997). Based on the possibility of using monoclonal antibodies (mAbs) for targeted therapy, extensive academic research as well as industrial research led to a broad variety of antibody formats. Over the last decades, mAbs became a famous tool for therapeutic applications and today, over 30 approved monoclonal antibodies are marketed of which 13 are found in the area of cancer treatment. The field of application ranges from cancer therapy to infectious diseases, inflammatory disorders and organ transplantations (Boyiadzis & Foon, 2008; Buss, Henderson, McFarlane, Shenton, & de, 2012; Nelson, Dhimolea, & Reichert, 2010; Sliwkowski & Mellman, 2013). Moreover, mAbs or fragments thereof can also be conjugated to chemotherapeutic drugs to yield so called antibody drug conjugates (ADCs) (Filpula, 2007; Kontermann, 2010).

The efficacy of therapeutic antibodies depends on antigen binding and secondary effects elicited by their constant region which can bind to immune effector cells. The latter can be tuned in many ways. For instance, it is possible to enhance effector functions such as complement-dependent cytotoxicity (CDC), phagocytosis and antibody-dependent cell mediated cytotoxicity (ADCC) (Carter, 2006). Beside antibody applications in cancer therapy and other diseases it is also possible to use the platform of bispecific antibodies as quantification tool for cell surface receptors. Bispecific antibodies can be coupled to fluorophores which in turn enable precise receptor quantitation (Metz et al., 2011; Panke et al., 2013).

Modification of antibodies by genetic engineering led to great improvement over the last decades. Since then, a variety of recombinant antibody formats emerged ranging from mono- and bivalent to bi- or multispecific molecules (Holliger & Hudson, 2005; Kontermann, 2010). In the context of this work, the following chapters will provide an outlook about genetic engineering and antibody modifications. Advantages and disadvantages of such modifications will be presented in the light of cancer therapy. The introduction spans basic characteristics of immunoglobulins (Ig) and has a focus on IgG isotypes.

2.2 Basic structure and functions of Immunoglobulins

Immunoglobulins are Y shaped glycoproteins which are produced by B cells as part of the adaptive immune system and are able to detect, tag and destroy foreign molecules. So called epitopes or antigenic determinants are recognized by the immune system where antibodies recognize linear or conformational epitopes of a given antigen. Epitopes constitute specific areas of an antigen whereas the same antigen can possess several epitopes. Such epitopes can be presented on viruses, yeast, bacteria and other non-host molecules (Janeway, Travers, Walport, & Shlomchik, 2001). Antibodies are highly specific with respect to antigen recognition and can initiate and recruit other parts of the immune system or destroy the target directly upon binding (Parker, 1993). Antibodies belong to the immunoglobulin superfamily which consists of five different isotypes in mammals that vary with respect to structure and immunological function. The different human antibody isotypes are IgA, IgD, IgE, IgG and IgM (Market & Papavasiliou, 2003; Woof & Burton, 2004).

Whereas IgD, IgE and IgG occur as monomers, the IgA isotype can be secreted as dimer and IgM is either present as monomer on the surface of B cells or secreted, in its most prevalent form, as pentamer (Geisberger, Lamers, & Achatz, 2006). The respective isotypes differ in several characteristic aspects such as in the distribution of N-linked carbohydrate groups, number and position of inter-chain disulfide bonds, the presence of a hinge region, the amount of heavy chain domains and the type of triggered immune response (Janeway et al., 2001). In the context of this work, the following chapters will focus on the IgG format and variants thereof. The main repertoire of immunoglobulin based immunity is provided by IgG which consists of four subclasses (IgG1, 2, 3 and 4) of which IgG1 is the most abundant in human serum with over 60% of all IgG subclasses (Hashira, Okitsu-Negishi, & Yoshino, 2000; Pier, Lyczak, & Wetzler, 2004). Nowadays, therapeutic antibodies are often IgG1 based isotypes which is partly due to superior effector functions such as ADCC, based on high affinity for Fc receptors and CDC, due to high complement activation properties (Salfeld, 2007). In addition, the half-life of IgG1 in blood plays an important role which is approximately 21 days (Clark, 1997).

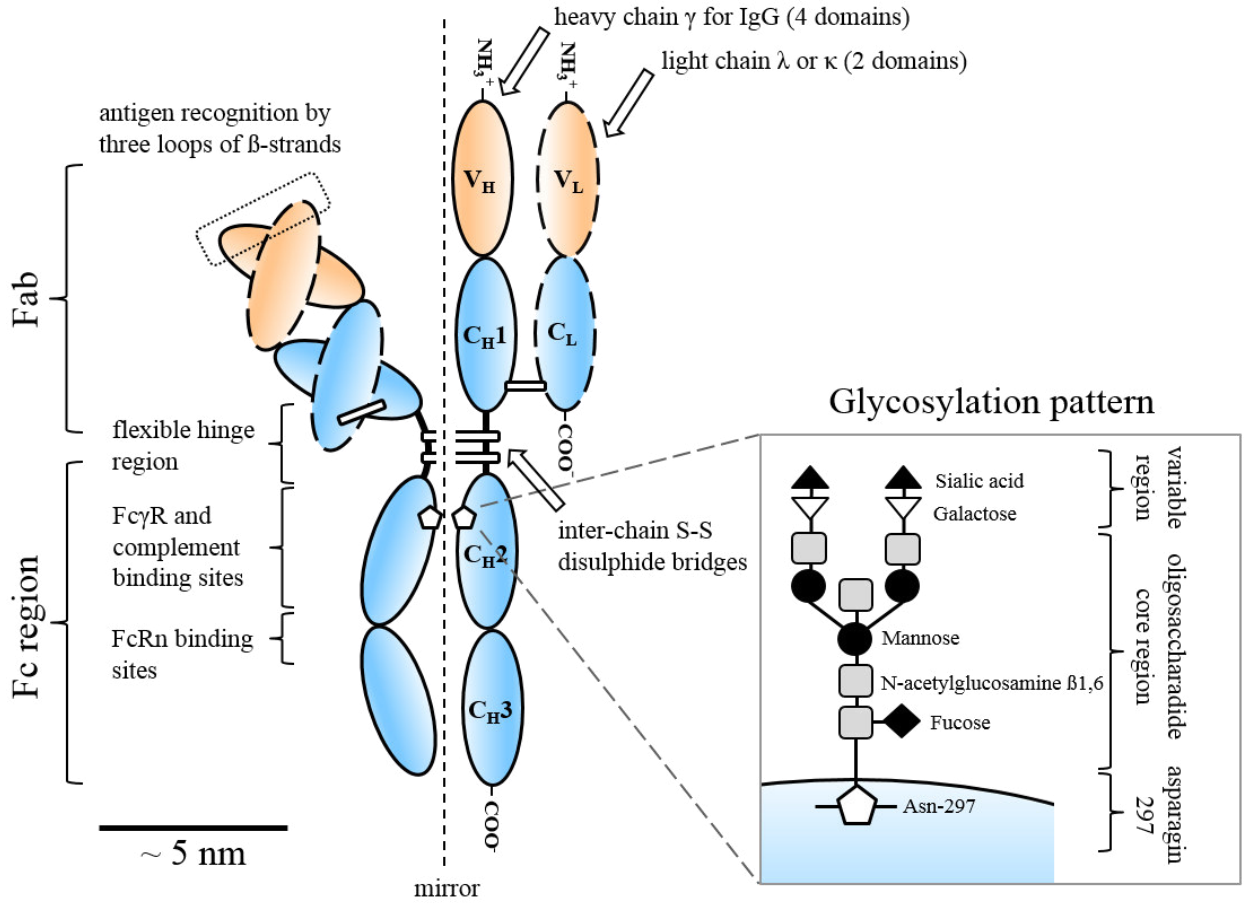

2.1 Basic IgG structure and function. FcγR, complement and FcRn binding sites are located in the Fc region whereas antigen recognition takes place at Fab fragment of V_H and V_L. Fc and Fab are connected by a flexible hinge region and the heavy (4 domains) and light (2 domains) chains are connected by a disulfide bond. Antibody glycosylation pattern is illustrated at conserved asparagine residue at position 297 in the C_H2 chain. The attached N-linked glycan comprises a variable region and an oligosaccharide core region. The illustration was modified and adapted from (Barb & Prestegard, 2011; Carter, 2006; Janeway et al., 2001)

With respect to structural properties, tetrameric IgG consists of 146 to 165 kDa in size depending on the isotype subclass and is build up by two pairs of identical polypeptide chains; two heavy and two light chains as illustrated in Figure 2.1. The heavy chain (HC) is approximately 50 kDa in size whereas the light chain (LC) 25 kDa (Janeway et al., 2001). The chains are connected to each other via disulfide bonds (Woof & Burton, 2004) and are organized into domains, each between 70 to 110 amino acids long (Putnam, Liu, & Low, 1979). The HC is structured into four protein domains of which three comprise the constant (C) domains C_H1, C_H2 and C_H3 and one variable (V) domain (VH). The LC is smaller in size and contains two domains, the V domain (VL) and one constant domain (CL) (Janeway et al., 2001; Putnam, Liu, & Low, 1979). Throughout all IgG isotypes two classes of LCs exists which are termed lambda (λ) and kappa (κ). Both LC classes do not occur at

the same time in one antibody. They show no functional differences. In contrast to that, five classes of different HCs (μ, δ, γ, α, and ε) define the respective isotype which can therefore be distinguished according to the constant region. All mammal isotypes possess different functional activities and effector functions (Janeway et al., 2001). Correctly assembled and folded domains comprise an antibody molecule with three similar sized globular fractions (2x Fab, 1x Fc region). These globular fractions are connected by a flexible amino acid stretch in the central part of the two HCs and are linked by disulfide bonds to each other (Adlersberg, 1976; Janeway et al., 2001). Upon proteolytic digestion of IgG by the cysteine protease Papain, disulfide bonds are cleaved on the amino-terminal side between the C_H1 and C_H2 domain and three globular fractions can be observed. Two identical fragment antigen binding fragments (Fab) are obtained which consists of the VH and C_H1 domain paired with the VL and CL domain. The third fragment is composed of paired C_H2 and C_H3 domains and exhibits no antigen binding activity but effector functions instead. This fragment was shown to crystalize readily and thus termed fragment crystallizable (Fc) (Janeway et al., 2001; Stelos & Pressman, 1962). Fc and Fab fragments are linked by the so called hinge region. This region facilitates dynamic movement of both Fab arms which has been shown by electron microscopy and nuclear magnetic resonance spectroscopy (Arata, Honzawa, & Shimizu, 1980; Ely et al., 1978; Silverton, Navia, & Davies, 1977).

Antigen-antibody interaction is a highly selective binding and mediated through the variable regions of the heavy and light chain (VH, VL). Antigen binding occurs through complement determining regions (CDRs) which are also defined as hypervariable regions and are located between three loops of ß-strands of VH and VL as denoted in Figure 2.1 (Janeway et al., 2001; Litman et al., 1993). Once antigen to antibody interaction occurs, aggregated IgG molecules are able to interact via their Fc region with Fcγ receptors (FcγRs). This type of receptor plays an essential role in the innate immune system and is found on effector cells or together with complement activation components (C1q being a subcomponent of the C1 complex of the classical pathway of complement activation) (Ravetch & Bolland, 2001). In the case of complement activation CDC is initiated. In consequence of antigen recognition and effector cell recruitment, ADCC can lead to the destruction of the target cell (Janeway et al., 2001; Pier et al., 2004).

Beside this role of the Fc region, it is also able to bind to the IgG neonatal Fc receptor (FcRn). FcRn was initially described as transporting IgG across epithelium from mother to fetus and is similarly in structure as the cell surface molecule major histocompatibility complex class I (MHC

class I) which presents epitopes to killer T cells (Jones & Waldmann, 1972). In terms of antibody half-life, Fc region to FcRn interaction results in fluid-phase uptake through this recycling receptor and to prolonged IgG half-life via returning IgG to the cell surface (Carter, 2006; Ober, Martinez, Lai, Zhou, & Ward, 2004). It has been shown that genetic engineering of IgG amino acid sequences can facilitate and improve binding to one or more interaction partners such as FcγRs, C1q, FcRn and target antigens (Filpula, 2007; Kontermann, 2010). The following chapter will describe a series of established and thesis relevant antibody modification strategies.

2.3 Aspects of antibody engineering and modification

Therapeutic antibodies represent a well-established class of drugs. This type of therapeutic agent is highly specific in terms of side-effects and has demonstrated its potency in a multitude of diseases such as cancer, autoimmune disease, inflammatory responses and immunosuppression (Abes, Dutertre, & Teillaud, 2009; Chan & Carter, 2010; Shuptrine, Surana, & Weiner, 2012). Improvement, with respect to clinical efficiency, spans a broad spectrum of antibody modification strategies and interdependent properties that can be altered (Carter, 2006). Fields of such improvement represent (i) immunogenicity, (ii) antigen binding affinity and specificity, (iii) effector functions, (iv) pharmacokinetics, (v) internalization properties and (vi) the molecular architecture of antibody formats (Carter, 2001b; Chowdhury & Wu, 2005; Presta, 2002). In the following chapters (2.3.1 – 2.3.6) each parameter will be introduced with the goal to provide a brief review about antibody properties that can be altered to increase clinical efficiency but also in the light of cell surface receptor quantification.

2.3.1 Immunogenicity

All drugs on protein basis are potentially immunogenic including therapeutic antibodies (Chirino, Ary, & Marshall, 2004). Patients often develop antibodies against therapeutic antibodies which are also referred to as anti-drug antibodies (Ritter et al., 2001). The development of such antibodies against administered therapeutic antibodies can lead to their direct neutralization, acceleration of clearance and finally to the termination of treatment (Carter, 2006). This obstacle was commonly observed after administering multiple doses of mouse derived antibodies. However, immunogenicity can be substantially reduced by the use of chimeric humanized mouse antibodies (Hwang & Foote, 2005). This reduction is achieved by replacing certain amino acid sequences of the variable regions of mouse derived antibodies with human sequences (Hwang & Foote, 2005).

The resulting chimeric antibody formats represent one of the first methods of reducing the risk of an immune response. Mouse derived constant regions are also replaced by human sequences in chimeric antibody formats but the obstacle of eliciting an immunogenic response remains. To further reduce immunogenicity, antibodies undergo the so called humanization process in which ideally only the CDR of the VH and VL chain remain of mouse origin. However, today therapeutic antibodies are of complete human origin which can be achieved by genetically modified mice or genetic engineering in combination with screening techniques (Lonberg, 2008; Lonberg, 2005; Hoogenboom, 2005; Green, 1999). Completely humanized therapeutic antibodies exhibit a significant lower immunogenic level and are common practice in some pharmaceutical companies (Hwang & Foote, 2005).

Nevertheless, a vast number of additional factors exist which influence immune response after antibody treatment. Immunogenicity cannot only be triggered by extrinsic factors, such as mouse derived amino acid sequences but also by intrinsic factors like antibody glycosylation patterns as illustrated in Figure 2.1. Additional parameters influencing immunogenicity are the presence of aggregated or misfolded antibodies, T-cell epitopes and chemical modifications such as deamidation describing a chemical reaction in which an amide functional group is removed (Shire, 2009; Carter, 2006; Clark, 2000).

2.3.2 Antigen binding affinity

The antigen binding affinity is the antibody's feature to recognize its specific antigen(s). This interaction represents a reversible non-covalent interaction in which the forces, that join the antibody-antigen complex, are based on weak protein to protein interactions. The type of forces include Van der Waals forces, hydrogen-, hydrophobic- and ion dipole- interactions. Antigen binding affinity is measured in terms of the association and dissociation constant K_a and K_d, respectively. In detail, K_d describes an equilibrium at which the propensity of larger molecules to dissociate into smaller molecules is equal. K_d is the inverse of the association constant K_a. The general reaction in which an antibody (A) binds to an antigen (B) can be described as follows (Watson et al., 2004):

$$AB \leftrightharpoons A + B$$

The association constant K_a and dissociation constant K_d, where [A], [B] and [A, B] represent concentrations of the respective molecules, are thereby defined as follows (Van Oss, 1995):

$$K_a = \frac{[AB]}{[A]\,[B]} = \frac{1}{K_d}$$

In other terms, the equilibrium of antigen binding and antigen dissociation of an antibody can also be described by the ratio of the so called on-rate ($k_{forward}$) and off-rate (k_{back}):

$$K_a = \frac{K_{forward}}{K_{back}} = \frac{on\ rate}{off\ rate}$$

The association and dissociation constant are measured in molar units (M) and correspond to an antibody concentration at which half of the antibody is bound to the antigen and the other half not. The smaller the K_d value the stronger the antigen to antibody binding ratio. Therapeutic antibodies consist of a K_d value in the low nM to sub-nanomolar range. Improvement of the antigen binding affinity can be a reasonable strategy to increase potency and to improve the pharmacokinetic profile of an antibody (Carter, 2006). Such increase in binding affinity is referred to as *in vitro* affinity maturation. The process is similar to *in vivo* affinity maturation, where B cells produce antibodies that are repeatedly exposed to the same antigen and thereby produce in several rounds of selection, antibodies with increasing antigen binding affinities (Janeway et al., 2001). *In vitro* affinity maturation is also based on rounds of mutation and selection, whereas the mutations can be introduced by radiation and the selection occurs with methods such as phage display libraries in combination with library construction strategies (Chowdhury & Wu, 2005; Hoogenboom, 2005; Roskos, Klakamp, Liang, Arends, & Green, 2007). An example for *in vitro* affinity maturation represents the study by Schier and colleagues who mutated the CDR of an antibody format called single chain Fv (scFv). The generated scFv (scFv C6.5) is specific for the prominent receptor tyrosine kinase (RTK) human epidermal growth factor receptor 2 (HER2/erb-B2/neu) and underwent *in vitro* affinity maturation via VL and VH chain mutations and thereby increased affinity from nano to picomolar range (Schier et al., 1996). In sum, affinity maturated antibodies can possess a higher therapeutic efficacy due to K_d values in the nM range and may also allow the reduction of dosage and possible adverse side effects. In the case of detection antibodies to quantify

cell surface proteins, a strong antigen affinity is favorable and thus, K_d values in the lower nM range.

2.3.3 Effector functions

Upon engineering therapeutic antibodies one has to consider a variety of aspects such as the implementation or modification of effector functions. Efficacy and potency can be increased by engineering antibodies exhibiting effector functions such as ADCC and CDC and also via *in vitro* affinity maturation, as described previously. However, effector functions might not always be beneficial but instead cause side effects (Carter, 2006). Respective modifications and therapeutic strategies depend on the field of application and possible obstacles. Although this thesis focuses on multispecific antibodies in cancer therapy, the case of the immunosuppressant mAb Muromonab-CD3 which is used after organ transplantations exemplifies the situation of undesired effector functions. This mouse derived monoclonal IgG2a antibody is used as immunosuppressive agent to prevent organ rejection after surgery (Smith, 1996). Even though Muromonab-CD3 is highly potent, severe drawbacks were encountered due to its mitogenic side effects. They lead to the stimulation of T cell proliferation and the production of cell signaling molecules (cytokines) through its interaction with the patients FcγRs (Chatenoud, 2004). The IgG2a backbone of Muromonab-CD3 and subsequent immune response after administration are a prominent example of unwanted effector functions. However, in other fields of applications the recruitment of the immune system shows to be beneficial and increases therapeutic potency such as in cancer therapy. In the case of the therapeutic mAb Herceptin which induces ADCC and the chimeric mAb rituximab which induces ADCC and CDC (Gennari et al., 2004; Idusogie et al., 2000; Weng & Levy, 2003; Clynes, Towers, Presta, & Ravetch, 2000) the effector functions which are mediated by a subclass of the FcγR family (FcγR IIIa) were found to be essential for therapeutic efficacy and success. FcγR IIIa is part of the leucocyte receptor family FcγR and represents the major mechanism to activate ADCC in natural killer cells (Cartron et al., 2002). Effector functions are mediated via the Fc region of antibodies that interact with FcγRs and components of the complement cascade. Due to this strong therapeutic effect, most licensed antibodies in the field of cancer treatment are IgG1 based isotypes which trigger the strongest ADCC and CDC response in comparison to other isotypes (Cartron et al., 2002; Lobo, Hansen, & Balthasar, 2004; Cartron et al., 2002). Within this clinical setting, the applied strategies aim for the destruction of target cells which present the antigen(s) of interest. Hence, involvement of ADCC and CDC can be essential

for the respective therapeutic strategy. To improve effector functions two general approaches can be applied:

(i) genetic engineering of the amino acid sequence of the Fc region
(ii) altering glycosylation patterns of the Fc region

A straight forward approach represents genetic engineering and Fc region modification to increase interaction with FcγRs and complement. With respect to the second approach, glycosylation is the process in which carbohydrate side chains are attached to the constant region of the light and heavy chain or the variable region which is illustrated in Figure 2.1 (Arnold, Wormald, Sim, Rudd, & Dwek, 2007). Antibody glycosylation is performed at asparagine residue 297 of the C_H2 domain which improves FcγR interaction and thereby ADCC (Carter, 2006; Shields et al., 2001). Another way to improve effector functions can be achieved by increasing the bisecting N-acetylglucosamine content which represents a monosaccharide derivative of glucose (Umana, Jean-Mairet, Moudry, Amstutz, & Bailey, 1999) or by reducing the fucose amount (Shields et al., 2002). Nevertheless, altering glycosylation patterns bears also the risk of inducing immunogenicity and may increase or decrease immunogenic properties of the antibody.

2.3.4 Pharmacokinetics

Antibody pharmacokinetics (PK) are of special interest for drug development and therapy. This term describes the study of determining the half-life of drugs which are administered to living organisms. Similar to genetic engineering of antibodies, which can improve for instance effector functions, the increase or decrease of terminal half-life is dependent on the therapeutic goal and field of application. The PK range, in which antibodies can circulate in plasma, is broad and can vary between minutes to weeks. Increasing half-life of a therapeutic antibody may be suitable in cases where high efficacy is desired. However, reduction of antibody half-life can be required in cases were prolonged exposure leads to side effects by unspecific binding (Carter, 2006). One strategy to tailor half-life properties is the modification of the interaction between IgG and FcRn. At a pH between 6.0 and 6.5 IgG can be taken up by vascular endothelial cells and is able to bind FcRn within endosomes. Once the pH turns back to neutral between 7.0 and 7.4 IgG is released (Ober et al., 2004; Ober, Martinez, Vaccaro, Zhou, & Ward, 2004). In consequence, mutations at the Fc region can increase or decrease the antibodies half-life due to altered Fc to FcRn interaction. Stronger interactions will lead to prolonged half-life due to salvage of the antibody whereas weaker

interactions to faster clearance and shorter terminal half-life. Alternative antibody formats such as antibody fragments which lack the Fc region face therefore the problem of rapid clearance (Holliger & Hudson, 2005). However, several strategies exist to increase PK properties of such antibody fragments. Three prominent ones are listed below:

(i) ability to bind IgG
(ii) ability to bind albumin
(iii) PEGylation

With respect to the first two strategies, these approaches take advantage of long living plasma proteins such as IgG or the globular protein serum albumin. Antibody fragments are engineered in a way that they are able to bind IgG or albumin which thereby prolongs their terminal half-life (Dennis et al., 2002; Holliger, Wing, Pound, Bohlen, & Winter, 1997). The third strategy is based on a chemical process termed polyethylene glycolylation (PEGylation). Polyethylene glycol (PEG) polymer chains are covalently attached to antibody fragments which result into an improved PK profile. Similar to the Fc region of IgG based formats, PEGylation of antibody fragments is able to prolong plasma half-life but omits, in contrast to IgG formats, side effects and immunogenicity mediated by effector functions of the Fc region (Chapman et al., 1999).

2.3.5 Internalization

The internalization rate of antibodies which have bound their respective antigen(s) can vary to great extent and depends on a multitude of factors such as the type of antigen, K_d values, cell type and almost no general rules can be applied which are valid for all antigens (Carter, 2006; Erickson et al., 2006). Certain therapeutic strategies such as the delivery of cytotoxic drugs or the inhibition of target receptors to antagonize their function, require antibody internalization (Wu & Senter, 2005). However, internalization properties of antibodies have also to be considered upon designing detection antibodies which are used to quantify cell surface receptors.

A prominent example in cancer therapy, where therapeutic efficiency correlates with successful antibody internalization are ADCs. This type of antibody class exhibits high antigen-specific selectivity and additionally carries potent cytotoxic molecules (Trail & Bianchi, 1999; Weinberg et al., 2005). After binding to the antigen of interest, which is in most cases a cell surface receptor, the ADC-antigen complex is internalized; a process termed receptor mediated endocytosis (Chari,

2008; Jaracz, Chen, Kuznetsova, & Ojima, 2005). In the next step endosomes deliver this complex for lysosomal degradation which finally leads to intracellular release of cytotoxic molecules that were initially carried as conjugates (Erickson et al., 2006). Various studies have shown that ADCs established a potent strategy to deliver cytotoxic molecules inside tumor cells via internalization and subsequent degradation and activation (Chari, 2008; Jaracz et al., 2005; Junutula et al., 2008; Sanderson et al., 2005).

In the context of this thesis, Metz and colleagues engineered multispecific antibodies with the purpose of targeted payload delivery (Metz et al., 2011). This approach represents a viable alternative to the use of ADCs where cytotoxic molecules are covalently labeled to antibodies in contrast to the novel payload delivery system (Metz et al., 2011). Here, bispecific antibodies were generated which can, on the one hand, recognize and bind tumor-specific antigens such as RTK growth factor receptors (e.g. HER2 and insulin-like growth factor 1 (IGF-1) receptor) and contain on the other hand a Dig binding module which is able to bind digoxygeninylated molecules like Dig-Doxorubicin. Successful payload delivery and co-internalization of antibody-payload was determined *in vitro* and *in vivo* (Metz et al., 2011). The high affinity Dig binding entity is a murine IgG derivative that was humanized and can be found in various diagnostic assays (Holtke, Seibl, Burg, Muhlegger, & Kessler, 1990; Holtke et al., 1995; Kessler, Holtke, Seibl, Burg, & Muhlegger, 1990; Kessler, 1991). In contrast to other technologies, such as regular ADCs which use chemical conjugation to cysteines, lysines or carbohydrates the described payload delivery approach has several advantages:

i) simple coupling reaction of payload to antibody
ii) defined payload to antibody charging ratio (Key concept which enables precise labeling of detection antibodies and receptor quantitation under modified conditions)
iii) defined position of payload attachment (Guarantees full functionality of detection antibodies due precise and no random chemical conjugation)
iv) target binding functionality remains intact (important for detection antibodies in quantitation experiments)
v) payload charging under physiological conditions is possible based on payload binding
vi) minimizing the risk of immunogenicity due to complexation of payloads without covalent modifications

It is important to point out that several of the listed points are key features of detection antibodies which are used for this thesis and are therefore based on the work of Metz and colleagues (Metz et al., 2011). In summary, targeted payload delivery and co-internalization of bispecific antibody formats can represent an alternative to conventional ADC strategies that rely on antibody internalization. In addition and of more significance for this work, the introduced approach is part of our key concept for cell surface receptor quantitation (chapter 2.6).

2.3.6 Molecular architecture

As introduced previously, a great number of therapeutic antibody formats are based on IgG1 formats which enable additional effector functions through the human Fc region (Jefferis, 2007; Reichert, 2008). Other IgG molecules, like IgG2 and IgG4, possess significant deficiencies in carrying out effector functions and are therefore only suitable for strategies that do not rely on interaction with ADCC and CDC (Swann et al., 2008). IgG3 based formats are also less frequently used for therapeutic approaches which is partly due to IgG3s significantly longer hinge region, in comparison to IgG1, rendering it more susceptible for proteolytic processing (Carter, 2006).

Beside the advantages of IgG1, the general modular domain architecture of antibodies lead to a variety of formats displaying a manifold and dynamic number of valencies and antigen specificities as described in chapter 2.5 and illustrated in Figure 2.2 and 2.3 (Holliger & Hudson, 2005; Kipriyanov & Le, 2004). Due to genetic engineering it is possible to fuse such modular antibody domains to other proteins such as toxins as for ADCs, protein fragments or enzymes (Adams & Weiner, 2005). A great therapeutic potential can also be found in antibody fragments which lack the Fc region (e.g. advanced cell surface detection antibodies). In settings were effector functions are undesired these small molecules are able to penetrate deeply into tumor tissue (Erickson et al., 2006). One advantage of such antibody fragments, in comparison to bivalent monovalent antibodies, is their lack in ability to cross-link target receptors and therefore unwanted receptor firing (Stuttle, Powling, Ritter, & Hardisty, 1991).

A vast number of strategies can be applied upon genetic engineering of antibodies. The respective modifications such as glycosylation, *in vitro* maturation to increase K_d, Fc mediated effector functions and the use to antibody fragments highly depends on therapeutic approach and field of application and has to be adapted for cell surface receptor quantitation studies. With this

background, the following chapters (2.4 and 2.5) will focus on antibody formats and antibody fragments that emerged.

2.4 The prototype of recombinant antibody molecules: Single chain variable fragment

With the technology of antibody engineering, Skerra and Plückthun first reported the expression of recombinant antibody fragments in *Escherichia coli* (Skerra & Pluckthun, 1988). The cloning of antibody repertoires by polymerase chain reaction (PCR), enabled to clone antibody genes without prior knowledge of the coding sequence (CS) on the respective clone (Orlandi, Gussow, Jones, & Winter, 1989; Benhar, 2007). Antibody phage display emerged as a tool to identify specific binders and select novel antibodies out of antibody libraries and is still today one of the most popular technologies to screen such libraries (Hoogenboom, 2005; Sergeeva, Kolonin, Molldrem, Pasqualini, & Arap, 2006). The most common format in such libraries was the prototype of recombinant antibody molecules, the so called scFv (Benhar, 2007; Marks et al., 1991).

As shown in Figure 2.2, scFvs constitute the complete antigen binding site of a standard IgG antibody. They are composed by two domains, the VH and VL chain, which are connected by a flexible linker of 15 amino acid residues. ScFvs are simple and straightforward in means of production, such as in bacteria, but can be problematic for therapeutic applications. Reducing conditions, that are encountered inside eukaryotic cells, can affect solubility properties and therefore lead to unpredictable behavior precluding intracellular expression in eukaryotic cells (Biocca, Ruberti, Tafani, Pierandrei-Amaldi, & Cattaneo, 1995). Due to their low molecular weight, which is approximately 28 kDa, scFvs possess a short plasma half-life (Holliger & Hudson, 2005). The most prominent approaches to increase stability represent disulfide stabilization and a modification in the selection process. With respect to the first strategy, heterodimers are converted into disulfide-stabilized Fv fragments (dsFv) in which the VH and the VL chain are stabilized by an inter-chain disulfide bond (Figure 2.2). The disulfide bond is engineered between structurally conserved framework positions which are distant from the CDRs (Reiter, Brinkmann, Lee, & Pastan, 1996). In the second strategy, Auf der Maur and colleagues developed a novel system that enables the selection of stable and soluble scFvs based on single-chain antibodies which are fused to a selectable marker. This marker can control gene expression and cell growth. By this means such antigen-independent selection process substantially improved the stability of scFvs (Auf der, Escher, & Barberis, 2001). It is important to keep in mind that scFvs lack the Fc region which is

necessary to mediate effector functions. ScFv are hence suitable for applications in which engagement of the immune system is not required or to omit biased signaling events in cell surface quantitation experiments as this work will investigate. Also strategies where bivalent binding of the target antigen may lead to a reduction of therapeutic efficacy (e.g. receptor dimerization and activation) are suitable fields of scFvs (Labrijn, Aalberse, & Schuurman, 2008).

2.5 Bi-and multispecific antibody formats

Based on the great diversity of antibody formats and their respective field of application they differ significantly in PK properties, avidity, immunogenicity, tissue penetration, size, steric properties, effector functions and binding stoichiometry. It is possible to categorize multispecific and multivalent antibodies into classes such as (Weidle, Tiefenthaler, Weiss, Georges, & Brinkmann, 2013):

i) IgG based formats
ii) none-IgG based formats

Various formats are based on fusions between both classes. For example, single domain antibodies (dAb), variable region fragments (Fv), scFvs, dsFvs, disulfide stabilized scFv (dsscFvs), Fab fragments and single chain Fabs (scFab) are commonly fused to Fc regions (Castoldi et al., 2012; Croasdale et al., 2012; Kontermann, 2010; Metz et al., 2011; Schanzer et al., 2011). These monovalent antibody fragments are illustrated in Figure 2.2 with their respective structural features.

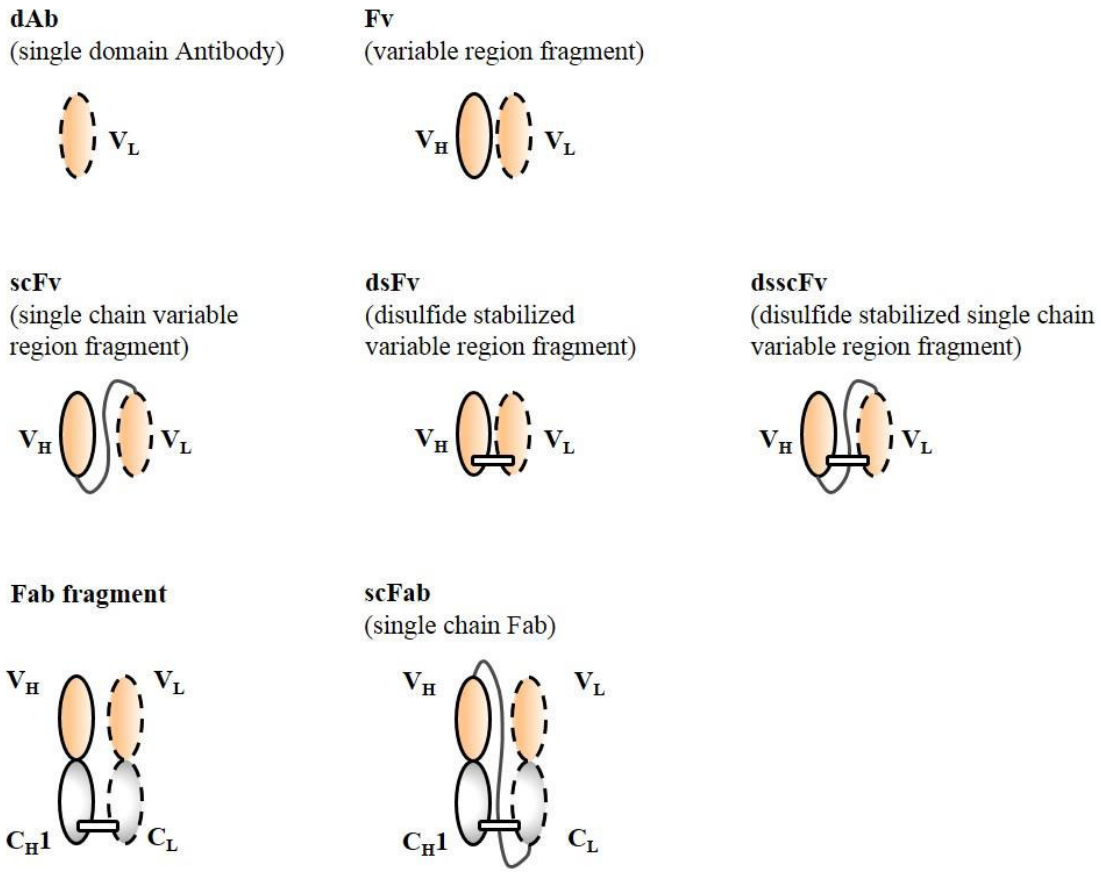

Figure 2.2 Monovalent recombinant antibody formats. V_H and V_L interaction can be stabilized and connected via single chains and/or a disulfide bonds.

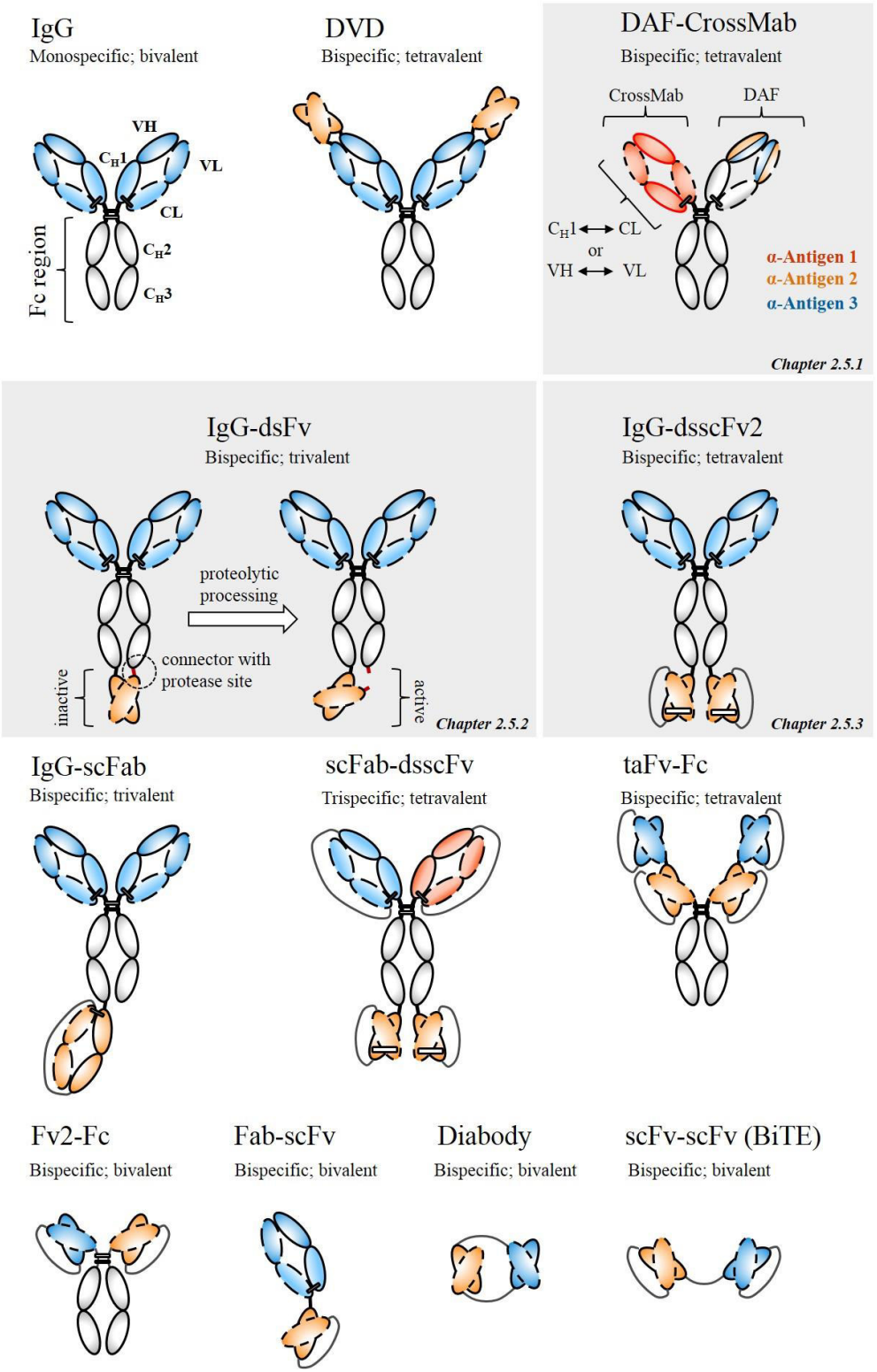

Figure 2.3. Multivalent and multispecific antibody formats. The thesis relevant formats DAF-CrossMab, IgG-dsFv and IgGdsscFv2 are shaded in grey. **taFv** = tandem scFv; **DVD** = dual-variable-domain; **DAF** = dual acting Fab; **BiTEs** = bispecific T-cell engagers. The illustration of antibody formats is adapted and modified from (Kontermann, 2012; Kontermann, 2010; Weidle et al., 2013).

None-IgG based and therefore Fc less formats are smaller in size (approximately 50-100 kDa) than IgG based antibodies (approximately 100-200 kDa) which emphasizes part of their different features and properties (Weidle et al., 2013). Because it is possible to fuse such antibody fragments at the C-terminus and N-terminus of IgG based formats or to other antibody fragments, a great variety of formats can be engineered as illustrated in Figure 2.3. These molecules can exhibit several valencies and bind to multiple antigens, depending on the combination of formats and technologies. For example, the bispecific and tetravalent dual variable domain antibody (DVD) represents an IgG based format which has been fused at its N-terminus to an Fv fragment. The Fv fragment consists of a VH and VL region of another specificity. Both domains are connected at each N-terminus by a variable linker to the VH and VL region of the Fc containing antibody (Kontermann, 2010). In contrast to such IgG based format, bispecific T-cell engagers or short BiTEs (Baeuerle & Reinhardt, 2009; Lutterbuese et al., 2010; Wolf, Hofmeister, Kufer, Schlereth, & Baeuerle, 2005) and diabodies (dbs) (Bostrom et al., 2009) exhibit no constant domain. These formats are generated by fusing two scFvs of different antibodies via a flexible linker to each other (Weidle et al., 2013). Although BiTEs contain no Fc region they are able to mediate effector functions via direct interaction with receptors of effector cells. For instance, BiTEs are able to bind and activate immune cells (cytotoxic T-cells or natural killer (NK) cells) with one arm and tumor-specific antigens with the other arm. In consequence, this strategy involving effector functions is more selective than Fc region containing formats (Baeuerle, Kufer, & Bargou, 2009). Besides direct binding of effector cells, bispecific antibody formats can also be engineered in a way to bind and inactivate two different antigens i.e. cell surface receptors. In line with this, so called dbs, single chain diabodies (scDbs), tandem scFvs (taFvs or scFv2) have been developed for retargeting of effector cells. These types of antibody fragments contain the VH and VL domains of two antibodies which are connected by a linker (Heiss et al., 2005; Kontermann, 2010). In summary, multi-specificity can be achieved by combining fusions of scFvs, Fabs, diabodies and tandem scFvs to Fc regions or by fusing antibody fragments of different antibodies with each other (Kontermann, 2010; Weidle et al., 2013).

Three of the illustrated antibody formats of Figure 2.3 are highlighted in grey and will be introduced in the next chapters. These antibodies were part of my research at Roche Diagnostics, Penzberg and are based on collaborations with other groups (Metz et al., 2012). The IgG-dsscFv2 is of special

interest for the cell surface receptor quantitation study whereas the IgG-dsFv cleavable linker molecule can be of interest as therapeutic concept in the Tetraspanin screen study.

2.5.1 DAF-CrossMab: Old players in new format

The trispecific dual-acting-fab (DAF) CrossMab combines two pairing technologies and can recognize three distinct antigens. Based on the CrossMab technology, the C_H1 and CL or VH and VL domains are exchanged leading to a significant reduction in mispaired LCs of heterodimeric IgG antibodies (left arm of DAF-CrossMab in Figure 2.3) (Klein et al., 2012; Schaefer et al., 2011b; Weidle et al., 2013). As for the two exchange options it has been shown that a C_H1 to CL exchange led to favorable purity with less side products and to a higher expression rate (Schaefer et al., 2011b). This pairing strategy is used together with the so called knobs-into-holes (kih) technology which was developed by Carter and colleagues and enforces correct binding of HCs (Atwell, Ridgway, Wells, & Carter, 1997; Carter, 2001a; Ridgway, Presta, & Carter, 1996; Zhu, Presta, Zapata, & Carter, 1997). Since the remaining arm of a CrossMab format is unmodified it is possible to apply the DAF concept and thereby generate the DAF-CrossMab. Here, separate parts of the DAF CDR region are able to recognize two epitopes of different origin, in contrast other antigen recognition strategies (Bostrom et al., 2009; Schaefer et al., 2011a).

2.5.2 IgG-dsFv with a cleavable linker

The second molecule of interest represents the bispecific and trivalent IgG-dsFv which is able to recognize two well-described RTK growth factor receptors which are targets in cancer therapy (cMET and HER3). As illustrated in Figure 2.3 this IgG based molecule detects HER3 in a bivalent manner whereas cMET is targeted by a dsFv composed of a VH and VL region (Metz et al., 2012). VH (cys44) and VL (cys100) are connected by interchain disulfide bonds since linker peptides can cause restricted antigen access (Jung, Pastan, & Lee, 1994; Metz et al., 2012; Reiter, Brinkmann, Jung, Pastan, & Lee, 1995; Reiter et al., 1996). The third entity, which is able to detect cMET, is tethered to the C-terminus of the C_H3 domain showing altered antigen binding properties because the CDR regions are directed against the C_H3 domain. Based on this arrangement and severe steric hindrance, the on-rates ($K_{forward}$) are significantly decreased whereas the off-rates (K_{back}) remain constant. This effect on cMET binding affinity was verified in surface plasmon resonance (SPR) experiments. Although VH and VL are connected to C_H3 by a sequence of connector amino acids, the VL to C_H3 sequence contains a protease site which enables binding to cMET after cleavage by

proteases (e.g. furin, matrix metalloproteases (MMP), urokinase-type plasminogen activation (uPA), PreScission). Upon proteolysis, full antigen binding affinity is restored (Metz et al., 2012).

2.5.3 Bispecific digoxigenin-binding antibodies

The so far introduced therapeutic approaches with bispecific antibodies focused either on simultaneous binding of two target antigens (Beck, Wurch, Bailly, & Corvaia, 2010; Joosten, Helsen, van de Loo, & van den Berg, 2008; van den Berg, Joosten, Helsen, & van de Loo, 1994) or direct recruitment and binding of effector cells (Linke, Klein, & Seimetz, 2010). However, bispecific antibodies are also capable of targeted payload delivery such as the antibody-drug conjugate Trastuzumab-DM1. This mAb is able to detect and bind the HER2 receptor and thereby to enrich the immunotoxin (DM1) at the site of interest (Krop et al., 2010; Metz et al., 2011). In relation to this, Metz and colleagues engineered bispecific antibodies that are able to bind cell surface receptors such as HER2 with one entity and the hapten digoxigenin (Dig) with the other. Their approach aims for targeted payload delivery by coupling digoxygeninylated immunotoxins to Dig-specific bispecific antibodies. As illustrated in Figure 2.3 Dig-specific dsscFvs are attached to the C-terminus of C_H3 domains via a peptide linker. The dsscFvs are able to bind digoxygeninylated payloads in a 2:1 ratio. The study could prove that the binding functionality of the BsAb-Dig-Immunotoxin complex was retained and other payload-compound combinations were investigated such as with fluorophores (Dig-GFP and Dig-Cy5) or chemotherapeutic agents (Dig-Doxorubicin) (Metz et al., 2011).

This therapeutic approach is feasible were digoxygeninylated payloads are bound to bispecific antibody formats which in turn target their respective cell surface antigen and thereby conduct targeted payload delivery. Other factors, like a stable serum half-life of complexed payloads support this approach. Even separate administration of bispecific antibodies and digoxygeninylated payloads under physiological conditions is possible due to the high affinity against Dig (Metz et al., 2011).

2.6 FACS based cell surface receptor quantitation

Quantitation of cell surface receptors by flow cytometry has already been described in the early 1980s and is best known as quantitative flow cytometry (QFCM) (Maher & Fletcher, 2005). This technique was early on applied in haematological diseases in order to analyze the implication of

cell surface proteins in development of these malignancies. Consequently, a variety of B-cell markers (e.g. CD2, CD19, CD20, CD22, CD38 and CD52) are now routinely quantified in different leukemias using QFCM (Arun et al., 2010; D'Arena et al., 2000; Ginaldi et al., 1998; Iyer, Hultin, Zawadzki, Davis, & Giorgi, 1998; Jiang et al., 2009). However, accurate quantitation of cell surface receptors is also of importance in other applications, as the analysis of cellular functions is often based on relative comparison of different cellular states. Exact quantitation of cell surface receptors is for various reasons attractive such as modelling of cellular networks, predictions on saturation conditions with therapeutic compounds and differentiation of normal and malignant state of cells. Finally, it also facilitates inter-laboratory comparisons (Zenger, Vogt, Mandy, Schwartz, & Marti, 1998).

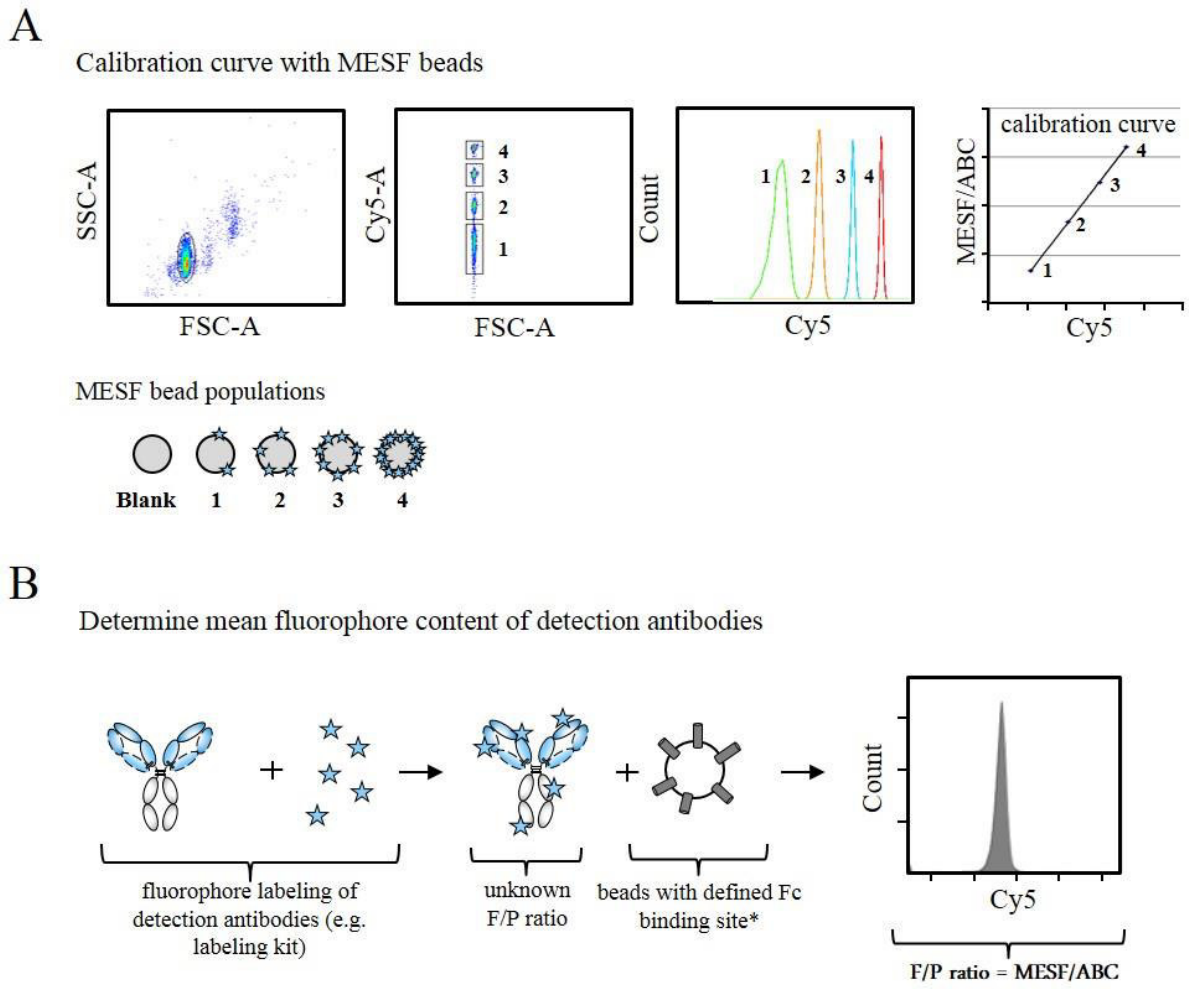

Figure 2.5. FACS based receptor quantitation. (A) A calibration curve by the use of MESF (molecules of equivalent soluble fluorochrome) is generated. After FACS analysis the respective bead populations are gated and the resulting MFI values translated into the absolute number of Cy5 molecules. (B) This step is used to determine the mean fluorophore content of detection antibodies. For this, detection antibodies are initially labelled with fluorophores and mixed with beads consisting of defined Fc binding sites and thus antibody binding sites. Together with the previously established calibration curve, the ABC (antigen binding capacity) value is used to translate the MFI detection antibody signal into absolute fluorochromes per antibody. This is done by dividing MESF with ABC which yields the F(fluorophore)/P(protein) ratio.

The quantitation of cellular antigens relies on beads with precisely defined numbers of reference molecules that are used as calibration standards as illustrated in Figure 2.5A. These bead populations are made up of one blank population and four fluorophore labelled populations, whereas each population consists of a varying but yet defined fluorophore content. Most common are beads from Quantum Simply Cellular, QuantiBRITE and QIFI for which similar sensitivity and accuracy was reported (Serke, van, Pardo, & Huhn, 1998). The absolute fluorophore loading of beads is determined by the comparison to a solution of known concentrations of this fluorophore,

yielding the so called molecules of equivalent soluble fluorophore (MESF) value (Schwartz et al., 2004). Upon FACS measurement of these reference beads, it is possible to determine a MESF calibration curve which is necessary to translate the obtained mean fluorescence intensity (MFI) values of samples into absolute receptor numbers. The principle can be compared to a standard protein assay where different concentrations of bovine serum albumin (BSA) are used to set up a calibration curve to determine unknown protein concentrations. In addition to calibration standards, inter-laboratory comparisons can be accomplished by the use of so called calibrated reference beads which are available to standardize procedures. The individual steps of quantitation experiments have been standardized and guidelines are available (D'hautcourt, 2002; Mittag & Tarnok, 2009; Schwartz & Fernandez-Repollet, 2001; Schwartz et al., 2004).

FACS-based receptor quantitation absolutely relies on the availability of fluorescently labelled antibodies. Most often, detection antibodies are labelled by a lysine-linker chemistry in which surface accessible lysines in the antibody chain are covalently linked to a fluorophore of interest vice versa. Usually, labelling reactions are stopped before complete labelling is achieved. Under such conditions it may happen that a certain population of antibodies does not carry a fluorescent label. Depending on the number and location of lysines in the antibody chain, the properties of labelled antibodies can change. As this labelling technique introduces fluorophores randomly, labelling of lysines near antigen recognition sites may lead to a population of antibodies with no or reduced activity. Consequently, the active concentration of detection antibodies vary and quantitation may be imprecise. The limiting factor in QFCM therefore is the labelling of detection antibodies which is usually unspecific, resulting in e.g. loss of antigen-binding, poor labelling reproducibility, heterogeneity of conjugated antibodies and shifted excitation and emission spectra (Schwartz et al., 2004). A strategy which is often used to compensate some of these problems is a special normalization step in which the fluorophore to antibody (F/P) ratio is quantified using beads which can bind a defined amount of labelled antibody (Lenkei et al., 1998). The normalization step is illustrated in Figure 2.5B in which a detection antibody is labelled with fluorophores and subsequently incubated with beads consisting of a defined antibody binding capacity (ABC). Due to the known ABC value it is possible to determine the F/P ratio by translating the gained MFI value into MESF (via a calibration curve, Figure 2.5) and divide the result by the ABC value. However, another strategy can be used to omit the need of a normalization step. A fluorophore that can be used in this respect is phycoerythrin (PE), which has a molecular weight of 200 kDa and a

high quantum yield. The size of the fluorophore enables purification of 1:1 antibody–fluorophore conjugates, but usually with a poor overall yield (Pannu, Joe, & Iyer, 2001).

As described previously, the advent of bispecific antibodies, easily available antibody variable domain sequences and falling prices for gene synthesis offers now a solution to generate a precise tool for receptor quantitation and internalization studies (Kontermann, 2012). Purification to near homogeneity is feasible, which is also reflected by the fact that such constructs are developed for therapeutic use in patients (Nieri, Donadio, Rossi, Adinolfi, & Podesta, 2009). This makes it possible to tailor the antigen-binding properties on the one side and allows engineering of site-specific fluorophore incorporation on the other. The study by Metz and colleagues has shown that attachment of a hapten-specific dssFv can be used to couple 'cargo' to a bispecific antibody (Metz et al., 2011).

2.7 Screening of Tetraspanins as promising tumor-relevant targets

Tetraspanins (Tspans) are transmembrane (TM) proteins. Out of 33 Tspan family members only approximately half have been described and more than nine show implications in cancer cell biology (see table 2.1). As I will summarize in the following chapters, these TM proteins play a role in tumor progression, metastasis formation and their expression patterns correlate with tumor prognosis of patients. Although their therapeutic relevance in cancer therapy is starting to emerge, single targeting is rather difficult since Tspans are expressed in a variety of tissues (Hemler, 2003; Lazo, 2007; Richardson, Jennings, & Zhang, 2011; Wright, Moseley, & van Spriel, 2004). A key feature of Tspans is their ability to form massive complexes with other molecules and to interact with growth factor receptors. Such properties can support a dual targeting approach by multispecific antibodies. For instance, inhibition of Tspan24 (CD151) has shown to sensitize breast cancer cells after HER2 RTK treatment with trastuzumab and reverse an acquired resistance phenotype (Yang et al., 2010). This data favors the rationale of a combinatory treatment against Tspans together with other tumor relevant molecules i.e. the generation of a bispecific antibody directed against Tspan24 and HER2. In relation to site-specific treatment, it has been shown that overexpression of Tspan8 and Tspan24 leads to upregulation of MMPs which are proteases being able to degrade extracellular matrix (ECM) proteins (Gesierich et al., 2005; Kanetaka et al., 2001; Le et al., 2006; Zhou et al., 2008). However, one has to consider tumor-specificity based on the ubiquitous expression of Tspans in the human body. Non-site-specific treatment could be overcome

by designing therapeutic antibodies in which the Tspan-specific entity is cleaved and activated by MMPs at the site of interest. Beside MMPs it has also been reported that Tspans are able to upregulate growth factor signaling in tumor cells via receptor-receptor interactions (i.e. cMET receptor) which further supports a co-targeting rationale (Klosek et al., 2005). In summary, the biological importance of Tspans is found in their interaction with other molecules (Hemler, 2003; Wright et al., 2004) making these TM proteins an ideal target for multispecific antibodies.

Table 2.1. List of all 33 human Tetraspanins. Tspan nomenclature according to HUGO Gene Nomenclature Committee (HGNC) and alternative Tspan names are summarized. Correlating or inversely correlating roles in tumor progression are listed including the respective studies. (Yanez-Mo, Barreiro, Gordon-Alonso, Sala-Valdes, & Sanchez-Madrid, 2009; Romanska & Berditchevski, 2011)

HGNC	Alternative names/ previously known as	Role in tumor progression	Literature
Tspan1	TM4-C, NET-1, TSP-1	correlates	(Chen et al., 2007; Chen et al., 2013; Scholz et al., 2009)
Tspan2	FLJ12082, TSN2, TSP-2	n.d.	n.d.
Tspan3	TM4-A, TM4SF8.1,2, TSP-3	n.d.	n.d.
Tspan4	TM4SF7, NAG-2, TSP-4	correlates	(Li et al., 2012)
Tspan5	NET-4, TSP-5, TM4SF9	may correlate	(Gao & Yu, 2008)
Tspan6	T245, TM4SF6, TSP-6	n.d.	n.d.
Tspan7	CD231, A15, MXS1, CCG-B7, TALLA-1, TM4SF2, DXS1692E	may inversely correlate	(Wuttig et al., 2012)
Tspan8	TM4SF3, CO-029, D6.1	correlates	(Kanetaka et al., 2001; Kuhn et al., 2007; Zhou et al., 2008)
Tspan9	NET-5, TNE5	n.d.	n.d.
Tspan10	Oculospanin (OCSP)	n.d.	n.d.
Tspan11		n.d.	n.d.
Tspan12	TM4SF12, NET-2	correlates	(Knoblich et al., 2013)
Tspan13	NET-6, FLJ22934, TM4SF13	correlates	(Arencibia, Martin, Perez-Rodriguez, & Bonnin, 2009; Huang et al., 2005a)
Tspan14	DC-TM4F2, BC002920, NEW2, TMSF14	n.d.	n.d.
Tspan15	NET-7, 2700063A19Rik, TMSF15	n.d.	n.d.
Tspan16	TM4-B, TM-8, TMSF16	n.d.	n.d.
Tspan17	CAD35489, FBX23, SB134, BC067105, NEW3, TM4SF17	n.d.	n.d.
Tspan18	BAB55318, AK027715.1, NEW6	n.d.	n.d.
Tspan19	XP_084868	n.d.	n.d.
Tspan20	Uroplakin Ib (UP1b), UPK1	correlates	(Olsburgh et al., 2003)
Tspan21	Uroplakin Ia (UP1a), UPIA, UPKA, MGC14388	correlates	(Kageyama et al., 2002; Romanska et al., 2013)
Tspan22	Peripherin, RDS, RP7, AVMD, PRPH, AOFMD, PRPH2, RD2, NMF193	n.d.	n.d.
Tspan23	Rom1, ROSP1	n.d.	n.d.
Tspan24	CD151, PETA3, SFA1, gp27, RAPH, MER2	correlates	(Sadej et al., 2009; Yang et al., 2008)
Tspan25	CD53, MOX44, OX-44	may correlate	(Yunta & Lazo, 2003a)
Tspan26	CD37, GP52-40	n.d.	n.d.
Tspan27	CD82, Kangai1, R2, 4F9, C33, IA4, ST6, GR15, KAI1, SAR2	inversely correlates	(Dong et al., 1996; Huang et al., 1998; Yang et al., 2000)
Tspan28	CD81, TAPA-1, S5.7	n.d.	n.d.
Tspan29	CD9, BA2, P24, GIG2, MIC3, MRP-1, BTCC-1, DRAP-27, 5H9	inversely correlates	(Mimori et al., 2005; Miyake et al., 1995)
Tspan30	CD63, MEL1, ME491, LAMP3, OMA81H, MLA1, NGA, LIMP	inversely correlates	(Woegerbauer et al., 2010)
Tspan31	SAS	n.d.	n.d.
Tspan32	TSSC6 (3 variants; UTR) PHEMX, MGC22455, ART1	n.d.	n.d.
Tspan33	MGC50844, Penumbra, New7	correlates	(Luu et al., 2013)

2.8 Biology of Tetraspanins and role in tumor progression

Before tumor cells are able to metastasize they have to undergo a multitude of orchestrated steps such as, in relation to cell motility, invasion, intravasation and extravasation. Essential factors to accomplish these steps include matrix degradation, cell migration, cell to cell and cell to matrix adhesion. It has been recently discovered that in all these cellular events so called Tspans are directly involved and even seem to play a role in regulatory function (Boucheix, Duc, Jasmin, & Rubinstein, 2001; Hemler, Mannion, & Berditchevski, 1996; Lazo, 2007; Richardson et al., 2011; Wright et al., 2004; Zoller, 2009) Such tumor promoting properties can partially be explained by the nature of Tspans. These TM proteins are able to form massive complexes with other molecules in the plasma membrane. Membrane proteins can have a great impact on the biology of cancer cells in relation to cellular interactions and signaling pathways that play a role in tumor adhesion and dissemination. The relevance of Tspans in cell biology but also with respect to cancer biology is rising but has received little attention so far (Boucheix et al., 2001; Hemler, 2003; Hemler, 2005; Lazo, 2007).

2.8.1 General features of Tspans

Tspans are found in a variety of tissues and are expressed in all eukaryotes (Hemler, 2003; Lazo, 2007; Richardson et al., 2011; Wright et al., 2004). The Tspan family consists of 33 proteins with unique structural features (Lazo, 2007; Tarrant, Robb, van Spriel, & Wright, 2003; Huang et al., 2005b). Tspans are hydrophobic TM type II proteins of a size between 20-50 kDa that exhibit four TM domains, two extracellular loops and two short cytoplasmic tails (Stipp, Kolesnikova, & Hemler, 2003). The extracellular portion of Tspans comprises of two loops which are termed small extracellular loop (SEL/EC1) and large extracellular loop (LEL/EC2) whereas a short sequence of intracellular amino-acids connects TM2 with TM3 (Figure 2.6) (Hemler, 2003; Hemler, 2005; Tarrant et al., 2003). The extracellular LEL/EC2 domain consists between 70-150 amino acids containing a conserved CCG motif of so far not fully clarified function.

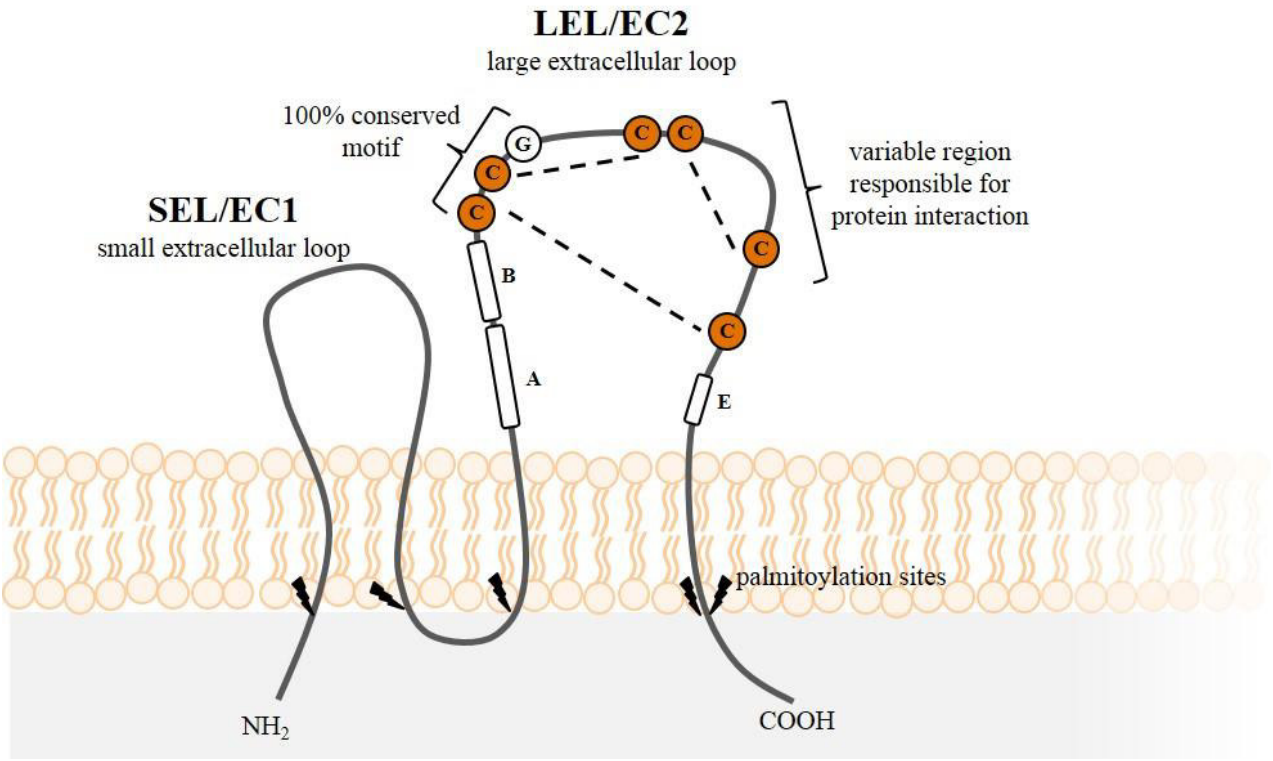

Figure 2.6. Structure and features of Tetraspanins. Schematic presentation of an unfolded Tspan with the extracellular loops SEL/EC1 and LEL/EC2, palmitoylation sites, the conserved signature Tspan CCG motif and A, B and E helices in the LEL/EC2 loop. Interaction with other proteins occurs at the variable region located in the LEL/EC2 loop. Tspans exhibit 2 to 4 disulfide bonds between orange shaded cysteine. The image is adapted and modified from (Lazo, 2007; Richardson et al., 2011; Hemler, 2008).

As illustrated in Figure 2.6, LEL/EC2 contains a constant region (A, B and E helices) and a variable region which is used to interact with proteins (Kitadokoro et al., 2001; Seigneuret, Delaguillaumie, Lagaudriere-Gesbert, & Conjeaud, 2001; Stipp et al., 2003). The conserved CCG residues determine and identify the protein signature of Tspans and include characteristic disulfide bonds (Lazo, 2007; Shoham, Rajapaksa, Kuo, Haimovich, & Levy, 2006). At intracellular and juxtamembrane regions, Tspans have palmitoylation sites which promote the formation of cholesterol rich microdomains. Palmitoylation represents the process in which fatty acids are covalently attached to cysteine, serine or threonine residues of proteins (Hemler, 2003; Hemler, 2005; Tarrant et al., 2003; Yanez-Mo et al., 2009). Studies have shown that the C-terminal cytoplasmic portion is likely to be responsible for communication with intracellular signaling molecules (Stipp et al., 2003). All Tspan family members exhibit low sequence homology but contain conserved secondary and tertiary structures (Yanez-Mo et al., 2009). The highest sequence homology with respect to the conserved regions are shared by the polar residues of the TM domains 1, 3 and 4 (Yanez-Mo et al., 2009).

2.8.2 How can Tspans interact with so many proteins? Tspan enriched microdomains (TEMs)

Significance of Tspans in tumor cell biology is most likely due to their ability of forming large complexes and the resulting interaction with other cell surface proteins in the plasma membrane. This ability constitutes for their complexity and the poor knowledge about them, although studies have shown that such formation is linked to tumor progression (Lazo, 2007; Tarrant et al., 2003; Yunta & Lazo, 2003b). The biology of Tspans can be considered as compartmentalized system and the resulting membrane complexes are termed Tetraspanin enriched microdomains (TEMs) or Tetraspanin webs (Levy & Shoham, 2005). TEMs contain different Tspans which interact with each other and form a Tspan core that in turn interacts with other molecules. Based on this compartmentalized system, it is likely that the molecule composition in TEMs determines the respective biological effect (Lazo, 2007).

TEMs have shown to play a role in tumor progression due to their ability of organizing other TM proteins like growth factor receptors, cell adhesion molecules, proteases and are therefore thought to promote adhesion, cell motility and cell proliferation (Berditchevski, 2001; Charrin et al., 2003a; Stipp et al., 2003). Also well-described kinases that are involved in signaling cascades important for cell proliferation and tumor progression (e.g. phosphatidylinositol-4 kinase (PI4K), protein kinase C (PKC)) are linked into TEMs (Boucheix & Rubinstein, 2001; Charrin et al., 2009; Hemler, 2005; Wright et al., 2004; Yanez-Mo et al., 2009). For instance, signaling can occur by a direct physical interaction between Tspan24 and PI4K where Tspan24 functions as connector between PI4K and integrins, which are TM receptors functioning as bridges for cell-cell and cell-ECM interactions (Berditchevski, 2001; Claas, Stipp, & Hemler, 2001). In another example the kinase PKC is activated upon Tspan25 (CD53) ligation (Barcia, Garcia-Vargas, Bosca, & Lazo, 1996; Bosca & Lazo, 1994; Lazo, Cuevas, Gutierrez del, & Orue, 1997) and can bind to intracellular sides of various Tspans (Zhang, Bontrager, & Hemler, 2001). Bound and activated PKC, in turn, is able to phosphorylate integrins which complexes with Tspan24 (Zhang et al., 2001). These examples underline the indirect implication of Tspans into signaling cascades important in tumor progression.

Tspans can be understood as molecular facilitators based on their participation in direct and indirect intracellular signaling i.e. signal modulation of receptors within TEMs (Lazo, 2007; Maecker, Todd, & Levy, 1997). The identification of tumor relevant Tspans in this work, based on a co-targeting rationale, is of special interest keeping in mind that the biological importance of Tspans are not

found in individual components but in the combination/interaction of Tspans with other molecules TEMs (Hemler, 2003; Wright et al., 2004).

2.8.3 TEMs are regulated by lipids and palmitoylation of Tspans

TEMs appear to be regulated by lipids. Palmitoylation controls association and therefore organization of membrane proteins via covalent modification (Lazo, 2007). A range of Tspans such as Tspan24 - Tspan30 can be palmitoylated at intracellular cysteines which facilitates the association to cholesterol rich complexes (Charrin et al., 2002; Charrin et al., 2003b). The initial assembly of TEMs is based on Tspan24, Tspan28 or Tspan29 homo- and heterodimerization in the Golgi (Kovalenko, Yang, Kolesnikova, & Hemler, 2004). Palmitoylation of Tspans is essential to promote the association of Tspan and Tspan-associated protein complexes and thereby to create TEMs (Berditchevski, Odintsova, Sawada, & Gilbert, 2002; Lazo, 2007; Yang et al., 2002). As an example, incorporation of Tspan24 into TEMs is facilitated via palmitoylated integrin together with palmitoylated Tspans such as Tspan28, Tspan29, and Tspan30 (Yang et al., 2004). It is important to discriminate between two types of Tspan complexes: i) palmitoylated Tspans which associate with integrins and form cholesterol rich complexes and ii) non-palmitoylated Tspans which are able to interact with signaling molecules (e.g. p130Cas, 14-3-3 or EWI). In consequence, interaction with Tspans can either occur as isolated complexes or as part of Tspans within TEMs (Lazo, 2007).

2.8.4 Integrins represent the main Tspan interaction partner

Even though the exact composition of TEMs is still not fully understood several key molecules in these microdomains have been identified. Besides signaling receptors and enzymes, adhesion molecules such as integrins have shown to play an important role (Yanez-Mo et al., 2009). In fact, the major type of Tspan interaction partners within TEMs are integrins (Berditchevski et al., 2001). Integrins are cell adhesion molecules which regulate actin filament rearrangement by intracellular signaling molecules. These proteins consist of two different chains, α and β, and overall 18 α and 8 β subunits in mammals (Brakebusch & Fassler, 2003; Juliano et al., 2004). However, integrins can also take part in tumor-related processes such as cell motility, adhesion, invasion and angiogenesis which makes the Tspan-integrin interaction of special interest (Hood & Cheresh, 2002; Janes & Watt, 2006; Ridley et al., 2003; Watt, 2002). In addition to this, integrins play a role in cell proliferation and gene regulation (Carragher, Westhoff, Fincham, Schaller, & Frame, 2003;

Lee & Juliano, 2004). Because most research focuses on individual Tspans only little is known about functional consequences upon Tspan-integrin interactions (Lazo, 2007). Via the cytoplasmic part of integrins (β1 chain) interaction with the ECM takes place at focal adhesions, which are large protein complexes connecting the cytoskeleton of a cell to the ECM (Hemler & Lobb, 1995). Direct interaction partners can be the focal adhesion kinase (FAK) which is a cytosolic protein tyrosine kinase regulating cell migration but also other proteins involved in cell signaling cascades (e.g. Src, paxillin, p130Cas) (Carragher & Frame, 2004). Based on this interaction, integrins are able to respond to changes in the extracellular environment and to regulate cell functions. Tspan-integrin interaction promotes the communication between cancer and neighboring cells underscoring the relevance of Tspans in tumor cell biology. The main integrin interaction partner for Tspans constitute integrins exhibiting a β1 subunit which is combined to α3, α4 or α6 and less common with α2 and α5 chain (Berditchevski, 2001). Besides mediating the adhesion to the ECM, β1 also signals via the integrin-linked kinase (ILacK) (Dedhar, 2000). In summary, integrins are able to transduce signaling by interacting with Tspans (Charrin et al., 2003a). This circumstance supports the overall rationale of designing multispecific antibodies targeting Tspans in combination with other molecules.

2.9 Tumor progression promoting Tspans

As mentioned previously, little is known about the Tspan family and approximately 5 out of 33 of these proteins have been relatively well described (e.g. Tspan24, Tspan27, Tspan28, Tspan29, Tspan30) whereas over nine have been correlated with tumor progression as summarized in table 2.1. Tspans represent interesting targets for therapeutic antibody generation due to several aspects:

i) tumor-relevant roles in TEMs
ii) interaction with other cell surface receptors (e.g. tumor relevant RTKs)
iii) tumor progression properties
iv) extracellular loops as target antigen

In the following chapters (2.9.1 and 2.9.3.), two Tspans were chosen to describe their role in tumor progression; First, Tspan24 represents a well characterized Tspan that has shown to regulate and promote neovascularization in breast cancer cells (Sadej et al., 2009) and second, Tspan8 (CO-029), exemplifying a poorly understood Tspan which is able to promote angiogenesis in pancreatic cancer cells (Gesierich, Berezovskiy, Ryschich, & Zoller, 2006; Nazarenko et al., 2010). But also

inversely correlated roles in tumor progression are found within Tspan family members. For instance, the biological function of Tspan29 (CD9) and Tspan27 (CD82) can be interpreted as metastasis suppressor (Dong et al., 1995; Zoller, 2009). Downregulation or loss of Tspan29 expression correlates with a variety of solid tumors (Miyake et al., 1995; Miyamoto et al., 2001; Sho et al., 1998; Si & Hersey, 1993; Wang et al., 2007a) and inversely correlates with the progression in hematopoietic malignancies (Yau et al., 1998; Yoon et al., 2010). Similar to Tspan29, Tspan27 is expressed in a broad range of epithelial tissues but is significantly downregulated or lost in the course of tumor progression (Dong et al., 1995; Jackson, Marreiros, & Russell, 2005; Liu & Zhang, 2006; Richardson et al., 2011) whereas expression levels inversely correlate with patient prognosis (Adachi et al., 1996; Yang et al., 2001).

2.9.1 Tumor progressing Tetraspanins: Tspan24

Beside Tspan29, Tspan24 is one of the best characterized Tspans and primary expressed in endothelial cells at basal and lateral cell to cell junctions but also in epithelial, muscle and haemopoeitic cells (Berditchevski & Odintsova, 1999; Sincock, Mayrhofer, & Ashman, 1997). Tspan24 can be clearly be correlated with tumor progression and is part of the rational why this work screens Tspans for anti-proliferative effects upon their inhibition. Several studies have identified Tspan24 to be upregulated in a variety of tumors such as breast, liver, pancreas, colon, prostate (Ang, Lijovic, Ashman, Kan, & Frauman, 2004; Hashida et al., 2003; Hirano et al., 2009; Ke et al., 2009; Novitskaya, Romanska, Dawoud, Jones, & Berditchevski, 2010; Sadej et al., 2009; Sauer et al., 2003; Yang et al., 2008) and that such upregulation is correlated with a lower survival rate of patients (i.e. 3.44 fold higher risk of death in breast carcinomas) (Ang et al., 2004; Hashida et al., 2003; Ke et al., 2009; Sadej et al., 2009; Tokuhara et al., 2001). Tspan24 is overexpressed in a third of cases in breast cancer (31%) and correlates with high grade subtypes (40%) and estrogen receptor negative subtypes (45%) (Yang et al., 2008). Animal models have shown that Tspan24 promotes metastasis formation by facilitating intravasation of tumor cells (Zijlstra, Lewis, Degryse, Stuhlmann, & Quigley, 2008) and tumor vascularization (Richardson et al., 2011; Sadej et al., 2009).

Three studies which were performed by Testa, Kohno, Yang and colleagues are of special interest for us and support Tspans as promising therapeutic targets for multispecific antibodies. Testa and colleagues developed a mAb (mAb 50-6) against Tspan24 and investigated metastasis formation

in vivo. As model system the human epidermoid cancer cell line HEp-3 cells was used and treated with this mAb. The antibody was found to specifically inhibit the formation of metastasis *in vivo* and to block HEp-3 migration *in vitro* in a chemotaxis assay. This study was one of the first to link Tspan24 as a positive effector of metastasis (Testa, Brooks, Lin, & Quigley, 1999). Several years later Kohno and colleagues investigated Tspan24 in relation to cell motility, invasion and metastasis in a set of three cancer cell lines of different tissue origin, each overexpressing Tspan24. Similar to mAB 50-6, the mAb which was developed by this group (mAb SFA1.2B4), was able to inhibit metastasis formation in the human colon cancer derived cell line RPMI4788 and the human fibrosarcoma cell line HT1080. By cell invasion and cell motility experiments, the study concluded that Tspan24 enhances cell motility, cell invasion and metastasis of cancer cells and that FAKs are needed for these steps (Kohno, Hasegawa, Miyake, Yamamoto, & Fujita, 2002). The third study by Yang and colleagues in 2010 (Yang et al., 2010) supports the approach of designing a multispecific antibody which targets Tspans on the one hand and a RTK on the other hand. As described previously, resistance to therapeutic antibodies and evasion to alternative signaling pathways can represent an obstacle in cancer therapy. Breast and lung cancers which are treated with the drug gefitinib, targeting the epidermal growth factor receptor (EGFR/HER1/ErbB-1), can lead to resistance by cMET amplification and phosphatidylinositol-4,5-bisphosphate 3-kinase (PI3K)/AKT pathway activation (Engelman et al., 2007). This pathway is an intracellular signaling pathway which plays an essential role in apoptosis and therefore in cancer (King, Yeomanson, & Bryant, 2015; Man et al., 2003; Peltier, O'Neill, & Schaffer, 2007). Similar problems were observed for anti-HER2 agents like the mAb trastuzumab (Roche) and the tyrosine kinase inhibitor lapatinib (GlaxoSmithKline) in human breast cancers (Esteva et al., 2002). The study by Yan and colleagues could reveal that the observed resistance is partly due to adhesion of human HER2 positive breast cancer cells to the extracellular glycoprotein und ECM component laminin-5 in the basement membrane and that knockdown of Tspan24 or integrins (e.g. $\alpha6\beta1$, $\alpha3\beta1$) can reverse the acquired resistance. Tspan24 knockdown in combination with trastuzumab is able to prevent HER2 activation and signaling through Akt and FAK. The researchers concluded that HER2 activity in mammary tumor cells is based on Tspan24 which supports integrin mediated adhesion to laminin-5 and that removal or inhibition of Tspan24 can overcome drug resistance (Yang et al., 2010).

In summary, Tspan24 seems to play a vital role in tumor cell movement and promotes metastasis formation. Several studies observed an increase in tumor cell migration and invasion upon

overexpression of Tspan24 whereas a knockdown resulted into inhibition (Ke et al., 2009; Klosek et al., 2005; Kohno et al., 2002; Yang et al., 2008). On molecular basis this acceleration i.e. in breast cancer is based on Tspan24 as master regulator of integrin function (e.g. α6β1, α6β4) in TEMs and results into signaling through FAK, the signaling G protein Ras-related C3 botulinum toxin substrate 1 (Rac1) and the serine/threonine intestinal cell kinase (ICK) (Yang et al., 2008). Tspan24 stabilizes the adhesion to other tumor cells and to laminin-5 through integrins (e.g. α3β1, α6β4) and by PKC-dependent actin cytoskeleton re-organization (Nishiuchi et al., 2005; Shigeta et al., 2003; Winterwood, Varzavand, Meland, Ashman, & Stipp, 2006). Overexpression of Tspan24 in hepatocellular carcinoma (HCC) cells is associated with MMP9 upregulation through the activation of cell signaling pathways (e.g. PI3K/AKT) leading to neoangiogenesis (Shi et al., 2010). But also increased motility and invasiveness can be observed upon Tspan24 overexpression and enhanced MMP9 expression (Hong et al., 2006). The presence of upregulated MMPs within the tumor microenvironment favors another therapeutic strategy. The approach of a multispecific antibody could be site-directed by tumor-specific antigens such as growth factor receptors (e.g. cMET receptor) whereas the Tspan-specific entity becomes active in the tumor environment by MMP9 cleavage. Even though the upregulation of MMPs is able to enhance peri-cellular proteolysis and therefore tumor progression, the exact mechanism by which the cell to cell/laminin interaction results into tumor progression, remains unclear (Richardson et al., 2011).

Tspans such as Tspan24 were also identified to upregulate growth factor signaling via cMET receptors in tumor cells, favoring thereby a co-targeting strategy by multispecific antibodies. In the study by Klosek and colleagues Tspan24 was determined as molecular linker between the cMET receptor and integrin α3/α6 which forms functional complexes. Via knock down experiments in human salivary gland cancer cells a complete stop in HGF stimulated cell growth and migration was observed (Klosek et al., 2005). As a consequence targeting the cMET receptor and Tspan24 simultaneously is likely to prevent the oncogenic function of this complex and thus cMET pathway activation and cell proliferation.

2.9.2 mAbs against Tspan24

On the basis of available literature and the described implementation in tumor progression Tspan24 was selected as an example. The vast majority of therapeutic antibodies that were generated against Tspans, were designed to target Tspan24. A list of Tspan24-specific mAbs is summarized in table

2.2. Due to distinct tissue and cell binding patterns i.e. their ability to detect integrin α6β1/α3β1 associated Tspan24, the investigated mAbs differ in function (Geary, Cambareri, Sincock, Fitter, & Ashman, 2001; Yamada et al., 2008). Based on previously described interactions by Tspan24 with other tumor relevant proteins such as growth factor receptors (e.g. cMET receptor, EGFR), Tspan24 was suggested by Haeuw and colleagues as scaffold to optimize the RTK–integrin cross-talk (Haeuw, Goetsch, Bailly, & Corvaia, 2011).

Table 2.2. Tspan24 therapeutic mAbs. *In vitro* and *in vivo* results of different mAbs against Tspan24. **N.d.** = not determined; ↑ = increase; ↓ = decrease. The table is based on the study by (Haeuw et al., 2011).

Anti- Tspan24 mAb	In vitro results	In vivo results	Literature
14A2.H1	↑ Aggregation of platelets	n.d.	(Ashman et al., 1991; Roberts, Rodgers, Drury, Ashman, & Lloyd, 1995)
11B1.G4	Platelet agonist	n.d.	(Fitter, Sincock, Jolliffe, & Ashman, 1999; Sincock, Mayrhofer, & Ashman, 1997)
TS151R	Inhibition of interaction with integrin	n.d.	(Serru et al., 1999)
TS151	Non-restricted	n.d.	(Charrin et al., 2001)
8C3	↓ Adhesion to laminin	n.d.	(Nishiuchi et al., 2005)
50-6	↓ Migration, ↓ Invasion, ↓ Angiogenesis	↓ Metastasis	(Testa et al., 1999)
SFA1.2B4	↓ Migration	↓ Metastasis	(Kohno, Hasegawa, Miyake, Yamamoto, & Fujita, 2002)
1A5	↓ Migration, ↑ Adhesion	↓ Metastasis	(Kohno, Hasegawa, Miyake, Yamamoto, & Fujita, 2002; Zijlstra et al., 2008)

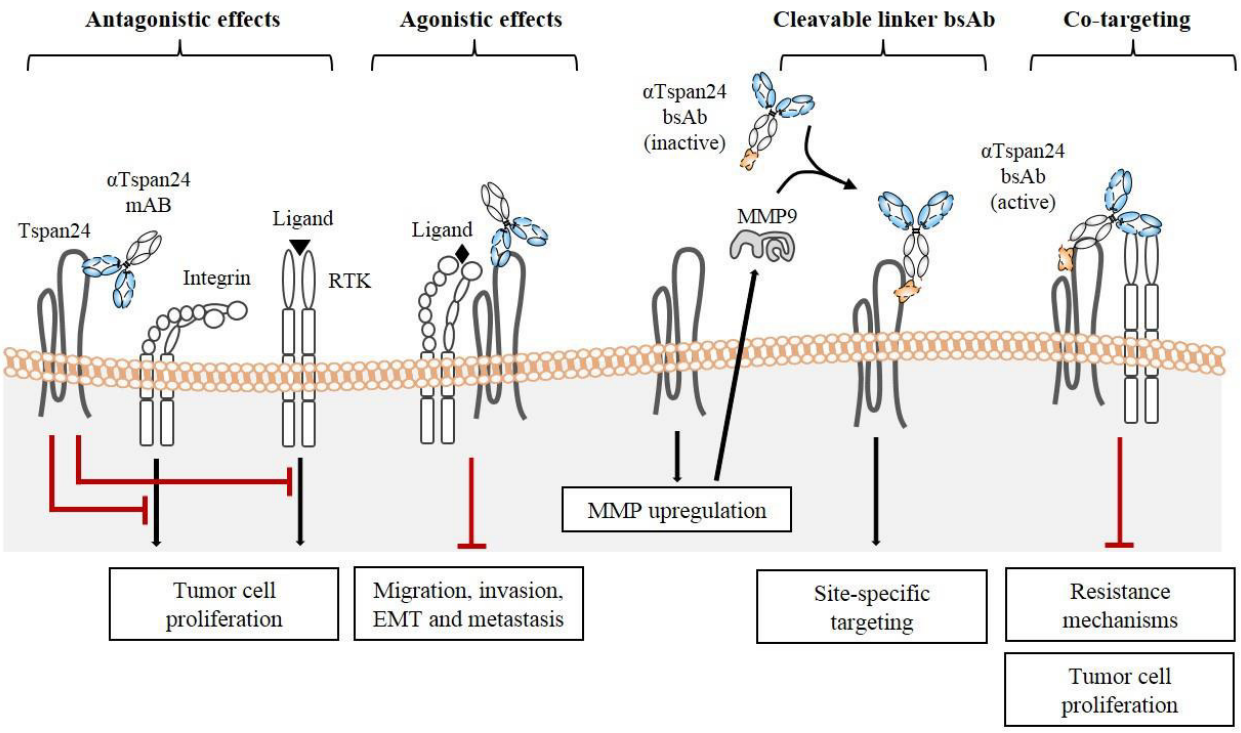

Figure 2.7. Potential mechanisms of targeting Tspan24 with different therapeutic antibody formats. Tspan24 targeting could be categorized into four different approaches: 1) antagonistic effects by prevention of integrin and RTK interaction; 2) agonistic effects via altered integrin interactions; 3) generation of site-specific BsAbs (cleavable linker) which are activated by MMPs; 4) Co-targeting of Tspans and RTKs to prevent resistance. The image is adapted and modified from (Haeuw et al., 2011).

In the light of this work Figure 2.7 illustrates possible mechanisms of Tspan24 inhibition and thereby Tspan targeting options. A straight forward targeting approach could represent the induction of an antagonistic effect via antibodies, by the inhibition of integrin association. Such antagonistic effect can be observed upon mAb treatment with 8C3 which inhibits integrin association (Nishiuchi et al., 2005). In consequence cell proliferation could be arrested. Beside antagonistic effects against Tspan24, antibodies could also exhibit an agonistic way of action by the activation of associated Tspan proteins or induced clustering with these (Haeuw et al., 2011). A study by Zijlstra and colleagues demonstrated an agonistic effect of a mAb (1A5) which led to the inhibition of metastasis formation due to enhanced ECM adhesion of tumor cells and thereby preventing detachment. The authors concluded that increased inhibition is most likely due to integrin activation via this mAb (Haeuw et al., 2011; Zijlstra et al., 2008) whereas increased cell to cell contacts might prevent epithelial–mesenchymal transition (EMT) (Fitter et al., 1999; Haeuw et al., 2011; Johnson, Winterwood, DeMali, & Stipp, 2009), a process in which cell to cell adhesion of epithelial cells is lost and migratory and invasiveness properties gained. Another strategy to

target Tspans could be the implementation of ADCC and CDC as described throughout chapter 2.3 and which is illustrated in Figure 2.7. In relation to the studies by Shi and colleagues and Hong and colleagues, who observed enhanced MMP9 expression correlating with Tspan24 overexpression, the cleavable linker approach (chapter 2.5.2) seems promising (Hong et al., 2006; Metz et al., 2012; Shi et al., 2010). In summary, several studies favored a co-targeting rational as illustrated in Figure 2.7. Especially on the basis of the work by Klosek and Yang, Tspan24 and cMET/HER2 receptor co-targeting would represent a promising therapeutic approach (Klosek et al., 2005; Yang et al., 2010).

2.9.3 Tumor progressing Tspans: Tspan8 (CO-029)

Another known but less well described tumor progression supporting Tspan represents Tspan8 (CO-029). Tspan8 was discovered by Szala and colleagues and initially described as tumor associated antigen (Szala et al., 1990). In relation to tumor progression, upregulation of Tspan8 correlates to several malignancies such as gastric, pancreatic, esophageal, hepatic and colorectal carcinomas. Increased expression of Tspan8 is found in proceeded stages of those tumors (Gesierich et al., 2005; Kanetaka et al., 2001; Le et al., 2006; Zhou et al., 2008). Several studies concluded that Tspan8 regulates and promotes tumor progression (Claas et al., 1998; Gesierich et al., 2006; Kanetaka et al., 2001; Le et al., 2006) and that high expression levels seem to correlate with a poor prognosis of patients with gastrointestinal tumors.

Metastasis assays in animal models, similar to Tspan24, reveal that increased levels of Tspan8 in esophageal and pancreatic tumors promote the formation of metastasis in distal organs (Claas et al., 1998; Zhou et al., 2008). These studies suggest that tumor cells which express Tspan8 metastasize without stopping at lymph nodes (Claas et al., 1998). Such overexpression can also lead intrahepatic metastasis formation of liver cancer cells (Kanetaka et al., 2003).

In relation to TEMs and proteins which are organized within, a forced Tspan8 expression results in the increase of invasive and migration properties of esophageal tumor cells (Zhou et al., 2008). The degree of tumor progression promotion by Tspan8 can be exemplified in animal models for pancreatic cancer cells. In these, Tspan8 stimulates tumor angiogenesis by endothelial cell progenitor maturation and migration, capillary sprouting and cell proliferation. Such stimulation in cell proliferation was also observed for Tspan24 by Novitskaya and colleagues and will be investigated in this work for all Tspans upon siRNA treatment (Novitskaya et al., 2010). Pancreatic

tumors that express Tspan8 secrete cell derived vesicles, so called exosomes which contain integrins and vascular cell adhesion molecule 1 (VCAM-1) which is known as adhesion molecule in endothelial cells but also in mediating pro-metastatic tumor-stromal interactions (Chen & Massague, 2012). Secreted exosomes induce the upregulation of vascular endothelial growth factor (VEGF), a signaling protein stimulating angiogenesis and vasculogenesis, and its corresponding receptor, chemokines and chemokine receptors. In addition, the expression of Tspan8 is upregulated in endothelial cells whereas VEGF, uPA and MMPs are upregulated in tumor adjacent fibroblasts (Gesierich et al., 2006; Nazarenko et al., 2010; Richardson et al., 2011). In summary, the expression of Tspan8 does not only influence other cells but also the TEM itself. In the case of colorectal and pancreatic cancer such upregulation leads to altered TEM components (e.g. epithelial cell adhesion molecules (EpCAM), C4.4A, claudin-7 and CD44v6) (Claas et al., 1998; Claas et al., 2005; Kuhn et al., 2007; Le et al., 2006).

Although Tspan24 and Tspan8 have shown to promote metastasis formation, both Tspans exhibit distinct mechanisms in doing so. In the study by Yue and colleagues Tspan24 and Tspan8 were stably knocked-down in BSp73ASML cells which are derived from rat pancreatic adenocarcinoma and known to be a highly metastatic cell line. The knockdown of Tspan24 and Tspan8 leads to an increased survival time (2-3 fold in comparison to wt) and to a delay in metastasis formation. However, Tspan24 facilitates metastasis formation by associating with proteases such as MMP9 and MMP13 more readily than Tspan8. This interaction leads to enhanced collagen and laminin111 degradation creating thereby a path for migrating tumor cells and promoting tumor invasiveness. Further, Tspan8 promotes metastasis by the recruitment of integrins with adhesion functions into motility promoting Tspan8 complexes. Such complexes are formed upon Src recruitment by Tspan8 and results into FAK activation (Yue, Mu, & Zoller, 2013).

In summary, Tpans can promote and facilitate metastasis formation in a variety of tumors. But of more importance for this work, Tspans seem to functionally interact with a broad range of tumor related cell surface molecules such as VCAM-1, EpCAM, integrins and growth factor receptors (cMET receptor, EGFR), to upregulate directly and indirectly the expression of MMPs, VEGF, uPA and to associate with protein kinases PI4K, FAK, Src and PKC.

3 Aim of studies

The first and main part of this work will focus on the strategy of using bispecific antibodies as receptor quantitation tool. The second part of this work will focus on target assessment of Tspans to generate data for a multispecific therapeutic antibody approach. Here, promising and tumor promoting Tspans will be screened via a proliferation assay based siRNA screen.

3.1 FACS-based Receptor Quantitation

In this study I applied a concept to couple fluorophores to generate bispecific tool antibodies, which enable highly reproducible and precise receptor quantitation. Initially, different formats were generated to compare and evaluate their properties in cell surface receptor quantitation. As antigens of interest the RTKs cMET, EGFR, HER2 and HER3 were chosen. These molecules are prominent oncogenes and pursued as drug targets in the clinic (Gherardi, Birchmeier, Birchmeier, & Vande, 2012; Yarden & Sliwkowski, 2001). By evaluating the quantitation of antigen cell surface expression in nine different cell lines, I here sought to determine if a Fab-scFv format is an appropriate tool antibody for standardized flow cytometric receptor quantitation. Finally, these antibodies were also tested to quantify proteins in intracellular vesicles, using confocal microscopy.

3.2 Tetraspanin Screen

In this study, I sought to determine proliferation promoting Tspans in a panel of different tumor derived cell lines. To accomplish this goal, an siRNA library screen consisting of Tspan-specific siRNAs against all 33 known Tspans was used. Initially 2D and 3D proliferation assays were performed to screen potential targets. Since individual members, of the yet relatively unknown Tspan family, correlate with tumor progression (Hemler, 2003; Richardson et al., 2011; Zoller, 2009) the goal of this study was to provide targets for future therapeutic antibody generation. A co-targeting rational by multispecific antibodies seems to represent a promising approach based on literature examples where Tspans interact with growth factor receptors and other tumor-relevant molecules (Boucheix et al., 2001; Hemler et al., 1996; Lazo, 2007; Richardson et al., 2011; Wright et al., 2004; Zoller, 2009). Together with RT-PCR and western blot analysis the screen sought to evaluate how many of the initially 33 targets lead to significant anti-proliferative effects upon mRNA knockdown.

4 Materials

4.1 Chemicals, enzymes and materials

1 kb ladder, 100 bp ladder	Invitrogen
2-mercaptoethanol	Gibco, Sigma
ACTB, GAPDH, probes	Roche
agarose	Invitrogen
Amersham ECL Western blotting reagents	GE Healthcare
ampicillin	Sigma
bacto agar	BD
bacto peptone	BD
bovine serum albumine	Sigma, Roche
Bradford protein assay solution	BioRad
bromphenol blue	BioRad
cOmplete Protease Inhibitor Cocktail	Roche
coomassie brilliant blue	Merck
CPRG (chlorophenol-red-β-D-galacto-pyranoside)	Roche
DEAE Dextran	GE Healthcare
DEPC	Gibco, Sigma
Dynabeads	Invitrogen
EDTA	Sigma
gelatine	Sigma
geneticin (G418)	Gibco, Invitrogen
iBlot® Transfer Stack, Regular	Invitrogen
Kanamycin	Sigma
Luciferase assay	Promega
LumiLight Plus Substrate	Roche
LightCycler 480 Sealing Foil	Life Technologies, Roche
LightCycler 480 Probes Master	Life Technologies, Roche
LightCycler 480 Multiwell Plate	Life Technologies, Roche
Lipofectamine 2000	Invitrogen
MagicMark™ XP Western Protein Standard	Invitrogen
Nonfat dry milk powder	AppliChem
NP-40	Roche
Nuclease-Free Water	Life Technologies
NuPAGE 4-12 % Bis-Tris Gel	Invitrogen
NuPAGE® Antioxidant	Invitrogen
NuPAGE® MOPS SDS Running Buffer	Invitrogen
NuPAGE® Sample Reducing Agent	Invitrogen
NuPAGE® Transfer Buffer	Invitrogen

Octyl-β-D-glucopyranosid	Sigma
Oligo(dT)	Roche
PhosphoSTOP	Roche
Pierce ECL Western Blotting Substrate	Pierce
poly-L-lysine solution	Sigma
Precision Plus Protein Kaleidoscope™ Standards	BioRad
Protein A / Protein G	Amersham, GE Healthcare
Qiashredder	Qiagen
restriction enzymes	New England Biolabs, Roche
RNAlater RNA Stabilization Reagent	Qiagen
Superscript II reverse polymerase	Invitrogen
SuperSignal West Pico Chemiluminescent	Pierce
T4 DNA ligase	New England Biolabs
TBST 10x	Roth
Triton X-100	Sigma
Trizol	Invitrogen
tryptone/peptone	BD
Tween 20	Calbiochem, BioRad
Universal ProbeLibrary Human ACTB Assay	Roche
Universal ProbeLibrary Human GAPD Assay	Roche
Universal ProbeLibrary Probes	Roche

4.2 Cell culture reagents

2-mercaptoethanol	Gibco, Sigma
poly(2-hydroxyethylmethacrylate)	Polysciences
Cell Freezing Medium-DMSO Serum free	Sigma
Collagen	Roche
DMEM high glucose	Gibco, Invitrogen
DMEM low glucose	Gibco
DMSO	Sigma
fetal calf serum (FCS)	Sigma
Fibronectin	Roche
Fugene® 6 transfection reagent	Roche
NEA (non essential amino acids)	Gibco, Invitrogen
Opti-MEM	Gibco, Invitrogen
PBS cell culture grade	Gibco
PS (penicillin,streptomycin, glutamine)	Invitrogen
Recombinant human IGF-I	PeproTech
Recombinant human heregulin-ß1	PrepoTech
Recombinant human HGF	Life Technologies

Recombinant human EGF	Invitrogen, Gibco
RPMI 1640	Gibco
sodium pyruvate	Gibco, Invitrogen
tissue culture plates	Falcon, Greiner
trypsin	Gibco, Invitrogen

4.3 Receptor quantitation reagents & material

7-AAD	BD
Alexa Fluor® 647 Antibody Labeling Kit	Ivitrogen
AlexaFluor647/Cy5 Reference Standards	Bangs Laboratories
Alexa Fluor® 647/Cy5	Bangs Laboratories
BD Cell Fix	BD
BD Quantibrite™ PE Beads	BD
CS&T (Cytometer Setup & Tracking) Beads	BD
Cy5 antibody Labeling Kit	Amersham
Cy5 mAb Labelling Kit	GE Healthcare
Cy5 FluoroLink Ab Labelling Kit	Pharmacia Biotech
DyLight 650 Antibody Labeling Kit	Pierce
FACS Canto II with HTS unit	BD
FCS	Gibco
FlowJo Version 7.6.1	Tree Star Inc.
PBS	Gibco
QuantiBRITE™ PE	BD
Quantum AlexaFluor647/Cy5 MESF	Bangs Laboratories
QuickCal Version 2.3	Bangs Laboratories
Simply Cellular anti-Human IgG	Bangs Laboratories

4.4 Antibodies

4.4.1 Antibodies for Receptor quantitation and FACS

Her2Fab1v1	*In house generated*
Her2Fab1v2	*In house generated*
Her3Fab1v1	*In house generated*
Human IgG whole molecule	Jackson ImmunoResearch
IgG-Dig	*In house generated*
Met1v1	*In house generated*
Met2v2	*In house generated*
MetFab1v1	*In house generated*
Monoclonal Anti-human ErbB3-Phycoerythrin	BD

4.4.2 Immunoblot antibodies

α-ß-Catenin	mouse, 1:2,000	BD #610154
α- c-erbB-2 Oncoprotein	rabbit, 1:1,000	Dako # A0485
α-cMyc XP™	rabbit, 1:1,000	Cell Signaling #D84C12
α-Cyclin D1	mouse, 1:2,000	Cell Signaling #2926
α-DDK	mouse, 1:1,000	Amsbio #TA50011-100
α-DDK tag mAb	mouse, 1:1,000	Origene #TA50011
α-EGFR	rabbit, 1:1,000	Millipore #06-847
α-EGFR phosho	rabbit, 1:1,000	Epitomics #1139-1
α-ErbB-3 (C-17)	rabbit, 1:200	Santa Cruz Biotechnology #sc-285
α-HER2/ErbB2	rabbit, 1:1,000	Cell Signaling #2242
α-Myc-tag (9B11)	mouse, 1:1,000	Cell Signaling #2276
α-Phospho-Akt	rabbit, 1:2,000	Cell Signaling #4060
α-Phospho-HER2	rabbit, 1:1,000	Cell Signaling #2244
α-Phospho-HER3/ErbB3	rabbit, 1:1,000	Cell Signaling #4791
α-Phospho-p44/42 MAPK	rabbit, 1:2,000	Cell Signaling #4370
α-rabbit	goat, 1:5,000	Jackson ImmunoResearch #111-035-04
α-rabbit	mouse, 1:3,000	Cell Signaling #7074
α-Tspan4	rabbit, 1:1,000	Abcam #ab95104
α-Tspan4	rabbit, 1:100	Aviva Systems Biology #ARP44756
α-Tspan8	rabbit, 1:500	Abcam #ab70007
α-Tspan13	rabbit, 1:100	Sigma # HPA007426
α-Tspan15	rabbit, 1:1,000	Abcam #ab105567
α-Tspan15	rabbit, 1:500	Sigma # AV46889

4.5 siRNA components

DharmaFECT1-4 TF reagent	Thermo Scientific	#T-2001-(1-4)
PLK positive control	Santa Cruz	#sc-36277
Non-Targeting siRNA#1-4	Thermo	#D-001810
cMET siRNA ON-TARGETplus	Thermo	#J-003156-14-0005
Target Sequence siRNA#1:	GAACUGGUGUCCCGGAUAU	
Target Sequence siRNA#2:	GAACAGCGAGCUAAAUAUA	
Target Sequence siRNA#3:	GAGCCAGCCUGAAUGAUGA	
Target Sequence siRNA#4:	GUAAGUGCCCGAAGUGUAA	

Eg5/Kif11	Thermo	#TATDB-000007
Target Sequence siRNA#1:	CUGAAGACCUGAAGACAAU	
Pre-designed Tspan4 siRNA	Ambion	#4392420-s224737
Target Sequence (5'-3'):	CACUUUUUAUAUUUACGU	
Pre-designed Tspan8 siRNA	Ambion	#AM16708-15096
Target Sequence (5'-3'):	GGGAUAUAAGGGAAAAU	
Pre-designed Tspan13 siRNA	Ambion	#AM16708-134312
Target Sequence (5'-3'):	CGUACAUCUCACUGGUAU	
Pre-designed Tspan15 siRNA	Ambion	#AM16708-20089
Target Sequence (5'-3'):	GGAGUUUCUGACUAAUCAA	
Tspan1 siRNA SMARTpool	Thermo	#M-003719-01-0003
Target Sequence siRNA#1:	CCAUGUAUCUGUACUGCAA	
Target Sequence siRNA#2:	GGUCUUUGCUCUUGGUUUC	
Target Sequence siRNA#3:	GGUAGUGCCUGCCAUCAAG	
Target Sequence siRNA#4:	GCAAAAGGCUCACGACCAA	
Tspan2 siRNA SMARTpool	Thermo	#M-017266-01-0003
Target Sequence siRNA#1:	AUACGAAACUCACGAGAUG	
Target Sequence siRNA#2:	GAGGUGCCAUAAAGGAGUU	
Target Sequence siRNA#3:	CGUCAUUGCUUUUGGACUA	
Target Sequence siRNA#4:	CCAUGUAUGAAGAGGCUUA	
Tspan3 siRNA SMARTpool	Thermo	#M-010735-02-0003
Target Sequence siRNA#1:	AGAGACAGCUGCAUUGUUG	
Target Sequence siRNA#2:	GUAGAGAUCCUGCUUACGA	
Target Sequence siRNA#3:	CCUAAGAUUUUAAGUACGA	
Target Sequence siRNA#4:	UGUAGGAUCAUAUGGCGUA	
Tspan4 siRNA SMARTpool	Thermo	#M-010625-01-0003
Target Sequence siRNA#1:	CGGACAAGAUUGACAGGUA	
Target Sequence siRNA#2:	CUGACUGGUUCGAGGUGUA	
Target Sequence siRNA#3:	AGGUGUGGCUUCAGGAGAA	
Target Sequence siRNA#4:	GCCAAGUGGUCAAGGCAGA	

Tspan5 siRNA SMARTpool	Thermo	#M-010634-01-0003
Target Sequence siRNA#1:	GAAGUCAGUUGUUGCAUCA	
Target Sequence siRNA#2:	GAAGUUGACCAGCAGAUUG	
Target Sequence siRNA#3:	GAAUUUGGUUAGCGAUAUC	
Target Sequence siRNA#4:	CAUCAGAGCAUAUCGGGAU	
Tspan6 siRNA SMARTpool	Thermo	#M-010624-02-0003
Target Sequence siRNA#1:	GCUGUAAACUUGAAGAUUG	
Target Sequence siRNA#2:	CAAAAUACGUUGCAUUGUU	
Target Sequence siRNA#3:	CAAGAGCGUUCUGCUAAUC	
Target Sequence siRNA#4:	UAUUAAAUGGUGUCGGAAU	
Tspan7 siRNA SMARTpool	Thermo	#M-021321-00-0003
Target Sequence siRNA#1:	GAACGAAACUGAUUGUAAU	
Target Sequence siRNA#2:	GUAACUAGUUUCAUGGAGA	
Target Sequence siRNA#3:	GGACUUACACGGACGCUAU	
Target Sequence siRNA#4:	CAGAAGGGUUGUUAUGAUC	
Tspan8 siRNA SMARTpool	Thermo	#M-010219-02-0003
Target Sequence siRNA#1:	UGAAUGAAACUCUCUAUGA	
Target Sequence siRNA#2:	GAUACUGGGUUUGGUGUUU	
Target Sequence siRNA#3:	UGAAUUAUGUGCCUGUCUA	
Target Sequence siRNA#4:	GCAAUAUGGGUACGAGUAA	
Tspan9 siRNA SMARTpool	Thermo	#M-012293-03-0003
Target Sequence siRNA#1:	UAAGAAGUACGACGCAUGA	
Target Sequence siRNA#2:	GCAGAGCUGAUCUUACUCA	
Target Sequence siRNA#3:	AAGAACGCCUGGAACAUCA	
Target Sequence siRNA#4:	UGGGUUGGGUGGCGAUUAU	
Tspan10 siRNA SMARTpool	Thermo	#M-018583-01-0003
Target Sequence siRNA#1:	CAGCAGAACCUGUACUUUA	
Target Sequence siRNA#2:	GAGCAGCUGCGUCAAGUAU	
Target Sequence siRNA#3:	CGGACGCAGCUCAGAGAGU	
Target Sequence siRNA#4:	GAGCUAAGGUCCAGGCCUC	
Tspan11 siRNA SMARTpool	Thermo	#M-034324-00-0003
Target Sequence siRNA#1:	GUGCCUAGCUCCUGCGAAU	
Target Sequence siRNA#2:	UCACCAAGCUGGAGCAGUU	
Target Sequence siRNA#3:	CGUACAUCCUGUUGCGGGA	
Target Sequence siRNA#4:	CUGCAUUCAGCACGGGAUU	

Tspan12 siRNA SMARTpool	Thermo	#M-012466-01-0003
Target Sequence siRNA#1:	GCAAACAGCUUUAAUACAC	
Target Sequence siRNA#2:	GUACAAUGGUCAGAUAUGG	
Target Sequence siRNA#3:	AUGAGGGACUACCUAAAUA	
Target Sequence siRNA#4:	UGAGAUGGAGGAGUUAUAA	
Tspan13 siRNA SMARTpool	Thermo	#M-012516-01-0003
Target Sequence siRNA#1:	GAGGUUGGUUGGAACAAUA	
Target Sequence siRNA#2:	GCCAUGUGCUCCAAUCAUA	
Target Sequence siRNA#3:	GCAGUGGGCAUCUUCUUGU	
Target Sequence siRNA#4:	GAUACAGGAACCAGAAAGA	
Tspan14 siRNA SMARTpool	Thermo	#M-014675-01-0003
Target Sequence siRNA#1:	GAUAUGAUGUCAGGAUUCA	
Target Sequence siRNA#2:	UCAGAAAGCUAACCAGUGC	
Target Sequence siRNA#3:	AGAGCAACAUCAAGUCCUA	
Target Sequence siRNA#4:	GGACGAUAUCGAUCUGCAA	
Tspan15 siRNA SMARTpool	Thermo	#M-017265-01-0003
Target Sequence siRNA#1:	CGACAACAUUCGAAGAGGA	
Target Sequence siRNA#2:	GCAAGAAUCAGUACCACGA	
Target Sequence siRNA#3:	GUUGAGCGGCAGAAAUAUA	
Target Sequence siRNA#4:	GCUCAUUGGUGGCGUGGUG	
Tspan16 siRNA SMARTpool	Thermo	#M-012485-01-0003
Target Sequence siRNA#1:	GAAAUCCACACUCCGUAUU	
Target Sequence siRNA#2:	GGGCCUCUCUGACGAAUGU	
Target Sequence siRNA#3:	GGUAUGGAGCGACUAAAGA	
Target Sequence siRNA#4:	CCCAGGAGUUGCUGUAAAU	
Tspan17 siRNA SMARTpool	Thermo	#M-031881-02-0003
Target Sequence siRNA#1:	GAGACCAGCUCAACCUCUU	
Target Sequence siRNA#2:	CCGGCAAGCACCAGCAUUU	
Target Sequence siRNA#3:	CGCACAAUCUAGUCGGUAA	
Target Sequence siRNA#4:	GGAGACAAAGACAUCGUGA	
Tspan18 siRNA SMARTpool	Thermo	#M-015297-02-0003
Target Sequence siRNA#1:	CAACGGGCCUGAAGACUUU	
Target Sequence siRNA#2:	GCAGGGCUGUUACACGGUG	
Target Sequence siRNA#3:	CCCGAGAAUUCUUCACCAA	
Target Sequence siRNA#4:	AAGCACUACCAGGGCAAUA	

Tspan19 siRNA SMARTpool	Thermo	#M-026901-01-0003
Target Sequence siRNA#1:	GAAAUCAGAUGGCUCCUAA	
Target Sequence siRNA#2:	GUGCAUGGCUCUUAUUAGA	
Target Sequence siRNA#3:	GAUAUAACCAAGUGGACUA	
Target Sequence siRNA#4:	GUGCAUGGUAUAAUGUUAA	
Tspan20 siRNA SMARTpool	Thermo	#M-017260-00-0003
Target Sequence siRNA#1:	GGAGCAGAAUUGAAUAUUA	
Target Sequence siRNA#2:	CAACAGCCCUCCAAACAAU	
Target Sequence siRNA#3:	GGACAAUUGCUGUGGCGUA	
Target Sequence siRNA#4:	GGACUGAGAAUAAUGAUGC	
Tspan21 siRNA SMARTpool	Thermo	#M-012360-00-0003
Target Sequence siRNA#1:	GCACAUGGACUACCUGUUC	
Target Sequence siRNA#2:	UGAUAGCCAUGUAUUUCUA	
Target Sequence siRNA#3:	GCUGAGACCAUAUGGGUGA	
Target Sequence siRNA#4:	GGUCCAUGGUCCUCACGUA	
Tspan22 siRNA SMARTpool	Thermo	#M-011102-01-0003
Target Sequence siRNA#1:	GGAGCGAUGUGAUGAAUAA	
Target Sequence siRNA#2:	GCAGGUGUUUCAUGAAGAA	
Target Sequence siRNA#3:	AGAAGAAGCGGGUCAAGUU	
Target Sequence siRNA#4:	GUUCAAAUGCUGCGGCAAC	
Tspan23 siRNA SMARTpool	Thermo	#M-017459-00-0003
Target Sequence siRNA#1:	GUAGAAGGCCUAUACCUGA	
Target Sequence siRNA#2:	CCAAGGAGGAUCUAUCUGA	
Target Sequence siRNA#3:	GACCCAGGGCUAUCUCUUU	
Target Sequence siRNA#4:	CGCCACGGGUACAAGGAUU	
Tspan24 siRNA SMARTpool	Thermo	#M-003637-03-0003
Target Sequence siRNA#1:	CAACAUGUGGCACCGUUUG	
Target Sequence siRNA#2:	CCUCAAGAGUGACUACAUC	
Target Sequence siRNA#3:	UCACAGGACUGGCGAGACA	
Target Sequence siRNA#4:	GUACAGGAGUCUCAAGCUG	
Tspan25 siRNA SMARTpool	Thermo	#M-011117-01-0003
Target Sequence siRNA#1:	GAAAACAAGUGUCUGCUUA	
Target Sequence siRNA#2:	UGAAUGAGUAUGUGGCUAA	
Target Sequence siRNA#3:	AUAAAUGGCACGAGUGAUU	
Target Sequence siRNA#4:	GGAGGGUUGCUAUGCGAAA	

Tspan26 siRNA SMARTpool	Thermo	#M-011604-01-0003
Target Sequence siRNA#1:	GCAGAAACCUGGACCACGU	
Target Sequence siRNA#2:	ACAACCGGCUCGCUCGAUA	
Target Sequence siRNA#3:	GUUCAUGACGCUCUCGAUA	
Target Sequence siRNA#4:	ACUCCACAAUCCUAGAUAA	
Tspan27 siRNA SMARTpool	Thermo	#M-003901-02-0003
Target Sequence siRNA#1:	GUAUCAAAGUCACCAAAUA	
Target Sequence siRNA#2:	CAUCGUGACUGAGCUCAUU	
Target Sequence siRNA#3:	GCACGUCCAUUCCGAAGAC	
Target Sequence siRNA#4:	UGACUGAGCUCAUUCGAGA	
Tspan28 siRNA SMARTpool	Thermo	#M-017257-02-0003
Target Sequence siRNA#1:	CCAAGGAUGUGAAGCAGUU	
Target Sequence siRNA#2:	GCCCAACACCUUCUAUGUA	
Target Sequence siRNA#3:	UCAGCAACCUCUUCAAGGA	
Target Sequence siRNA#4:	CCACCAACCUCCUGUAUCU	
Tspan29 siRNA SMARTpool	Thermo	#M-017252-00-0003
Target Sequence siRNA#1:	UGAAAUAGCUGCGGCCAUC	
Target Sequence siRNA#2:	GAUAUUCCCACAAGGAUGA	
Target Sequence siRNA#3:	UUAAGGAAGUCCAGGAGUU	
Target Sequence siRNA#4:	CCAAGAAGGACGUACUCGA	
Tspan30 siRNA SMARTpool	Thermo	#M-017256-01-0003
Target Sequence siRNA#1:	GAGAUAAGGUGAUGUCAGA	
Target Sequence siRNA#2:	AAGGAGAACUAUUGUCUUA	
Target Sequence siRNA#3:	GGAUUAAUUUCAACGAGAA	
Target Sequence siRNA#4:	GAUGGAGAAUUACCCGAAA	
Tspan31 siRNA SMARTpool	Thermo	#M-003703-01-0003
Target Sequence siRNA#1:	UGUAAUCUCUUGCUCAUGU	
Target Sequence siRNA#2:	CAUCAUCGGCGGAGUCAUU	
Target Sequence siRNA#3:	GAGAAAGUUUAGCGAAUAU	
Target Sequence siRNA#4:	AGCAAUGAGAUUUCGGAAU	
Tspan32 siRNA SMARTpool	Thermo	#M-021411-01-0003
Target Sequence siRNA#1:	GAGCGUCCCUGGAGAAGAA	
Target Sequence siRNA#2:	CCAAGAGGAUGCUCGGGUA	
Target Sequence siRNA#3:	CCAAGAGGAUGCUCGGGUA	
Target Sequence siRNA#4:	GUACCAGGCUGUGCACCAA	

Tspan33 siRNA SMARTpool	Thermo	#M-018311-00-0003
Target Sequence siRNA#1:	ACACAGCAACCUAUUCUUA	
Target Sequence siRNA#2:	GGUCUCAGAACAUGUAUUU	
Target Sequence siRNA#3:	CUGCAGAACCUCAUUGAUU	
Target Sequence siRNA#4:	UGUCUACGCUCGGCUAAUG	
Tspan4 Pool	Thermo	#L-010625-02-0005
Tspan4 siRNA#1	Thermo	#J-010625-17
Tspan4 siRNA#2	Thermo	#J-010625-18
Tspan4 siRNA#3	Thermo	#J-010625-19
Tspan4 siRNA#4	Thermo	#J-010625-20
Tspan8 Pool	Thermo	#L-010219-02-0005
Tspan8 siRNA#1	Thermo	#J-010219-05
Tspan8 siRNA#2	Thermo	#J-010219-06
Tspan8 siRNA#3	Thermo	#J-010219-07
Tspan8 siRNA#4	Thermo	#J-010219-08
Tspan13 Pool	Thermo	#L-012516-02-0005
Tspan13 siRNA1	Thermo	#J-012516-17
Tspan13 siRNA2	Thermo	#J-012516-18
Tspan13 siRNA3	Thermo	#J-012516-19
Tspan13 siRNA4	Thermo	#J-012516-20
Tspan15 Pool	Thermo	#L-017265-02-0005
Tspan15 siRNA1	Thermo	#J-017265-17
Tspan15 siRNA2	Thermo	#J-017265-18
Tspan15 siRNA3	Thermo	#J-017265-19
Tspan15 siRNA4	Thermo	#J-017265-20

4.6 Lysis buffers and other buffers

Lysis buffer 1 (Birgit Bossenmaier)	50 mM Hepes, pH 7.5, 150 mM NaCl, 1.5 mM $MgCl_2$, 100 mM NaF, 10 mM NaPyrophosphate, 1 mM EGTA, 10 % Glycerol, 1 % Triton X-100
Lysis buffer 2 (Birgit Bossenmaier)	50 mM Hepes, pH 7.5, 150 mM NaCl, 1.5 mM $MgCl_2$, 100 mM NaF, 10 mM NaPyrophosphate, 1 mM EGTA, 10 % Glycerol, 1 % Triton X-100, 10 µg/mL Aprotinin, 1 mM PMSF, 1 mM Na-Orthovanadate
Lysis buffer 3 (Diana Weininger)	50 mM Tris-Cl, pH 7.5, 150 mM NaCl, 1 % NP40, 0.5 % DOC, 10 µg/mL Aprotinin, 0.5 mM PMSF, 1 mM Na-Orthovanadate
Lysis buffer 4 (ELISA)	10 mM Tris-Cl, pH 7.5, 100 mM NaCl, 1 mM EDTA, 1 mM EGTA, 1 % Triton X-100, 10 % Glycerin, 0.1 % SDS, 0.5 % DOC, 1 mM PMSF, 1 mM NaF, 2 mM Na-Orthovanadate, 10 µg/mL aprotinin
NET buffer	10 mM Tris-Cl, 100 mM NaCl, 25 mM EDTA Final pH 8.0
RIPA buffer	50 mM Tris-Cl, pH8.0, 150 mM NaCl, 1 % Igepal CA-630, 0.5 % deoxycholate (DOC), 0.1 % SDS

4.7 Commercial available Kits

Alexa Fluor® 647 Antibody Labeling Kit	Ivitrogen
Ama® cell line Nucleofector® kit	Lonza
Annexin-V-FLUOS Staining kit	Roche
ApoTox-Glo ™	Promega
Caspase-Glo® 3/7 assay	Promega
Cell proliferation ELISA, BrdU	Roche
CellTiter-Glo	Promega
Cy5 antibody Labeling Kit	Amersham
Cy5 FluoroLink Ab Labelling Kit	Pharmacia Biotech
Cy5 mAb Labelling Kit	GE Healthcare
DyLight 650 Antibody Labeling Kit	Pierce
Gel extraction kit	Qiagen
HiSpeed Plasmid Maxi Kit	Qiagen
Luciferase Reporter gene Assay	Roche
Micro BCA™ Protein Assay Kit	Pierce
N-Glycosidase F Deglycosylation Kit	Roche
Nuclear extraction kit	Active Motif
PCR purification kit	Qiagen
Quick change II mutagenesis kit	Stratagene
Rapid DNA Ligation Kit	Roche

Rapid DNA Dephosphorylation and Ligation Kit	Roche
RNase-Free DNase Set	Qiagen
RNeasy Mini Kit	Qiagen
Steady-Glo	Promega
Steady-Glo® Luciferase Assay System	Promega
Transcriptor First Strand cDNA Synthesis Kit	Roche

5 Methods

5.1 Basic cell culture

A431, A549, BxPc3, HCT116, Hs746T, MDA-MB-175 VII, NCI-H1993, NCI-H322M, NCI-H441, SNU-5 and T47D were obtained from ATCC (Manassas, VA, USA). DU145 and HT29 were obtained from the NCI (Bethesda, MD, USA). NCI-H596 from Chugai Pharmaceuticals Co., Ltd. and MKN45 were purchased from the DSMZ (Leipzig, Germany). All cell lines were supplemented with 10 % fetal calf serum (FCS), 2 mM L-glutamine (Gibco) and non-essential amino acids (Pan Biotech) unless stated otherwise. NCI-H596 were maintained in RPMI high glucose, supplemented with L-glutamine, 1 mM sodium pyruvate, 10 mM HEPES (Pan Biotech) and 10 % FCS. A431, A549, A549-B34, BxPc3, DU145, HCT116, NCI-H1993, NCI-H322M, NCI-H441, NCI-H596, and HT29 were maintained in RPMI 1640 medium. The cell line A549-B34 is genetically altered and overexpresses the HER3 receptor and was kindly provided by Dr. Birgit Bossenmaier (Mirschberger et al., 2013). For MKN45, RPMI 1640 medium containing 20 % FCS was used. SNU-5 cells were maintained in Iscove's modified Dulbecco's media supplemented with 15 % FCS. Hs746T cells were maintained in Dulbecco's modified Eagle's medium (DMEM) high glucose and T47D in RPMI high glucose medium. For MDA-MB-175 VII DMEM:F12 medium containing 10 % FCS was used. The following table summarizes the main cell cultures were used for this work and their respective culturing conditions and properties.

Cell Line	Tissue origin	Status	Origin	Medium	Reference
A431	skin	carcinoma	ATCC	RPMI1640, 10 % FCS	(Faust & Meeker, 1992)
A549	lung	carcinoma	ATCC	RPMI1640, 10 % FCS	(Giard et al., 1973)
A549-B34	lung	carcinoma	Roche	RPMI1640, 10 % FCS, 500 µg/ml G418	(Mirschberger et al., 2013)
BcPx3	pancreas	adenocarcinoma	ATCC	RPMI1640, 10 % FCS	(Loor, Nowak, Manzo, Douglass, & Chu, 1982)
Du145	prostate	carcinoma	NCI	RPMI1640, 10 % FCS	(Papsidero et al., 1981)
H1993	lung	adenocarcinoma	ATCC	RPMI1640, 10 % FCS	(Phelps et al., 1996)
H441	lung	adenocarcinoma	ATCC	RPMI1640, 10 % FCS	(Bepler et al., 1989)
HCT116	intestine	adenocarcinoma	ATCC	RPMI1640, 10 % FCS	(Schroy, III et al., 1995)
Hek293	kidney	normal	ATCC	Eagle`sMEM with Earle`s BSS, 10 % FCS	(Graham, Smiley, Russell, & Nairn, 1977)
Hs746T	gastric	adenocarcinoma	ATCC	DMEM high glucose, 10 % FCS	(Smith, 1979)
HT29	colon	adenocarcinoma	NCI	RPMI1640, 10 % FCS	(Didier et al., 1996)
MDA-MB175	breast	carcinoma	ATCC	DMEM:F12, 10 % FCS	(Siciliano, Barker, & Cailleau, 1979)
MKN45	gastric	adenocarcinoma	DSMZ	RPMI1640, 20 % FCS	(Koga, Aoyagi, Imaizumi, Miyagi, & Shirouzu, 2011)
NCI-H322M	lung	carcinoma	ATCC	RPMI1640, 10 % FCS	(Gazdar et al., 1990)
NCI-H596	lung	carcinoma	Kamakura	RPMI high glucose, 10 % FCS	(Takahashi et al., 1989)
SNU-5	gastric	carcinoma	ATCC	IMDM, 15 % FCS	(Park et al., 1987)
T47D	breast	carcinoma	ATCC	RPMI 1640 High Glucose, 10 % FCS	(Judge & Chatterton, Jr., 1983)

Cell lines were maintained at 37 °C in a 5 % CO_2-gassed atmosphere. Briefly, cells growing in suspension were sub-cultured upon reaching a concentration of approximately $1x10^6$ cells/mL and cultured between $1x10^5$ and $1x10^6$ cells/mL. Adherent cells were grown to confluency. For sub-culturing the medium was removed and cells were treated with 2 mL Accutase ® (Sigma). After cell detachment, fresh medium was added and cells were dispensed into new culture flasks.

Long term storage was performed by resuspending $1x10^6$ - $5x10^6$ cells in 90 % FCS with 10 % DMSO. All reagents and storage vessels were cooled down do 4 °C and the freezing procedure was carried out on ice. Cells were frozen overnight at –80 °C in isopropanol containing freezing boxes (Nalgene). Finally the cells were transferred into liquid nitrogen.

5.2 FACS-based receptor quantitation

5.2.1 General procedure of FACS-based receptor quantitation

Cell surface receptors were quantified using fluorophore-labelled bispecific antibodies as detection antibodies in combination with Quantum MESF beads (Bangs Laboratories) as calibration tool. The fluorescence intensities of bound bispecific antibodies were quantified via Quantum MESF beads leading to the corresponding MESF units and the number of absolute cell surface molecules was then calculated via the known F/P ratio of the labelled bispecific antibodies.

In detail, cell lines growing in the logarithmic phase were harvested by the use of Accutase ® (Sigma Aldrich) at the respective experimental time points. Based on our findings, similar culturing periods were essential to deliver significant data. Cells were counted and 2×10^5 cells were dispersed in duplicates into v-bottom 96-MTP wells (Nunc). After centrifugation, a washing step with ice-cold PBS (Gibco) containing 2 % FCS was performed on ice. In the meantime, detection antibodies were coupled to Dig-Cy5 in a 1:1.2 or 1:2.4 molar ratio in PBS (2 % FCS) (see following tables) and incubated for 10 min in the dark at room temperature.

Molar ratio calculation table 1:

	Ratio conjugate:Ab	M Ab [g/mol]	C Ab [mg/mL]	M conjugate [g/mol]	C conjugate [mg/mL]	V Ab:Conjugate
IgG-Dig	2.4	150,000	3.00	1,167.55	0.5	8.92
Met1v1	1.2	126,509	1.01	1,167.55	0.5	44.70
Met2v2	2.4	201,211	0.56	1,167.55	0.5	64.11
MetFab1v1	1.2	75,822	1.27	1,167.55	0.5	21.31
Her2Fab1v1	1.2	75,266	3.16	1,167.55	0.5	8.50
Her2Fab1v2	2.4	102,526	1.85	1,167.55	0.5	9.89
Her3Fab1v1	1.2	75,818	1.34	1,167.55	0.5	20.19

Master mix calculation table 2:

	Concentration [mg/mL]	Final concentration Ab [µg/mL]	20 µg/mL Ab = Vol Ab [µL]	Volume [µL]	+ Volume conjugate Dig (1:10 prediluted) [µL]	+ Volume buffer [µL]
IgG-Dig	3.00	20	5.3	800	6.0	789
Met1v1	1.01	20	15.8	800	3.5	781
Met2v2	0.56	20	28.6	800	4.5	767
MetFab1v1	1.27	20	12.6	800	5.9	781
Her2Fab1v1	3.16	20	5.1	800	6.0	789
Her2Fab1v2	1.85	20	8.6	800	8.7	783
Her3Fab1v1	1.34	20	11.9	800	5.9	782

Fifty µL of Dig-Cy5 coupled antibodies were added to the cells, thoroughly resuspended and incubated on ice in the dark. After 45 min of incubation the cell suspension was washed three times with ice-cold PBS (2 % FCS) and spun down at 300× g for 5 min. Samples were resuspended in 200 µL fixation buffer (1× BD CellFix) and subjected to flow cytometric analysis (BD, FACS Canto). Data acquisition comprised of SSC-A, forward scatter (FSC)-A, FSC-W and Cy5 channel. FSC threshold for events was set between 10,000 and 12,000. Photomultiplier tube (PMT) for Cy5 channel was kept constant at 446. Overall, 10,000 events of the desired and gated populations were recorded. HTS unit settings were: 100–150 µL sample, flow rate 2 µL/s, mixing volume 80–100 µL, mixing five times with a speed of 200 µL/s and a washing step with 200–600 µL. Data analysis was performed with FlowJo (Tree Star) and XLfit (IDBS).

5.2.2 MESF reference standard and MESF calibration beads

To facilitate cell surface receptor quantitation from low to high receptor numbers a unified window of analysis (UWA) was defined. Cell lines with different cMET receptor expression level (none, low, intermediate, high) were subjected to receptor quantitation and fluorescence settings were adjusted in a way that all fluorophore intensities, corresponding to the respective receptor levels, could be analyzed under such conditions. To define a UWA, the Cy5 Reference Standard (Bangs Laboratories) was analyzed under the pre-defined target fluorescence settings and median fluorescence intensity was recorded. The Reference Standard was used to adjust fluorescence settings according to the pre-defined median value upon using other FACS machines or after FACS maintenance for example. Cell samples and Quantum MESF beads (Bangs Laboratories) were

measured at the same day, in the same buffer and at equal fluorescence settings according to the UWA. Adjustments of FCS/SSC were performed to optimize sample analysis without altering the Cy5 channel. The Quantum Cy5 MESF Kit (Bangs Laboratories) is comprised of five bead populations of calibrated fluorescent standards: 4 bead populations with different and defined levels of Cy5 fluorescence intensities and one blank population. The recorded Cy5 median values were entered in the QuickCal template version (FACSDivaScale). The resulting calibration curve associated fluorescence median values to standardized fluorescence intensity units (MESF) and allowed the assignment of MESF values to labeled cell samples. Calculation of the blank population into MESF units led to the detection threshold.

MFI values were translated into MESF values by the use of Cy5 MESF Calibration Beads (Bangs Laboratories). One drop of each bead population was added into 500 µL 1× Cell Fix (BD) in PBS containing 2 % FCS and mixed thoroughly. The same procedure was applied for Cy5 MESF blank control. The use of a Cy5 reference standard (Bangs Laboratories) guaranteed similar flow cytometric conditions between experiments and was used to calibrate the FACS Canto prior use (UWA). For this purpose, MESF calibration beads and MESF reference standard were measured at the same PMT settings as the subsequently analyzed cells. The PMT for the Cy5 channel was kept at 446. Overall, 5,000 events of the desired and gated populations were recorded. HTS unit settings were: 100–150 µL sample, flow rate 2 µL/s, mixing volume 80–100 µL, mixing five times with a speed of 200 µL/s and a washing step of 200–600 µL. Data analysis was performed with FlowJo (Tree Star) and XLfit (IDBS).

5.2.3 Simple cellular beads (SCB)

To determine the F/P ratio of a detection antibody consisting of an unknown amount of fluorophores, the following method was applied. Simple cellular anti-human IgG beads have a defined ABC value and thus a defined amount of Fc binding sites for human IgG. After bead saturation by detection antibodies, the fluorescence intensities were recorded and calculated into the corresponding MESF units via MESF Quantum beads (Bangs Laboratories). By dividing the obtained MESF value with the ABC value, the effective F/P ratio of the analyzed detection antibody was determined.

In detail, to 100 µL of a BsAb-Dig-Cy5 solution at a concentration between 10 to 100 µg/mL, one drop of simple cellular® anti-human IgG beads was added and incubated for 30 min on ice in the

dark. Samples were then washed twice with 2 mL ice-cold PBS (2 % FCS) and centrifuged at 300× g for 5 min. For flow cytometric analysis (BD, FACS Canto), 500 µL of ice-cold PBS (2 % FCS) was added to the samples which were then analyzed in the SSC-A, FSC-A, FSC-W and Cy5 channel. HTS unit settings were: 100–150 µL sample, flow rate 2 µL/s, mixing volume 80–100 µL, mixing five times with a speed of 200 µL/s and a washing step of 200–600 µL. In total, 10,000 events were recorded, exported as FCS 3.0 files and data analysis was performed with FlowJo (Tree Star) and XLfit (IDBS).

5.2.4 Receptor quantitation with QuantiBRITE

To evaluate PE-labeled HER3 mAb (R&D Systems) the QuantiBRITE™ PE fluorescence quantitation kit was applied. It contains lyophilized pellets of four bead populations which are conjugated with different amounts of PE molecules. The beads were resuspended in 500 µL PBS (2 %FCS, 1× BD Fix) and analyzed by flow cytometry. HTS unit settings were: 100–150 µL sample, flow rate 2 µL/s, mixing volume 80–100 µL, mixing five times with a speed of 200 µL/s and a washing step of 200–600 µL. Singlets were gated in the SSC and FSC plot and the resulting PE levels used to determine the ABC of an unknown cell population.

5.2.5 Labeling of antibodies with Cy5

Parental Met1v1 and Met2v2 antibodies were covalently labelled with Cy5 by the use of Cy5 mAb Labeling Kit (GE Healthcare). In brief, antibodies were equilibrated in PBS (pH 7.3) at 1 mg/mL. 100 µg of antibody was conjugated according to the manufacturer's instructions for 30 min at room temperature. Free dye was separated from conjugated antibodies by size-exclusion chromatography. Cy5-labeled antibodies were stored light protected at 2–8 °C.

5.2.6 mRNA expression profiling

Total RNA was isolated from cells using the RNeasy Mini Kit (Qiagen). From this material, cDNA synthesis was performed using a cDNA synthesis kit (Roche). The resulting double-stranded cDNA was purified with a Microarray Target Purification Kit (T7) (Roche). Purified cDNA was then transcribed into cRNA using the Roche Microarray RNA Target Synthesis Kit (T7) (Roche Applied Science) and further purified with RNeasy Mini-Spin Columns (RNeasy Mini Kit). All kit procedures were performed according to the manufacturers instructions. Twenty µg of the purified cRNA were fragmented in a total volume of 40 µL (adjusted with diethylpyrocarbonate-water)

using 8 µL of 5× fragmentation buffer (200 mM Tris-acetate, pH 8.1; 500 mM potassium acetate and 150 mM magnesium acetate) at 94 °C for 35 min. Thirty µL of fragmented cRNA solution were mixed with control oligonucleotide, staggered control cRNAs, herring sperm DNA, acetylated BSA and hybridization buffer in a total volume of 300 µL. This hybridization mix was loaded onto Affymetrix Human Genome U133 Plus 2.0 arrays and incubated in a roller device for 16 hours. Hybridization solution was removed, the arrays were washed and stained as recommended by Affymetrix and then scanned with an Affymetrix GeneChip Scanner 3000 (7G). For the cell line H1993 a slightly modified protocol (L8) was used. Here, after total RNA isolation with the RNeasy Kit double-stranded cDNA was generated, transcribed into biotinylated aRNA and then purified using the GeneChip 3´ IVT Express Kit (Affymetrix). All samples were measured in triplicates and analyzed using in-house software.

5.2.7 Quantitative confocal immunofluorescence analysis of bispecific antibodies

Cells were grown on calibrated glass coverslips to a confluency of 80 %. Subsequently, cells were incubated with 10 µg/mL of BsAb/Dig-Cy5 complex for 60 min at either 4 or 37 °C, washed, fixed and immediately imaged on a Leica SP5X confocal microscope using hybrid detectors (HyD) in photon counting mode. Imaging conditions were as follows: 63×/1.2 NA water immersion lens, white light laser excitation at 649 nm at 25 % laser intensity, emission band pass at 656–758 nm, HyD setting at 100 %, Pinhole AU = 1.2 corresponding to an optical section thickness of 1.062 µm, pixel size 72.9 nm and 12 bit resolution. For quantification, solutions with defined concentrations of Cy5 were measured and a calibration curve was established. Measured gray levels were then translated into a pseudocolor intensity map and absolute concentrations of Cy5, respectively, which were then assigned to the labelled cells.

5.2.8 Antibody construction, expression and purification

To generate cell surface detection antibodies (Met1v1, Met2v2, MetFab1v1, Her2Fab1v1, Her2Fab1v2, Her3Fab1v1) variable HC regions were ordered as gene synthesis containing a Kozak sequence and leader peptide with flanking 5′ BamHI and 3′ KpnI sites. The sequences were derived from available patents (HER2: US5772997; HER3: WO2011076683; cMET: US2007/0092520; Dig scFv: WO2011/003557). The KpnI site was located in the C_H1 domain of the human IgG1 CS. The LCs were ordered as complete cds in form of a gene synthesis with 5′ BamHI and 3′ XbaI sites. The scFv anti-Dig fusion construct was ordered in the order of variable HC, linker, followed by

variable LC and contained an additional disulfide bridge (VHCys44 and VLCys100) (Jung et al., 1994). The scFv construct was cloned as described previously (Metz et al., 2011). For Met2v2, one HC and one LC plasmid were prepared. With respect to Met1v1, two different HCs and one LC plasmid were prepared. The two HC plasmids contained the kih mutation T366W (knob) and T366S, L368A and Y407V (hole) in the C_H3 domain of the human IgG1 backbone as previously published (Merchant et al., 1998; Ridgway et al., 1996). An additional disulfide bond was engineered into the C_H3 domains of the two HCs: S354C (knob) and Y349C (hole) (Merchant et al., 1998; Ridgway et al., 1996). For MetFab1v1, a LC and one HC consisting of VH-C_H1 coupled to scFv were constructed. The resulting Fab-scFv construct has been described previously (Lu et al., 2002).

Antibody expression and purification was performed as following. First, antibody chains were co-transfected in HEK293F cells (Invitrogen) as previously described (Metz et al., 2011). After 7 days of incubation, cell culture supernatants were harvested and filtered through a 0.22 mm Millipore Express PLUS PES membrane (Millipore). Antibodies with Fc part were bound to a protein A Sepharose column (GE Healthcare) and washed with phosphate-buffered saline (PBS) (Gibco). Antibodies without Fc part were applied to a Kappa-Select column (GE Healthcare) and similarly washed with PBS. Elution of antibodies was achieved at pH 3.0 for protein A and at pH 2.5 for Kappa-Select. If required, further purification by size-exclusion chromatography was performed as described (Metz et al., 2011). The protein concentration of purified antibodies was determined by measuring the OD at 280 nm, using a molar extinction coefficient calculated according to Pace and colleagues (Pace, Vajdos, Fee, Grimsley, & Gray, 1995).

5.3 Protein analysis

5.3.1 Whole cell extract preparation from eukaryotic cells

Cell cultures were rinsed at least two times with pre-warmed PBS and treated with 2 mL of Accutase ® (Sigma). Depending on the degree of attachment, cells were incubated 5 to 15 min at 37 °C. Afterwards, cells were harvested and spun for 5 min at 300 g, resuspended in ice-cold PBS and again spun down to remove residual growth medium and PBS. Approximately $1x10^7$ cells were resuspended in 800 µL lysis buffer (buffer composition was dependent on the experiment. See 4.6) which was supplemented with 0.5 mM PMSF, 1 x protease inhibitor mix, 1 mM NaF and 40 mM sodium orthovanadate. The amount of buffer was adjusted depending on the number and type of

cells. Subsequent steps were performed on ice. The cell suspension was then incubated for 15 min at 4 °C and inverted several times. Cell debris was spun down for 15 min at 14,000 g at 4 °C and protein concentration was determined by Bradford or BCA. Usually, 50 µg of total protein extract was used for immunoblot analysis.

5.3.2 SDS-PAGE and Immunoblot

After cell harvesting (chapter 5.3.1), 10 µL of lysate was used for protein concentration determination (chapter 5.3.3). For standard applications 50 µg of total protein lysate was used. The amount of cell lysate was adjusted and sample buffer (Invitrogen), sample reducing agent (Invitrogen) and water calculated to the same volume and mixed on ice. The samples were then heated up to 70 °C for 10 min and collected by a quickspin. Afterwards, samples and 5 µL of protein standard (Biorad; Invitrogen) were loaded onto a 1-1.5 mm NuPAGE Bis-Tris gradient gel (4-12 %) (Invitrogen) with 1x MOPS buffer (Invitrogen). Fivehundred µL of antioxidant (Invitrogen) was added into the cathode part of the chamber. Samples resolved at 200 V for approximately 50 min. Next to the run, the samples were either transferred by wet blot or semi-dry blot onto nitrocellulose or PVDF membranes (Invitrogen). PVDF membranes were previously activated in methanol. To pre-incubate the gel, an equilibration buffer was mixed as follows:

- 2x NuPage buffer (Invitrogen)
- 10 % methanol
- 1:1000 antioxidant

The gel was pre-equilibrated for 20 min in 100 mL equilibration buffer under mild agitation and then transferred into the iBlot (Invitrogen) using program 2 for 6 min. All steps were carried out according the iBlot manual. Afterwards the membrane was either dried, stored in TBS-T or PBS-T until development.

For immunoblotting the membrane was incubated at least for 2 hours in 5 % BSA (Roche) TBS-T. Afterwards three washing steps for 10 min in TBS-T followed under mild agitation. The primary antibody was added and incubated between 4 hours and 3 days according to experimental settings and antibody properties. Usually, an overnight incubation period at 4 °C followed. Primary antibodies were diluted in 1-5 % milk (Roche) or BSA (Roche) in the case of phosphorylation-detecting antibodies. Three 10 min washing steps in TBS-T followed under mild agitation. The secondary antibody was added in 1 % BSA or milk TBS-T and incubated for 1 hour at RT. Another

3 x 10 min washing step was performed. At last, the membrane was dried and covered with developing reagent. Following reagents were used:

- Highest sensitivity SuperSignal West Pico (Pierce)
- High sensitivity Lumi-LightPLUS Western Blotting Substrate (Roche)
- Medium sensitivity Pierce ECL-Western Blotting Substrate (Pierce)
- Low sensitivity Amersham ECL Western Blotting (GE Healthcare)

Visualization was carried out under the Roche Lumi-Imager Workstation (Roche).

5.3.3 BCA protein assay

To determine an unknown protein concentration of a sample 100 µL of the BCA standards (0, 5-200 µg/mL) (Thermo Scientific) were pipetted as duplicates into a 96-well plate (Corning). The protein sample was diluted 1:50 – 1:100 in water ad 100 µL and added in duplicates into a 96-well. Afterwards, 100 µL of BCA reagent (25 MA: 24 MB: 1MC) (Thermo Scientific) was pipetted into all wells and mixed thoroughly. The 96-well plate was covered with an adhesive aluminum foil and incubated at 37 °C for 2 hours. Finally the absorbance was measured in a TECAN infinite reader (Tecan) at 562 nm.

5.3.4 Protein Expression and Purification - Transfection

Small scale test expressions were performed with 30 mL of 0.5 x 10^6 FreeStyleTM 293-F (HEK293F, Invitrogen) cells/mL and seeded one day prior transfection. For transfection, plasmid DNA (30 µg DNA/mL culture volume) was mixed with 1.2 mL Opti-MEM® I Reduced Serum Medium (Invitrogen) and further resuspended with 40 µL of 293FectinTM Transfection Reagent (Invitrogen). The mixture was incubated for 15 min at RT and added drop wise to the cells. Twenty-four hours post transfection, culturing flasks were fed with 300 µL 200 mM L-Glutamine (Sigma-Aldrich) and 600 µL of Feed7 (see below for composition). Seventy-two hours post-transfection the cell concentration, cell viability and glucose concentration in the medium was determined using an automated cell viability analyzer (Vi-CELLTM XR, Beckman Coulter) and a glucose meter (Accu-CHEK® Sensor comfort, Roche). In addition, the flasks were fed with 300 µL of L-glutamine, 300 µL non-essential amino acids solution (PAN^{TM} Biotech), 300 µL 100 mM sodium pyruvate (Gibco, Invitrogen), 1.2 mL Feed7 and ad 5 g/L glucose D-(+)-Glucose solution 45 % (Sigma). Six days post-transfection, antibodies were harvested by centrifugation at 3500 rpm in a X3R Multifuge (Heraeus) for 15 min. The supernatant was sterile filtered through a Steriflip filter

unit of 0.22 mm Millipore Express PLUS PES membrane, (Millipore) and stored at -20 °C until further use or at -80 °C for long term storage.

Composition of 1 L feed7:

- L-Asparagine 2 g (Gibco, Sigma)
- HyPep 1510 (Sojapepton) 30 g
- Ammonium-Fe(III)-Citrate 85.5 mg
- Ethanolamine reinst 0.3 mL
- T044 0.3 mL
- D-Glucose 6.5 g (Sigma)
- FreeStyle Medium ad 1 L (Invitrogen)

5.3.5 Protein Expression and Purification - Protein Quantification

Proteins were quantified by affinity chromatography using the automated Ultimate 3000 system (Dionex) with a pre-packed Poros® A protein A column (Applied Biosystems). All samples were loaded in buffer A (0.2M Na_2HPO_4, [$2H_2O$] at pH 7.4) and eluted in buffer B (0.1M citric acid, 0.2M NaCl at pH 2.5). To determine protein concentration an extinction coefficient of 1.62 was used for all samples.

5.3.6 Protein Expression and Purification – Immuno-precipitation

Immunoprecipitation was performed with 30 µg of protein which was diluted in PBS supplemented with 5 % Tween®20 (PBS-T at a pH 7.4) (Fluka Analytical) at an equal reaction volume for all samples. 126 µL Dynabeads® Protein A consisting of 0.24 µg human IgG per µL Dynabeads® binding capacity (Invitrogen), were added and the solution was incubated for 90 to 120 min at RT and 20 rpm to allow binding of human IgG Fc to protein A being linked to magnetic beads. The total reaction volume was 1.4 mL. Next, the beads were washed three times with 1 mL PBS-T, centrifuged for 30 seconds at 400 x g to collect the solution at the bottom of the tube. The supernatant was discarded and Dynabeads® were incubated with 30 µL of 100 mM citrate at pH 3 (Citric acid monohydrate) (Sigma) to elute the proteins. Afterwards the solution was neutralized with 3µL of 2M Tris at pH 9 (Fisher Scientific).

5.3.7 Protein analysis - Reducing and Non-Reducing SDS-PAGE

In total, 7 µL of the previously eluted proteins were mixed with 2 x NuPAGE® LDS Sample buffer (Invitrogen) and another 7 µL was mixed with 2 x sample buffer containing 10 % NuPAGE®

Sample Reducing Agent (Invitrogen). Samples were heated to 70 °C for 10 min and loaded onto a pre-cast NuPAGE® 4- 12 % BisTris Gel (Invitrogen). The gel was run for 45 min at 200 V and 125 mA. Afterwards the gel was washed three times with Millipore water and stained with SimplyBlueTM SafeStain (Invitrogen) for 2-10 min. The gel was de-stained overnight in Millipore water.

5.3.8 Protein analysis - Analytical HPLC

Proteins were analyzed using the Agilent HPLC (High-Performance Liquid Chromatography) 1100 (Agilent Technologies) with a TSK-GEL G3000SW gel filtration column with 7.5 mm ID x 30 cm (TosoHaas Corp.). For this, 18 µL of the eluted proteins were loaded onto the column in Buffer A (0.05 M K_2HPO_4/KH_2PO_4 in 300 mM NaCl, pH 7.5) and separated based on size.

Next, reducing and non-reducing SDS-PAGE was performed where 7 µL of the eluted proteins was mixed with 2 x NuPAGE® LDS Sample buffer (Invitrogen). Simultaneously another 7 µL was mixed with 2 x sample buffer containing 10 % NuPAGE® Sample Reducing Agent (Invitrogen). Samples were heated to 70 ° for 10 min and loaded onto a pre-cast NuPAGE® 4- 12 % BisTris Gel (Invitrogen). The gel was run for approximately 45 min at 200V and 125 mA. Afterwards the gel was washed three times with Millipore water and stained with SimplyBlueTM SafeStain (Invitrogen). Finally the gel was de-stained overnight in Millipore water and imaged.

5.4 RT-PCR analysis

The reverse transcription polymerase chain reaction (RT-PCR) is based on PCR which is used to amplify and simultaneously quantify targeted DNA molecules. This technique allows the detection and quantification of specific sequences in a DNA sample. The first step to quantify gene expression of small amounts of RNA is to amplify the gene transcript. Therefore RNA samples were first reverse transcribed into cDNA via the enzyme reverse transcriptase.

5.4.1 RNA Isolation:

For RNA isolation the RNeasy kit (Qiagen) was used according to the manufactures instructions. Small cell pellets consisting of 5-10 x 10^6 cells were mixed with 700 µL of RLTM buffer containing 1 % ß-Mercaptoethanol (Gibco). Samples were then homogenized transferring them into QIAshredder tubes (Qiagen) followed by a 2 min centrifugation step. To purify RNA, samples

were washed with 600 µL 70 % ethanol in an RNeasy spin column (Qiagen) and centrifuged for 15 seconds at 8,000 x g. The flow-through was discarded and 700 µL of RW1 buffer (Qiagen) was added into the column and centrifuged for 15 seconds at 8,000 x g. This washing step was performed twice. After discarding the flow-through 500 µL of RPE buffer (Qiagen) was pipetted into the RNeasy spin column and centrifuged for 15 seconds at 8,000 x g. This step was repeated with 400 µL RPE buffer and a 2 min centrifugation step at 10,000 x g. Finally, purified RNA was eluted by adding 40 µL RNase free water (Qiagen) on top of the column followed by a 1 min centrifugation at 8,000 x g. At this point it was possible to store the samples at -80 °C.

5.4.2 cDNA synthesis and RT-PCR

For cDNA generation the Transcriptor First Strand cDNA Synthesis Kit (Roche) was used according to the manufactures instructions. The annealing step was performed with 1 µL oligo(dT)18 primer and 1 µg RNA filled up to 13 µL with RNase free water (Qiagen). Samples were then incubated at 65 °C for 10 min. cDNA synthesis was achieved by adding 7 µL of master mix solution (Roche) to the sample. The master mix contained:

- 4 µL 5x RT buffer
- 0.5 µL Protector
- 2 µL dNTP-Mix
- 0.5 µL RT-Enzyme

The PCR program was set to:

- 55 °C for 30 min
- 85 °C for 5 min
- Cool down to 4 °C

For long term storage it was possible to stop at this step and freeze the sample to -80 °C. The master mix was then prepared for the RT-PCR reaction with the LightCycler 480 Probes Master kit (Roche) and previously selected Universal Probe Library (Roche) primers and probes. All steps were performed on ice and the master mix consisted of:

- 7.5 µL Roche water
- 10 µL Roche Master Mix
- 0.5 µL Primer Reverse (50 pmol)
- 0.5 µL Primer Forward (50 pmol)
- 0.5 µL Primer Probe

- 0.5 µL Probe
- 1 µL cDNA

After mixing all components the master mix was pipetted into a 96 well RT-PCR plate (Roche) and sealed by LightCycler 480 Sealing Foil (Roche). Finally the 96 plate was quick-spinned for 20 seconds and placed into the Light Cycler 480 II (Roche).

The Light Cycler 480 II settings were:

- 10 min 95 °C
- 40 Cycles a 10 seconds 95 °C plus 1 min 60 °C

5.5 Cellular based assays

5.5.1 Proliferation assay

The Promega cell viability assay represents one method to indirectly determine the amount of viable cells on the basis of ATP release after cell lysis. Viable and metabolic active cells contain ATP and due to the luciferase reaction it is possible to determine the proportionate ATP level. The enzyme Luciferase catalyzes luciferin in the presence of Mg^{2+}, O_2 and ATP to Oxyluciferin. The ATP level and therefore the resulting luminescence is proportional to the viability of analyzed cells treated in this work by siRNA, therapeutic antibodies or other agents.

CellTiter-Glo Buffer (Promega) and lyophilized CellTiter-Glo Substrate (Promega) was equilibrated to RT prior use and mixed in a 1:1 ratio. The growth medium of the cells in 96-well plates was replaced with fresh RPMI/DMEM and equilibrated to RT for approximately 30 min to prevent background. Next, 100 µL of the combined CellTiter-Glo reagent was added on top of the 100 µL medium of each well. The plate was shaken at 300 rpm for 2 min on an orbital shaker to induce cell lysis and stabilize the luminescent signal. An incubation period of 10 min at RT followed. Before analysis, the CellTiter-Glo-medium mix was transferred into an opaque 96-well (Sigma) and luminescence quantified using a 96-well plate reader (Infinate 200 Pro, Tecan) with an integration time of 0.25-1 seconds/well. Incubation periods and the amount of cells per 96-well varied between the analyzed cell lines (1,000 to 15,000 cells) and had to be adjusted according to the experimental set-up. Luminescence was then recorded via a 96-well plate reader (Infinate 200 Pro, Tecan).

5.5.2 Apoptosis assay

The respective cell lines were seeded at 1,000 to 10,000 cells per 96-well plate for 24 hours at 37 °C in a 5 % CO_2-gassed atmosphere before treatment. Cells were treated with therapeutic antibodies at a 0.2 µM concentration and pre-incubated for 15 min. Apoptosis was evaluated using a Caspase 3/7 luminescent assay (Promega) after two days of incubation according to the manufacturer's instructions. Ten µM Staurosporin was added 3 hours before readout as positive control and unspecific huIgG was used as negative control.

5.5.3 Poly-HEMA 3D culture

This assay was performed to facilitate 3D mammalian cell cultures. Basically, the Poly-2-hydroxyethylmethacrylate (HEMA) layer prevents cell attachment and thus forcing 3D clustering. In the first step a Poly-HEMA (Polysciences Inc.) master mix was prepared to cover 96-well cell culture plates by mixing following components:

- 4.2 mL Poly-HEMA stock solution (Polysciences Inc.)
- 5.0 mL ddH_2O sterile filtered
- 90.8 mL absolute ethanol

Each well was then covered with 100 µL of the master mix (for a 6-well plate 3 mL) and dried over a 3-5 days incubation period at 37 °C. Finally, the Poly-HEMA covered plates were used similar as standard cell culture plates.

5.5.4 Collagen 3D culture

Covering a cell culture plate with collagen represents another method to facilitate 3D cell cultures, besides Poly-HEMA coating. For this, a vial of lyophilized Collagen (Roche) was dissolved with 5 mL sterile 0.2 % acetic acid (v/v) yielding a final concentration of 2 mg/mL. To cover 6-well plates a 1:50 dilution was performed by mixing 25 µL of the stock solution with 975 µL PBS (Gibco) resulting in a final concentration of 50 µg/mL Collagen and thus 50 µg Collagen per 6-well. The Collagen solution was carefully spread and air dried for 2-3 hours at RT under laminar flow to prevent contaminations. In the last step the plates were carefully washed with 1 mL PBS (Gibco) and ready for use.

5.5.5 Fibronectin covered culture vessels

Cell culture plates were covered with fibronectin to promote 3D cell growth in cell culture experiments. For this, Fibronectin (Roche) was dissolved in 5 mL sterile water for 60 min at 37 °C yielding a concentration of 1 mg/mL. The stock solution was then diluted to 50 µg/mL and 100 µL added into 96-wells corresponding to 2 µg Fibronectin per well. The plates were incubated at 37 °C for 1 hour, remaining solution was removed by PBS (Gibco) and the Fibronectin covered plates were stored under sterile conditions until use.

5.5.6 ACEA

The ACEA system is a cell-based assay which enables to monitor a range of parameters such as cell viability, cell number and the degree of cell adhesion over a period of time in real time. The ACEA device (ACEA) is composed of a cradle located in a cell culture incubator which holds a 96-well microtiter E-Plate (Roche). These E-plates contain thin gold electrodes which measure the impedance of a given 96-well by applying an electrical field that is influenced by cell density and cell shape. Thus, increased cell adhesion and cell growth lead to higher electrode impedance. The system can be used to measure cytotoxic effects on mammalian cells over time such as siRNA or therapeutic antibody treatment. The microtiter E-Plate was first primed by the addition of 100 µL complete medium per well. Next, 60 µL of complete medium and the desired cell amount (1,000 to 10,000 cells) was added per well. At this point it was possible to perform siRNA transfections by adjusting the volumes and adding 40 µL of the transfection mixture on top of the 160 µL (described in paragraph 4.6). An incubation period of 24 hours at 37 °C with a 5 % CO_2 atmosphere followed. The device schedule was programmed as follows:

- Add Step (1) = Sweep 1 with an Interval 1 min
- Add Step (2) = Sweep 1,000 with an Interval 15 min
- Add Step (3.1) = Sweep 180 with an Interval 1 min
- Add Sub-Step (3.2) = Sweep 2,000 with Interval 10 min

Step 3 had to be performed as quickly as possible to avoid temperature and pH variations which in turn can influence the ACEA readout. The data was analyzed by the xCELLigence software.

5.6 siRNA transfection

Efficient siRNA delivery is critical for successful gene silencing. The standard transfection technique of this study represented DharmaFECT (Thermo Fischer). This method is based on lipid mediated transfection and exhibits rather low toxicity in contrast to e.g. Lipofectamine (Invitrogen). The DharmaFECT reagents are available as four distinct siRNA-specific formulations to accommodate for different target cell lines whereas DharmaFECT-1 showed to be the most efficient for the cell line panel of this study. Two distinct transfection methods were used. I determined following conditions to be most effective for siRNA transfections in combination with cell viability experiments:

- siRNA amount per 96-well = 1 pmol
- concentration of siRNA = 2.5 - 10 nM
- DharmaFECT reagent per 96-well = 0.2 - 0.4 µL
- simultaneous siRNA transfections during cell seeding without 24 hours pre-culturing of cells

The supplier recommends treating and transfecting cells 24 hours post seeding. Instead, higher transfection efficiencies and viability results were obtained upon combining seeding and transfection at the cell culture start.

5.6.1 siRNA transfection 24 hours post seeding

Cells were seeded in triplicates at a ratio of 1,000 to 40,000 cells per well in 100 µL complete medium. An incubation period of 24 hours at 37 °C with 5 % CO_2 followed. In order to transfect 10 wells of a 96-well plate a working solution of 0.2 µM of the respective siRNA was prepared in 100 µL serum free RMPI/DMEM medium and incubated for 5 min at RT. Next, the working solution was combined with 100 µL of previously prepared DharmaFECT transfection solution consisting of 95-99 µL serum free RPMI/DMEM and 1-5 µL DharmaFECT-1 reagent. An incubation period of 20 min followed. Longer incubation periods had to be performed on ice. In the last step, 20 µL of the siRNA-DharmaFECT solution were mixed with 80 µL complete medium per well and added to the cells after discarding the old medium. Cells were incubated at 37 °C and 5 % CO_2 until readout by a cell proliferation assay (Chapter 5.5).

5.6.2 siRNA transfection and cell seeding at the same day

Cells suspensions were prepared at a ratio of 1,000 to 40,000 cells per well in 70 µL complete medium. At the same time, the transfection mix was prepared. In order to transfect 10 wells of a 96-well plate a working solution of 0.2 µM of the respective siRNA was mixed in 100 µL serum free RPMI/DMEM medium and incubated for 5 min at RT. Next, the working solution was mixed with 100 µL of previously prepared DharmaFECT transfection solution consisting of 95-99 µL serum free RPMI/DMEM and 1-5 µL DharmaFECT-1 reagent. An incubation period of 20 min followed. Longer incubation periods had to be performed on ice. In the last step 20 µL of siRNA-DharmaFECT solution were combined with 80 µL of cell suspension per well. Cells were incubated at 37 °C and 5 % CO_2 until readout via cell proliferation assays (Chapter 5.5).

5.7 Cloning

5.7.1 Bacterial Strains

XL10-Gold® Ultracompetent Cells (Stratagene) were used for transformation after cloning experiments with inserts bigger than 1,000 bp. For smaller inserts and retransformations One Shot® TOP10 Chemically Competent E. coli (Invitrogen) were used. Competent cells were grown on Luria Bertani (LB) agar plates (ImMedia™ Amp Agar) containing 100 µg/mL ampicillin (Invitrogen) at 37 °C.

5.7.2 Gel Extraction

Restriction fragments were separated in 1 % agarose gel TAE buffer (40 mM Tris-acetate at pH 7.8, 20 mM sodium acetate, 2 mM EDTA) containing ethidium bromide (0.5 µg/mL). The gel was run at 150 V for 50 min. Fragments were extracted and purified by the use of illustra GFX™ PCR DNA and gel band purification kit (GE Healthcare). Here, the bands of interest were cut out and subsequently dissolved in DNA capture buffer (GE Healthcare) by heating up the samples to 60 °C. The solution was then transferred to a GFX MicroSpin column. DNA was captured by the silica membrane and washed once for salt removal. Finally, plasmid DNA was eluted in 50 µL 10 mM Tris-HCI at pH 8.0. DNA concentration was determined using the NanoDrop ND-1000 Spectrophotometer (Nano-Drop Technologies).

5.7.3 Ligation

For all DNA ligation reactions the Rapid DNA Ligation Kit (Roche) was used. Ligation reactions were carried out according to the manufacturer's instructions. For specific reactions, vector and insert DNA were mixed at a molar ratio of 1:3 containing 50 ng of vector DNA to increase the probability of insertion. Finally, 2 µL DNA dilution buffer, 10 µL T4 DNA Ligation Buffer and 1 µL T4 DNA Ligase were added and incubated for 1 hour at RT.

5.7.4 Transformation and Retransformation

For transformation experiments XL10 Gold (Stratagene) cells were thawed on ice for approximately 15 min. For each ligation mix 25 µL of cell suspension was transferred to a pre-chilled 1.5 mL Eppendorf tube. Subsequently, 2 µL of ligation mix was added and incubated for 30 min on ice. Bacterial cells were then heat shocked at 42 °C for 30 seconds followed by a 2 min incubation period on ice. Nine-hundred µL of pre-warmed S.O.C. medium (Invitrogen) was then added and an incubation period of 1 hour at 37 °C and 250 rpm followed. Usually three dilutions of each sample (1:1, 1:10 and 1:100) were plated on an LB agar plate containing 100 µg/mL ampicillin and incubated at 37 °C overnight. Transformations and re-transformations with TOP10 cells (Invitrogen) were performed similar except following modifications: The cells were stored and used in 50 µL aliquots and for re-transformation 6 µL of ligation mix instead of 2 µL was used. In addition the incubation period before plating was omitted.

5.7.5 Miniprep

Five colonies of each transformation experiment were picked and used to inoculate 3.5 mL LB-Amp (100 µg/mL) of an overnight culture at 37 °C and 225 - 250 rpm. The next morning, 1.8 mL of each culture was used for miniprep and the remaining culture was stored at 4 °C. Minipreps were performed with the help of the QIAprep® Miniprep kit (Qiagen) which is based on the modified alkaline lysis method of Birnboim and Doly (Birnboim & Doly, 1979). Unless stated otherwise, all centrifugation steps were performed at 17,900 x g and at RT. The cells were harvested through centrifugation for 3 min at 6,800 x g. Afterwards, the supernatant was discarded and the cell pellet resuspended in 250 µL resuspension buffer. 250 µL lysis buffer was added and samples were mixed by inversion and incubated for a maximum of 5 min at RT. Next, 350 µL neutralization buffer was added, samples were mixed immediately by inversion and precipitated cellular debris was spun

down for 10 min. The supernatant which contained the plasmid DNA was then transferred to QIAprep spin column and centrifuged for 60 seconds. The DNA in the column was washed with 750 µL PE buffer to remove salts and finally the plasmid DNA was eluted in 30-50 µL elution buffer. All minipreps were subjected to a control digest followed by fragment separation on a 1 % agarose gel to verify successful ligation.

5.7.6 Maxiprep

Next to re-transformations a single colony was picked to inoculate a 3.5 mL LB-Amp pre-culture. After 8 hours, 250 µL of the pre-culture was used to inoculate a 250 mL overnight culture. 12 to 16 hours later the bacterial cells were harvested by a centrifugation step at 6,000 x g, at 4 °C. Maxipreps were performed with the help of the HiSpeed® Plasmid Purification Maxi Kit (Qiagen) that starts with a modified alkaline lyses procedure. Here, cell pellets were resuspended in 10 mL resuspension buffer and lysed by the addition of 10 mL lysis buffer for 5 minutes at RT. 10 mL of chilled neutralization buffer was then added and the precipitated bacterial lysates were cleared by filtration through a QIAfilter Cartridge. The filtrate was subsequently transferred to an anion exchange resin and washed with 60 mL of a medium salt buffer to remove RNA, proteins and low molecular weight contaminations. The plasmid DNA was eluted in 15 mL of high salt buffer. In order to desalt and concentrate the solution, plasmid DNA was precipitated by the addition of 10.5 mL isopropanol. Finally, precipitated DNA was bound to a QIAprecipitator Module, washed with 2 mL of 70 % ethanol and eluted in 1 mL TE buffer. Maxipreps were subject to a control digest followed by fragment separation on a 1 % agarose gel to verify the amplified construct.

5.7.7 Sequencing

The sequencing of the engineered constructs was performed externally.

6 Results

6.1 FACS-based Receptor Quantitation

Flow cytometry is an attractive option for quantitation of cell-surface receptors on intact cells as this technique is available in many molecular biology laboratories. The exact quantitation of cell-surface receptors is for various reasons attractive. Among them (Zenger et al., 1998):

i) modeling of cellular networks
ii) predictions on saturation conditions with therapeutic compounds
iii) differentiation of normal and malignant state of cells
iv) inter-laboratory comparison

As part of this thesis, the FACS-based receptor quantitation study focused on establishing a method to quantify receptor numbers with BsAbs. I sought to improve the quality of receptor detection in comparison to standard quantitation methods such as custom fluorophore labeling and the QuantiBRITE assay but to also challenge non-FACS-based techniques such as the radioligand binding assays and kinetic extrapolation (KEX). Up to date, radioligand binding assays represent the gold standard in receptor quantitation.

6.1.1 Principle of cell surface quantitation with BsAb Dig detection antibodies

Instead of focusing on targeted payload delivery as in one of our previous studies, the approach in my thesis modified the Dig-based technology to enable precise cell surface receptor quantitation. Essential parameters represent the hapten Dig and bispecific antibodies with high affinity against Dig. Digoxygeninylation of payloads can include the coupling to chemotherapeutics, nucleic acids, peptides, proteins but also to fluorophores such as Cy5 which is a key feature of the applied quantitation strategy (Kessler, 1991; Metz et al., 2011).

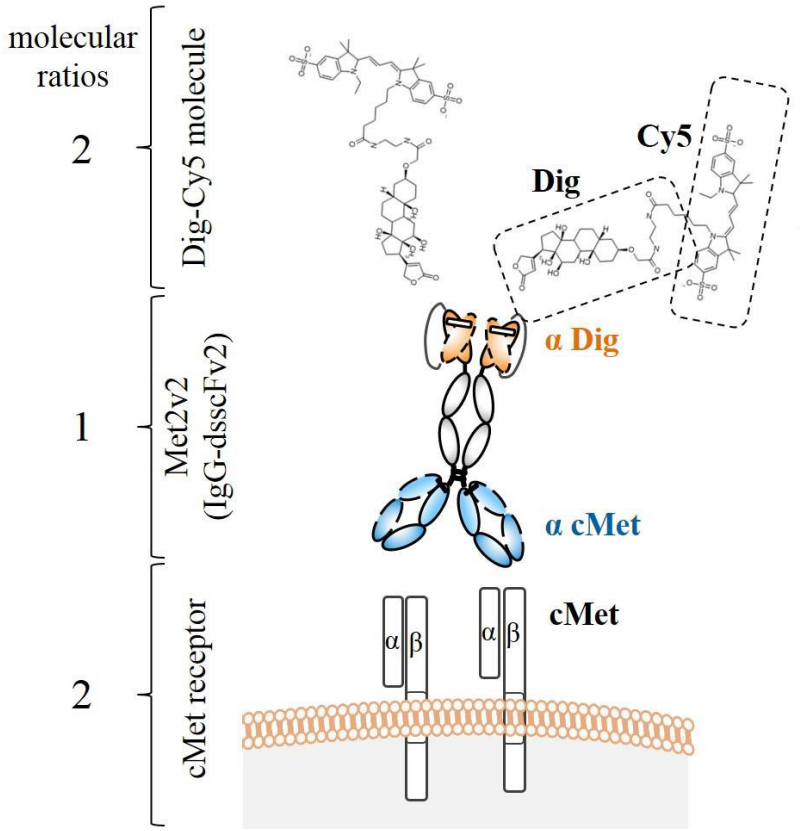

Figure 2.4. Molecular ratio of detection antibody, fluorophore and antigen. Based on the BsAb Met2v2 (IgGdsscFv2) a defined detection antibody to digoxygeninylated Cy5 ratio is generated. Each Met2v2 molecule is able to bind two digoxygeninylated Cy5 molecules and in turn detect two cell surface cMET receptors as illustrated.

The great advantage of using digoxygeninylated fluorophores such as Cy5, is to quantify under defined fluorophore to antibody to cell surface receptor ratios as illustrated in Figure 2.4. Unlike other quantitation techniques, that are carried out with detection antibodies (detailed description in chapter 6.1.22 – 6.1.24), the fluorophore to antibody ratio is known and neither a chemical conjugation step to attach fluorophores nor the subsequent normalization step is required to determine the amount of bound fluorophores (Panke et al., 2013). Due to simple Dig to antibody binding, it is possible to interchange fluorophores (Dig-Cy5, Dig-Alexa488…) but retain bispecific detection antibodies at the same time. This circumstance make this novel quantitation technology a dynamic and cost efficient tool which will be assessed in this work.

6.1.2 Workflow of receptor quantitation

A typical FACS based receptor quantitation requires a five step workflow and includes establishing suitable recording conditions for the FACS measurement, the use of MESF calibration beads to translate gathered MFI values into absolute receptor numbers and the determination of the fluorophore content of the applied detection antibodies:

(i) Performance check of FACS machine
(ii) Creation of UWA enables inter-machine comparison
(iii) Calibration curve with MESF beads which carry defined amounts of fluorophores
(iv) Determine mean fluorophore content of detection antibodies
(v) FACS analysis of cells which were incubated with conjugated detection antibodies

Since quantitation experiments are carried by our novel bispecific Dig detection antibody the fourth step, which determines the mean fluorophore content of detection antibodies, can be omitted.

6.1.3 Selecting cell lines according to cMET gene count and mRNA data

For this study, cMET receptor expression was addressed in a panel of nine cell lines based on its prominent role in the development and implication in cancer. Cell lines were chosen according to three criteria: i) different tissue origin, ii) absence and presence of gene amplification of cMET, iii) high and low cMET mRNA values. This particular selection enables to answer the question whether this novel quantitation tool exhibits a broad range of applicability or not and to investigate correlations between mRNA and protein levels in relation to absolute receptor numbers.

Table 6.1.1 Gene count and mRNA data of the selected cell line panel. The cell lines were selected according to different criteria such as tissue origin, absence or presence of gene amplifications, high or low cMET mRNA values. For comparison reasons, absolute mRNA values were normalized and set in relation to DU145 = 100% (absolute value = 1357). The corresponding standard deviation (STD) is presented in percent. (n.d. = not determined; * = below detection limit; ** H1993 was measured with method L8 instead of L4 as described in 5.2.6).

Cell Line	Tissue Origin	Gene Count	mRNA Absolute	mRNA Normalized	STD in Percent [%]
T47D	breast	**1.45**	*	*	*
DU145	prostate	**2.11**	1,357	**100**	± 3.5
A549	lung	**n.d.**	1,764	**130**	± 8.8
HT29	colon	**2.09**	2,171	**160**	± 5.1
H441	lung	**3.07**	3,663	**270**	± 4.0
SNU-5	gastric	**5.31**	n.d.	**n.d.**	n.d.
Hs746T	gastric	**11.0**	4,478	**330**	± 4.0
MKN45	gastric	**8.96**	4,749	**350**	± 9.8
H1993**	lung	**10.64**	6,513	**480**	± 2.4

Table 5.1.1 summarizes tissue origin, gene count and mRNA data of the nine cell lines. cMET gene count values were obtained by high resolution analysis of SCNAs (somatic copy-number alterations) and assembled by Beroukhim and colleagues (Beroukhim et al., 2010). With respect to the generated Affymetrix data, mRNA values were normalized to DU145 and set to 100% to facilitate inter-cell line comparison. This cell line displayed relatively low expression levels of cMET (absolute value = 1357) and a gene count of 2.11 as listed in table 5.1.1. In line with DU145, the cell lines A549 and HT29 exhibited similar cMET gene counts and mRNA values. Overall, DU145, HT29 and A549 constitute low to moderate cMET expressing cell lines. As medium to strong cMET expressing cell line, H441 was chosen. With a threefold cMET gene count and 2.7 fold increased mRNA levels (in comparison to DU145) this cell line is predicted to exhibit a higher cMET protein level than the previous three cell lines. T47D was chosen as cMET negative cell line with the lowest gene count of 1.45 and for which no mRNA signal was detectable (Table 5.1.1).

As positive controls and therefore high cMET expression cell lines, Hs746T, MKN45 and H1993 were chosen. These cell lines displayed the highest gene count (>8) and highest mRNA levels (>3 fold) in relation to DU145. Unfortunately, no mRNA data was available for SNU-5 but a gene count of 5.31 indicates high cMET expression levels. This is also confirmed by various studies investigating cMET protein expression in SNU-5 (Asaoka et al., 2010; Liu et al., 2011; Smolen et al., 2006).

In summary, gene count values and mRNA expression data correlates, albeit the fold difference for the mRNA value was rather modest. The selected panel of cell lines ranged from cMET negative (T47D) to low/moderate (DU145, A549, HT29) and high (Hs746T, MKN45, H1993) expressing cells with respect to gene count and mRNA value. Based on the data of table 5.1.1, I expect the novel quantitation tool to be assessed in a panel of broad range cMET protein expressing cell lines.

6.1.4 Analysis of cMET expression on protein level

To further investigate cMET protein expression in the selected cell lines, immunoblot analysis was performed prior receptor quantitation experiments. The aim of this analysis was to detect cMET protein in the respective cell lines in which previously, gene count and mRNA levels were determined. In addition, I sought to confirm to have selected a suitable panel of cell lines which consist a diverse range of cMET protein expression. Cell lysates were prepared three days after seeding and analyzed for the presence of total and phosphorylated cMET protein as shown in Figure 6.1.1.

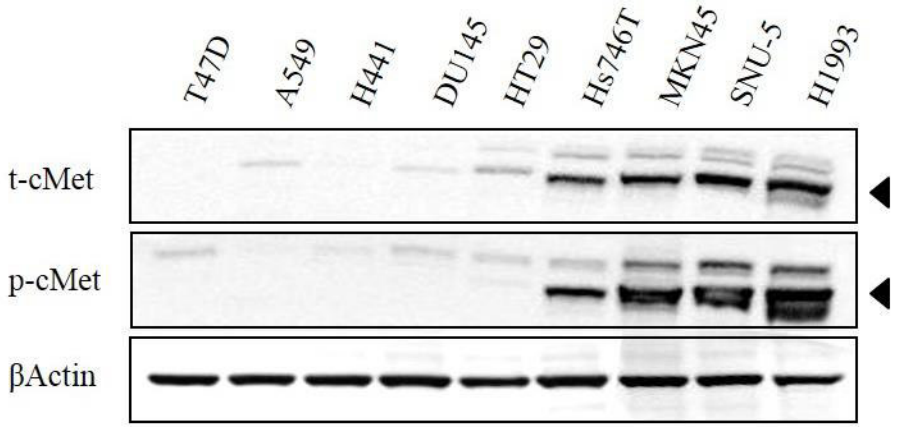

Figure 6.1.1 Immunoblot analysis of total and phosphorylated cMET. Cell lysates were harvested three days after seeding and analyzed for total (t) and phosphorylated (p) cMET. Protein amounts were determined via a Micro BCA assay and a total of 50µg protein was loaded for each sample. The arrow head indicates t- and p-cMET.

With respect to total cMET, H1993, SNU-5, MKN45 and Hs746T showed a strong protein abundance at approximately 145 kDa representing the mature cMET ß subunit (arrows in Figure 6.1.1). The smaller 30 kDa α subunit was not visible with the used immunoblot antibody due to a lack of cross-reactivity. A second band at 170 kDa was observed representing the pre-cursor protein which has not been cleaved by the pro-protein convertase furin. The strong cMET signal for H1993, SNU-5, MKN45 and Hs746T correlated with the gene count and mRNA data. This was also observed in A549 and H1993 previously by Ma and colleagues (Ma et al., 2005). No cMET signal was detected in T47D at any exposure level supporting the rationale of choosing T47D as cMET negative cell line. The weak band at 200 kDa in the phospho cMET blot for T47D is most likely unspecific since no total cMET was detected. Low to moderate cMET expressing cell lines DU145, A549 and HT29 showed weaker band intensities in comparison to high expressing cell lines. However, no signal could be determined for H441, although this cell line exhibits a cMET gene count of 3 and 2.7 fold cMET mRNA in comparison to DU145. Various studies confirm the presence of cMET in H441 (Chess, Ryan, & Finkelstein, 1998; Christensen et al., 2003; Dua, Zhang, Parry, & Penuel, 2011) and thus indicating a detection deficiency of the total cMET-specific immunoblot antibody.

I successfully detected the cMET protein in 10 out of 12 cell lines whereas T47D was chosen as cMET negative control. Based on the rationale of the selected cell lines and similar to table 5.1.1, it was possible to differentiate between strong cMET protein expressing and low cMET protein expressing cell lines. Due to the limited dynamic range of immunoblot analysis, the comparison between both data sets was rather moderate but a correlation could be seen. Overall, it was possible

to confirm a diverse cMET protein expression range within the selected panel of cell lines rendering them suitable for $cMET^{low}$ to $cMET^{high}$ receptor quantitation analysis.

6.1.5 Converting MFI into MESF values by using a standard

To establish FACS-based receptor quantitation a standard is necessary to translate resulting MFI values of FACS experiments into absolute receptor numbers. For this purpose, commercially available MESF standard beads from Bangs Laboratories were used carrying a defined number of Cy5 fluorophores per bead population. To guarantee precise quantitation, it is essential to test the standard according to quality and linearity of the provided beads.

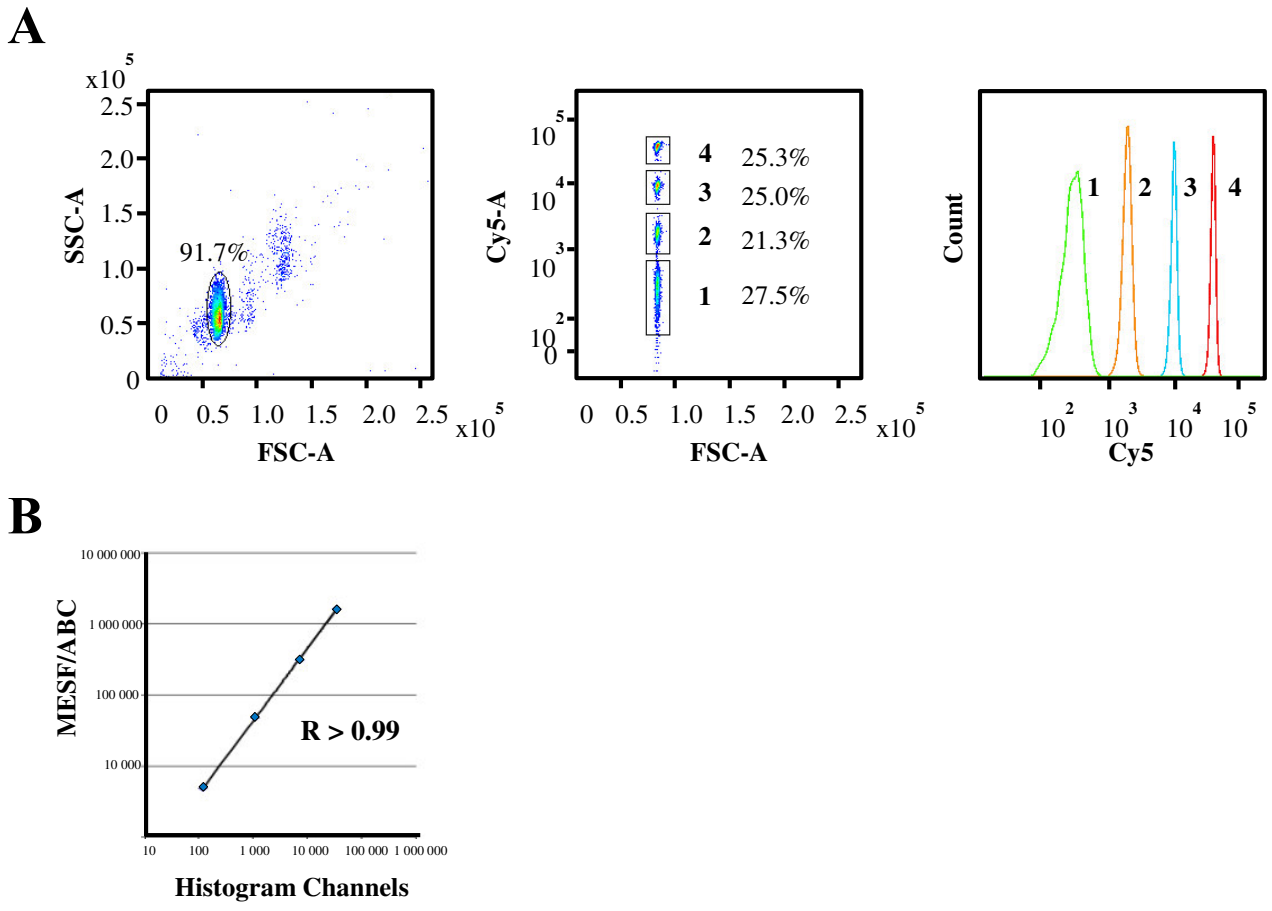

Figure 6.1.2 Quality control of MESF calibration beads. (A) FACS gating strategy of the analyzed MESF calibration beads. Over 90% of the combined bead populations were gated, separated into four populations and shown in the Cy5 channel overlay. The numbers indicate the different bead populations. (B) The four resulting MFI values were used to set up a standard curve and translate MFI into MESF. The correlation coefficient was R > 0.99.

Each of the four bead populations corresponds to one MESF value which in turn correlates to fluorescence intensity of a given number of fluorochrome molecules in an aqueous solution. For example, bead population number 1 of the standard, which has an MESF value of 100, exhibits the same fluorescence intensity as 100 Cy5 molecules in a solution. In order to translate MFI values into absolute receptor numbers the MESF beads were used to set up an MESF calibration curve. The fluorescence intensity of each bead population was set against the fixed MESF value provided by the supplier. Figure 6.1.2A demonstrates the quality control of the obtained beads, gating strategy and the generation of a MESF calibration curve. In the first step the beads were analyzed in FSC (forward-side scatter) and potential dimers were excluded. Over 90% of the combined bead populations were gated and the respective single bead populations 1 to 4 are shown in the Cy5-A/FSC-A channel. The four resulting MFI values were then processed by a pre-programmed online spreadsheet (Bangs Laboratories) to generate the calibration curve (Figure 6.1.2B). The overall correlation coefficient of the curve was $R > 0.99$ and was determined for each experiment involving MESF calibration beads without loss in quality. The lower detection limit was at 831 +/-38 MESF units and the higher at 1,655,554 MESF units.

In conclusion, I was able to reproducibly setup a high quality standard using MESF standard beads. After gating approximately 90% of the four bead populations, the resulting standard curve, which is necessary to translate MFI values into MESF, was determined with a correlation coefficient of $R > 0.99$. It is possible to conclude, that no loss in precision can be expected on the basis of MFI to MESF conversation errors.

6.1.6 Custom antibody labeling requires a subsequent normalization step

After having established the MESF standard, the next step in a FACS-based quantitation study is the generation of suitable detection antibodies. Common quantitation methods, such as custom fluorophore labeling, require the generation of fluorophore labeled detection antibodies by kits in combination with a subsequent normalization step. Due to the BsAb technology in combination with Dig-Cy5, which will be discussed in detail in chapter 6.1.7, this study will try to omit this step. However, labeling was exemplarily performed with three antibody constructs to investigate custom labeling efficiency and to enable comparison between the respective quantitation techniques.

Table 6.1.2 Custom fluorophore labeling and normalization. Three antibody constructs Ab1, Ab2 and Ab3 were custom labeled with the fluorophore Cy5 by the Amersham Biosciences kit. The F/P ratio was determined by the use of SCB (Bangs Laboratories).

Construct	Normalization (F/P ratio)
Ab1 (IgG-DIG)	0.98
Ab2 (Met2v2)	0.37
Ab3 (Met1v1)	0.87

Custom labeling of detection antibodies is commonly done by unspecific labeling techniques such as lysine-linker chemistry where surface accessible lysines in the antibody chain are covalently coupled to a fluorophore of interest. Because such reaction results in an unknown antibody to fluorophore ratio, this method requires a normalization step in which the mean fluorophore content per protein/detection antibody is determined (F/P ratio). The normalization step is performed in a separate experiment by the use of so called Simple Cellular Beads (SCB) (Bangs Laboratories). I labeled three different antibody species with the fluorophore Cy5 according to the manufacturer (Amersham Biosciences). The F/P ratio was then determined in the normalization step and results are shown in table 6.1.2. As the values indicate not all antibodies were successfully labeled. For instance, only every third antibody construct was labeled for antibody species Ab3 (F/P = 0.37).

Custom fluorophore labeling in combination with the necessary normalization step emphasized four major problems: i) Not all antibodies of the same antibody species were labelled with equal amounts of fluorophore; ii) The overall efficiency of labeling varied significantly; iii) Due to unspecific lysine-linker chemistry some antibodies can lose functionality at the antigen binding site; iv) Custom labeling required normalization by SCB which may represent another source of error.

6.1.7 Designing BsAbs for improved receptor quantitation

As introduced in the previous chapter, common FACS-based quantitation techniques (e.g. custom fluorophore labeling) exhibit a range of limitations leading to imprecise results. I addressed following questions to approach these limitations and to set up a novel quantitation tool:

A) Is it possible to improve the error-prone labelling step and to generate a homogenous detection antibody species?

B) Can the normalization step, which is needed to determine the F/P ratio, be omitted?

C) How can detection tools with respect to antibody formats be improved?

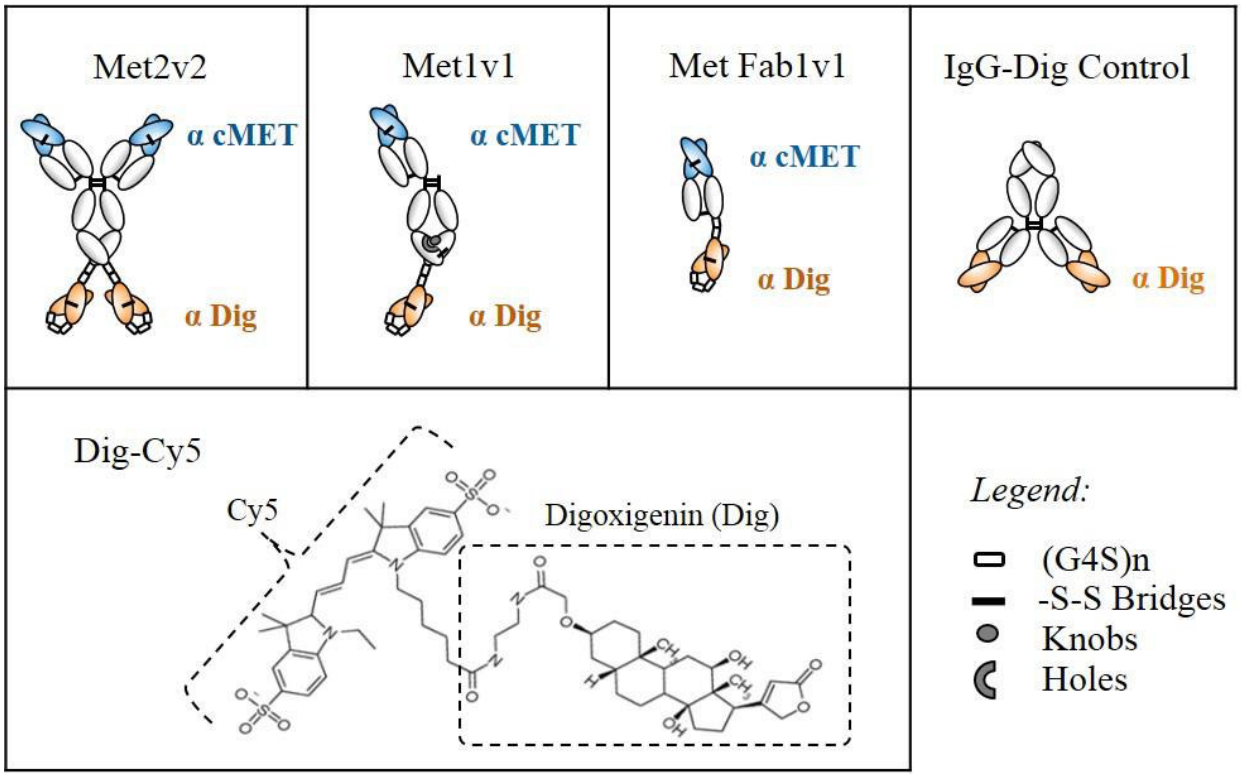

Figure 6.1.3 Proof-of-Concept molecules based on BsAb technology for receptor quantitation of cell surface cMET. Schematic presentation of different BsAb formats (variable regions are shaded) and the fluorophore coupled hapten Dig (Dig-Cy5). The three BsAbs (Met2v2, Met1v1 and MetFab1v1) are specific for cMET as biological target and Dig. As unspecific binding control, IgG-Dig was generated which lacks cMET-specificity.

To address these questions three proof of concept BsAbs were designed as shown in Figure 6.1.3. As key idea, the generated BsAb constructs are able to recognize a biological target on the one side (i.e. cMET receptor) and the hapten Dig on the other side. Dig is covalently linked to the fluorophore Cy5 (Dig-Cy5) resulting in a defined F/P ratio and thereby omitting the usual normalization step. Based on the Dig mediated fluorophore- BsAb coupling strategy, proof of concept molecules were designed according to three considerations: (i) FACS-based quantitation methods work with regular IgG formats as detection antibodies. These formats are bivalent and as such can bind to one or two antigens leading to inaccurate quantitation. In line with this, the first

BsAb construct which was generated, represents a bispecific 2v2 format which is able to bind two cMET receptors and two Dig-Cy5 molecules (ii) To ensure monovalent cMET receptor binding, a second BsAb 1v1 antibody format was designed which can bind one receptor and one Dig-Cy5 molecule (iii) The constant region of IgG based detection antibodies can interact with FcRn as described previously. This circumstance can result in FcRn-antibody interaction and thus false positive MFI values. To investigate such undesired interaction a third and constant-region-omitting antibody was designed (Fab1v1). Figure 6.1.3 illustrates the different antibody constructs which were used for the study. All BsAbs are specific for the RTK cMET as biological target in addition to the hapten binding entity which is specific for Dig-Cy5. As unspecific binding control an IgG based IgG-Dig antibody was generated which is able to bind Dig-Cy5 but not cMET.

6.1.8 Dig coupled fluorophores enabling a precise F/P ratio

Dig was originally found as steroid (390 Da) in plants such as *Digitalis purpurea*, *Digitalis orientalis* and *Digitalis lanata* and is commonly attached to sugars forming glycosides (Polya, 2003). In biotechnology, this small molecule is broadly used to label IgG and represents an alternative to the biotin-streptavidin system. One major advantage of Dig over biotin is that it is not constitutively present in mammalian cells, thus reducing endogenous background in immunohistochemical applications. Antibodies against Dig have been generated already more than 20 years ago (Kessler, 1991). Due to its high immunogenicity, the hapten Dig is used in various applications such as ELISA and has become a standard as immunohistochemical maker for non-radioactive in situ hybridization (Eisel, Grünewald-Janho, & Krushen, 2002).

For the receptor quantitation study I took advantage of the small size of Dig and the possibility to covalently couple it to other small molecules such as fluorophores. Metz and colleagues have determined the crystal structure of murine anti-Dig Fab binding Dig. In addition, a panel of Dig coupled compounds were generated via digoxygeninylation and analyzed for functionality. It could be confirmed that the antibody accommodate modifications of Dig and linker-mediated fusion of small molecules or proteins to Dig (Metz et al., 2011). In consequence, we generated Dig-Cy5 which constitutes the fusion of Dig to the fluorophore Cy5 (Figure 6.1.3). digoxygeninylation of Cy5 was done via NHS (N-hydroxysuccinimide) ester conjugation to amines. Previous studies have shown that coupling/labeling of BsAb to Dig-Cy5 is quantitative and stable (Metz et al., 2011).

The homogeneity of Dig-Cy5 was confirmed to be >96% by re-analysis of the purified product in analytical HPLC.

6.1.9 Generation of proof-of-concept BsAb constructs

The antibodies Met2v2, Met1v1 and MetFab1v1 bound in low nM affinities their respective biological target and to Dig at 15.8 nM for the 2v2 format (Metz et al., 2011). The design of Met2v2 and IgG-Dig was based on formats in which scFv (single-chain Fv) were fused to C-termini of IgG HCs according to Coloma and Morrison (Coloma & Morrison, 1997).

The first formats, Met2v2 and IgG-Dig contain two disulfide stabilized scFv fusions at the C-terminus of the human IgG1 HC which were connected by a repeating glycine serine motif (G4S) as illustrated in Figure 6.1.3. Previous studies have shown that the G4S connector facilitates free access to the Dig binding site (Metz et al., 2011).

The second format which was generated represents the bispecific Met1v1 containing only one scFv and one Fab arm (Figure 6.1.3) and thus being monovalent for cMET and Dig. To prevent homo-dimerization and enforce heterodimer pairing of the two HCs containing the scFv and Fab, respectively, the kih mutation strategy was applied. This strategy, to reduce nonproductive assembly, was first introduced by Paul Carter and colleagues (Merchant et al., 1998; Ridgway et al., 1996). To achieve hetero-dimerization, single amino acid substitutions were introduced into C_H3 domains of the Fc chain resulting into T366W (knob) mutation in one HC and T366S, L368A and Y407V (hole) mutations into the other HC. The kih strategy relies on the fact that the respective HCs exhibit a so called C2 symmetry. With respect to antibody stability but also in terms of dimerization, studies have shown that the disulfide bridge of the human IgG C_H3 domain is important (McAuley et al., 2008). Therefore an additional disulfide bridge was engineered for the C_H3 domain of the Met1v1.

The third construct which was generated represents a Fab1v1 in which the Fab-scFv fusion lacks the constant Fc region. Like Met1v1, the engineered Fab1v1 is monovalent (Dig/cMET) and binds specifically to cMET as described previously (Lu et al., 2002).

6.1.10 Proof-of-Concept BsAbs can be expressed and purified at high quantities and purities

Expression plasmids containing heavy and light chain of the respective BsAb constructs were co-transfected to HEK293-F. Transiently expressed BsAbs were affinity purified from the cell supernatant by either protein A, in the case of a conserved Fc region, or by Kappa-Select if Fc was lacking (Fab1v1). In a second step BsAb were subjected to size-exclusion chromatography.

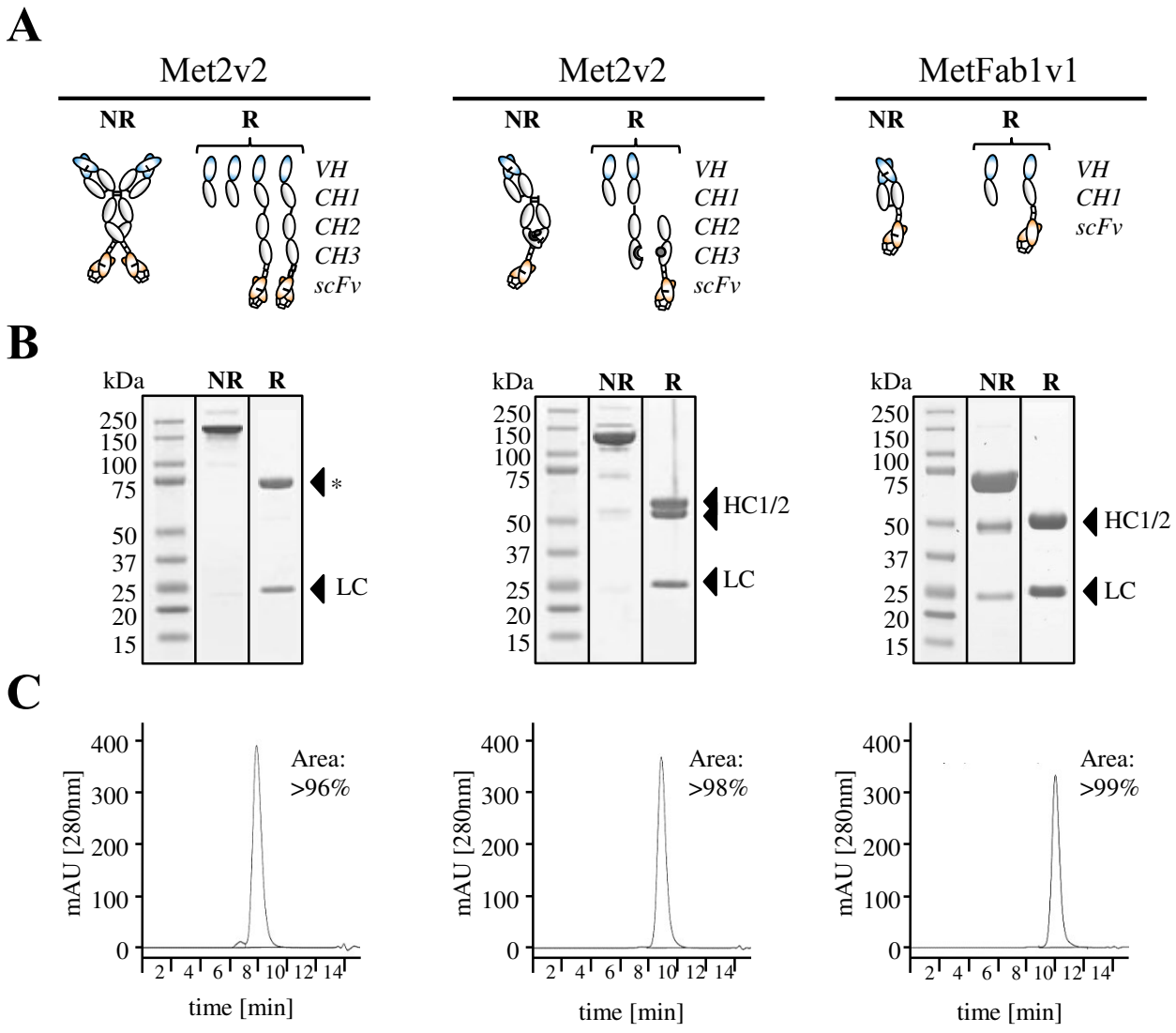

Figure 6.1.4. SDS-PAGE and analytical HPLC analysis of three BsAb formats which are destined for FACS-based receptor quantitation. (A) Schematic presentation of different BsAb formats under non-reducing (NR) and reducing (R) conditions. The corresponding chain sequence is listed on the side (VH = variable region, CH = constant region, scFv = single chain variable fragment). (B) Coomassie stained SDS-PAGE at non-reducing (NR) and reducing (R) conditions. In the order as presented in A. * = light chain with scFv, LC = light chain, HC1/2 = indicates the two different HCs. (C) Analytical HPLC of Protein A and size-exclusion chromatography purified BsAbs. The determined homogeneity was >96%.

Figure 6.1.4 shows SDS-PAGE and analytical HPLC analysis of the antibodies Met2v2, Met1v1 and MetFab1v1 and illustrates the structure in the "native" and reduced state.

For each construct SDS-PAGE analysis was performed under non-reducing (NR) conditions to investigate its native structure and under reduced (R) conditions to "break-up" disulfide bridges and quaternary protein folding (Figure 6.1.4B). At NR conditions the total size of Met2v2 was approximately 200 kDa. The size is due to its LCs with 25 kDa and the HCs with 75 kDa containing each a scFv (VH-C_H1-C_H2-C_H3-scFv) as indicated in Figure 6.1.4A. The size of the second antibody Met1v1 was approximately 125 kDa under reducing conditions whereas three bands could be observed under NR conditions. The band at 25 kDa assembled the LC and the two bands at 50 kDa were HC1 (VH-C_H1-C_H2-C_H3) and HC2 (C_H2-C_H3-scFv). HC2 lacked the Fab part but consisted of a scFv fusion instead leading to a similar size as HC1. The smallest antibody MetFab1v1 was 75 kDa in size and segmented under NR conditions to its LCs at 25 kDa and to the Fab region of the HC at 50 kDa including a scFv (VH-C_H1-scFv). The two weaker bands, which can be observed under reducing conditions, implied that parts of the MetFab1v1 antibody degraded during the boiling step. Overall, SDS-PAGE analysis confirmed protein purity of the three engineered BsAbs.

Structural integrity was confirmed by analytical HPLC as shown in Figure 6.1.4B. Here, antibody purities over 96% were determined. Theoretical antibody masses were confirmed in mass spectroscopy (data not shown). In summary, three proof of concept BsAbs were generated in mg quantities and at high homogeneity (>96%). With the gained high purity antibodies it was possible to conduct initial experiments in establishing the novel FACS-based quantitation method.

6.1.11 Binding stability of BsAb to fluorophore coupled Dig

After engineering, expressing and purifying the respective BsAbs, their binding stability to the fluorophore coupled Dig (Dig-Cy5) was investigated. Only stable Dig-Cy5 to BsAb interaction guarantees reliable quantitation data in FACS analysis. This non-covalent binding stability was tested by the use of SCB.

In the first step, BsAbs were non-covalently coupled to Dig-Cy5 prior each experiment. To fully saturate the mAb or scFv(s), Dig-Cy5 was added in a 1.2:1 and 2.4:1 molar ratio according to Metz and colleagues, respectively (residual Dig-Cy5 was not removed by size exclusion or other methods)

(Metz et al., 2011). After coupling, Dig-Cy5 BsAbs were incubated together with SCB at varying times. SCB are commercially available beads consisting of single bead populations which carries a defined number of anti-Fc binding sites. This sites recognize human IgG and thus the engineered BsAbs except MetFab1v1. Such non-covalent binding stability was tested by the use of these beads. After binding of Dig-Cy5 coupled antibodies to SCB, the MFI was investigated by flow cytometry and respective values are shown in Figure 6.1.5. For this experimental setup, Met2v2 and Met1v1 were used with i) varying antibody incubation periods and ii) varying numbers of washing steps after the incubation with SCB. The supplier recommended an incubation period of 45 min followed by two washing steps. As depicted in Figure 6.1.5, incubation of Dig-Cy5 and SCB led to MFI values below 80 emphasizing no unspecific binding of Dig-Cy5 to the beads. Also individual measurement of SCB resulted in MFI values below 30 which demonstrated a very low auto-fluorescence of SCB. In consequence, MFI values above 80 were due to Dig-Cy5 coupled BsAb which bound to SCB.

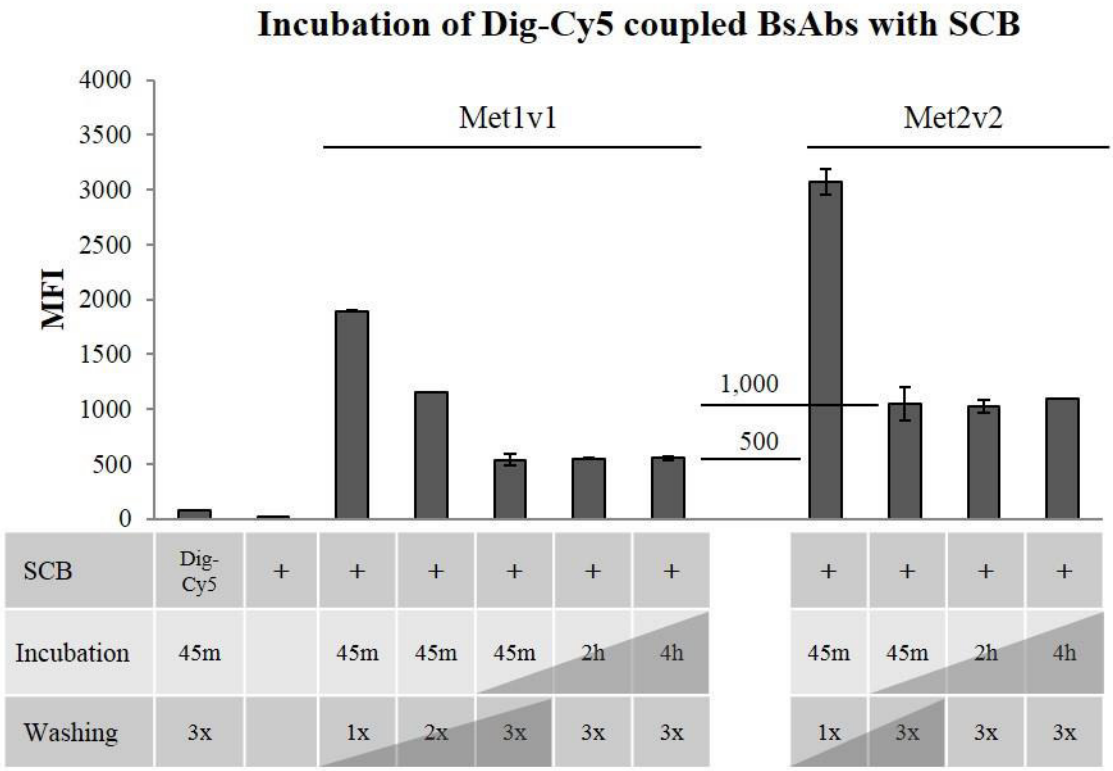

Figure 6.1.5. Binding stability analysis of DIG-Cy5 to Met1v1 and Met2v2 via SCB. Incubation times of fluorophore coupled BsAbs with SCB and the number of washing steps next incubation were varied. The resulting MFI value is set against the respective experimental conditions. Increasing washing steps led to decreasing MFI signal intensity whereas prolonging incubation periods from 45 min to 4 hours revealed no loss MFI signal.

A constant MFI value was expected after the incubation of Dig-Cy5 coupled BsAb with SCB, due to a defined number of anti-Fc binding sites. However, as depicted for Met1v1 and Met2v2 the number of washing times correlated to signal intensity. The highest MFI value was obtained after one washing step (Met1v1 >1,800; Met2v2 >3,000), whereas the lowest after three washing steps (Met1v1 <600; Met2v2 <1,100). This observation can be either due to weak SCB to BsAb binding or due to unstable Dig-Cy5 to BsAbs binding. To further investigate the Dig-Cy5 BsAb interaction, Met1v1 and Met2v2 were incubated with SCB over a period of 45 min, 2h and 4h but keeping the amount of washing steps constant (3x). As shown in Figure 6.1.5 the MFI signal remains uniform over 4 hours for both antibodies. No fluorophore bleeding could be observed. Upon comparison of the MFI values of Met1v1 and Met2v2 with each other, a ratio of 2 was calculated (Met1v1 ~ 530 MFI; Met2v2 ~ 1050 MFI). This ratio matched the theoretical F/P ratio of both BsAbs which is 1 and 2, respectively, and supported the assumption of stable Dig-Cy5 to BsAb binding. The study by Metz and colleagues investigated the binding affinity of Dig-Cy5 to the BsAbs via SPR and determined a low nanomolar affinity of 15.8 nM indicating a strong coupling of Dig-Cy5 to BsAbs (Metz et al., 2011).

In summary, it was possible to demonstrate a stable Dig-Cy5 to BsAb coupling over four hours without loss in signal intensity. Also the theoretical MFI ratio of 2, between Met1v1 and Met2v2, could be determined. In addition, the study by Metz and colleagues further supported our finding by SPR analysis which determined a strong, nanomolar affinity of the respective BsAbs to Dig-Cy5 (Metz et al., 2011). The observed loss in signal correlates with the number of washing steps, emphasized a weak SCB to BsAb binding instead. It is noteworthy, that stable Dig-Cy5 to BsAb coupling is essential for accurate receptor quantitation which could be demonstrated. As mentioned previously, this novel quantitation technique omits normalization via SCB due to a known F/P ratio of the detection antibodies. The gained data, however, suggested a weak SCB to antibody interaction. The question arises: Does the normalization step via SCB represent an error-prone step and thereby lead to imprecise quantitation data?

6.1.12 F/P ratio analysis of BsAbs by SCB

After verifying a stable Dig-Cy5 BsAb interaction, I investigated SCB as normalization tool. In the previous paragraph, a weak BsAb to SCB binding was assumed which would result into biased and therefore inaccurate quantitation data for quantitation techniques relying on this normalization step.

To follow up the question, SCB were used to determine the amount of fluorophores which bind to the generated BsAbs and thus the F/P ratio of our constructs.

Usually, this normalization step is performed for custom fluorophore labeled antibodies exhibiting an unknown F/P ratio. The F/P ratio is needed to translate MFI values into MESF values which represent the absolute receptor numbers. For Met1v1 and Met2v2 the F/P ratio is known (1 and 2) and thereby no normalization step is required. However, this circumstance can be used to access the accuracy by SCB by comparing the actual F/P ratio with the one determined via SCB.

Table 6.1.3 Analysis of Dig-Cy5 to antibody ratio using SCB. Fluorophore coupled BsAbs (IgG-Dig, Met1v1, Met2v2) were incubated at two different concentrations with SCB. The MESF value was calculated and the measured F/P ratio compared to the actual F/P ratio. (* = (Metz et al., 2011)

Sample	Concentration (µg/mL)	MESF	F/P ratio*	Measured F/P ratio
IgG-Dig	10	160,166	2	0.8
IgG-Dig	100	179,147	2	0.9
Met1v1	10	68,812	1	0.4
Met1v1	100	70,750	1	0.4
Met2v2	10	120,225	2	0.6
Met2v2	100	128,571	2	0.7

Factor 2

Factor 1.5-1.8

Factor 2-3

For this, two different concentrations of Dig-Cy5 coupled IgG-Dig, Met2v2 and Met1v1 were used to guarantee complete saturation of the SCB (10µg/mL and 100µg/mL BsAb). As shown in table 6.1.3 no concentration-dependent differences were observed, confirming the saturation of beads by BsAbs. The gained MFI data was translated into MESF values via MESF standard beads as discussed previously in paragraph 6.1.3. The displayed MESF values were not normalized for the number of Dig-Cy5 molecules per antibody. Instead, I listed the known F/P ratios (Metz et al., 2011) and the measured F/P ratios. The ratios which were determined by SCB were calculated by dividing MESF values by the ABC value (194,461) which is provided by the supplier. For all antibody constructs and concentrations the measured F/P ratio was significantly lower than the

actual F/P ratio (2-3 fold). Also, ratio comparison of Met1v1 to Met2v2 led to a factor of 1.5-1.8 instead of 2.

The F/P ratio analysis of BsAbs by SCB resulted into inaccurate normalization data. The actual F/P ratios (1 and 2) are supported by i) a defined F/P ratio for each BsAbs format upon generation (Figure 6.1.3), ii) size exclusion chromatography studies by Metz and colleagues (Metz et al., 2011) and iii) the experimentally determined F/P ratios as shown Figure 6.1.5. In summary, it was possible to demonstrate that the SCB facilitated normalization step in custom labeled antibodies introduced a significant error margin which resulted into false F/P values.

6.1.13 Concentration-dependent analysis of BsAb cell surface binding to cMET^{high} H1993

Working concentrations for the respective BsAb constructs were determined to ensure complete cMET receptor saturation upon receptor quantitation. The amount of required antibody depends on the absolute receptor number. Therefore, the cMET^{high} expressing cell line H1993 was used. H1993 is known to have a significant cMET gene amplification and to overexpress cMET receptors (Lutterbach et al., 2007). Immunoblot analysis of Figure 6.1.1 determined highest cMET protein out of the investigated cell line panel.

A

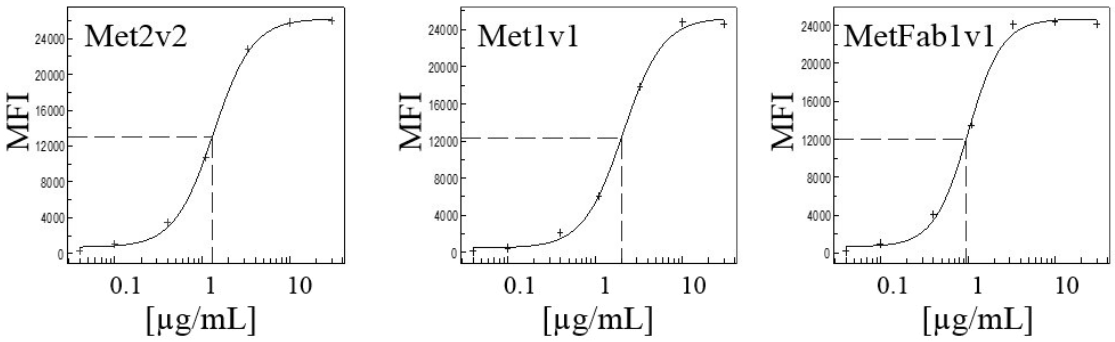

B

Construct	IC_{50} [µg/mL]
Met2v2	1.98
Met1v1	1.29
MetFab1v1	0.95

Figure 6.1.6. Concentration-dependent analysis of BsAb cell surface binding to cMET on H1993. (A) Saturation curves of BsAb constructs Met2v2, Met1v1 and MetFab1v1 were generated in the $cMET^{high}$ expressing cell line H1993. (B) The corresponding IC_{50} value were calculated to determine the final BsAb working concentration. A theoretical saturation was reached at 4 µg/mL for all three constructs.

Saturation curves of Met2v2, Met1v1 and MetFab1v1 were generated as shown in Figure 6.1.6A. The corresponding IC_{50} values were calculated and summarized in table 6.1.6B. As depicted, the values ranged between approximately 1 and 2 µg/mL. To achieve complete cMET receptor saturation in H1993 and the remaining eight cell lines, a BsAb concentration of 4µg/mL BsAb was needed. To guarantee full saturation, 10 µg/mL was defined as working concentration for all constructs and used throughout all quantitation experiments.

6.1.14 Establishing the "Unified Window of Analysis" for linear quantitation conditions

I expected to observe significant variations in receptor numbers in the selected panel of nine cell lines. This assumption was based on collected mRNA data (table 6.1.1), gene count variations (table 6.1.1) and varying cMET protein expression levels (Figure 6.1.1). One challenge for accurate receptor quantification was to establish a linear quantification window including the lowest but also highest cMET expressing cell line. Hence, the so called UWA had to be first defined together with the use of reference standard beads (Bangs Laboratories) as shown in Figure 6.1.7.

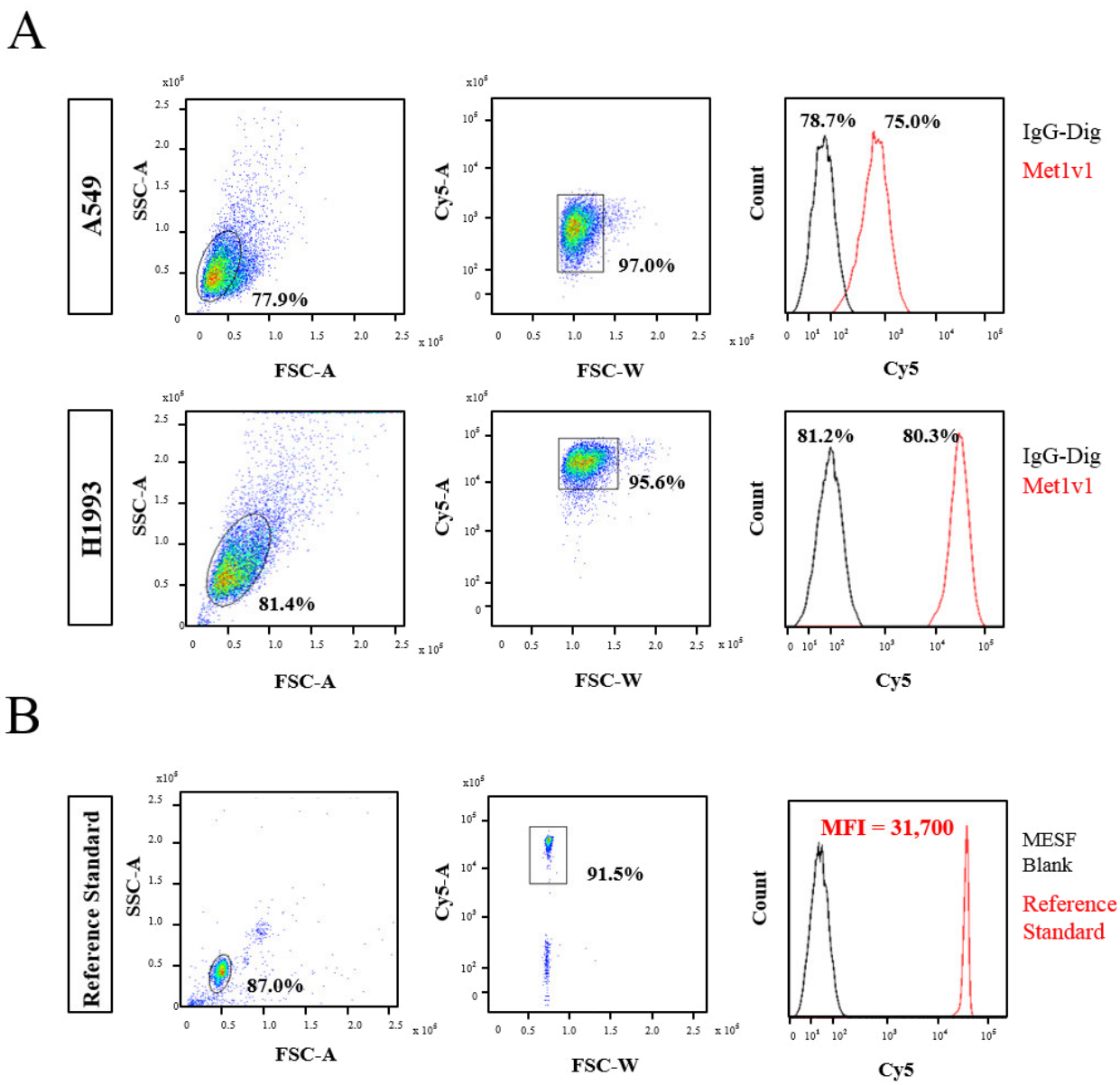

Figure 6.1.7 Establishing the UWA. (A) Exemplary scatter profile of a cMET^{low} and cMET^{high} (A549, MKN45) cell line with additional Cy5 histogram analysis for Met1v1 (red) and IgG control (black). (B) Scatter profile of reference standard (Bangs laboratories) to define the UWA. An MFI value of 31,700 was determined by the reference beads (red curve). The MESF blank (black curve) was used as blank control.

The UWA was established by staining the cMET low expression cell line A549, as well as the cMET high expressing cell line H1993, with Met1v1. FACS settings for Cy5 signal detection were adjusted in a way that corresponding Cy5 intensities of both cell lines could be recorded, without exceeding the detection window. Once appropriate detection conditions were established it was possible to define UWA by the use of Cy5 reference standards (Bangs Laboratories). The reference standard consisted of a single bead population with an assigned MESF value. After analyzing the

reference standard under this pre-defined Cy5 conditions (Cy5 channel/amplifier: 446) the median fluorescence intensity was recorded (MFI=31,700) as exemplified in Figure 6.1.7B. In other words, UWA can be re-established once the Cy5 channel parameters are adjusted in a way that reference beads lead to an MFI of 31,700. This defined MFI value can be used to re-adjust Cy5 fluorescence settings upon using different FACS machines or to recalibrate the system after FACS laser maintenance.

Figure 6.1.7A shows the scatter profile and gating strategy of A549 and H1993 which were stained with Dig-Cy5 labeled Met1v1. First, the main cell population was gated in the Side Scatter (SSC)/Forward Scatter (FSC) profile to exclude cell aggregates and dead cells. Gated populations accounted 70% to 85% for all tested cell lines except Hs476T and SNU-5 (60-65%). These cell lines contained a high degree of aggregates and cell debris. The presence or absence of a live-dead marker, to exclude apoptotic cells, did not influence the quantitation results (data not shown) and was therefore excluded in FACS measurements. In the second step, resulting events of the SSC-A/FSC-A scatter profile events were analyzed via a Cy5-A/FSC-W scatter plot to exclude cell duplets and triplets. The hereby gated populations accounted over 95% for all cell lines indicating a low amount of cell duplets with respect to the initial SSC-A/FSC-A gate. In the third step, previously gated events were analyzed by a Cy5 histogram. The recorded Cy5 signal intensity for H1993 was significantly higher than for A549, reflecting different levels in cMET protein expression. In addition, signal intensity of IgG-Dig is shown. This control antibody was used to determine unspecific binding of Met1v1. A clear differentiation between control antibody and Met1v1 was visible for each cell line (Except T47D= neg. ctrl.). Values in the Cy5 histogram represented the overall percentage of cells which were gated from the initial cell population in the SSC-A/FSC-A scatter plot. In the final step, unspecific MFI signals (IgG-Dig) were always subtracted from the measured BsAb MFI (i.e. Met1v1). The resulting value was then matched against the calibration curve (Figure 6.1.2) to yield the final MESF value which reflected the total receptor number. The MESF value was not necessary to determine the UWA.

In summary, I could successfully establish the UWA for nine cell lines. The system was set up by the use of $cMET^{low}$ and a $cMET^{high}$ expressing cell lines to guarantee a broad and linear detection range. Together with the reference standard, the determined Cy5 channel settings were fixed to enable reproducible experimental conditions at an MFI of 31,700. The hereby determined settings were not changed and used throughout the course of all experiments.

6.1.15 Cell culture dependent cell surface expression of cMET

After setting up the UWA, cMET receptor quantitation experiments were performed for all cell lines with the detection antibody Met1v1. It is well known that the number of cell surface proteins can vary with culture conditions. Studies indicate that expression levels of cellular proteins can depend on cell confluency which is changed during cell growth and division (Su, Wang, Ghishan, Kiela, & Tang, 2009). Moreover, Kornilova and colleagues could demonstrate such process for the HER2 receptor (Kornilova, Taverna, Hoeck, & Hynes, 1992). They discovered that HER2 protein content varied significantly depending on cell density in mammary epithelial cell lines such as HC11 and 31E (Kornilova et al., 1992). The question arose, whether the poor reproducibility was based on "altered cMET protein expression levels during cell proliferation".

Table 6.1.4 Receptor quantitation of cell lines with BsAb Met1v1. The mean MESF values of at least three biological replicates were calculated for A549, MKN45, DU145, HT29 and SNU-5. The corresponding STDs are shown as absolute MESF value and in percent.

Cell Line	Met1v1		
	Mean MESF	STD (MESF)	STD in Percent [%]
A549	25,839	± 11,806	45,7
MKN45	616,344	± 133,830	21,7
Du145	5,163	± 2,208	42,8
HT29	11,522	± 4,541	39,4
SNU-5	1,187,700	± 112,694	9,5

With respect to initial quantitation experiments, the calculated receptor numbers (MESF values) varied significantly for A549, MKN45, DU145 and HT29 as shown in table 6.1.4. Determined standard variation for this cell lines ranged between 20 and 45 percent. Although the Dig-Cy5 coupling procedure, the UWA and the FACS measurement itself were standardized and kept at constant parameters, poor quantitation reproducibility was observed. Quantitation data for cell lines such as SNU-5 were highly reproducible in the same experimental setup (table 5.1.4). The only varying condition represented the culturing time of cells before FACS analysis. Here, cells were harvested after a culturing period between 60 to 80 hours (three days post seeding) at approximately 80% confluency.

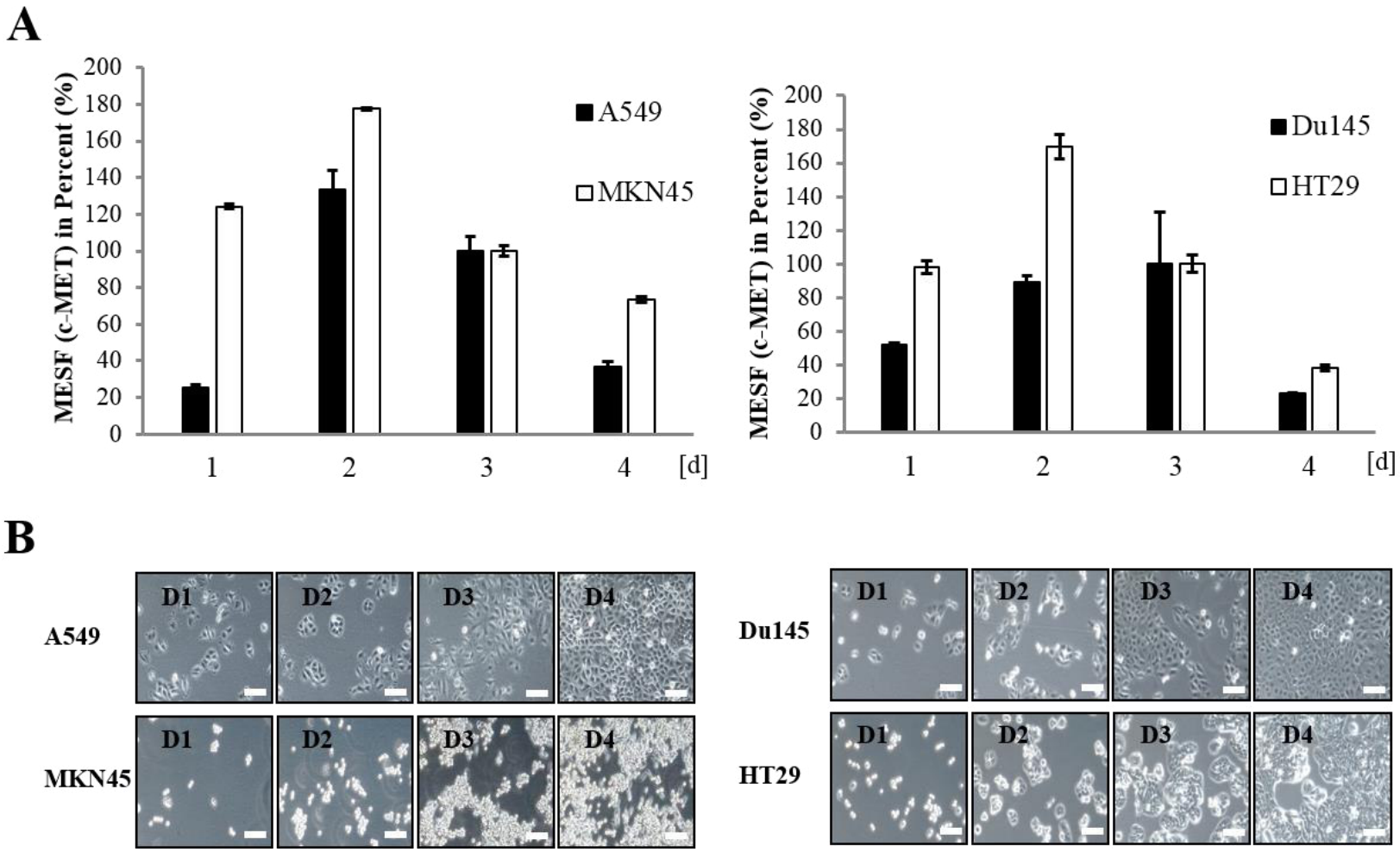

Figure 6.1.8 Influence of culture duration on cell surface expression levels of cMET. (A) Time-course receptor quantitation experiment with Met1v1 in A549, MKN45, DU145 and HT29. Absolute MESF values of day 3 were set to 100%. (B) Prior FACS analysis, bright field pictures were taken at each day (Days1-4; Magnification 100x).

A time-course experiment was designed for A549, MKN45, DU145 and HT29, which quantified cMET receptor levels after every 24 hours of cultivation. The results are summarized in Figure 6.1.8. Since MKN45 harbors a nine-fold cMET gene amplification (Beroukhim et al., 2010) and exhibited significantly higher MESF values over A549, DU145 and HT29, the gathered quantitation results are normalized to percentages. In addition, this type of data presentation enabled a simplified inter-cell line comparison related to the cMET expression level dynamics. Data normalization was performed at day three where MESF values were set to 100%. To monitor cell confluency, cells were simultaneously analyzed via bright field microscopy prior FACS measurement.

Significant variations in cMET protein expression were observed for all cell lines over the entire culturing phase (Figure 6.1.8). The determined receptor amounts revealed an overall 2 to 4-fold change in cMET protein levels, whereas A549 exhibited the highest variation. Here, cMET levels increased approximately five-fold from day one to two. Cell lines A549, MKN45 and HT29 shared a similar expression dynamic in which cMET receptor levels increased after seeding, reached a maximum at day two and continued to fall till confluency was reached. Sub-confluent cells (~30%) at day two exhibited the highest cMET levels whereas the lowest level was reached at full confluency (100%). Although DU145 exhibited a similar trend, this cell line did not reach its cMET level maximum at day two. Instead, receptor levels remained constant over two days (day two-three).

In terms of cell morphology, MKN45 presented a change of cellular morphology as cMET induces an EMT transition phenotype (Tsarfaty et al., 1994) and cell scattering (Bhargava et al., 1992). Cells appeared roundish and loosely adherent in bright field microscopy (Figure 6.1.8A). The morphology correlated with nine-fold cMET gene amplification in MKN45 (Beroukhim et al., 2010) and 20 to 80-fold increased receptor amounts over adherent and differentiated A549, DU145 and HT29.

According to evaluated data of Figure 6.1.8 it was possible to determine the cause of previously poor quantitation reproducibility. I demonstrated dynamic cMET protein expression in A549, MKN45, DU145 and HT29 over one culturing passage. Cell surface expression of cMET appeared to correlate with cell confluency and cMET receptor numbers increased/varied up to five-fold. As a consequence, quantification experiments that were performed within a window of 60 to 80 hours

post cell seeding, exhibited significant variation in cMET receptor numbers and led to poor reproducibility. To bypass this issue and to obtain reproducible quantitation data, the following experiments were strictly performed 70-75 hours after seeding.

6.1.16 Part I: Quantitation of cMET on tumor cells with Met1v1

After defining essential parameters to generate reproducible quantitation data such as i) the amount of antibody needed to saturate cMET receptors, ii) the establishment of an UWA and iii) the identification of appropriate cell culture conditions, cMET receptor quantitation was started in nine cell lines. Gained data was then compared to previously determined mRNA and gene count values shown in table 6.1.1.

Table 6.1.5 Flow cytometric quantitation of cMET cell surface levels with Met1v1. Nine cell lines were quantified at Day 3. cMET receptor numbers and the corresponding STD are shown as MESF values whereas the STD was also calculated in percent. Flow cytometric experiments were performed at least in three biological replicates with two technical replicates per measurement. (n.d. = not detectable).

Cell Line	Met1v1		
	Mean MESF	STD (MESF)	STD in Percent [%]
T47D	n.d.	n.d.	n.d.
Du145	7,000	± 1,057	15.1
HT29	9,440	± 2,219	23.5
A549	37,224	± 6,878	18.5
H441	109,909	± 36,334	33.1
Hs746T	152,191	± 33,867	22.3
MKN45	698,653	± 40,066	5.7
Snu5	1,145,582	± 149,106	3.5
H1993	1,173,664	± 100,686	13.0

The initial cMET receptor quantitation was performed with a bispecific, cMET/Dig monovalent 1+1 format (Met1v1) based on following rationale: cMET dimerization is a well characterized biological process which occurs after stimulation by the hepatocyte growth factor (HGF)

(Birchmeier, Birchmeier, Gherardi, & Vande Woude, 2003; Comoglio, Giordano, & Trusolino, 2008; Maulik et al., 2002). Because bivalent antibody formats, such as the Met2v2, may bind only one dimerized receptor, imprecise quantitation data could be generated. To circumvent this, the MetFab1v1 was generated since this BsAb has only one cMET binding site.

Table 6.1.5 summarized the quantified cMET receptor levels of the selected cell line panel and the corresponding standard deviation (STD). Absolut receptor numbers are displayed as MESF values and the STD in percent. Quantification experiments for individual cell lines were performed at least in three biological replicates. The overall STD ranged between 3.5 to 33.1% whereas no correlation to $cMET^{low}$ or $cMET^{high}$ expressing cell lines could be observed. I suggested, that the obtained deviations were cell line-specific and not based on the technical procedure or the low cMET protein expression levels. For instance, the $cMET^{high}$ cell line H1993 exhibited a STD of 13% similar to DU145 at 15.1% which represented a $cMET^{low}$ cell line. The lowest receptor numbers were determined for DU145 with less than 10,000 receptors per cell whereas SNU-5 and H1993 showed the highest cMET levels with more than 1.1 million receptors per cell. For the $cMET^{negative}$ cell T47D no receptors could be detected supporting immunoblot analysis (Figure 6.1.1) and specificity of Met1v1. Comparing the cMET receptor values to table 6.1.1 (cMET gene count and mRNA) only weak correlations could be drawn. For example, the multiple gene amplifications of MKN45 and H1993 (8.96 and 10.64) were reflected by high receptor numbers at 700,000 and 1,170,000, respectively. However, Hs746T exhibits an 11-fold cMET amplification, being the highest gene count in the selected cell line panel, but only 150,000 receptors. Also $cMET^{negative}$ T47D was reported to have an average cMET gene count of 1.45 but showed no cMET receptor signal.

In summary, it was possible to quantify cMET receptor in a broad range of cMET expressing cell lines over three log scales. Highly reproducible data was obtained in which the observed error is most likely cell line-specific. In relation to gene count data and mRNA expression levels only a weak correlation can be draw.

6.1.17 Part II: Comparing the bivalent Met2v2 with Met1v1 in quantitation experiments

The use of detection antibodies which are bivalent, for the antigen to be quantified possess a significant disadvantage. Such antibodies are able to bind their antigen i.e. cell surface receptors in a mono- or bivalent fashion and thereby introduce error. Davis and colleagues demonstrated that mono- and bivalent binding influenced receptor quantitation experiments (Davis, Abrams, Iyer,

Hoffman, & Bishop, 1998). To investigate the quantitation accuracy between monovalent binders (Met1v1) and bivalent binders (Met2v2), the following quantitation experiment was performed with Met2v2.

Table 6.1.6 Comparison of cMET cell surface level quantification by Met2v2 and Met1v1. Nine cell lines were quantified at day 3. cMET receptor numbers and the corresponding STD are shown as MESF values and in percent. Met1v1 values of table 5.1.5 were included for data comparison and the factor of Met2v2 and Met1v1 was calculated. Flow cytometric experiments were performed at least in three biological replicates with two technical replicates per measurement. (n.d. = not detectable).

Cell Line	Met1v1	Met2v2			Factor
	Mean MESF	Mean MESF	STD (MESF)	STD in Percent [%]	Met2v2/ Met1v1
T47D	n.d.	n.d.	n.d.	n.d.	n.d.
Du145	7,000	11,211	± 2,009	17.9	1.6
HT29	9,440	15,460	± 1,898	12.3	1.6
A549	37,224	45,096	± 6,530	15.5	1.2
H441	109,909	137,252	± 42,899	31.3	1.2
Hs746T	152,191	235,601	± 5,958	2.3	1.5
MKN45	698,653	752,311	± 47,944	6.4	1.1
Snu5	1,145,582	1,417,397	± 91,892	6.5	1.2
H1993	1,173,664	1,188,770	± 11,388	0.1	1.0

Table 6.1.6 summarized the obtained quantitation data for Met2v2 including the STD in MESF values and in percent. The obtained error after Met2v2 quantification was comparable to Met1v1. Here, the highest STD was also found for H441 with 31.3% (For Met1v1 33.1%). The consistency of error for both data sets underlines the high reproducibility of the quantitation tool and suggests a cell line driven error, as assumed in the previous chapter.

All cell lines showed higher cMET levels in comparison to Met1v1 quantified cells. This observation can be explained by the binding properties of Met2v2. This antibody is able to either detect two cMET receptors, by binding one receptor with each Fab arm, or just one cMET receptor via single receptor binding. The resulting Met2v2/Met1v1 ratio ranged from 1.0 to 1.6 as calculated

in the last column of table 5.1.6. In theory, a bivalent (α-cMET receptor) antibody pool which binds in 50% of all events two receptors and in the remaining events single receptors would yield a factor of 1.5, in comparison to a monovalent binder. Pure monovalent binding would results in a ratio of two. I observed that $cMET^{high}$ expressing cell lines (>500,000 receptors) such as MKN45, SNU-5 and H1993 exhibited only minor differences in receptor numbers upon comparison to Met1v1 generated data. For these cell lines the Met2v2/Met1v1 factor ranged between 1.0 and 1.2. Conversely, the analysis of $cMET^{low}$ expressing cell lines (< 200,000 receptors) showed no such pattern but a Met2v2/Met1v1 ratio between 1.2 and 1.6 and thereby a significant difference in receptor numbers.

In summary, I could demonstrate the disadvantage of using bivalent detection antibodies in receptor quantitation studies for certain cell lines. Although high receptor expressing cell lines seemed not to be as susceptible as low expressing ones, the introduced binding options of Met2v2 (mono- or bivalent) led to inaccurate quantitation data. In fact, receptor amounts were altered 1.2- to 1.6-fold for cell lines exhibiting less than 200,000 receptors (in comparison to Met1v1 collected data). In conclusion, the use of bivalent (α-cMET receptor) detection antibodies introduced a huge error margin simply because mono- or bivalent binding properties cannot be predicted.

6.1.18 Part III: Improving Met1v1 by omitting the constant region

As described in chapter 6.1.7, the generated detection antibodies for this study were IgG based. Out of the five antibody classes (IgA, IgD, IgE, IgG, IgM) IgG represents the most prevalent class in serum and non-mucosal tissue. Since several decades IgG is known to be actively transferred during pregnancy from mother to fetus and thus to guarantee passive immunity (Brambell, 1966; Morphis & Gitlin, 1970). This highly specific transport mechanism is carried out by the so called FcRn receptor) (Simister & Rees, 1985; Simister & Mostov, 1989) and is found for example in syncytiotrophoblasts which transport IgG from maternal circulation to fetal capillaries (Leach et al., 1996; Simister, Story, Chen, & Hunt, 1996; Kristoffersen, 1996). FcRn is expressed in several organs and tissues whereas the main site of IgG transport is found to be in the vascular endothelium (Borvak et al., 1998; Ward, Zhou, Ghetie, & Ober, 2003). FcRn consists of an MHC-class-I structure and is able to bind the C_H2-C_H3 hinge region (Fc region) of an IgG molecule as described in the introduction (Leach et al., 1996; Rodewald, 1976; Simister & Rees, 1985; Simister & Mostov, 1989). In terms of accurate receptor quantitation, such binding of detection antibodies to FcRn

would result into false positive quantitation events. To investigate possible FcRn-Met1v1 interactions, the MetFab1v1 detection antibody was generated which lacks the C_H2-C_H3 hinge region as described in chapter 6.1.9. Both constructs (MetFab1v1, Met1v1) were engineered as 1+1 formats and should consist equal cMET binding properties.

Table 6.1.7 Comparison of cMET cell surface level quantification by Met1v1 and MetFab1v1. The listed cell lines were quantified at Day 3. cMET receptor numbers and the corresponding STD are shown as MESF values and in percent. To determine FcRn-Met1v1 interaction the data set of Met1v1 (Table 5.1.6) was included and the ratio to MetFab1v1 calculated. Flow cytometric experiments were performed at least in three biological replicates with two technical replicates per measurement. (n.d. = not detectable).

Cell Line	Met1v1	MetFab1v1			Factor
	Mean MESF	Mean MESF	STD (MESF)	STD in Percent [%]	Met1v1 / MetFab1v1
T47D	n.d.	n.d.	n.d.	n.d.	n.d.
Du145	7,000	5,511	± 1,180	21.4	1.3
HT29	9,440	9,139	± 2,339	25.6	1.0
A549	37,224	34,360	± 87	> 0.1	1.1
H441	109,909	109,270	± 39,611	36.2	1.0
Hs746T	152,191	150,603	± 24,984	16.6	1.0
MKN45	698,653	783,259	± 61,171	7.8	0.9
Snu5	1,145,582	1,226,230	± 129,951	10.6	0.9
H1993	1,173,664	1,178,566	± 40,577	3.4	1.0

Table 6.1.7 summarized the determined MESF values by MetFab1v1 and the corresponding STD in percent. With respect to data reproducibility, the STD was comparable to the data set of Met1v1 and Met2v2. The STD ranged between 1 and 36 percent. As anticipated in the previous two quantitation experiments (5.1.14-15), the observed error variations among cell lines are likely to be cell line-specific. This hypothesis is supported by considering STDs of H441 and MKN45. H441 exhibited the highest error in all three receptor quantitation set ups (33.1%, 31.3%, 36.2%) which was observed throughout the experimental series. On the other hand, cell lines such as MKN45 showed a very low STD error (5.7%, 6.4%, 7.8%) for the respective antibody constructs.

In general, the determined MESF values were very close to the dataset of Met1v1. This observation is also supported by calculating the Met1v1/MetFab1v1 ratio which ranged between 0.9 and 1.1 (except DU145 = 1.3 ratio). Ratios above 1 are obtained if Met1v1 measurement results in higher MESF values than MetFab1v1 quantitation. Such an increase can be explained, for example, by unspecific binding of Met1v1 to FcRn. However, upon data analysis no significant decrease in MESF values for MetFab1v1 quantified cells were observed except for DU145. This cell line showed a 1.3-fold increase in MESF values for Met1v1. Affymetrix analysis though, determined DU145 to be negative for FcRn mRNA (Data not shown). Considering affymetrix data, an FcRn-Met1v1 interaction as cause for increased and therefore unspecific cMET MESF values becomes rather unlikely.

In conclusion, it was not possible to demonstrate a higher cMET-specificity of MetFab1v1 over Met1v1 in the selected cell line panel. Upon comparison to previously established quantitation data of Met1v1, a Met1v1 to FcRn interaction could not be determined. As a result, FcRn interactions were either too low in numbers to alter cMET quantitation quality or simply not present. It is worth mentioning that the calculated STD for MetFab1v1 was similar to Met2v2 and Met1v1 for each cell line. Differences in reproducibility are therefore likely to be cell line-specific. Taking quantitation parts I, II and III together (Chapter 6.1.16-18), I established a 1+1 format based, highly reproducible cMET protein quantitation tool for nine cell lines that covers three logs of receptor numbers .

6.1.19 The FcRn - IgG interaction requires special physiological conditions

Based on the results of previous cMET quantitation experiments a possible FcRn-Met1v1 interaction was rather unlikely. In addition, the experiments were conducted at standard cell culture conditions with a pH between 7.2 and 7.4. To achieve high affinity binding between FcRn and IgG studies have shown that an acidic pH environment of > 6.5 is required whereas no binding occurs at a physiological pH of 7.4 (Jones & Waldmann, 1972; Rodewald, 1976; Simister & Rees, 1985). For this purpose I chose the colon derived adenocarcinoma cell line Colo205 which expresses cMET and contains in addition a four-fold FcRn gene amplification. The FcRn affymetrix value for Colo205 is over 950 (see for comparison Figure 6.1.1). With this experiment I sought to i) investigate the FcRn-Met1v1 interaction under optimal FcRn-Met1v1 binding conditions and to ii) evaluate quantitation results caused by this unspecific binding.

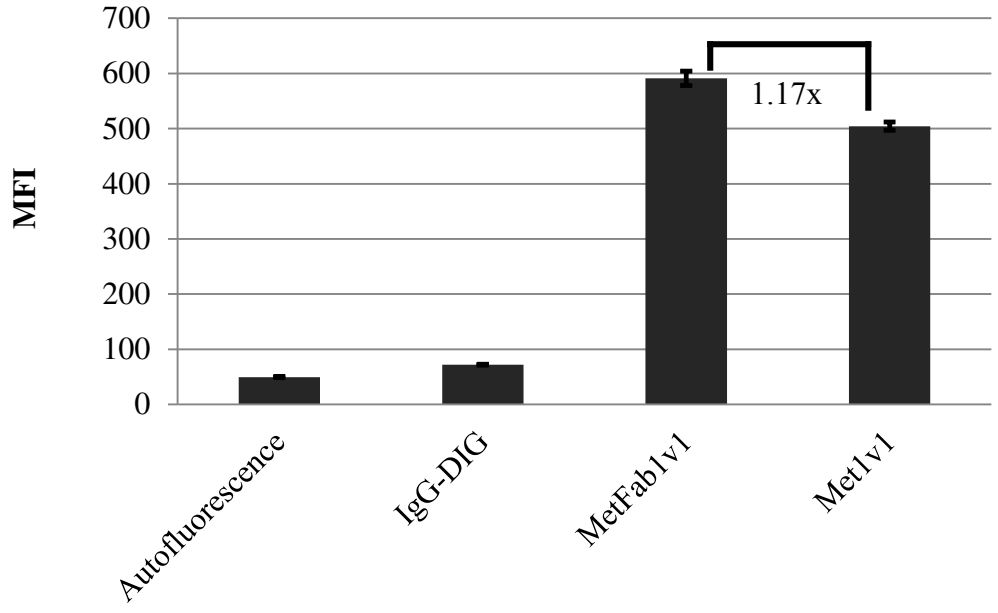

Figure 6.1.9 cMET quantitation in Colo205 at pH 6.1. Colo205 cells were quantified by Met1v1, MetFab1v1 which lacked the C_H2-C_H3 hinge region and IgG-DIG as control antibody. The experiment was conducted at a pH of 6.1 to facilitate FcRn- IgG interaction.

Figure 6.1.9 shows a simple cMET quantitation experiment for Colo205 at an acidic pH of 6.1. As control, the auto-fluorescence of Colo205 was assessed and the amount of bound IgG-Dig. In theory, under acidic conditions the control IgG-Dig antibodies would bind to FcRn in same ratios as Met1v1. Only MetFab1v1 does not interact with FcRn due to a lack of C_H2-C_H3 hinge region as described previously. The results in Figure 6.1.9 demonstrated relatively low MFI values by Met1v1 and MetFab1v1 which, in terms of MESF values, correspond to approximately 20,000 cMET receptors. Astonishingly, MetFab1v1 possessed a 1.17-fold increased MFI over Met1v1 quantified cells and not vice versa. The IgG-Dig control exhibited an MFI of only 20 and therefore it is close to background noise. Together with the observed Met1v1 and MetFab1v1 data FcRn interaction appeared unlikely even under optimized conditions.

In summary, a significant FcRn to IgG interaction which would alter specificity of cMET receptor quantitation could not be determined. Even under optimized pH condition and subsequent experiments (data not shown) such interaction was not obtained. In relation to the so far established receptor quantitation a possible interference by FcRn can be excluded. However, certain experimental questions might require the use of Fc-less Fab constructs as detection antibodies.

6.1.20 Generation of detection antibodies against tumor relevant targets HER2 and HER3

With the aim to demonstrate a broad application range of the established quantitation tool and to expand our analysis to other cell surface proteins, I chose HER2 and HER3 as prominent tumor targets. HER2, also known as ErbB2/neu is part of the epidermal growth factor receptor family and stimulates cell proliferation via the well characterized RAS-MAP kinase pathway (Olayioye, 2001; Hudis, 2007). Over 30% of all breast cancers exhibit a *HER2* gene amplification which is associated with a high recurrence rate and poor prognosis (Tan & Yu, 2007). Like HER2, HER3 (ErbB3) belongs to the family of RTKs but lacks an active kinase domain. To trigger receptor activation, heterodimerization with other EGF receptor family members is required which leads to cell proliferation and differentiation via the HER3/PI3K pathway (Guy, Platko, Cantley, Cerione, & Carraway, III, 1994; Yarden & Sliwkowski, 2001). HER3 is highly expressed in various cancer models (Sithanandam et al., 2003) and activation of the HER3/PI3K pathway correlates with malignant phenotypes of adenocarcinomas (Kobayashi, Iwamatsu, Shinohara-Kanda, Ihara, & Fukui, 2003). To enable HER2 and HER3 protein quantification, two additional Fab1v1 constructs were generated as illustrated in Figure 6.1.10.

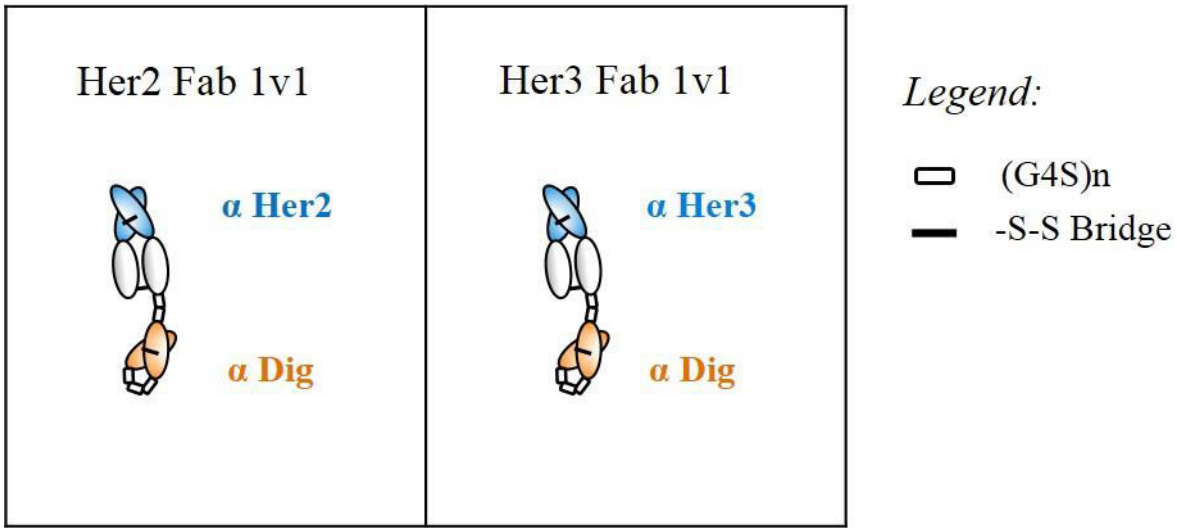

Figure 6.1.10 Proof of concept molecules based on BsAb technology to quantify the cell surface receptors HER2 and HER3. Schematic presentation BsAbs (variable regions is shaded) which are specific for distinct biological target (HER2, HER3) and DIG. Both constructs were engineered as Fab-scFv fusions omitting the C_H2-C_H3 hinge region.

Similar to MetFab1v1, the HER2/3-specific constructs Her2Fab1v1 and Her3Fab1v1 contained a Fab-scFv fusion lacking the constant Fc region. Hence, unspecific binding to FcRn was prevented. The engineered Fab1v1 constructs bound their target receptors HER2 and HER3 in a monovalent

fashion, as described previously (Lu et al., 2002). In summary, both proof of concept molecules were generated in mg quantities and at high homogeneity comparable to the cMET-specific BsAbs.

6.1.21 Quantitation of HER2 and HER3 protein levels on tumor cells

HER2 and HER3 receptor quantitation was performed in the same cell line panel as cMET. Cell lines were not changed since growth conditions, UWA and FACS settings were already determined and optimized for the respective cell line panel. In the first step, mRNA values were measured to evaluate HER2 and HER3 protein levels. The summarized results of HER2 and HER3 cell surface protein quantification and affymetrix analyses are shown in table 5.1.8 (HER2) and 5.1.9 (HER3), respectively. The STD of target receptors was presented as MESF and in percent.

Table 6.1.8 Flow cytometric quantitation of HER2 cell surface levels with Her2Fab1v1. HER2 mRNA levels were determined by affymetrix analysis including the respective STD. For HER2 protein quantification, cell lines were analyzed at Day 3. Absolute receptor numbers and the corresponding STD are shown as MESF values. In addition, the STD was also calculated in percent. Flow cytometric experiments were performed at least in three biological replicates with two technical replicates per measurement. (* H1993 was measured with method L8 instead of L4 as described in 5.2.6).

Cell Line	HER2				
			Her2Fab1v1		
	mRNA	STD	Mean MESF	STD (MESF)	STD Percent [%]
A549	139	± 12	6,230	± 1,163	18.7
Hs746T	161	± 3	7,610	± 888	11.7
DU145	229	± 4	11,066	± 997	9.0
HT29	364	± 32	22,354	± 3,113	13.9
MKN45	405	± 4	27,041	± 3,974	14.7
H1993*	139	± 13	29,231	± 1,355	4.6
SNU-5	n.d.	n.d.	31,752	± 3,322	10.5
T47D	565	± 23	32,637	± 6,762	20.7
H441	465	± 11	32,722	± 6,152	18.8

In reference to HER2 analysis of table 5.1.8, HER2 mRNA expression could be determined for all cell lines by affymetrix analysis. The signal intensity ranged from 139 to 465, which was of rather modest intensity. HER2 cell surface proteins were quantified and determined MESF values ranged between 6,230 and 32,722 (table 5.1.8). No correlation between mRNA and protein level could be observed. For instance, A549 and H1993 share the same HER2 mRNA quantity (Affymetrix = 139), whereas on protein level 6,230 and 29,230 receptors were determined for these cell lines. Similar to cMET quantitation experiments the overall reproducibility of HER2 quantitation was very good, which is reflected by the low STD ranging between 9.0 and 20.7%. Because cell lines were analyzed by one antibody construct (Her2Fab1v1) it was difficult to hypothesize about a cell line driven error. However, similar to the cMET data, H441 exhibited one of the highest STDs among the analyzed cell lines (18.8%).

Table 6.1.9 Flow cytometric quantitation of HER3 cell surface levels with Her3Fab1v1. Similar to HER2 analysis, at first HER3 mRNA levels were determined by affymetrix analysis. The corresponding STD was included. For HER3 protein quantification, cell lines were analyzed at Day 3 and the absolute receptor numbers and corresponding STDs are represented as MESF values. The STD was also calculated in percent. All flow cytometric experiments were performed at least in three biological replicates with two technical replicates per measurement. (* H1993 was measured with method L8 instead of L4 as described in 5.2.6).

Cell Line	HER3				
			Her3Fab1v1		
	mRNA	STD	Mean MESF	STD (MESF)	STD Percent [%]
Hs746T	1	± 3	900	± 326	36.0
A549	21	± 4	1,498	± 266	17.8
DU145	159	± 24	2,751	± 429	15.6
SNU-5	n.d.	n.d.	3,175	± 696	21.9
HT29	1,472	± 57	4,020	± 86	> 0.1
T47D	2,436	± 71	5,080	± 1,641	32.3
MKN45	1,473	± 30	7,403	± 1,310	17.7
H441	1,105	± 168	8,297	± 1,932	23.3
H1993*	163	± 5	8,482	± 450	5.3

The results of HER3 cell surface protein quantitation and mRNA analyses are shown in table 6.1.9. In comparison to HER2 mRNA levels, the obtained values for HER3 showed a broader distribution and ranged between 1 and 2,436. For example, A549 and Hs746T revealed almost no HER3 mRNA signal (1-21), whereas DU145 and H1993 exhibited rather modest expression levels (159-163) and the remaining cell lines over 1,100. HER3 receptor quantitation determined MESF levels between 900 and 8,500. The STD was similar to cMET and HER2 quantitation experiments and ranged between 0.1 and 23.3%, except for Hs476T (STD=32.3%) and T47D (STD=36.0%). Overall, less HER3 receptors could be quantified (900-8,400) for the selected cell lines in comparison to HER2 (6,200-32,700), although HER3 mRNA values were higher than HER2. For example, the affymetrix value of approximately 150 corresponded to 29,200 HER2 proteins but only 8,400 HER3 proteins.

Despite rather low mRNA levels of HER2 and HER3 in comparison to cMET, it was possible to quantify both surface receptors for the selected tumor cell lines. In contrast to cMET quantitation, with receptor values in the range of approximately 500,000 to 1,200,000 I could also demonstrate accurate quantitation for low receptor expressing cell lines as for HER2 (< 33,000) and HER3 (< 10,000) receptors. The obtained reproducibility was high and is reflected by small STDs. Correlation between mRNA and protein levels was weak underscoring the necessity to directly determine protein levels to be able to draw meaningful conclusions on the presence of protein on the cell surface. All in all, I could successfully demonstrate a broad application range (low-high receptor numbers) of the novel FACS-based receptor quantitation tool.

6.1.22 Improving the detection efficiency and range for low receptor expressing cell lines

Receptor quantification in cMET overexpressing cell lines such as H441, Hs746T, MKN45, SNU-5 and H1993, containing *cMET* gene amplifications, led to overall receptor numbers of 100,000 to 1,000,0000 (see table 6.1.5) (Beroukhim et al., 2010). Although it was possible to even quantify receptor numbers which were several logs smaller, such as the HER3 protein in A549 (~1,500 MESF), certain experimental conditions can require even a greater sensitivity. For instance:

i) The analysis of cell lines consisting of extremely low receptor numbers which fall below the MESF calibration curve.
ii) Dig coupled fluorophores possessing a weak quantum yield and therefore require a stronger signal.

Under these circumstances, the engineered 1+1 format might not be optimal and reach its detection limit. In response we generated a 1+2 format as illustrated in Figure 6.1.11. The construct was specific for HER2 and generated according to Her2Fab1v1. It contained two Dig-specific ScFv fusions at the C-terminus of the heavy and LC instead of one resulting into a 1+2 format. The monovalent Her2Fab1v2 is able to detect a single HER2 receptor while exhibiting two Dig binding sites and thus delivering a two-fold increased signal intensity.

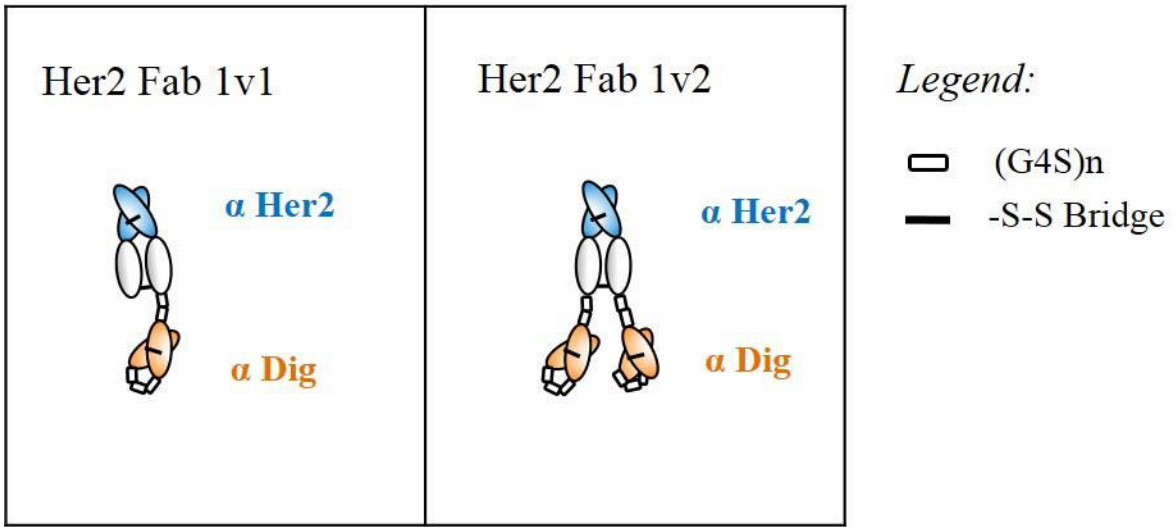

Figure 6.1.11 The proof of concept molecule Her2Fab1v2 represents a 1+2 format to quantify HER2 receptors. Schematic presentation BsAb (variable regions is shaded) which are specific for HER2. In contrast to Her2Fab1v1, the novel 1+2 format Her2Fab1v2 contains two Dig-specific ScFv fusions at the C-terminus of the heavy and light chain instead of one. The construct was engineered as Fab-scFv fusions omitting the C_H2-C_H3 hinge region.

I wondered whether the monitored number of molecules would increase in a linear fashion or whether the antibody would deliver a brighter fluorescent signal due to a shift in the detection limit. Based on the so far collected receptor quantitation experiments, the HER2 receptor was found to be an ideal target to investigate the novel format. HER2 cell surface protein was found to be expressed very low throughout all cell lines (6,200 to 32,700) in contrast to cMET for example (7,000 to 1,117,000 MESF). Similar to previously generated cMET, HER2 and HER3 antibody constructs, protein expression, purification and integrity of HER2Fab1v2 were comparable in quality and quantity (data not shown).

6.1.23 Her2Fab1v2 is able to increase the protein detection signal in a linear way

All cell lines were quantified by Her2Fab1v2 under previously established conditions. Table 6.1.10 summarizes and juxtaposes the generated Her2Fab1v2 and Her2Fab1v1 data. STD was presented in MESF and in percent. In the last column the ratio between both constructs is calculated. HER2 quantitation with HerFab1v2 showed to be highly reproducible. STDs between 3.7% and 25.3% were observed for the respective cell lines. The reproducibility was also similar and close to the standard which were observed by MetFab1v1 quantitation in table 5.1.5 (Except for HT29 with STD=23.5% and 3.7%). Since the amount of fluorophore binding entities was doubled for Her2Fab1v2, the ratio between Her2Fab1v1 and Her2Fab1v2 was of special interest. A ratio of two indicates a two-fold increase in fluorescence intensity at equal receptor binding numbers. Out

of nine cell lines the factor 2.0 was determined five times, a factor between 1.9 and 2.2 was calculated four times and only T47D exhibited a factor of 2.5. Because the Her2Fab1v1 determined HER2 receptor values for T47D and H411 were similar in numbers (32,600 and 32,700 MESF) but the ratio in comparison with Her2Fab1v2 different (2.5 and 2.0), I can therefore conclude that the fluorescence signal increased in a linear fashion and did not led to a shift in detection. Such a shift in detection and brighter fluorescence signal would have been observed systematically in all cell lines and not only in T47D. The ratio of 2.0 also demonstrated a precise Dig-Cy5 to antibody coupling supporting the fluorophore-Dig binding data of section 5.1.9.

Table 6.1.10 Flow cytometric quantitation of HER2 cell surface levels with Her2Fab1v2. For HER2 receptor quantification cell lines were analyzed at Day 3 post seeding. Non-normalized receptor numbers and corresponding STDs are represented as MESF values. The STD was also calculated in percent. In the last column the ratio between Her2Fab1v2 and Her2Fab1v1 was calculated. All flow cytometric experiments were performed at least in three biological replicates with two technical replicates per measurement. (*The determined MESF values were not corrected and normalized for the number of scFvs).

Cell Line	Her2Fab1v1	Her2Fab1v2			Factor
	Mean MESF	Mean MESF*	STD (MESF)	STD in Percent [%]	Her2Fab1v2/ Her2Fab1v1
A549	6,230	12,219	± 3,157	25.3	**2.0**
Hs746T	7,610	16,629	± 2,578	15.5	**2.1**
DU145	11,066	20,524	± 2,317	11.3	**1.9**
HT29	22,354	45,029	± 1,683	3.7	**2.0**
MKN45	27,041	53,227	± 4,559	8.6	**2.0**
H1993	29,231	59,036	± 4,358	7.4	**2.0**
SNU-5	31,752	72,193	± 8,871	12.3	**2.2**
T47D	32,637	80,677	± 14,938	18.5	**2.5**
H441	32,722	66,913	± 11,847	17.7	**2.0**

In summary, I observed a very good two-fold increase in MESF signal, except for T47D, if the values were not corrected for the number of scFvs. This finding confirmed a linear increase in the monitored signal if the number of fluorophores is doubled. As a result, this approach is feasible and will benefit for targets with even lower cell surface expression levels.

6.1.24 Part I of technology comparisons: Custom fluorophore labeling

To assess the full potential of the novel FACS-based receptor quantitation tool in relation to other quantitation techniques, three experimental approaches were followed (chapter 6.1.24-26). In the first approach, I compared the widely-used custom fluorophore labeling to our BsAb based quantitation method.

In custom fluorophore labeling, fluorescent moieties are covalently coupled to the antibody of interest. This technique was initially reported over 70 years ago by Coons and colleagues (Coons, Creech, Norman Jones, & Berliner, 1942; Coons & Kaplan, 1950). This widespread method of covalent binding is achieved via haptenylation of amino groups by N-hydroxysuccinimide esters (NHS-ES) (Pitt, Lindemeier, Habbes, & Veh, 1998) and is referred to lysine linker chemistry. Today, various haptens such as fluorophores, Dig, biotin but also enzymes are commercially available as already activated NHS-ES. Activated esters react with primary amino groups of the detection antibody and thereby introduce the hapten of interest. However, this technique can exhibit essential drawbacks. For instance, due to the presence of multiple primary amino groups which do also occur in the active binding site of antibodies, lysine linker chemistry can result into hapten conjugation that alters antigen binding properties or completely inactivates the antibody (Werthen & Nygren, 1988; McCormack, OKeeffe, MacCraith, & OKennedy, 1996).

As experimental system I chose the cMET^{high} cell lines MKN45 and H1993. Both cell lines revealed almost identical MESF values upon Met1v1 and Met2v2 quantitation with ratios between 1.0 and 1.1 (see table 5.1.6). Similar MESF values with different antibody constructs enabled further comparison options for the experimental setup. For custom fluorophore labeling the parental Met1v1 and Met2v2 antibodies were used and labeled with Cy5 via lysine linker chemistry. By this approach, all antibody species contained the same cMET antigen binding site but were coupled to Cy5 by different fluorophore labeling techniques. Thus, a direct comparison between both methods was possible. The parental antibodies did no carry additional scFvs and were termed MetAb1 (parental Ab of Met1v1) and MetAb2 (parental Ab of Met2v2). As described previously, custom fluorophore labeling required a normalization step which is needed to determine the average amount of fluorophores per antibody. The results were summarized in table 5.1.2. For MetAb1 and MetAb2 an F/P ratio of 0.87 and 0.37 was determined by SCB, respectively. The F/P ratio of 0.37, which was calculated for MetAb2, indicated an theoretical average of 0.38 Cy5 molecules per MetAb2.

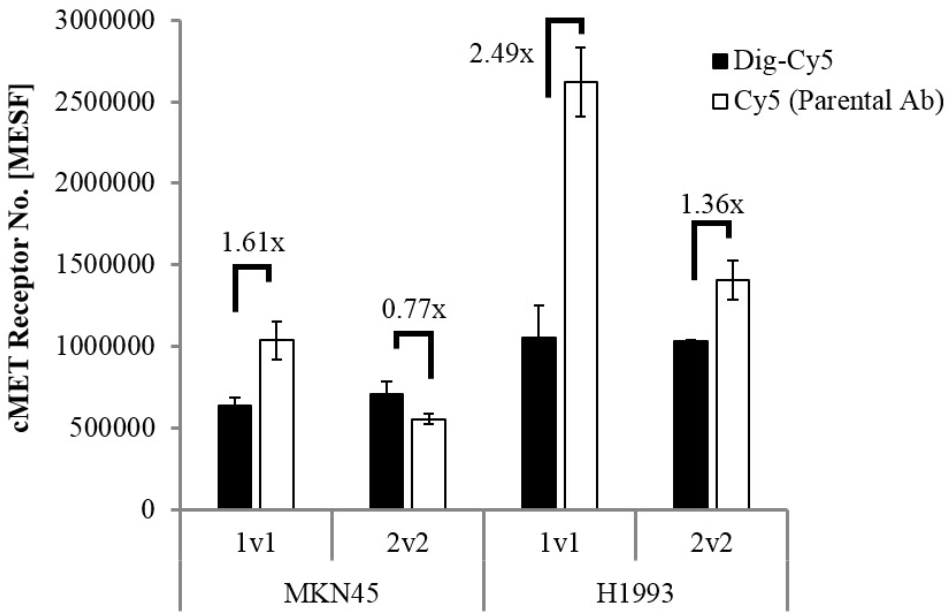

Figure 6.1.12 Comparison of BsAb Dig-Cy5 based receptor quantitation with custom fluorophore labeling. cMET receptor quantitation in MKN45 and H1993 with either Dig-Cy5 BsAbs (black bars) or lysine-coupled Cy5 mAbs (white bars). For custom fluorophore labeling the parental Met1v1 and Met2v2 BsAbs were used which lacked the scFvs and termed MetAb1 and MetAb2. (1v1 constructs: Met1v1 and MetAb1; 2v2 constructs: Met2v2 and MetAb2).

The set of custom labeled antibodies, together with Dig-Cy5 coupled BsAbs were used to quantify cMET protein levels in MKN45 and H1993. The results are shown in Figure 6.1.12. Black bars represented Dig-Cy5 BsAbs (Met1v1, Met2v2) and white bars custom Cy5 labeled antibodies (MetAb1, MetAb2). Significant differences between both quantitation methods could be observed. For example, a 2.5-fold increased MESF value was determined by MetAb1 in comparison to Met1v1 in H1993. In addition, bivalent MetAb2 detected less cMET protein than its monovalent MetAb1 counterpart for both cell lines. Based on the design and binding properties of the mono- and bivalent parental antibodies, such finding is unlikely to be true. On the other hand, our generated Met1v1 and Met2v2 led to similar receptor numbers for the respective cell lines as observed previously (Figure 6.1.5 and Figure 6.1.6). To some extent, the apparent differences between custom labeled antibodies MetAb1 and MetAb2 can be explained by the normalization step with SCB. As I demonstrated in previous experiments (chapter 6.1.6 table 6.1.3), SCB determined F/P ratios which were up to three-fold lower than the actual F/P ratio (F/P Met2v2 = 0.6) which was determined by Metz and colleagues (Metz et al., 2011).

In summary, I provided a consistent quantitation dataset which was generated by Dig-Cy5 BsAbs in contrast to custom labeled antibodies which displayed several discrepancies. In combination

with the obligatory normalization step, custom fluorophore labeling exhibited following disadvantages:

(i) The need of a normalization step after custom fluorophore labeling
(ii) A heterogeneous pool of labeled antibodies (F/P < 1)
(iii) The possibility of inactivated detection antibodies
(iv) Detection antibodies with altered binding properties

The obtained data clearly favored the use of Dig-Cy5 coupled BsAbs as quantitation method of choice upon comparison to custom fluorophore labeling.

6.1.25 Part II of technology comparisons: PE labeling

In the second approach to rank the novel FACS-based quantitation tool, I investigated PE labeled detection antibodies. This method circumvents several of the drawbacks in custom fluorophore labeling.

For this, I obtained commercially available PE labeled detection antibodies. These detection antibodies rely on the fluorophore PE which is covalently coupled to IgG via the reaction of maleimide groups to free sulfhydryl (Hardy, 1986). PE is of special interest in FACS analysis and represents one of the brightest dyes being used. This is partly due to its huge extinction coefficient ($\mathcal{E}$=1.96x10^6 cm^{-1} M^{-1}) and the excellent quantum efficiency (Quantum yield = 0.84). PE emits at 573 nm and is able to be excited by common argon lasers making it suitable for most FACS applications (van der Weij-De Wit CD et al., 2006). Based on its large size of 240 kDa, PE labeled antibodies are commonly coupled and purified in a 1 to 1 ratio whereas the overall antibody-fluorophore yield is reported to be poor (Pannu et al., 2001). Because of the known stoichiometry it is possible to quantify proteins which were detected by PE labeled antibodies with the help of QuantiBRITE standards and therefore to omit the otherwise necessary normalization step by SCB. Similar to Cy5 MESF reference standards, QuantiBRITE beads exhibit a defined number of reference molecules which are used as calibration standards. In summary, the quantitation of cell surface proteins via PE labeled antibodies is clearly favored over custom fluorophore labeling due to:

(i) A known antibody fluorophore ratio (Usually 1:1)
(ii) Precise and defined labeling of the antibody

(iii) Omission of the error-prone normalization step

(iv) The possibility to purify PE labeled antibodies based on their size.

To compare the generated Dig-Cy5 BsAbs to PE-based detection, commercially available anti-HER3-PE antibody was obtained (R&D Systems). As experimental system I chose the cell lines A549-B34, H441 and MDA-MB175 based on high HER3 mRNA (Affymetrix) and protein (Immunoblot analysis) expression levels. A549-B34 was genetically altered and stably overexpresses HER3. The cell lines were quantified by Her3Fab1v1 and by anti-HER3-PE detection antibodies in combination with QuantiBRITE. Figure 6.1.13 summarized the determined MESF values for HER3. For all three cell lines the HER3 cell surface receptor could be quantified and receptor numbers ranged between 5,700 and 11,900. In relation to the different quantitation methods, A549-B34 and H441 showed higher MESF values after HER3Fab1v1 quantitation in comparison to HER3-PE.

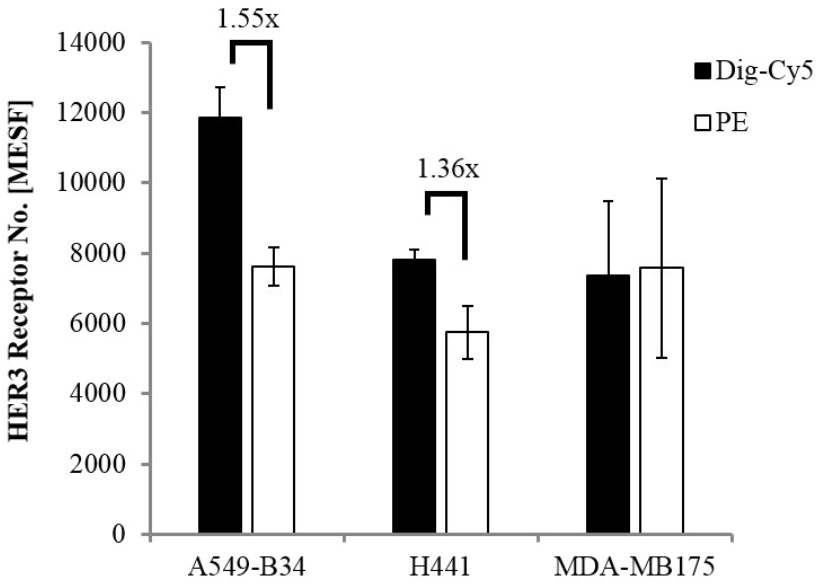

Figure 6.1.13 Comparison of BsAb Dig-Cy5 based receptor quantitation to PE-conjugated mAb based quantitation. HER3 receptor levels in A549-B34, H441 and MDA-MB175 were determined at day 3 by FACS analysis. Dig-Cy5 Her3Fab1v1 and anti HER3-PE antibody together with QuantiBRITE were assessed.

The ratio of the respective MESF values was approximately 1.5 and 1.3 for two of the cell lines and can be explained by the antibody formats. The observed differences displayed monovalent versus bivalent α-HER3 entities and support the circumstance of using high affinity monovalent binders such as the generated 1+1 formats i.e. Her3Fab1v1 instead of bivalent mAbs (See Figure 7.1). Similar ratios were also observed previously upon comparison of the monovalent cMET

binder Met1v1 to the bivalent Met2v2 antibody in table 6.1.6 yielding ratios between 1.0 and 1.6. For MDA-MB175 both methods determined similar HER3 receptor amounts of 7,400 and 7,600 MESF values. Interestingly, the STD for this cell line was significantly higher than in A549l-B34 or H441. Because the deviation was similar for both quantitation methods (33.6% and 28.5%), this finding supports the hypothesis of a cell line-specific error/variation in receptor numbers.

In summary, it was possible to quantify HER3 receptors in three cell lines by the use of Dig-Cy5 coupled BsAbs and by PE-conjugated mAbs. However, the Dig-Cy5 method showed to be more precise due to the monovalent nature of the used detection antibodies (1+1 format) in contrast to the bivalent PE-mAb (2+1). Keeping the different binding possibilities of PE-conjugated mAb in mind and normalizing the determined MESF values to monovalent binding (ratio ~ 1.5), very similar MESF values were obtained for both techniques. In addition, the obtained STDs were similar in range for both quantitation methods. The use of Dig-Cy5 coupled BsAb (1+1 format) was favored over bivalent PE-conjugated detection antibodies even though both quantitation techniques were similar in accuracy.

6.1.26 Part III of technology comparisons: Literature data on EGFR Receptor quantitation

The previous two chapters focused on common FACS-based receptor quantitation methods: i) Custom fluorophore labeling of detection antibodies and ii) the use of PE conjugated detection antibodies. It was possible to determine significant advantages of the designed Dig-Cy5 BsAbs over standard antibody formats and thus, to achieve a higher quantitation accuracy. However, the gold standard in receptor quantitation represents the so called radioligand binding assay which uses, for example, ^{125}I labeled EGF to detect EGF receptors. But also other techniques are used like the recently described real time detection device “Ligand Tracer” which uses kinetic extrapolation or short KEX, to determine receptor numbers (Barta, Bjorkelund, & Andersson, 2011). This chapter will focus on quantitation techniques which are not FACS-based and compare the Dig-Cy5 BsAb technology to available literate data. To facilitate inter-method comparison, I investigated the same surface receptor as the listed studies in table 6.1.11.

Table 6.1.11 Literature abstract of EGFR quantitation studies in A431. The table summarized EGFR quantitation studies corresponding STD in percent and the respective method(s) of quantitation. Overall, an EGFR receptor density of 1.5 to 3 million per A431 cell was determined. The last study listed, was performed within the scope of this dissertation and used Dig-Cy5 coupled BsAbs as detection tool.

Receptor Numbers x10^6	Standard Deviation	Literature	Method of Quantitation
2-3	n.d.	Fabricant *et. al*., 1977	Radio ligand binding assay: ^{125}I-EGF binds EGF-Receptor
2,6	n.d.	Haigler *et al*., 1978	Radio ligand binding assay: ^{125}I-EGF binds EGF-Receptor
2-3	n.d.	Wrann & Fox, 1979	Radio ligand binding assay: ^{125}I-EGF binds EGF-Receptor
2	n.d.	Adamson & Rees, 1981	Radio ligand binding assay: ^{125}I-EGF binds EGF-Receptor
2.4	30%	Buss, Kudlow, Lazar, & Gill, 1982	Radio ligand binding assay: ^{125}I-EGF binds EGF-Receptor
1,5	n.d.	Chatelier *et al*., 1986	FACS assay: Fluorescent EGF Ligand without calibration standard
3.6	n.d.	Kamata et al., 1986	Radio ligand binding assay: ^{125}I-EGF binds EGF-Receptor
0.5	n.d.	Lopez *et al*., 1992	FACS assay: Biotinylated mAb against EGFR in conjugation with streptavidin-bound fluorochrome. Quantum microbeads as standard
0.335 [1)] 3.15 [2)]	40% 47%	Brotherick *et al*., 1994	1) FACS assay: Conjugated mAb IgG2 against EGFR (Custom labeling) and Quantum simply Cellular beads standard 2) Radio ligand binding assay:^{125}I-EGF binds EGF-Receptor
2.1 [1)] 1.5 [2)]	17% 22%	Barta *et al*., 2011	1) Real time detection devive LigandTracer: KEX, ^{125}I-EGF and [^{125}I]-Cetuximab 2) Radio ligand binding assay: ^{125}I-EGF and [^{125}I]-Cetuximab
1.84 [1)] 1.65 [2)]	48% 26%	Novy *et al*., 2012	1) Real time detection device LigandTracer: KEX, ^{125}I-EGF and [^{125}I]-Cetuximab 2) Radio ligand binding assay: ^{125}I-EGF and [^{125}I]-Cetuximab
1.554	5.8%	Panke *et al*., 2013	FACS assay: BsAbs (Fab) binding target receptor and Dig-Cy5 in a monovalent fashion

Initial literature research revealed that several studies were performed to quantify EGFR which is also known as HER1/ErbB1. EGFR is of special interest in cancer therapy and belongs to the like named EGFR family of RTKs which consists of four members in total (EGFR, HER2, HER3 and HER4). Because EGFR family members regulate various physiological processes and participate in cell proliferation, apoptosis, cell motility, neovascularization they can play and essential role during cancerogenesis (Cheng et al., 2011; Normanno et al., 2006). EGFR overexpression or altered activation mechanisms lead to increased cell proliferation, invasion, metastasis formation and are often correlated to a poor prognosis for patients (Hirsch, Varella-Garcia, & Cappuzzo, 2009; Wang et al., 2009; Wang et al., 2007b). The overexpression of EGFR is found in various cancer cell lines such as in A431. This cell line was frequently quantified for EGFR protein levels in several studies (table 6.1.11). A431 was originally derived from a human epidermoid carcinoma and contains an unusually high density of EGF receptor numbers (Fabricant, De Larco, & Todaro, 1977; Haigler, Ash, Singer, & Cohen, 1978) and increased *EGFR* copy numbers (5.45) as Moroni and colleagues could demonstrate (Moroni et al., 2005).

Out of 12 studies listed in table 6.1.11, nine determined EGFR numbers either exclusively via radioligand binding assay or together with other quantitation methods. The radioligand binding assay was first introduced by Carpenter and colleagues 1975 and is still valid with only minor assay modifications (Carpenter, Lembach, Morrison, & Cohen, 1975). In this quantitation method, cells are exposed to ^{125}I labeled EGF (Gow & Wardlaw, 1975). Labeled mono-iodinated and di-iodinated EGF species are then separated by DEAE-cellulose chromatography. Carpenter and colleagues could demonstrate equivalent biological activities of ^{125}I labeled EGF to unlabeled EGF. In the next step, cells were incubated with ^{125}I labeled EGF in the presence or absence of excess unlabeled EGF to determine unspecific binding. Finally, Scatchard analysis was performed using varying amounts of ^{125}I EGF (Carpenter et al., 1975; Cohen, Carpenter, & King, Jr., 1980).

Beside radioligand binding assays and FACS-based quantitation assays, Barta and colleagues introduced 2011 a novel technique to quantify receptor numbers on cell lines (Barta et al., 2011). A real-time detection device termed LigandTracer (Ridgeview Instruments AB, Uppsala, Sweden) is able to measure ligand-receptor interaction and to apply interaction kinetic modeling. Kinetic modeling is also characterized as kinetic extrapolation or short KEX. Based on KEX, the device circumvents the requirement of receptor saturation leading to a reduced reagent consumption. Two

of the listed studies focused on the comparison between the novel KEX technique and radioligand binding.

Table 6.1.11 summarized EGFR quantitation results in A431 for 12 studies which were collected by FACS-based assays, radioligand binding, KEX and by the use Dig-Cy5 coupled BsAbs. The determined receptor numbers varied significantly among the different methods (inter-assay) but also within identical methods (intra-assay). Taken all studies together, 1.5 to 3 million EGF receptors were determined for A431. It is important to note, that less than half of the listed studies provided STDs for their quantitation results. Studies which did, determined STDs between 17 to 47% (Except Dig-Cy5 BsAbs with 5.8%).

Although most experiments were performed via the radioligand binding assay representing the gold standard in receptor quantitation, this method showed poor intra- and inter-assay reproducibility. The intra-assay reproducibility was reflected by STDs between 26% and 47% whereas five out of nine studies did not provide STDs. In relation to the reproducibility among different studies, the determined EGFR amounts vary between 1.6 to 3.6 million corresponding to an error of approximately 70%. Also the assay detection sensitivity showed to be poor and is in the range of hundred thousand receptors.

Three studies of table 6.1.11 were conducted by FACS-based assays using either i) fluorescent EGF ligands, ii) biotinylated mAbs against EGFR in combination with streptavidin bound fluorochromes or iii) custom labeled mAbs together with Quantum simply cellular beads. Only the study by Brotherick and colleagues, which used custom fluorophore labeled mAbs, provided a STD (40%) and an average of 0.335 million EGF receptors for A431 cells (Brotherick et al., 1994). The studies by Chatelier and colleagues and by Lopez and colleagues determined 1.5 and 0.5 million EGF receptors, respectively (Chatelier et al., 1986; Lopez et al., 1992). Similar to radioligand binding assays, both studies exhibited an overall assay sensitivity in the range of hundred thousand receptors.

Two recent studies used KEX technology to quantify EGFR and compared the gained data to radioligand binding assays (Barta et al., 2011; Novy, Barta, Mandikova, Laznicek, & Trejtnar, 2012). Here, 2.1 and 1.84 million EGF receptors were determined via KEX with a STD of 17% and 48%, respectively. Radioligand binding resulted in 1.5 and 1.65 million EGF receptors with a STD of 22% and 26%, respectively. Comparing KEX quantitation to the sum of radioligand

binding studies, the novel KEX technology exhibits a higher inter-assay reproducibility and also detection sensitivity. KEX enables to quantify down to hundred- to ten thousand receptors.

The final study listed in table 6.1.11 was performed with the FACS-based Dig-Cy5 BsAb technology. Similar to MetFab1v1 and Her2Fab1v1, we generated a Her1Fab1v1 detection antibody which lacked the C_H2-C_H3 hinge region and therefore enabled exclusive EGFR binding. According to the previously established assay conditions, EGFR was quantified in A431 by the monovalent Her1Fab1v1 (1+1 format). In three biological replicates 1.554 million EGF receptors were determined with a STD of 5.8%. As shown with my experiments (cMET, HER2 and HER3 quantitation) the assay detection sensitivity is in the range of ten thousand to thousand receptors. In comparison to KEX, radioligand binding assays and the three listed FACS studies, the use of Her1Fab1v1 detection antibodies showed highest intra-assay reproducibility and sensitivity.

In summary, EGFR quantitation studies based on radioligand binding assays exhibited the lowest reproducibility and sensitivity among the listed EGFR quantitation studies. Both, intra- and inter assay reproducibility was poor and most studies did neither provide a STD nor the amount of biological replicates which were performed. But also the three FACS-based assays (except Dig-Cy5 BsAbs) lacked reproducible results. Here, an average of 0.4 to 3.6 million EGF receptors per A431 cell was determined. However, the recently established KEX technology was able to improve receptor quantitation significantly. The obtained EGF receptor amounts varied between 1.84 and 2.1 million with an error of 48% and 17%, respectively. Also in terms of sensitivity the KEX technology was able to quantify down to the range of hundred to ten thousand receptors. Overall, the highest reproducibility and sensitivity was achieved by the use of Dig-Cy5 BsAbs (Her1Fab1v1). It was possible to determine in three biological replicates an average of 1.55 million EGF receptors with a STD of 5.8%. The assay detection-sensitivity was up to three logs higher than radioligand binding and was therefore able to quantify down to the range of ten thousand to thousand receptors. Taken together, I believe that these findings confirm that not just comparable but also more precise values can be obtained using Dig-Cy5 coupled BsAbs for receptor quantitation.

6.1.27 Visualizing Receptor Quantitation: Distribution of cMET on the surface of tumor cells

In the last experiment I tried to quantify cMET receptor numbers by confocal microscopy. Similar to FACS-based quantitation, a soluble MESF standard (Bangs Laboratories) was commercially

obtained. Quantitative confocal microscopy could be used, for instance, to determine receptor numbers in tissue samples of patients.

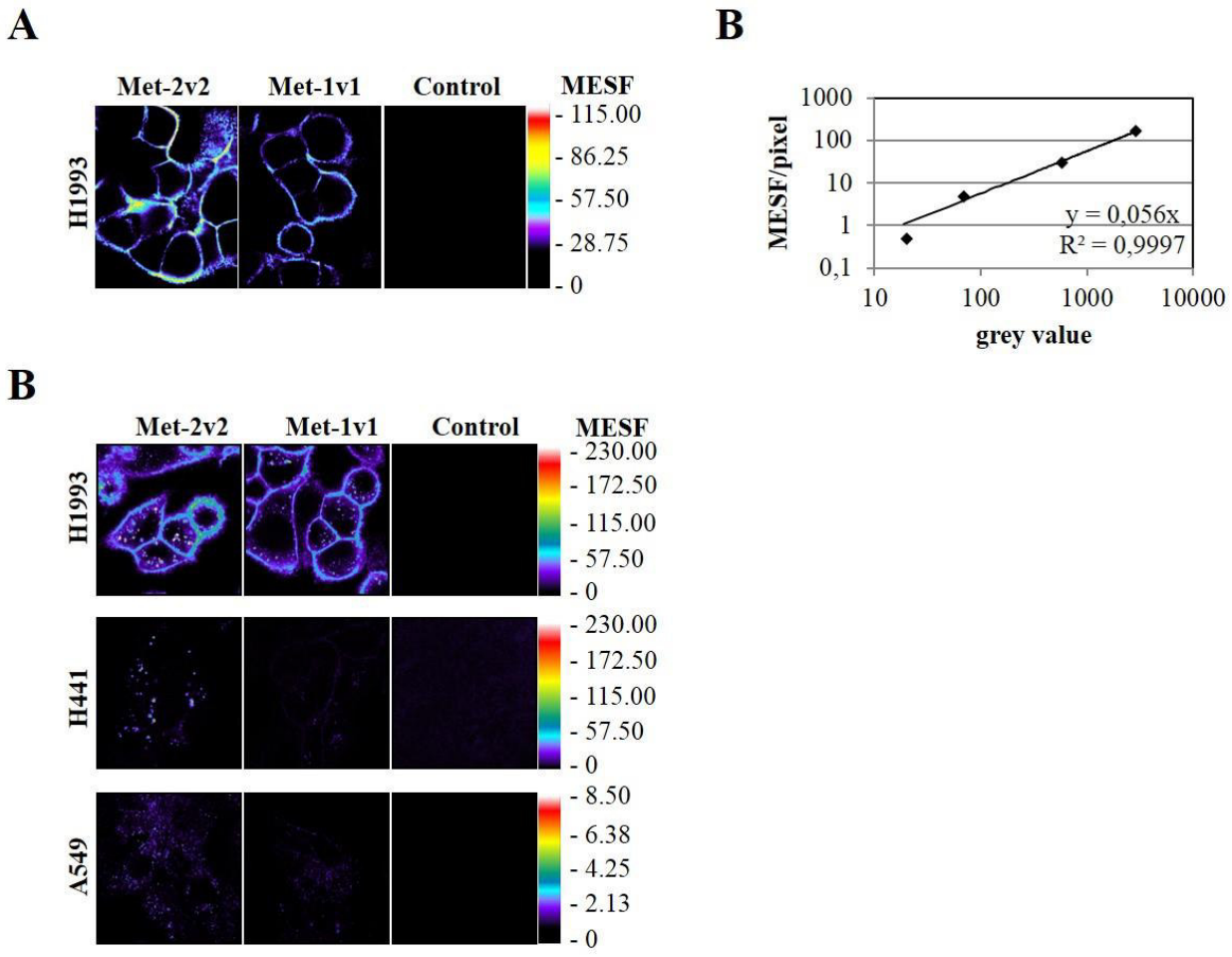

Figure 6.1.14 Visualization of the cMET receptor on tumor cells by confocal microscopy. (A) Analysis of cMET cell surface expression in H1993 with Met2v2, Met1v1 and a negative control. The cells were analyzed and stained at 4°C. (B) Grey value plot of defined Cy5 dye concentrations in solution. The measurements were taken at 10 µm distance from the coverglass surface. (C) Analysis of cMET cell surface expression in H1993, H441 and A549 cells. The cells were incubated for 1 hour at 37°C. Obtained signals for Met2v2 were corrected for the number of Dig binding scFv per antibody.

The BsAbs Met1v1 and Met2v2 were used for quantitative confocal microscopy analysis in conjunction with HyD. This method allowed us to infer the absolute number of labeled biomolecules at a subcellular level of resolution (Digman, Dalal, Horwitz, & Gratton, 2008)Leica Microsystems, 2012). In a first experiment, I incubated the cMET^{high} expressing cell line H1993 at 4°C with Met2v2 and Met1v1. Under these conditions, which were similar to the FACS-based

receptor quantitation, we observed in confocal microscopy a homogenous receptor expression on the cell surface (Figure 6.1.14A). The overall signal for Met1v1 was lower than for Met2v2 (As observed in FACS-based assays). To quantify the obtained signals, solutions of defined concentrations of Cy5 were analyzed in parallel and the resulting fluorescent signal was used to calculate the absolute concentration (for details see materials and methods). The signal was linear over a large log range and translated into a pseudocolor map representing the absolute concentrations (Figure 6.1.14B). In a second experiment, the bispecific antibodies were added at 37°C to three different cell lines with different expression levels of cMET (Figure 6.1.14C). The differences in staining intensity were clearly visible and correlated with the quantitation experiments. This method allowed the quantitative assessment of local concentrations of molecules of interest in subcellular domains at a high level of optical resolution afforded by high end confocal microscopy.

In summary, confocal quantitation was possible for the visible cellular structures and organelles - but not so easily achieved for the whole cell. At 37°C the BsAb significantly internalized which was visible as punctuate pattern corresponding to endosomes and lysosomal organelles.

6.2 Identifying tumor proliferation promoting Tetraspanins as target for BsAbs formats

The second part of this work will not concentrate on multispecific antibodies as a tool but focus on target assessment for such antibodies. Promising and tumor promoting molecules will be assessed in the light of providing data which could enables the generation of a novel, multispecific antibody against the determined targets.

The second part of this thesis sought to investigate Tspans on their potential proliferative effects in a panel of cancer cell lines. This yet relatively unexplored but in tumor progression implicated TM proteins represent promising targets in cancer therapy. The performed screen was carried out to identify novel targets to allow therapeutic antibody generation. As described previously, Tspans can organize into TEMs and thereby interact with a variety of other proteins such as growth factor receptors and act, most likely, as scaffolding factors. Beside single siRNA knock-down of individual Tspans I also combined Tspan knock-down with RTK targeting by therapeutic antibodies based on the interactions and cross-talk of Tspans with other RTKs.

6.2.1 Screening 33 Tetraspanins in 6 cell lines by siRNA knock down

I sought to determine anti-proliferative effects in cancer cells by down-regulating Tspans on mRNA level. For this purpose siRNA pools (each targeting one Tspan) were transfected into a panel of different cell lines to silence Tspan expression. Six cancer cell lines were investigated for anti-proliferative effects after the individual knockdown of 33 Tspans. Cell lines were chosen by three criteria: (i) similar tissue origin such as for A549, NCI-H322M and NCI-H596 all being derived from lung cancers, (ii) by different tissue origin such as BxPc3 (pancreas adenocarcinoma), HCT116 (colon carcinoma) and the respective lung cancer cell lines and (iii) the elevated expression of tumor relevant RTKs such as EGFR, HER2, HER3 and cMET receptors by affymetrix analysis. By this strategy I sought to investigate a broad spectrum for possible therapeutic applications and to cover the distinct biological functions of Tspans in different tissues and tumor related effects.

In respect to the experimental set-up the initial screening experiments were based on cell viability assays. A standard viability assay includes the seeding of a defined number of cells, siRNA transfection which targets individual Tspan mRNA and finally the addition of Cell Titer Glo (CTG) as readout to determine the relative numbers of viable cells. CTG is a metabolic assay in which

cells are lyzed. Only metabolically active and therefore viable cells are able to convert Luciferin (component of CTG) with the help of ATP and Luciferase to Oxyluciferin which results in luminescence. The more viable cells, the more ATP is present and therefore a higher luminescence can be detected by a luminometer.

6.2.2 The use of control siRNAs to determine transfection efficiencies and screening quality

A panel of different positive and negative siRNA controls was used during the screening process. As mock/scrambled siRNA, the commercially available Non Template Control (NTC) (ThermoFisher) was obtained. This negative control is composed of a pool of four single NTC siRNA species (1 to 4) similar to Tspan siRNA pools. As positive control, Eg5 and polo-like kinases 1 (PLK-1) siRNA were applied. Eg5, also known as kinesin-like protein KIF11, is known to play a role in cell motility and cell division by regulating spindle formation (Sawin, LeGuellec, Philippe, & Mitchison, 1992; Kashina, Scholey, Leszyk, & Saxton, 1996; Ferenz, Gable, & Wadsworth, 2010). Upon mRNA silencing, centrosome migration halts and cells arrest in mitosis. Due to genomic, transcriptional and biological heterogeneity between cancer cell lines, a second positive control was evaluated in form of PLK-1 siRNA. On cellular bases, PLK-1 helps to regulate cell cycle by activating CDK/cyclin complexes which mediate the G2/M-phase transition and represents a key positive regulator of mitosis, meiosis and cytokinesis (Lee, Yuan, Kuriyama, & Erikson, 1995; Glover, Hagan, & Tavares, 1998). PLK-1 knock-down results in growth inhibition and apoptosis in esophageal and prostate cancer cell lines (Bu, Yang, Li, & Song, 2008; Reagan-Shaw & Ahmad, 2005).

In summary, the use of NTC, Eg5 and PLK-1 enabled to determine the overall transfection efficiencies and the siRNA screening quality. To be able to evaluate individual Tspan knock-down efficiencies the screen relied on a potent positive control. To guarantee strong anti-proliferative effects I decided to run two positive control in parallel, Eg5 and PLK-1.

6.2.3 Optimization of siRNA transfection is essential to generate significant screening data

Before commencing the actual screening process, in which proliferation promoting Tspans were investigated, it was essential to optimize the two most sensitive parameters of the experimental set-up. These parameters were (i) the amount of cells per siRNA transfection and (ii) the identification of the experimental endpoint. Under optimal conditions, anti-proliferative effects can be assessed

in a broad experimental window (Δcell viability) between mock- and positive control- siRNA treated cells. This highly dynamic scenario is illustrated in Figure 6.2.1 which represents a theoretical set of experiments underlining the critical endpoint parameter.

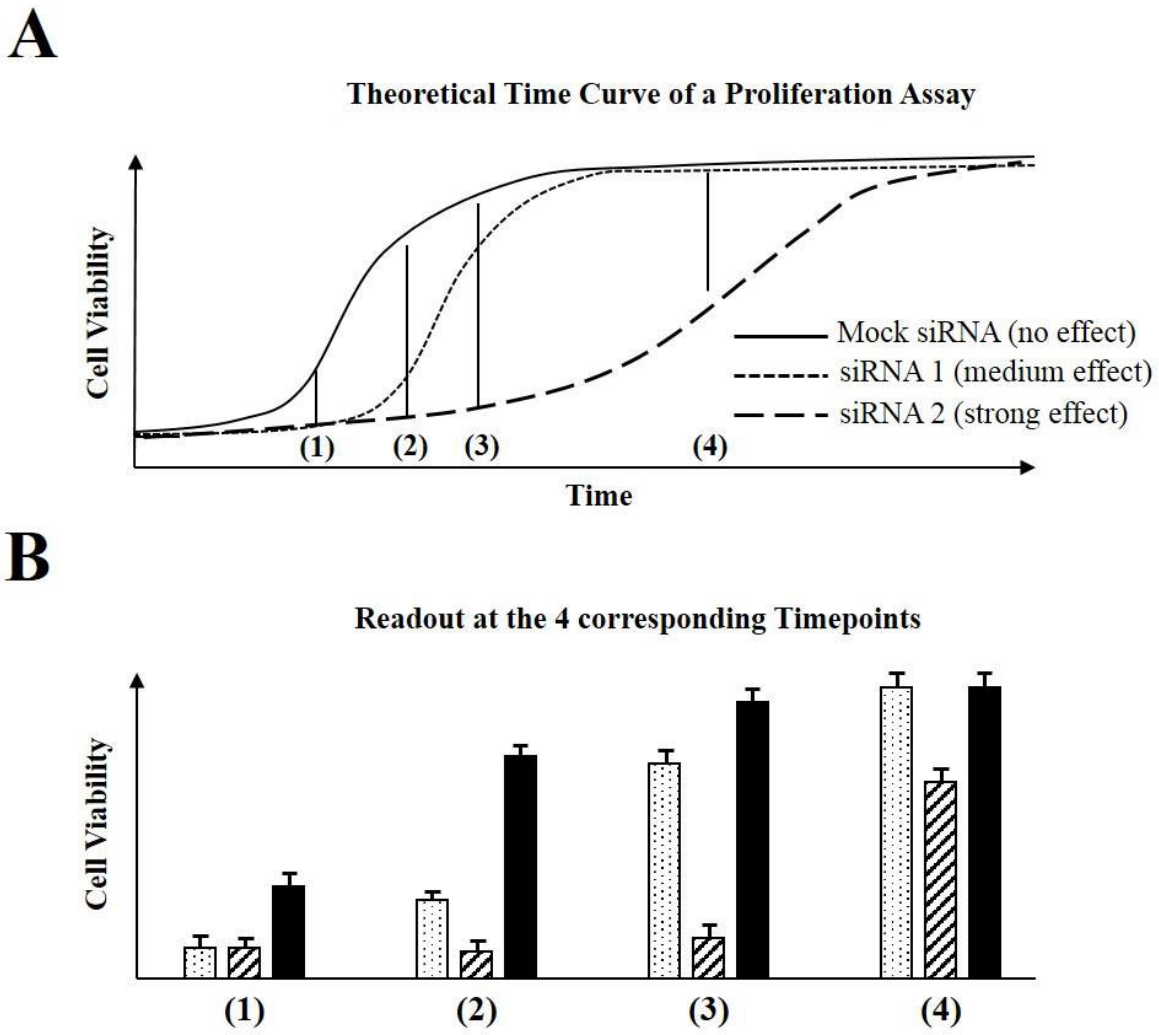

Figure 6.2.1 Theoretical transfection conditions: Determining the optimal endpoint of an siRNA transfection experiment. Exemplary growth curves and corresponding bar charts. (A) Theoretical growth curves of cells which are untreated and treated with two different siRNAs. Depending on the potency of the respective siRNA effect (medium strong; strong) different growth curves can be observed. Four possible experimental end-points are denoted (1-4). (B) Proliferation assay read-out of the four different end-points 1-4. Although the bars are derived from the same experiment this example emphasizes the importance of choosing an appropriate assay termination time-point. Time-point 2 results in the most significant data evaluation.

The three exemplary growth curves of Figure 6.2.1A represent one cell line which was treated by different siRNAs with distinct effects in cell viability. Cells were transfected with mock siRNA

(no effect), siRNA1 (medium effect) and siRNA2 (strong effect). The growth curves can be used to describe the assay's significance in relation to four different experimental endpoints (1-4). The endpoint is characterized by CTG treatment and subsequent data evaluation as shown in Figure 6.2.1B. Mock siRNA treated cells exhibit a standard cell growth pattern starting with an initial lag phase, followed by an exponential growth phase and finally a stationary phase. siRNA1 exhibits a medium strong anti-proliferative effect whereas siRNA2 shows a strong anti-proliferative effect leading to altered growth patterns. Depending on the time-point at which the experiment is stopped, different conclusions about the respective siRNA and thus the protein of interest can or cannot be made. It is noteworthy to mention, that the illustrated growth curves are unknown for the 33 investigated Tspans and that only one timepoint can be analyzed (as shown in Figure 6.2.1B). For instance, the assay stop at the earliest time-point 1 and the latest time-point 4 would suggest either similar anti-proliferative effects by siRNA1 and siRNA2 or no effects by siRNA2 as shown in the corresponding bar chart of Figure 6.2.1B. Stopping the experiment at time-point 3 would imply a strong siRNA1 effect but almost no anti-proliferative effects of siRNA2. In conclusion, termination of the siRNA experiment at timepoints 1, 3 and 4 would not reflect their actual anti-proliferative effects. However, before mock treated cells reach full confluency but are still growing 2, the stop of the experiment would conclude a strong anti-proliferative effect of siRNA1 and a medium strong effect of siRNA2.

In summary, the choice of the experimental endpoint represents a crucial parameter in determining actual anti-proliferative effects on the investigated siRNAs and thus on the protein of interest. A too early or late assay termination will result into misleading conclusions and the loss of medium strong effects. The optimal timepoint to stop the assay and perform CTG readout is just after the exponential growth phase and before reaching the stationary phase of mock treated cells. Cells which have not been successfully transfected will overgrow the remaining cell population by time and alter the assay outcome (i.e. timepoint 4).

6.2.4 The amount of cells per transfection correlates with the transfection efficiency

The second parameter which influences readout and data evaluation of a screening experiment represented the amount of cells per transfection. In the course of optimization studies it has been shown that cell numbers directly correlate with transfection efficiencies. Figure 6.2.2 exemplifies two representative proliferation assays of NCI-H596 cells that were seeded at different cell ratios

(10,000 and 20,000 cells per 96-well). The results were normalized to NTC (NTC= 100% cell viability) transfected cells. Both experimental runs were performed with the respective siRNA controls to draw conclusions about experimental conditions such as transfection efficiencies, toxicity of the transfection reagent and quality of control siRNAs. High transfection efficiencies will lead to massive cell death in cells which were treated by positive siRNA controls such as PLK-1 or Eg5. The window between positive siRNA controls and NTC treated cells represented the actual transfection efficiency.

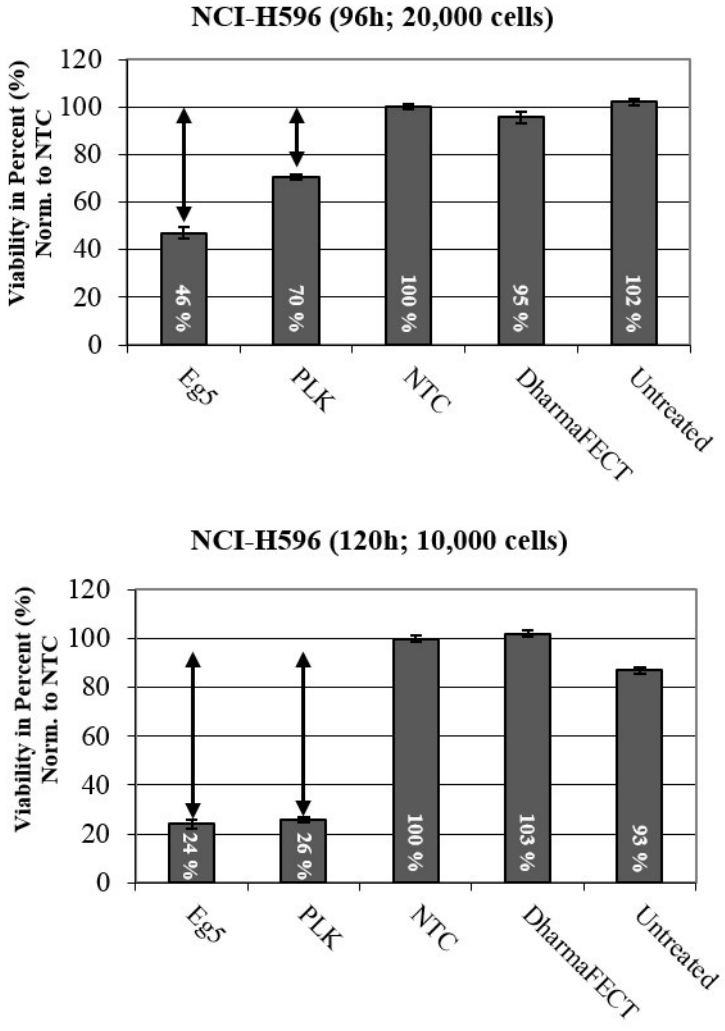

Figure 6.2.2 Optimization of siRNA transfection conditions. Two proliferation assays for NCI-H596 are shown. Cells were treated by a set of controls (positive controls: Eg5, PLK-1; negative controls: NTC, DharmaFECT, Untreated cells) to investigate assay conditions. Values were normalized to NTC=100%. For NCI-H596 the use of 20,000 cells per 96 well resulted in less pronounced transfection efficiencies in comparison to 10,000 cells. The use of lower cell numbers led to an approximately 75% window whereas the higher numbers to only to 30-50%.

The first proliferation assay in Figure 6.2.2 shows NCI-H596 which were seeded at 20,000 cells per 96-well and the experiment was stopped after 96 hours. The results indicated a drop in cell viability to 46% or 70% upon Eg5 and PLK-1 treatment, respectively. However, varying experimental conditions can increase the quality of the screen significantly. In the second proliferation assay 10,000 cells per 96-well were seeded and the assay was terminated after 120 hours. At these parameters cell viability dropped to 24% and 26% after Eg5 and PLK-1 treatment, respectively. Such decrease in cell seeding numbers led to higher transfection efficiencies. In consequence, the screening window was broader and less pronounced siRNA effects could be detected. Since DNA transfection reagents such as Lipofectamine 2000 are reported to exhibit cytotoxic effects (Zhong et al., 2008) the used siRNA transfection reagent DharmaFECT was also investigated. The proliferation assays in Figure 6.2.2 showed no anti-proliferative effects upon comparison between untreated cells and DharmaFECT treated cells. Both negative controls, NTC and DharmaFECT showed similar cell viabilities in comparison to untreated cells.

Concluding, the amount of seeded cells represented the second major parameter influencing transfection efficiencies and thus data generation. I could observe a direct correlation between the amount of cells and transfection efficiency; the lower the cell seeding ratio, the higher the transfection efficiency. Even though no anti-proliferative effects were observed for DharmaFECT reagent treated cells or by NTC, it is important to mention that every cell line may respond differently. The transfection optimization process which defined these respective parameters was performed for each cell line individually.

6.2.5 Tetraspanin screen as single siRNA- and combinatory siRNA-antibody treatment

After establishing optimal transfections conditions for each cell line the actual screening process was started. In general, two experimental approaches were designed to a) identify anti-proliferative effects upon individual Tspan mRNA knockdown and b) to determine possible synergistic effects caused by combining individual siRNA silencing with therapeutic antibody treatment. The first approach targeted exclusively individual Tspans whereas the second approach focused on a combinatory treatment of one Tspan and one RTK such as EGFR, HER2, HER3 or cMET.

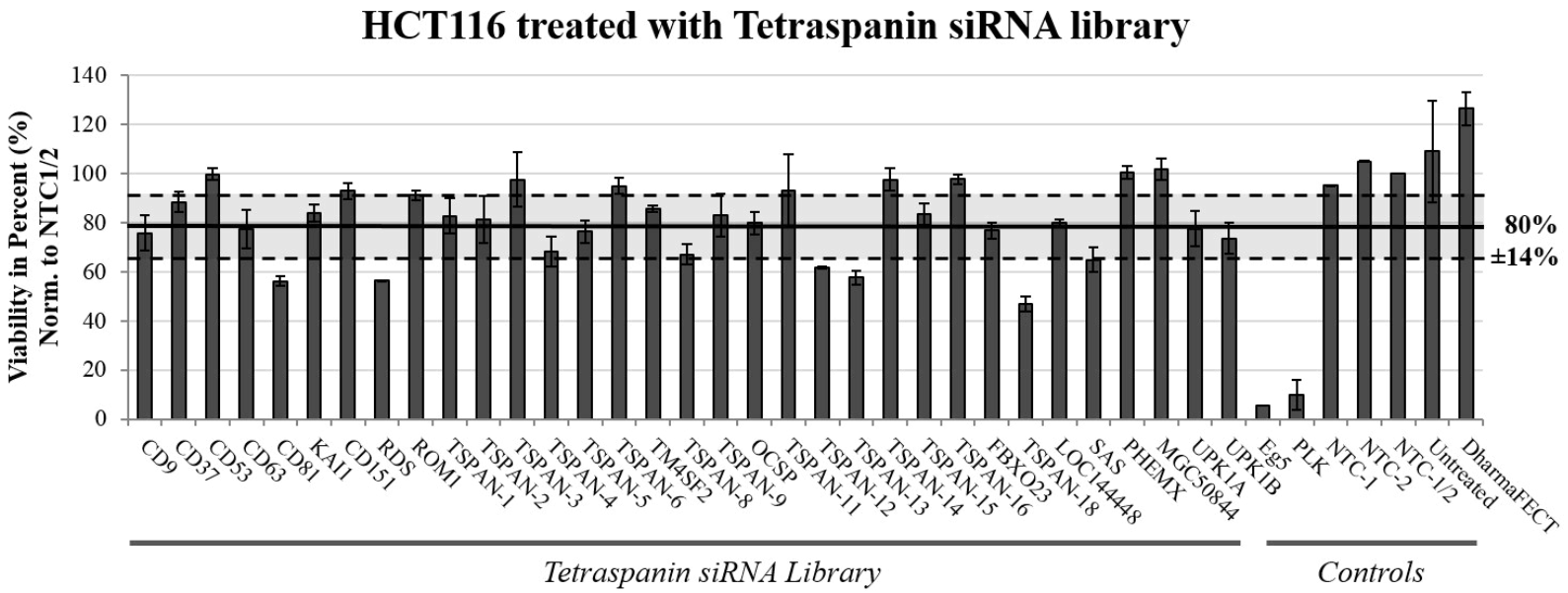

Figure 6.2.3 Representative screening example of HCT116 by the Tetraspanin siRNA library. The Figure illustrates a proliferation assay of HCT116 cells being transfected by individual Tspans of the siRNA library and the respective controls. All values were normalized to the NTC control and are shown in percent. To identify hits, the overall anti-proliferative effect of the library was averaged and only siRNAs which were stronger than the combination of average and STD considered as possible hits. For this dataset CD81 (Tspan 28), RDS (Tspan22), Tspan4, Tspan8, Tspan12, Tspan13, Tspan18 and SAS (Tspan31) were recorded as hits.

Figure 6.2.3 shows the results of one typical screening experiment that was performed. The CTG readout was categorized into two sections: Samples which were treated by the Tspan siRNA library and cells being treated by screening controls. CTG results for the lung cancer cell line HCT116 were converted into percent and normalized to the average of NTC1 and NTC2 (= 100% cell viability). In the given proliferation assay therapeutic antibodies were not combined. Positive controls Eg5 and PLK-1 showed a drop in cell viability down to 5-10% indicating a strong anti-proliferative effect and high transfection efficiencies whereas the NTC was similar to untreated cells. To evaluate promising Tspan hits the following procedure was applied: First, the average anti-proliferative effect of the combined siRNA screen was determined including the SD. Only siRNAs showing stronger effects and thus not being within the STD of the mean combined siRNA effect were considered as possible hits. For example, in Figure 6.2.3 the averaged anti-proliferative effect of each siRNA is approximately 20% with a STD of 14%. The calculation is highlighted by a line representing the mean and a dotted line representing the corresponding STD. Only samples which were below this STD window and exhibiting cell viability values below 66% were considered as possible hits. It is important to mention that the average siRNA library effect varied significantly between different cell lines. In the given example eight Tspan proteins were considered as possible hits for this experimental run (Tspan8, Tspan12, Tspan13, Tspan18, Tspan22 (RDS), Tspan28 (CD81) and Tspan31 (SAS)) whereas Tspan8 knock-down showed the strongest anti-proliferative with a cell viability drop to 33%. In this way, the data set of promising Tspan hits was determined for each screening experiment (single and combinatory treatment).

Based on the given experimental set up (6 cell lines, 33 Tspans, 4 therapeutic antibodies) a comprehensive data set was generated. To identify possible hits for further investigation I applied the described screening calculations for each screening run. In the next step of this study the gathered hits were summarized and evaluated.

6.2.6 Summarizing the screening results of 33 Tetraspanins in 6 cell lines

The screening summary and overview for 8 out of 33 Tspans is shown in table 6.2.1. Anti-proliferative effects were calculated in percent for the respective Tspans-cell line combination which were either treated alone (Tspan siRNA) or in combination (Tspan siRNA+ Ab).

Table 6.2.1 Exemplary screening summary of 8 out of 33 Tetraspanins in 6 cell lines. The table summarizes data evaluation of single siRNA treatment and the combinatory siRNA-antibody treatment. Possible hits are shaded in grey. The anti-proliferative effect in percent was calculated for each Tspan- cell line combination. The strongest effects ranged between 60 and 70% reduction in cell viability.

	BxPc3	A549	HT29	HCT116	NCI-H322M	NCI-H596
Tspan2	40%, 3% 37% +*αHer1 Ab* 35% +*Herceptin* 41% +*Pertuzumab* 37% +*αHer3 Ab*	9%, 12%, 13%	16%, 13%	19%, 10%	4%, 19%	17%, 31% 35% +*αHer1 Ab* 32% +*Pertuzumab* 36% +*αHer3 Ab*
Tspan4	15%, 6%	5%, 4%, 6%	7%, 6%	32%, 16% 45% +*αHer1 Ab* 53% +*Pertuzumab* 44% +*αHer3 Ab*	50%, 31% 61% +*Pertuzumab* 58% +*αHer3 Ab*	19%, 11%
Tspan5	10%, 5%	20%, 23%, 14% 15% +*αHer1 Ab* 20% +*Herceptin* 19% +*Pertuzumab* 28% +*αHer3 Ab*	11%, 4%	24%, 11%	35% 55% +*Pertuzumab*	1%, 0%
Tspan8	22%, 5%	23%, 22%, 17% 20% +*αHer1 Ab* 22% +*Pertuzumab* 31% +*αHer3 Ab*	11%, 25% 22% +*Her1 Ab*	33%, 24% 27% +*αHer1 Ab* 29% +*Herceptin* 37%, 23% +*Pertuzumab* 41% +*αHer3 Ab*	52%, 26% 47% +*Pertuzumab* 59% +*αHer3 Ab*	15 %, 9%
Tspan13	14%, 1%	13%, 12%,10%	10%, 19%	43%, 22% 27% +*αHer1 Ab* 27% +*Herceptin* 21% +*Pertuzumab* 44 +*αHer3 Ab*	28%, 23%	19%, 16% 34% +*Pertuzumab* 29% +*αHer3 Ab*
Tspan15	17%, 14%	15%, 16%, 9% 3% +*αHer1 Ab* 11% +*Pertuzumab* 32% +*αHer3 Ab*	9%, 10%	17%, 14% 46% +*αHer1 Ab*	32%, 21%	10%, 1%
Tspan22	39%, 16% 34% +*αHer1 Ab* 43% +*Pertuzumab* 41% +*αHer3 Ab*	27%,29%, 13% 36% +*αHer1 Ab* 34% +*Pertuzumab* 32% +*αHer3 Ab*	18%, 33% 25% +*αHer1 Ab* 8% +*Pertuzumab*	44%, 26% 66%, 28% +*αHer1 Ab* 35% +*Herceptin* 39%, 24% +*Pertuzumab* 49% +*αHer3 Ab*	9%, 17% 48% +*αHer3 Ab*	19%, 14% 28% +*αHer1 Ab* 30% +*αHer3 Ab*
Tspan32	22%, 15%	22%, 25%, 19% 18% +*αHer1 Ab* 21% +*Herceptin* 17% +*Pertuzumab* 29% +*αHer3 Ab*	0%, 6%	0%, 10%	10%, 4%	3%, 1%

For all single siRNA treatments at least two biological replicates were performed which are represented by two values (anti-proliferative effect in percent). Depending on whether the determined anti-proliferative effect was within the STD of the respective experiment or not, the box is shaded grey. Only grey shaded boxes represent possible “hits” according to the set criteria such as Tspan2 knockdown in BxPc3. In this example, the combinatory treatment with therapeutic antibodies was also found to lead to a significant anti-proliferative effect. The obtained effects differed between the respective Tspans and cell lines. For instance, Tspan32 showed exclusively in A549 a significant decrease in cell viability whereas Tspan22 in all six cell lines. Also differences between single and combinatory treatment were observed. Tspan15 exhibited a weak anti-proliferative effect in HCT116 after single siRNA treatment (~15%) but strong effects (~45%) upon combined siRNA and therapeutic Her1 antibody treatment.

Overall, the strongest anti-proliferative effects ranged between 60% and 70%. The data summary was conducted for all 33 Tspans and eight are shown exemplarily in table 6.2.1. Based on the generated data set, it was possible to determine potential hits and to continue with the next experimental steps. It is important to note that the determined hits, at this point of rge experimental series, did not undergo any kind of quality control yet and have therefore to be understood as potential targets. Such quality control will be described in the following chapter.

6.2.7 Investigation of Tetraspanin mRNA levels to evaluate screening results

After the initial screening process individual mRNA levels of the respective Tspans were quantified by RT-PCR. Quantification of Tspan mRNA levels helped drawing conclusions about previously determined hits of table 6.2.1 and identifying possible siRNA off target effects. After generating complementary DNA (cDNA) transcripts from mRNA the Universal ProbeLibrary System® (Roche) was applied to quantify mRNA expression levels. This system is based on 8-9 nucleotide short hydrolysis probes which are labeled at the 5' end with fluorescein and at the 3' end with a dark quencher dye. These probes hybridize in the amplicon region of the target sequence and, upon template replication, the probes fluorophore is cleaved by the polymerase 5´nuclease activity. Cleavage results in a fluorescence signal since the quencher dye is not in close proximity of the fluorophore any longer.

Table 6.2.2 mRNA analysis by RT-PCR for 8 Tetraspanins in 6 cell lines. The table shows for each Tspan- cell line combination two values. The first value represents the mean cycle number at which the Tspan, our gene of interest (GOI), appeared for the respective cell line. The second value represents the cycle number difference between the GOI and the mean housekeeping gene (HKG). For Tspan- cell line combinations showing ND (Not Determined) no mRNA signal for the respective Tspan was obtained. Grey shaded boxes refer to combinations which were determined as hits during the screening experiments.

	BxPc3	A549	HT29	HCT116	NCI-H322M	NCI-H596
RT-PCR	Mean: Cycle TSPAN Mean: 2 HKG - GOI	Mean: Cycle TSPAN Mean: 2 HKG - GOI	Mean: Cycle TSPAN Mean: 2 HKG - GOI	Mean: Cycle TSPAN Mean: 2 HKG - GOI	Mean: Cycle TSPAN Mean: 2 HKG - GOI	Mean: Cycle TSPAN Mean: 2 HKG - GOI
Tspan2	34.0 9.7	37.8 13.8	40 12.6	37.1 11.8	36.1 14.0	36.3 12
Tspan4	29.5 5.2	28.2 4.0	31.5 4.0	29.9 4.4	29.9 7.6	27.5 3.0
Tspan5	30.8 7.0	32.9 9.0	33.6 6.0	30.8 5.3	30.0 7.9	29.4 5.0
Tspan8	28.9 4.9	31.6 8.0	28.4 1.3	31.6 6.6	28.9 7.0	29.5 5.6
Tspan13	29.5 5.5	30.9 6.6	32.7 5.2	31.9 6.5	25.8 3.2	28.5 4.1
Tspan15	32.7 8.2	32.3 8.7	34.0 7.0	35.4 9.9	28.6 6.0	32.6 9.2
Tspan22	n.d.	n.d.	n.d.	n.d.	n.d.	n.d.
Tspan32	n.d.	n.d.	n.d.	n.d.	n.d.	n.d.

Fluorescence intensity is proportional to cleavage cycles and thus enables quantitative mRNA investigation (Freeman, Walker, & Vrana, 1999; Schmittgen et al., 2000). The obtained Cross-threshold (Ct) value correlates with the mRNA abundance of the respective target. Ct values higher than 35 cycles represent low mRNA levels whereas Ct values between 20 and 25 correlate with high mRNA levels (Wong & Medrano, 2005; Greenbaum, Colangelo, Williams, & Gerstein, 2003; Karlen, McNair, Perseguers, Mazza, & Mermod, 2007).

RT-PCR analysis was performed for the respective 33 Tspans in all cell lines. For comparison reasons and to evaluate the screening data, table 6.2.2 shows the results of RT-PCR analysis for the same eight Tspan as in table 6.2.1. Cell lines which were found to be negative for Tspan mRNA were labeled with not determined (n.d.). The remaining Tspan-cell line combinations display two values. The upper value represents the cycle at which the Ct was reached for the respective Tspan. In addition, each RT-PCR sample was also analyzed for the Ct cycle of two housekeeping genes (HKGs) (GapDH and Actin B). The average cycle difference between the Tspan mRNA Ct and both HKGs is indicated by the second value. For example, in BxPc3 the Ct cycle for Tspan2 was at 34.0. The averaged Ct of both HKG was 9.7 cycles earlier and thus at cycle 24.3. Grey shaded boxes represent the previously determined hits of table 6.2.1. The overall Tspan Ct value was between 26 and 36 except for Tspan22 and Tspan32 which exhibited no mRNA signals (n.d.). Averaged HKG Ct values were found to be between cycle 22 and 25 which is conform to the literature since HKGs are commonly expressed at high numbers (Turabelidze, Guo, & DiPietro, 2010). Ct values and therefore mRNA expression of Tspan2, Tspan4, Tspan5 and Tspan8 were very similar throughout all cell lines. Obtained Ct values varied only between two to three cycles. In contrast to that, Tspan13 and Tpsan15 showed higher mRNA expression variations (4-6 Cts) between the respective cell lines. Except Tspan22 and Tspan32, the remaining Tspans were found to be expressed in all cell lines and the highest mRNA value was determined for Tspan13 in NCI-H596 (Ct = 28.5) and Tspan8 in HT29 (Ct = 28.4) and NCI-H596 (Ct = 28.5).

Comparing the screening results of table 6.2.1 (proliferation assays) to the mRNA analysis in table 6.2.2 the following assumption could be made: It was possible to verify that Tspan2, 4, 5, 8, 13 and 15 mRNA were expressed in the respective hits and that the siRNA was able to reduce mRNA levels. However, it was not possible to determine Tspan22 and Tspan32 mRNA for any cell line although the transfection of the respective siRNAs led to hits (table 6.2.1). It is likely that previously determined hits for Tspan22 and Tspan32 were off-target related or . Especially

Tspan22 siRNA was found in every cell line to generate significant anti-proliferative effects even though no Tspan22 mRNA was present. With the datasets of the screening summary and RT-PCR analysis it was possible to narrow the initial number of Tspan hits down.

In summary, the first quality control to investigate the previously determined hits by proliferation assays was RT-PCR analysis. Upon comparing both data sets with each other inconsistencies were observed. Although certain Tspan siRNAs such as Tspan22 exhibited anti-proliferative effects, no mRNA expression could be verified in the respective cell lines. These findings are most likely due to off target effects and such hits were excluded.

6.2.8 Evaluation of the datasets leads to four promising Tetraspanin candidates

At this point of the experimental series the study focused on the evaluation of the screening and RT-PCR results. Figure 6.2.4 summarizes different criteria for Tspan hits which were need to be fulfilled for further investigation.

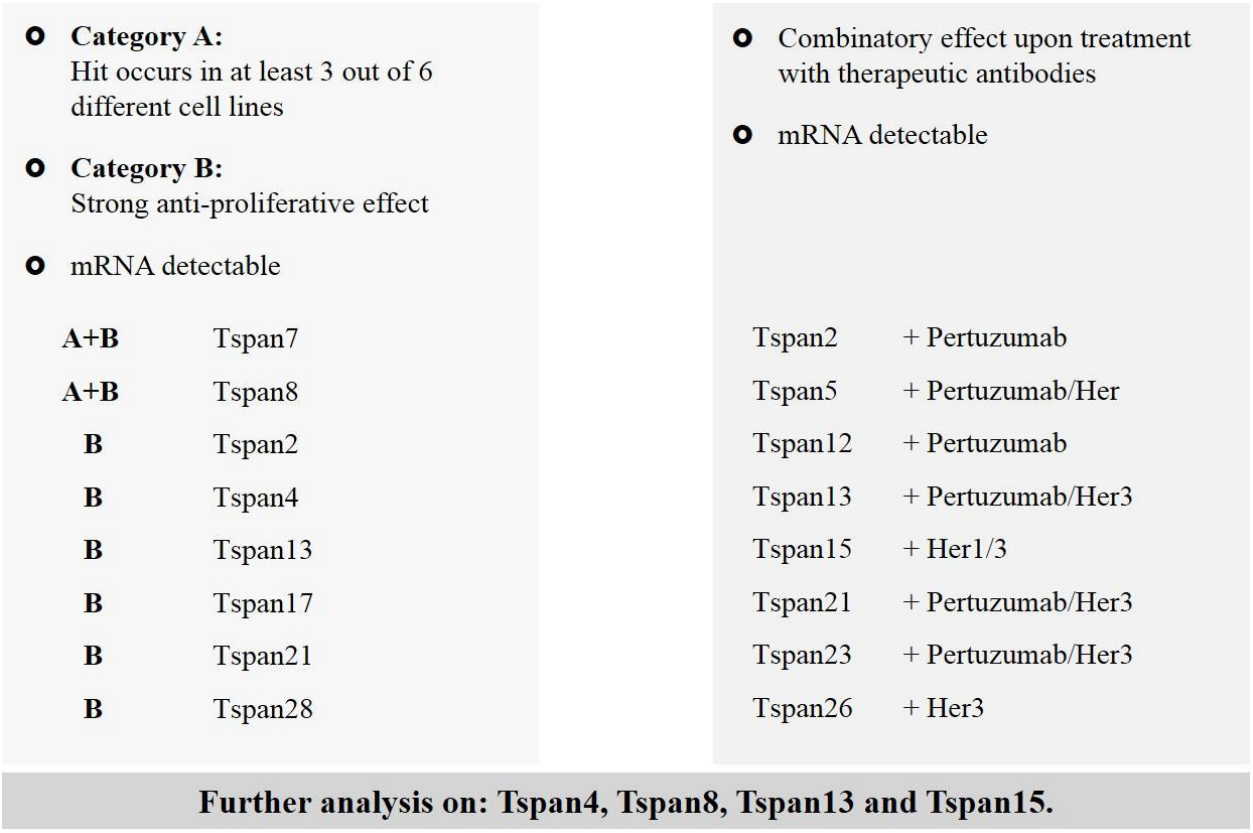

Figure 6.2.4 Categorization and evaluation of the most promising Tetraspanin hits. After proliferation and RT-PCR analysis the remaining hits were categorized according to (A) their occurrence in at least 3 out of 6 cell lines and (B) to very strong anti-proliferative effects (>60%). siRNA- antibody combinations which resulted into significant anti-proliferative effects were listed on the right side.

The overall prerequisite was the verification of mRNA presence for the respective Tspan. In order to determine the most promising set of hits, the Tspan dataset was categorized. The left box in Figure 6.2.4 classifies the hits into two categories: A) hits occurring in at least three out of six cell lines; B) hits exhibiting particularly strong anti-proliferative effects (30-60%). For example, Tspans such as Tspan7 and Tspan8 fell into both categories and were thus labeled with A+B. The right box summarizes all hits exhibiting a significant effect for the combinatory treatment with therapeutic antibodies. The predominant therapeutic antibody was Pertuzumab (six out of eight hits)

and Her3 targeting antibodies (five out of eight hits). Based on this categorization and data evaluation the project continued by focusing on the most promising hits: Tspan4, Tspan8, Tspan13 and Tspan15.

6.2.9 Reduction of siRNA amounts per transfection antagonizes off-target effects

In order to further increase siRNA derived data quality and to reduce possible off-target effects, the used siRNA pools were investigated in a titration experiment in HT29 and HCT116. Figure 6.2.5 shows the titration of Tspan8 and Tspan15 siRNA in HCT116. RT-PCR was used as readout and the resulting mRNA levels were normalized to the HKG Actin B whereas the mRNA levels of untreated cells (0 nM) were set to 1. Since the initial screening process was conducted at 100 nM the titration ranged from 1 nM to 100 nM. Both bar charts in Figure 6.2.5 revealed that the use of 10 to 100 nM concentrations for Tspan8 and Tspan15 siRNA resulted into a comparable mRNA silencing.

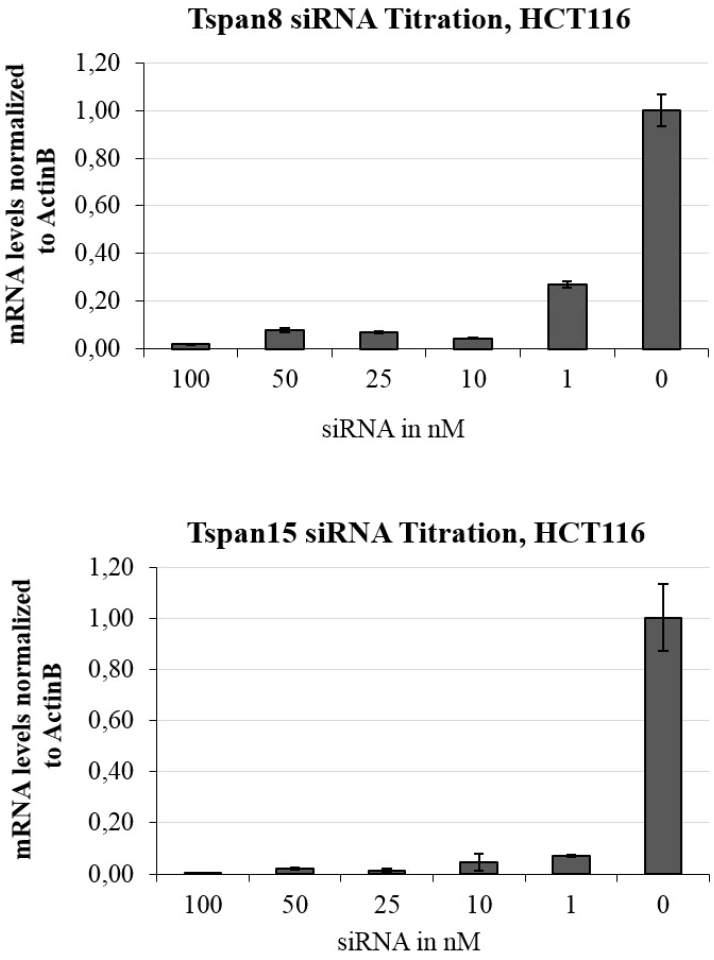

Figure 6.2.5. siRNA pool titration of Tspan8 and Tspan15 in HCT116. The results show RT-PCR analysis of HCT116 cells which were transfected by different siRNA amounts of Tspan8 and 15. mRNA levels were normalized to untreated cells and set to 1. As depicted, the original 100 nM siRNA concentration can be diluted up to 10 times without losing mRNA knock-down efficiency. In consequence, future siRNA experiments were conducted at 10 nM concentrations to reduce off-target effects.

This observation was also confirmed for Tspan4 and Tspan13 (Data not shown). In summary, following siRNA experiments were carried out at 10 nM siRNA concentrations per transfection to antagonize off target effects.

6.2.10 Transfection of Tetraspanin siRNA leads to morphological changes in HT29

Beside significant anti-proliferative effects, also morphological changes were observed in bright field analysis for HT29 after Tspan13 mRNA silencing. As described previously, Tspans play a significant role in orchestrating cell to cell contacts and are also known to maintain tissue integrity (Hemler, 2001; Zoller, 2009).

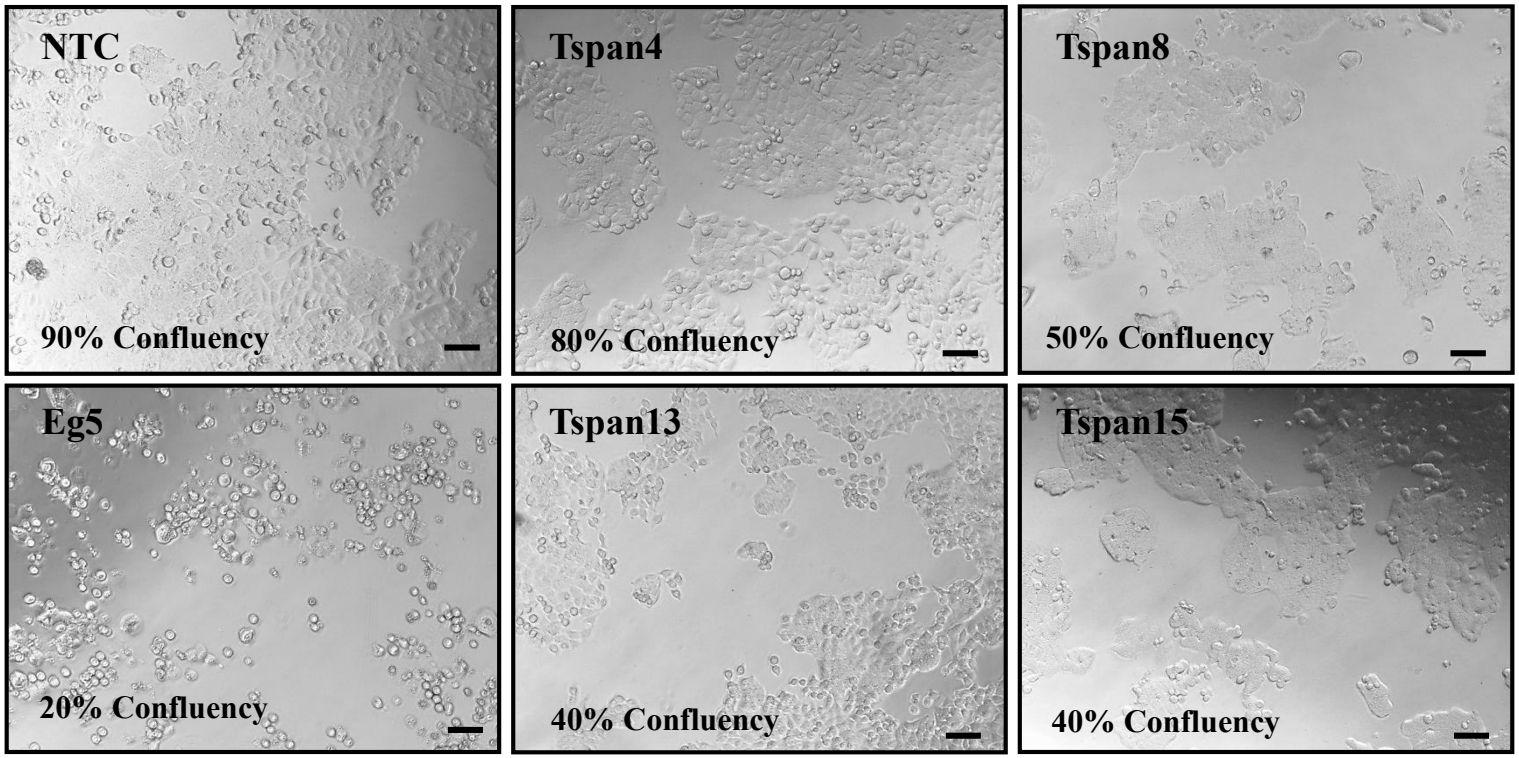

Figure 6.2.6 Morphological changes after Tetraspanin siRNA transfection in HT29. Bright field images were taken four days post siRNA transfection of Tspan4, Tspan8, Tspan13, Tspan15 and the controls NTC and Eg5 at a 100x magnification. In contrast to NTC control treated cells, Tspan8 and Tspan15 mRNA down-regulation leads to morphological changes such as the disappearance of cell borders and the fusion to cell clusters. Tspan4 is comparable to NTC whereas Tspan13 treated cells show a clear reduction in confluency (40%).

To further investigate these observations the screening experiment was repeated in a 6 well plate with HT29 and HCT116. Changes in morphology were only seen in HT29 cells. Figure 6.2.6 shows bright field images of HT29 which were treated by Tspan4, 8, 13 and 15 and the controls Eg5 and NTC at standard transfection conditions. Images were taken at a 100x magnification. NTC control treated cells consisted of approximately 90% confluency and single cell boarders were clearly visible. Cells which were treated with Eg5 siRNA exhibited signs of apoptotic behavior (i.e. rounding up) (Hacker, 2000), a significant drop in confluency (< 20%) and were not able to cluster (compare to NTC). Down-regulation of Tspan4 led to minor reduction in cell confluency (>80%) but no detectable change in cell morphology and single cells could still be distinguished. HT29 which were transfected with Tspan13 siRNA showed a more pronounced drop in confluency (>50%) emphasizing the anti-proliferative effect of Tspan13 mRNA silencing. For both siRNA treatments the morphology was still comparable to NTC. However, knockdown of Tspan8 and Tspan15 mRNA led not only to confluency levels below 50% but also to a clear change in cell morphology. Single cell borders could hardly be recognized and cells seemed to have fused with each other. It is important to mention that standard proliferation assays were not able to visualize/translate this effect.

In conclusion, I was able to observe distinct changes in cell morphology upon Tspan mRNA silencing. Such changes are reasonable based on the biological function of Tspans and will be further investigated in the next experimental setup. The so far performed 2D proliferation assays were suitable to display anti-proliferative effects but lacked the possibility to display morphological changes.

6.2.11 Morphological analysis by the use of the ACEA system

Based on previous findings in HT29 (Figure 6.2.6) Tspan silencing seemed to have an impact on cell morphology. To investigate the impact of Tspan down-regulation the Real-Time Label-Free Cellular Analysis (RTCA) system (ACEA Biosciences Inc.) was used.

The ACEA system is a cell-based assay which allows to monitor parameters such as cell viability, cell numbers, the degree of cell adhesion and cell morphology over a period of time in real-time. The device is composed of a cradle located in a cell culture incubator which holds 96-well microtiter E-Plates. These E-plates contain thin gold electrodes which measure the impedance of a given 96-well by applying an electrical field as illustrated in Figure 6.2.7.

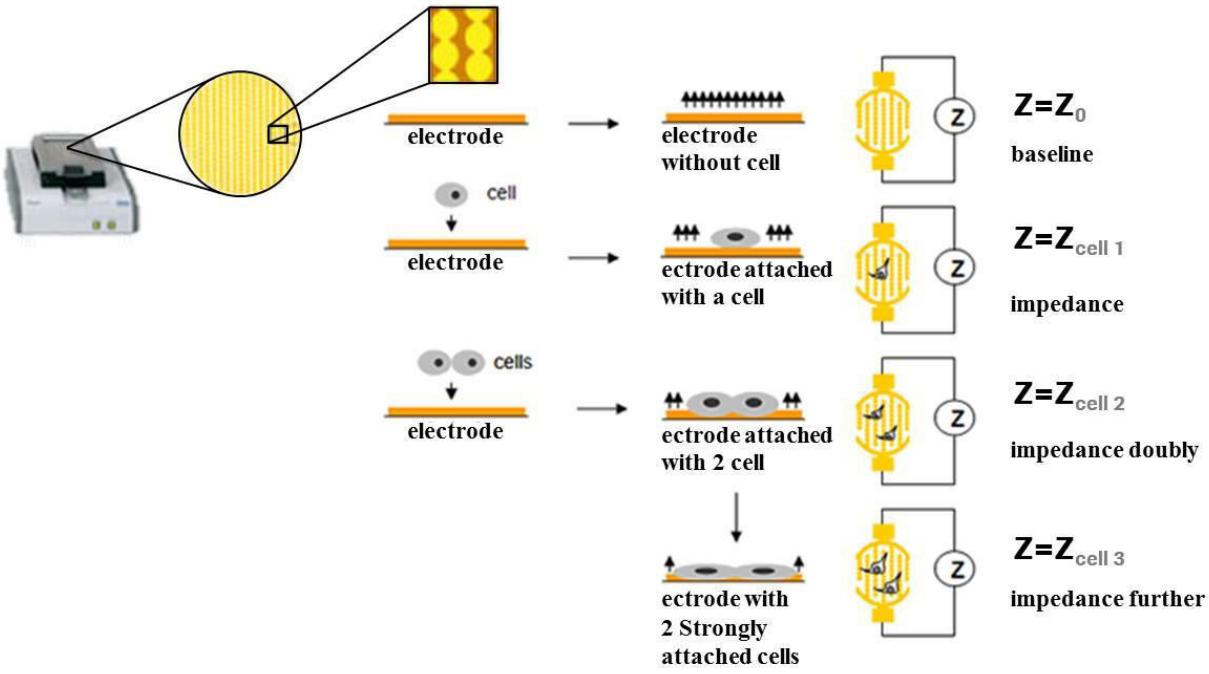

Figure 6.2.7 Working principle of the cell based ACEA system. The ACEA system consists of 96 well E-plates being covered with thin gold electrodes. The electrodes enable the impedance measurement at real time by applying an electrical field. The degree of impedance is correlated to the amount of cells which successfully attach to the E-plate.

The field is influenced by cell density and cell shape. Increased cell adhesion or cell growth will result in cell spreading which in turn leads to higher electrode impedance. The measured impedance is translated to cell index (CI) values. In order to use this system for siRNA experiments, transfection assays were optimized for the respective cell lines and device (e.g. timepoint of transfection, cell numbers). It was possible to establish siRNA transfections within the ACEA setting for the cell lines HT29 and HCT116.

6.2.12 ACEA analysis of siRNA treated HCT116 and HT29 cells

In Figure 6.2.8 the results of ACEA analysis and the corresponding standard proliferation assays were compared with each other. Both assays were performed simultaneously and terminated at the same time-point. HT29 and HCT116 were treated by Tspan4, 8, 13, 15 siRNA and the controls NTC and Eg5. HCT116 revealed a broad CI window (CI = 1.7) between NTC and Eg5 transfected cells (Figure 5.2.8A). The run was stopped 97h after siRNA transfection because NTC treated cells were about to enter lag phase. The strongest effect and thus lowest CI value was obtained in Tspan4

siRNA treated cells (CI = 0.9). A similar ratio was also observed in the corresponding CTG assay (Figure 6.2.8B) in which cell viability dropped down to 23% upon Tspan4 siRNA transfection.

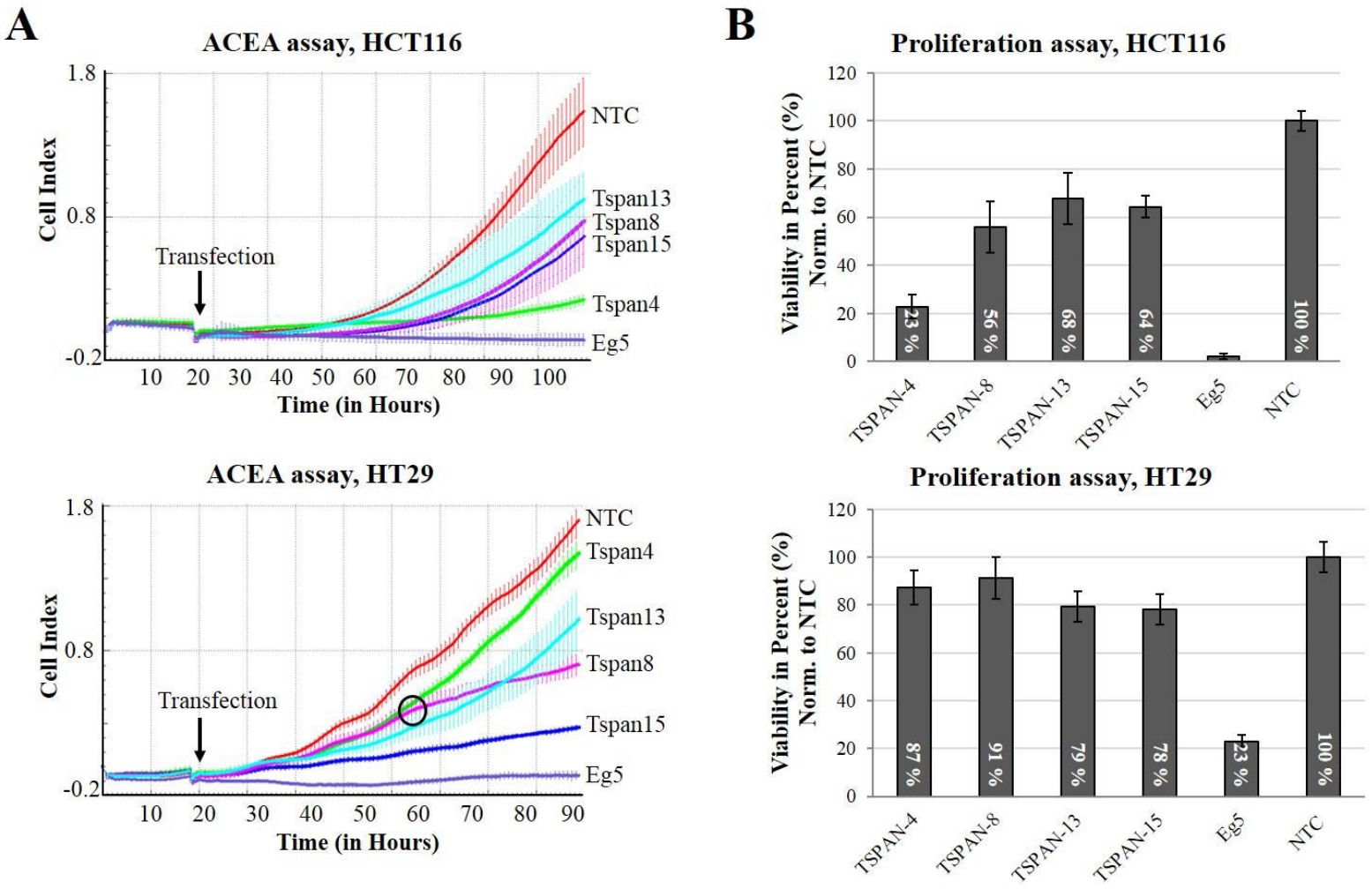

Figure 6.2.8 ACEA and proliferations assay analyses of HCT116 and HT29 after Tetraspanin mRNA knockdown. (A) ACEA data indicate the strongest morphological changes after Tspan4 and Tspan15 transfection for HCT116 and HT29, respectively. For HT29, Tspan8 treatment results in similar CI values as Tspan4 till 65h after seeding (Indicated by a circle). After this period the CI value drops. (B) At the end of the ACEA run cells were analyzed via a proliferation assay. The two datasets for HCT116 are comparable whereas HT29 does not show strong effects on proliferation level in contrast to the obtained ACEA data. The experiments points out the need of different methods to investigate the effects of Tspan knock-down.

Also Tspan8, 13 and 15 siRNA transfection in HCT116 were comparable in both readout systems. ACEA analysis of the respective Tspans led to approximately 50% of the NTC CI value whereas CTG analysis resulted into drops in proliferation and cell viability to approximately 60%. However, HT29 cells revealed a different result. For this cell line the ACEA experiment was stopped after 80h post siRNA treatment. NTC treated cells reached a CI of 1.7 units whereas the respective Tspan siRNAs lead to broadly distributed CI values of 0.2- 1.5 units. The lowest value was obtained for Tspan15 siRNA treated cells (CI = 0.2) whereas Tspan4 siRNA showed only minor effects (CI = 1.5) and was close to NTC (CI = 1.7). CIs for Tspan8 and Tspan13 were 0.7 and 1, respectively. Another observation can be made upon comparison of the growth curves between Tspan4 and Tspan8 treated cells. Even though both curves are identical till 60h after seeding, cells which were treated with Tspan8 siRNA suddenly ceased cell proliferation. This observation was seen in all biological replicates.

Comparing the gained HT29 ACEA data with the corresponding proliferation data, no correlation could be seen. Although both datasets for HCT116 resembled each other, the exclusive analysis of HT29 by a standard proliferation assay would not have revealed the morphological alterations caused by Tspan15 and Tspan8 siRNA. In fact, the proliferation data for HT29 showed only weak anti-proliferative effects between 9-22%. ACEA analysis instead could illustrate the significant effects caused by Tspan15 and Tspan8 silencing in HT29 on the CI value of these cells. Previously observed changes in morphology after bright field analysis could be confirmed by ACEA experiments.

Because initial screening data showed in some cases stronger anti-proliferative effects upon combined Tspan-Antibody treatment over single treatment, all combinations were investigated by the ACEA system. Similar to previous findings (HT29; Tspan8, Tspan15) the initial screening on CTG basis might have missed morphological effects of combinatory targeting. HCT116 and HT29 cells were transfected with the four respective Tspan siRNAs and were combined with either GA201 (αHer1), Herceptin (αHER2), Pertuzumab (αHER2), 205 (αHer3) or AK18 (αIGF1R). Unfortunately, except for the combination of Pertuzumab and Tspan15 in HCT116 no other combination showed changes in cell morphology and growth behavior. The ACEA analysis in which Tspan15 and the HER2 receptor were targeted is shown in Figure 6.2.9. NTC reached a CI value of 1.4 and the combination of NTC and TSPAN-15 1.3 units which indicated a very weak effect of Pertuzumab on HCT116. Single Tspan15 siRNA treatment resulted into a drop of the CI

value to 0.9 units (approximately 65% of NTC). However, combining Tspan15 siRNA and Pertuzumab treatment led to a strong drop from 1.4 to 0.3 CI units (approximately 20% of NTC).

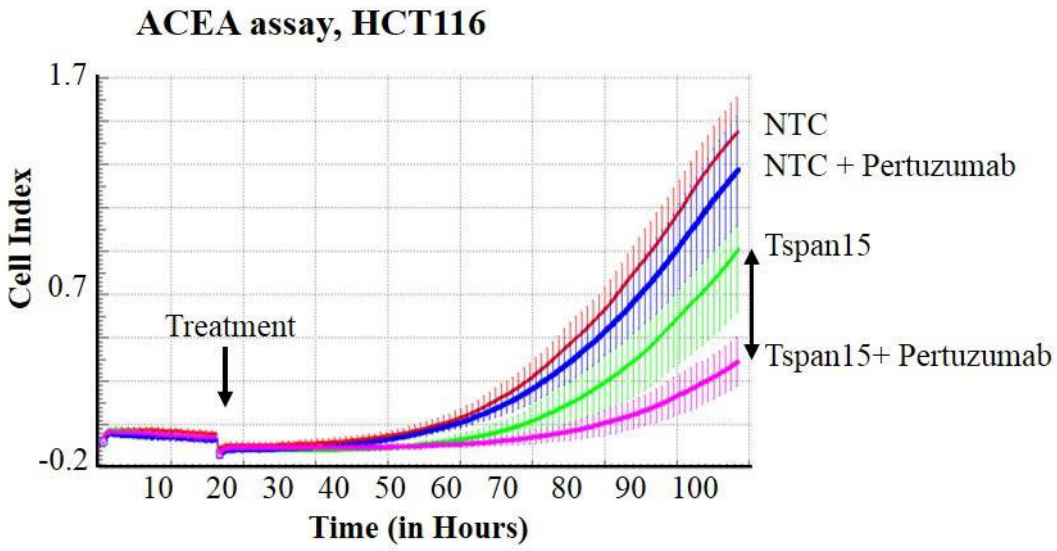

Figure 6.2.9 ACEA analyses in HCT116 after combinatory siRNA and antibody treatment. After screening all antibody- Tspan siRNA combinations on the ACEA platform only Pertuzumab and Tspan15 showed additive effects. Upon combining both treatments the CI value drops to 0.4 whereas Tspan15 to 0.8, Pertuzumab to 1.3 and NTC control treated cells to 1.5.

In summary, I could demonstrate that initial 2D proliferation analysis on CTG basis is not sufficient to display all effects of Tspan siRNA silencing but that it was suitable to determine reasonable targets for further investigation. The ACEA device could reveal morphological alterations in HT29 upon Tspan8 and Tspan15 silencing which were previously seen in bright field analysis.

6.2.13 Morphological changes in a three dimensional model system

Up to this point of the study all assays were performed as monolayer cultures and therefore 2D. However, 3D *in vitro* models can represent the more appropriate system to investigate tumor development and treatment. Studies have shown that 3D models can alter the molecular behavior of cells in comparison to conventional 2D systems (Shaw, Wrobel, & Brugge, 2004; Lee, Kenny, Lee, & Bissell, 2007). For example HER2 receptors are more frequently activated in 3D systems such in the spheroid model resulting into increased response to the monoclonal antibody Herceptin (Pickl & Ries, 2009).

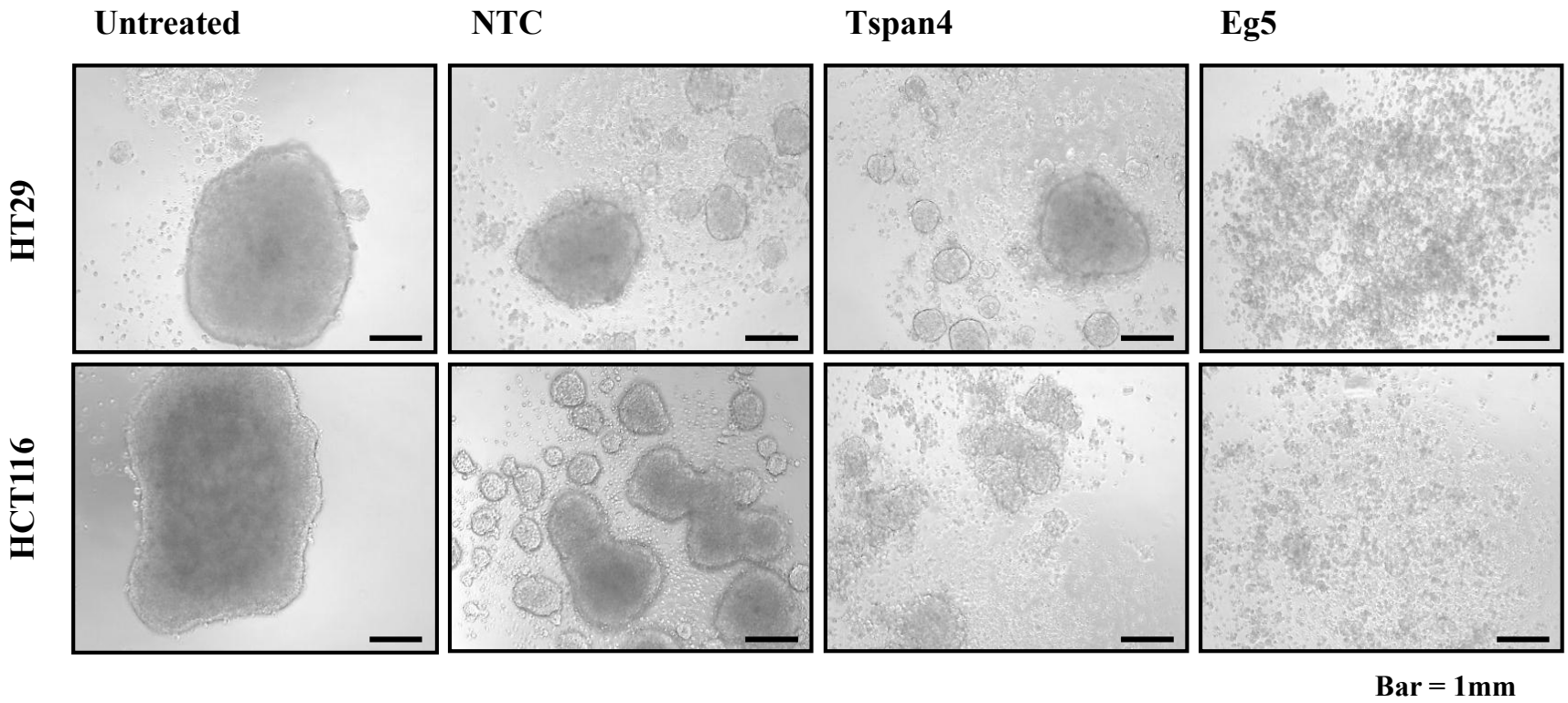

Figure 6.2.10 Establishing a three dimensional model system on PolyHema bases to investigate Tetraspanin down-regulation. Bright field images of HT29 and HCT116 cells are shown which were grown on PolyHema coated plates and treated by NTC, Tspan4 and Eg5 siRNA. Magnification = 100x. As depicted, both cell lines are able to form spheres under such conditions (Untreated cells) and also upon NTC siRNA treatment. Tspan4 treatment led to massive cell death in HCT116 and reduced sphere formation in comparison to NTC treated cells. Positive control siRNA treatment with Eg5 resulted into no sphere formation but cell death.

Due to the role of Tspans in cell to cell contact, adhesion and proliferation (Hemler, 2005; Zoller, 2009) the following experimental series was performed in a spheroid model system: Conventional cell culture plates were covered by polyHEMA which prevented cell attachment to the culture vessel and forced the formation of spheroids.

Before investigating the impact of Tspan down-regulation in this spheroid model, the system had to be optimized for siRNA transfections. As shown in Figure 6.2.10 the assay was successfully established for the cell lines HCT116 and HT29. Unfortunately, the remaining cell lines were not able survive in the 3D environment or the siRNA transfections itself were too stressful in this setting. Bright field analysis in Figure 6.2.10 shows that untreated cells were able to form large spheroids whereas Eg5 transfected cells showed no cluster formation but only single cells. In 2D transfection experiments it was possible to perform a washing step 24h post transfection in order to remove the siRNA transfection reagent and thus to minimize cell stress. Because in 3D assays this washing step could not be performed the transfection reagent remained which explains the differences in spheroid formation between untreated and NTC treated cells. Even though spheroids were formed, the observed cell aggregations for HT29 and HCT116 were smaller for NTC treated cells over untreated cells. Transfection of Tspan4 siRNA in HCT116 led to massive cell death and no cluster formation. Knockdown of Tspan4 prevented spheroid formation and was comparable to Eg5 treatment.

6.2.14 3D analysis reveals strong anti-proliferative effects by Tspan4 and Tspan15 siRNA

After optimizing 3D system conditions for HT29 and HCT116, cells were treated with the respective Tspan siRNAs. Figure 6.2.11 shows two representative proliferation assays for both cell lines. The anti-proliferative effects in HCT116 were strong and ranged between 40 to 60% in comparison to NTC. Strongest inhibition was caused by Tspan4 siRNA leading to a 60% cell growth inhibition. Comparing 3D results to initial 2D screening led to similar but more pronounced effects in 3D analysis. The use of the spheroid model system enhanced the anti-proliferative effects in HCT116 which are caused by the respective siRNAs over 2D system analysis (17-46%). However, HT29 PolyHema assays revealed a different picture. The strongest anti-proliferative effect was shown by Tspan4 with 33% growth inhibition followed by Tspan13 with 24%. Tspan8 and Tspan15 silencing seemed not to result into anti-proliferative effects in 3D cultures. Comparing

these findings with the 2D screening data leads to no correlation. In the initial 2D screening Tspan8 was considered as possible hit in HT29 whereas Tspan4 silencing showed no effect.

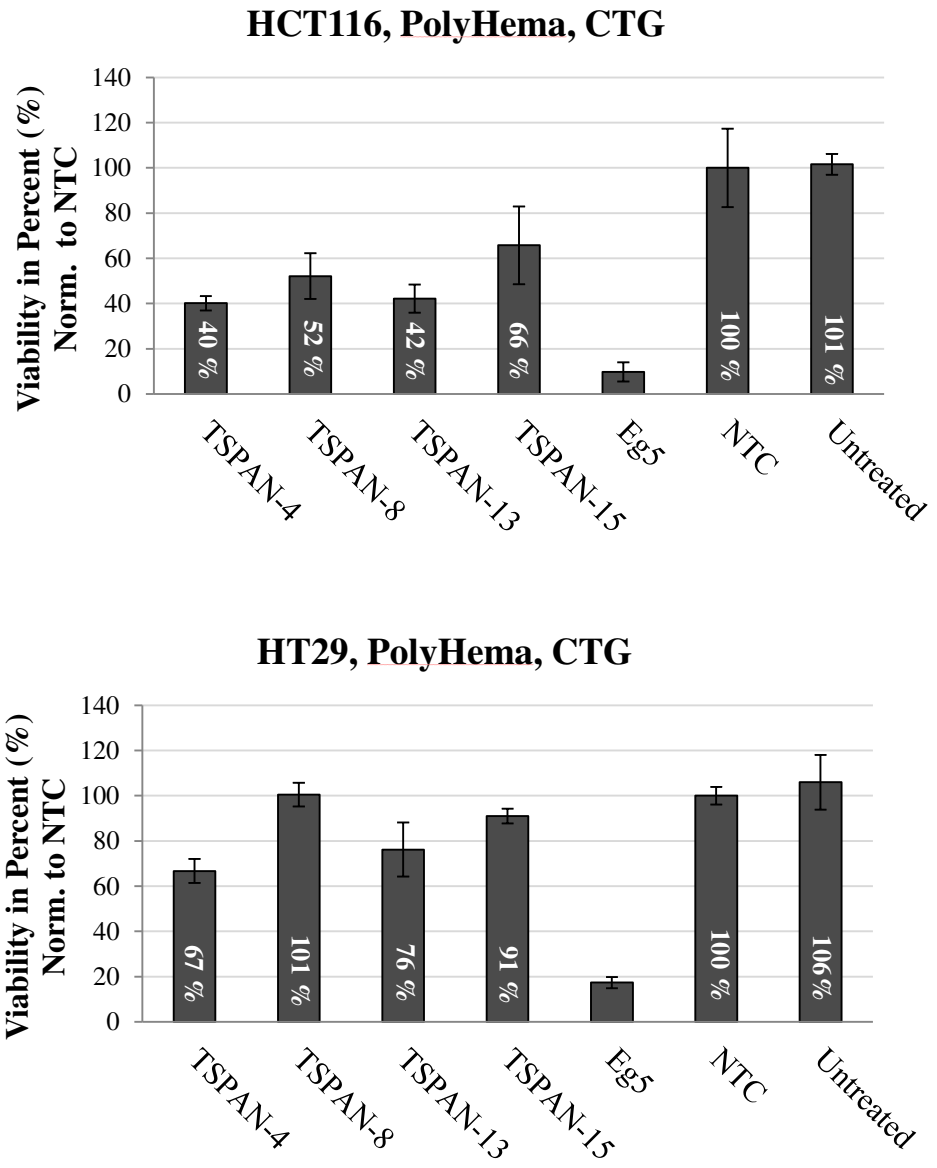

Figure 6.2.11 PolyHema assay of HCT116 and HT29. The cell lines HCT116 and HT29 were grown on PolyHema covered plates and read out by a CTG proliferation assay after Tspan siRNA treatment. The values were normalized to the respective NTC control which was set to 100%. The anti-proliferative effects of the four Tspan siRNAs are very strong (35-60%) in HCT116. In HT29 no effect can be observed for Tspan8 treatment and only 10% for Tspan15. Tspan4 shows a 33% anti-proliferative effect.

The results shown in Figure 6.2.11 are representative of a total of at least three biological replicates which were conducted with six technical replicates per sample. Upon comparison of reproducibility of the determined dataset two exceptions were noted; Tspan8 and Tspan13 down-regulation led to

varying results. Biological replicates were not reproducible in HCT116 or HT29 and ranged between 0% to 90% cell growth inhibition. In contrast to that, Tspan4 and Tspan15 were highly reproducible leading to 60% and 40% cell inhibition in HCT116, respectively. The observed effects for these Tspan siRNAs in HT29 were also highly reproducible without exceptions.

6.2.15 Low 3D reproducibility of Tspan8 and Tspan13 leads to single siRNA evaluation

During the course of the study it I tried to minimize the risk of possible siRNA off-target effects by correlating RT-PCR analysis to proliferation data. First, only hits which were found to express the respective Tspans were considered for further analysis. Of the initial 33 Tspan a range of "hits" could be excluded leading to four Tspans. In the second step, the initial siRNA amounts were downscaled by a factor of 10 to finally 1 pmol per transfection at a 10 nM concentration. 3D analysis led to highly reproducible (Tspan4, Tspan15) but also to varying data (Tspan8, Tspan13). Based on the observed variations the following chapters 6.2.16 and 6.2.17 will focus on off-target identification. Each Tspan siRNA is composed of a pool of four single siRNAs which targets one individual Tspan. The following experiments compared each of the four siRNAs on proliferation- and RT-PCR-level with each other. The so far used siRNA pool was also investigated to enable comparison between single siRNA and pool effects.

6.2.16 Single siRNA No.4 leads to contradictory results for proliferation and RT-PCR data

After 3D analysis the final and most promising Tspans, Tspan4 and Tspan15, were investigated on siRNA off-target effects. Low reproducibility and varying anti-proliferative effects of Tspan8 and Tspan13 led to the exclusion of these potential targets. Figure 6.2.12 shows the dataset of Tspan4 siRNA in HCT116 which was analyzed on proliferation and RT-PCR level. Single siRNAs were analyzed at two concentrations, 2.5 and 10 nM since each siRNA in the pool is fourfold diluted. As shown with the proliferation assay of Figure 6.2.12A Tspan4 pool siRNA exhibits a 50% anti-proliferative effect in comparison to NTC which was set to 100%. This effect is comparable to the data I observed for 3D culturing (60%) in HCT116. The single siRNA treatments at 2.5 nM and 10 nM are similar in trend. siRNA (1) and (3) did not exhibit anti-proliferative effects in contrast to siRNA (2) and (4). The treatment of cells with siRNA (2) led to a reduction in cell proliferation to 64% to 73% whereas siRNA (4) resulted in complete cell death. At both nM concentrations the cell viability dropped below 8%. To the corresponding proliferation assay experiment, the siRNA effect on Tspan4 mRNA levels was investigated. Gained mRNA levels were normalized to NTC

treated cells and set to 1. Treatment of HCT116 with the pool siRNA led to 3 fold decrease in total mRNA. The 2.5 and 10 nM concentrations of the siRNA (1), (2), (3) and (4) were comparable at both concentrations. Interestingly, siRNA (2), (3) and (4) showed a similar down-regulation (4-5 fold) whereas siRNA (1) led almost to no mRNA silencing.

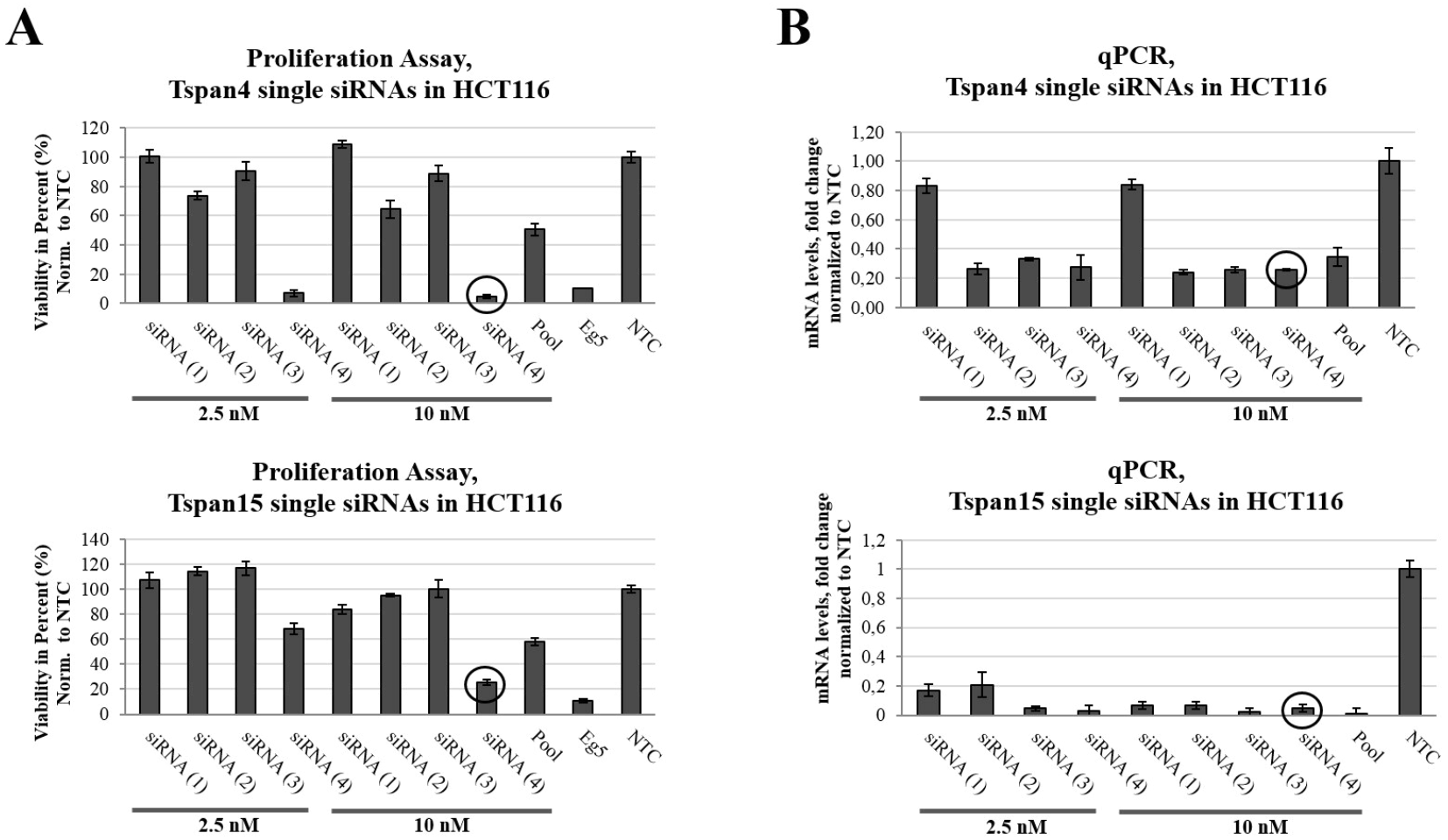

Figure 6.2.12 Proliferation assay and RT-PCR analyses of Tspan4 and Tspan15 single siRNAs in HCT116. (A) Proliferation assays of single siRNAs 1 to 4 of Tspan4 and Tspan15 at two different siRNA concentrations. For Tspan4 no significant difference between the 2.5 nM and the 10 nM concentration could be detected whereas the 10 nM concentration showed stronger effects for Tspan15. In both cases siRNA (4) exhibited the strongest anti-proliferative effect. (B) RT-PCR analysis of mRNA down-regulation after single siRNA treatment. mRNA levels of NTC treated cells were set to 1. Single siRNA treatment for Tspan4 showed no differences between both nM concentrations similar to Tspan15 except for the mRNA levels of siRNA (1) and (2). The overall down-regulation was comparable between the single siRNAs except siRNA (1) for Tspan4 which showed a poor down-regulation (0.8). Even though similar mRNA knockdown efficiencies were be observed by the four single siRNAs, the respective proliferation data led to varying anti-proliferative effects (siRNA 4).

Even though siRNA (4) treatment resulted in similar mRNA knock-down levels as siRNA (2) and (3) it showed a 10 fold stronger anti-proliferative effect. This finding suggests additional anti-proliferative effects by siRNA (4) over the remaining single siRNAs. The second dataset in Figure 6.2.12 investigated Tspan15. On proliferation level, siRNA pool treatment resulted into a 40% anti-proliferative effect. Using the higher nM concentration led to stronger effects in the case of Tspan15 silencing. For 2.5 nM only siRNA (4) exhibited a 30% anti-proliferative effect whereas (1), (2) and (3) showed no growth inhibition. The use of siRNA (4) at 10 nM led to anti-proliferative effects of 75%, similar as Tspan4 siRNA (4). The remaining siRNAs (1), (2) and (3) led at 10 nM to growth inhibitions below 20% cell viability. With the help of RT-PCR analysis the respective siRNA were analyzed on their effect at mRNA levels. In contrast to Tspan4, the mRNA levels of Tspan15 were down-regulated more than 15 fold (all single siRNAs) at 10 nM. Correlating the RT-PCR data with the proliferation data, siRNA (4) led to a higher anti-proliferative effect over the remaining single siRNAs although exhibiting similar mRNA down-regulation patterns. The same observation was also made for single siRNA (4) of Tspan4 and suggested additional anti-proliferative effects.

6.2.17 Off-target analysis of single siRNA (4) on protein level

Single siRNA analysis revealed that Tspan4 and Tspan15 single siRNA (4) led to stronger and more pronounced anti-proliferative effects at similar mRNA down-regulation patterns in comparison to the remaining single siRNA species. Based on these findings the probability of off-target effects caused by Tspan4 siRNA (4) and Tspan15 siRNA (4) was reasonable. To disprove such off-target effects the next step of this study investigated the impact of Tspan mRNA silencing on protein level. Due to Tspan biology (e.g. 4 TM spanning regions) and the ability to cluster into TEMs it was extremely difficult to visualize Tspans by western blot analysis. In addition, few immunoblot antibodies were available against Tspan 4 and Tspan15.

A panel of immunoblot antibodies for Tspan4, 8, 13 and 15 were ordered from five different suppliers and a variety of western protocols focusing on the extraction and visualization of TM proteins for western blot analysis was tested. The assay optimization was done in five cell lines exhibiting high Tspan mRNA levels. During an intensive assay optimization process and primary antibody incubation periods over four days it was possible to visualize Tspan4 in A549 cells and Tspan15 in HCT116 but not Tspan8 and Tspan13. The results are shown in Figure 6.2.13. The

respective cell lines were transfected with Tspan4 and Tspan15 pool siRNA, the corresponding single siRNAs 1-4 and by the NTC control. The observed signal for Tspan15 matched the actual protein size of 32 kDa whereas the signal corresponding to Tspan4 appeared too high at around 70 kDa. Tspan4 is reported to have a size of 26 kDa. With respect to the different transfections one can see that siRNA number (4) showed for both cell lines and for both siRNAs the strongest decrease in protein amounts. This observation was in line with the gained proliferation data.

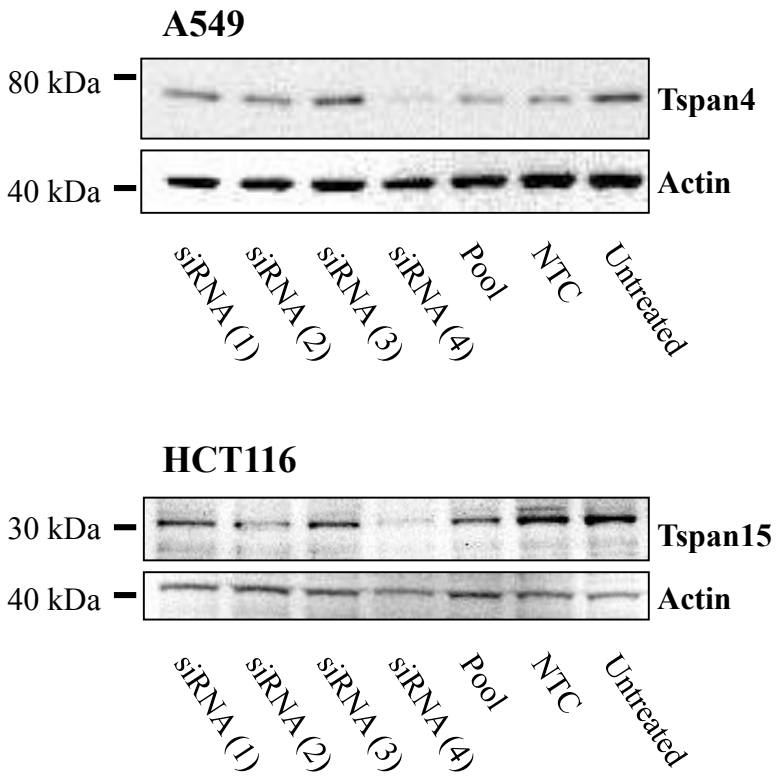

Figure 6.2.13 Immunoblot analysis of Tspan4 and 15 in A549 and HCT116. It was possible to detect Tspans on immunoblot level for A549 and HCT116. Tspan4 and 15 siRNA (4) transfection led to the strongest decrease in protein amount in both cell lines. The immunoblot signal representing Tspan4 occurred too high at around 60 kDa whereas its actual size is 26 kDa. The immunoblot band size of Tspan15 correlated with its actual size of 33 kDa.

In summary, I could successfully correlate anti-proliferative effects which were observed for single siRNAs in proliferation assays with actual Tspan protein down-regulation in immunoblot analysis. Silencing of Tspan4 and Tspan15 by siRNA pools and more precisely single siRNA (4) reduced cell growth in HCT116 and HT29 and is likely to play a role tumor promoting role.

6.2.18 FACS based receptor quantitation as tool to evaluate siRNA knock-down

One obstacle of the performed Tspan screen represented the evaluation of Tspan knock-down by siRNA transfection. The study was further hampered by the fact that Tspans represent relatively unknown TM proteins and thereby a limited number of commercial siRNAs but also immunoblot antibodies were available. A common procedure to evaluate *in vitro* siRNA knock-down experiments represents the combination of RT-PCR and immunoblot analysis. Based on the rather limited detection range of such protein expression analysis I investigated siRNA silencing in combination with the recently establish FACS based receptor quantitation.

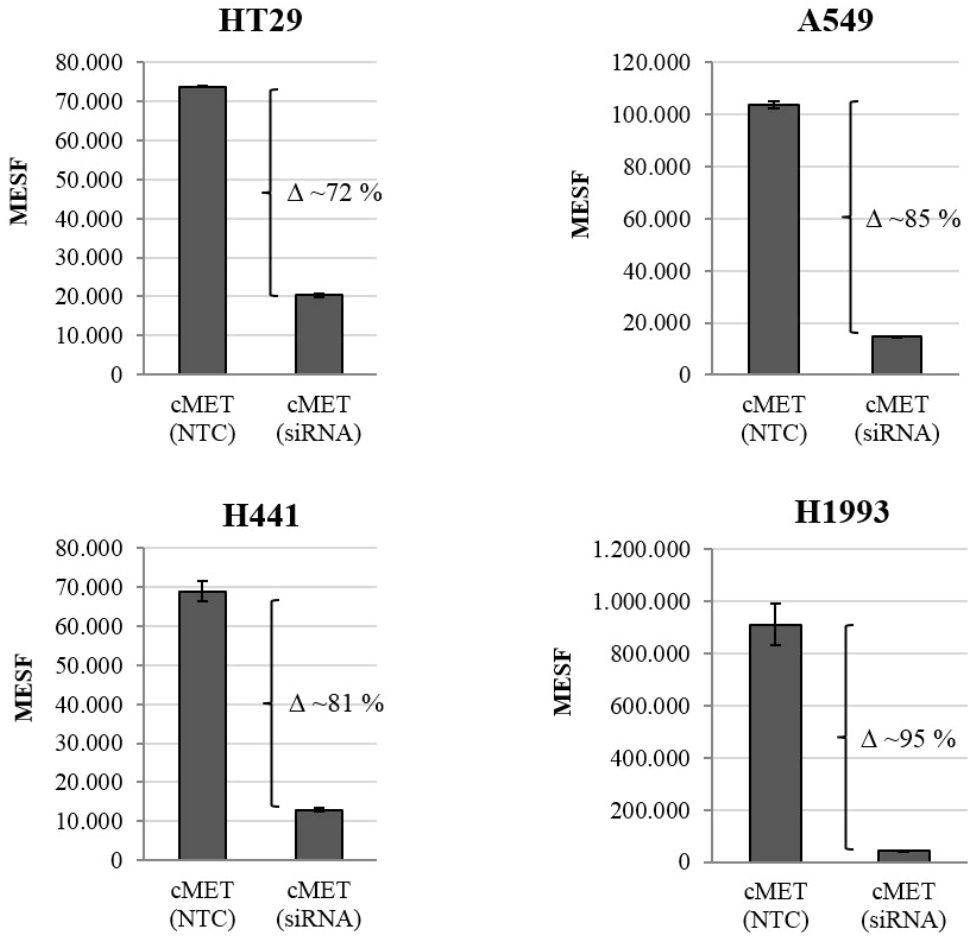

Figure 6.2.14 FACS based cMET receptor quantitation after siRNA treatment. HT29, A549, H441 and H1993 cells were quantified 4 days post siRNA transfection (cMET siRNA, NTC). cMET receptor quantitation was performed with the MetFab1v1 format.

In Figure 6.2.14 the cell lines HT29, A549, H441 and H1993 were transfected with cMET silencing siRNA and quantified after four days post transfection by FACS based receptor quantitation

(MetFab1v1). cMET receptor down-regulation of up to 95% was obtained (H1993) in comparison to NTC treated cells and the overall efficiency ranged between approximately 72% to 85% for the remaining cell lines. It is noteworthy to mention that transfection conditions were not optimized and higher efficiencies and thus higher receptor down-regulations can be obtained upon further optimization.

I concluded that the recently established FACS based receptor quantitation tool represented a another option to investigate siRNA silencing. Receptor quantitation is fast forward method in which precise receptor amounts can be obtained within one day to evaluate and correlate transfection conditions to transfection efficiencies. In future studies, Tspan targeting BsAbs might be used to investigate Tspan silencing.

7 Discussion

7.1 FACS-based Receptor Quantitation

In the presented work I introduced receptor quantitation with BsAb as an alternative to custom fluorophore labelled Abs, PE-conjugated Abs or other techniques such as the radio ligand binding assay. A BsAb, specifically a Fab-scFv construct, with an antigen-specific part and a hapten-binding moiety which allows coupling of fluorophores for receptor quantitation experiments was engineered. With regard to the field of use I do see the versatility of the system advantage: (i) monovalency for the antigen-binding site delivers a precise antibody to antigen ratio; (ii) quantitative and site-specific labeling is feasible without eventually affecting the antibody-binding properties and yielding only one product; (iii) the precise labeling ratio makes it unnecessary to use another error-prone normalization step with SCB; (v) although not specifically shown, omitting the Fc part reduces the risk of unwanted binding to FcRn receptor molecules.

Generation of Dig specific BsAb detection antibodies

The application of recombinant antibody technology to receptor quantitation can be easily implemented if a therapeutic antibody is generated. One part of this effort is sequencing and kinetic characterization of obtained binders. In this case, selection of a suitable antibody from a lead series or the use of the therapeutic antibody itself is feasible. The variable sequence information of antibodies already in use in flow cytometric experiments could also be derived from existing Hybridomas. However, a DNA isolation and sequencing step is then required before a BsAb can be generated.

The use of hapten coupled detection antibodies

The hapten coupling method is in my opinion a different but good alternative to covalent coupling, as larger amounts of different hapten-conjugated fluorophores can be easily produced, which enables versatile and flexible coupling of different fluorophores to one BsAb. This would also enable multiplexing of different cell surface antigens as long as the fluorophore excitation and emission spectra do not overlap. Multiplexing for receptor quantitation experiments is challenging but has been described previously by Wang and colleagues who provide a calibration strategy for multicolor flow cytometry that enables to determine the number antibodies bound per cell (Wang, Gaigalas, Marti, Abbasi, & Hoffman, 2008). In addition, hapten coupling separates the protein

component from the small molecule fluorophore. The latter is usually much longer stable and easier to handle. Instead of small molecules the technique very likely also accommodates quantum dots which already have been used for antigen quantitation experiments (Buranda, Wu, & Sklar, 2011). The advantage of quantum dots over fluorophore tags is that they can be photoexcited over a wide spectral range and are therefore not limited to their spectral region of resonance (Buranda et al., 2011). The next generation of hapten coupled BsAb detection antibodies could be based on quantum dots instead of fluorophores.

Doubling the F/P ratio leads results into a linear increase in signal strength

I could demonstrate that the signal strength increases linearly if another hapten-specific scFv is conjugated, doubling the amount of fluorophore per antibody. As control group, the previously established Her2Fab1v1 was compared in quantitation experiments to Her2Fab1v2. The ratio between the respectively quantified cell surface HER2 receptors was calculated and determined to be approximately 2.0, underlining a linear increase in signal strength. With respect to possible applications, this approach could be employed to increase the signal strength for targets with a low cell surface expression as shown for the HER2 receptor in A549 and Hs746T. Furthermore, instead of increasing the number of hapten-specific scFv one could also design a Dig-containing small molecule which carries more than one fluorophore, further enhancing the signal strength. Combining such modified Digs with two hapten-specific scFv could quadruplicate the signal. According to the generated data it is likely that the signal strength increases in a linear fashion. Such quantification of cell surface receptors at lower expression levels could be applied on broad basis such as for oncological targets and for screening purposes. The exact quantification is for various reasons attractive and applicable: modeling and simulation of cellular networks, predictions on saturation conditions with therapeutic compounds, dose-response studies and the differentiation of normal and malignant state of cells. The novel tool could further enable pre-clinical mode of action studies where the change in total receptor numbers and receptor ratios could be determined. Pharmacodynamic properties such as clearance of drug candidates via receptor internalization could be easily investigated. With respect to clinical relevance the quantitation of proteins in patient material such as leukocytes could be a possible field of application.

Can MESF values be set equal to absolute receptor numbers?

The precision of the hereby generated cell surface receptor quantitation tool relies to great extent on the use of standardized measurements such as microspheres as external standards which are required to calculate MESF values. In consequence, a lack of defining fluorescence intensity through standardized measurements leads to arbitrary units or to relative terms such as “negative”, “dim”, “intermediate” or “bright”. Obstacles of quantitative measurements and the interpretation of fluorescence signals are for instance PMT settings, instrument variations (laser power, filter sets), environmental factors (buffer pH, temperature) and the labeling efficiency of detection antibodies in terms of F/P ratios. In consequence, quantitative fluorescence analyses require the highest level of standardization to generate significant data. Based on the novel Fab-scFv Dig approach it is possible to generate homogeneous F/P ratios and by the simultaneous use of fluorophore labeled bead populations as standards, varying factors such as instrumental settings and environmental factors can be cancelled out. Also the use of Quantum™ MESF microspheres as external standards enable standardized measurements of fluorescent intensity. Microspheres are labelled with the same fluorochromes as the detection antibodies and are environmentally responsive to temperature or pH (Bangs Laboratories - Tech Notes 103 & 821). However, one essential question arises: Can the calculated MESF values of this study be set equal to absolute receptor numbers?

To discuss this question the exact definition of MESF units has to be considered. Even though MESF units were used over the past three decades, a precise definition was only recently established and published in the Journal of Research of the National Institute of Standards and Technology (NIST). As described previously, the MESF concept states that a sample which is labeled with fluorophores exhibits the same fluorescence intensity as an equivalent number of molecules of the same fluorophore free in a solution (Schwartz et al., 2004; Gaigalas et al., 2001; Schwartz et al., 2002; Wang et al., 2002). MESF units are defined in the context of the so called “fluorescent measurement model” which relates physical characteristics to fluorescent signals (Schwartz et al., 2002). The model clearly identifies the parameters which play a role upon comparison of samples to standards and therefore enables the differentiation between instrumental biases and physical characteristics of the fluorescent solution. The relation between the measured fluorescence intensity and fluorescent yield is implemented whereas the fluorescence yield is the product of the concentration of fluorophores and the molecular quantum yield (Gaigalas et al., 2001; Schwartz et al., 2002; Schwartz et al., 2004; Wang et al., 2002). In consequence, the fluorescence

yield of two solutions can be compared and this fact represents the basis of the use of standards to quantify fluorescence intensity in flow cytometry. The fluorescent measurement model relates the measured FI to the fluorescent yield and is described by following formula (Schwartz et al., 2004):

$$i_F = \left[ge\Omega\varepsilon\Phi \int Q(\lambda)\, s(\lambda)T(\lambda)d\lambda\right]c$$

Where:

i_F	=	*measured fluorescence intensity*
g	=	*photomultiplier (PMT) gain*
e	=	*elementary charge*
Ω	=	*aperture and collection optics*
Q(λ)	=	*quantum efficiency of the PMT at λ*
T(λ)	=	*filter characteristics at λ*
ϵ	=	*molar extinction coefficient at the excitation wavelength*
Φ	=	*quantum yield*
s(λ)	=	*normalized emission spectral function at λ*
c	=	*concentration of the fluorochrome*

The comparison of the fluorescent yield of two solutions through the measured fluorescence intensity is difficult due to various parameters as indicated by the formula. However, upon comparison of a standard to an unknown sample some factors can be canceled out if the measurement takes place on the same instrument at similar conditions (e.g. g, e and omega). The remaining factors can be summarized by the factor "x" resulting in following fluorescence intensity equation (Schwartz et al., 2004):

$$i_F = X\Phi c$$

In other words: If the standard and the sample are measured under equal instrumental conditions and if the excitation and emission spectra of the fluorophores are equal, it is possible to state that the measured fluorescence intensities is the same as comparing the respective fluorescent yields to each other (Schwartz et al., 2004). Therefore, a standard with a known concentration of fluorophores is equivalent to the concentration of an unknown sample. The discussion can be expanded to fluorophores which were immobilized to microspheres representing the standards of the performed study. However, the greatest error source upon comparing and translating MESF values in a quantitative manner represents the quantum efficiency of the fluorochrome and its spectral response (Wang et al., 2002). As shown by Schwartz and colleagues and by Wang and

colleagues, changes in the microenvironment such as in conjugated antibodies can lead to spectral shifts. But also mere binding of detection antibodies to cells can lead to spectral shifts and thus altered signals (Schwartz et al., 2004; Wang et al., 2002). To discuss this problem the study by Metz and colleagues is important. They determined the excitation maximum (nm) and emission maximum (nm) of the respective components and constructs which are part of this study. The results of their excitation and emission analysis are shown in the following table 7.1 (Metz et al., 2011).

Table 7.1. Excitation and emission maxima of different Cy5 molecules.

Molecule	Excitation maximum (nm)	Emission maximum (nm)
Cy5	652	680
Dig-Cy5	647	674
mAb bound to Dig-Cy5	657	678

Even though minor shifts can be observed Metz and colleagues concluded, that fluorescent properties of the respective compounds were not affected upon digoxygeninylation (Metz et al., 2011).

In summary, flow cytometric MFI values correlate with beads which were normalized to MESF values of a defined calibrator solution. As the steric and electrostatic conditions of an antibody–fluorophore are different and spectral shifts can occur, one can only refer to this standard and not define absolute receptor numbers as it might be possible by mass spectrometry. A possible solution to overcome this issue might be the measurement and evaluation of the emission spectrum and implement it into the factor X of the fluorescent measurement model.

The Dig BsAb has a defined antigen binding site

If a bivalent mAb format is replaced by a monovalent binder it is of importance that the antibody affinity is very high, specifically a low k_{off} is desired, to prevent dissociation under washing conditions. Similar considerations are valid for the hapten-binding site. However, I did not observe loss of antibody or hapten in our experimental setting. For all antibody-derived quantitation experiments it has to be considered that the antigen-binding site can have a major influence on quantitation. Antigen binding can be influenced by various factors, e.g. co-receptor expression or ligand presence masking the binding site, changes in the glycosylation pattern or splice variants

lacking the antigen-binding site. In this line, the use of fluorophore coupled detection antibodies is of clear advantage over site- unspecifically labelled detection antibodies. Such heterogeneous species of detection antibodies may contain altered antigen binding sites which can result in the inactivation of the antibody (Werthen & Nygren, 1988; McCormack, O'Keeffe, MacCraith, & O'Kennedy, 1996). It is also arguable whether spectral shifts, as discussed previously, are more pronounced in such a heterogeneous antibody population. A number of studies demonstrated that the presence of multiple fluorophores which are in close proximity, in custom labelled antibodies, led to a decrease in fluorescence intensity due to fluorophore quenching (Chapple, Johnson, & Davidson, 1990; Deka et al., 1996; Der-Balian, Kameda, & Rowley, 1988; Gruber et al., 2000; Haugland, 1995; Petrou, Mastichiadis, Christofidis, & Kakabakos, 2007). A recent study by Vira and colleagues investigated the functionality of custom labelled detection antibodies for anti-hemaglutinin (HA) monoclonal antibodies (Fc125) (Vira, Mekhedov, Humphrey, & Blank, 2010). The Fc125 antibody was labelled with fluorescein isothiocyanate (FITC) at varying F/P rations and finally evaluated by a kinetic ELISA assay. Similar to other studies, the researchers observed problems upon under- and over- antibody labelling which led to a decrease in fluorescence but also reagent related problems occurred that produced a large non-specific background (Vira et al., 2010; McKay, Forman, & White, 1981; Holmes & Lantz, 2001; Goding, 1976; Chantler & Batty, 1983; Panchuk-Voloshina et al., 1999). Coupling of FITC to Fc125 led to minor changes in the avidity whereas higher levels of FITC resulted in the inactivation of a significant fraction. Vira and colleagues concluded that an optimal F/P ratio is essential to minimize un- and over-labelling but also avoid inactive antibodies. They developed a technique to calculate such ratio for Fc125 (F/P = ~1.6 – 5) (Vira et al., 2010). In terms of quantitative flow cytometry the avoidance of custom fluorophore labelling is clearly revealed, even though it might be possible to calculate the degree of inactivation and altered antigen binding of custom labelled antibodies to a certain extend.

Variations in the number of cell surface receptors during cell culture

Using a BsAb for receptor quantitation as described here still faces the problem that a huge variability is introduced by the cell culture conditions. Cell culture confluency has a large impact on receptor expression as observed. This necessitates rigorous adherence to cell culture protocols to achieve reproducible results. Therefore, the seeding conditions and time of analysis are fundamental parameters which need to be reported in order to facilitate comparison between studies of one receptor type in a certain cell line.

Gill and Lazar investigated in a study the effect of EGF stimulation in A431 cells with respect to cell proliferation, EGFR amounts and phosphotyrosine content (Gill & Lazar, 1981). The data reveals a crucial fact to understand and perform reproducible receptor quantitation experiments. An inverse relationship between cell density and EGF affinity of EGRF was shown and EGFR amounts increased from 0.5 pmol of labeled 125I-EGF per 10^6 cells at low cell densities to 5.7 pmol at high cell densities. But variations in EGFR numbers which are in correlation to cell densities are also observed in other cell lines. BSC1 cells, for instance, decrease EGFR levels at higher cell densities whereas the receptor amounts increase for BALB/c-3T3 cells at higher cell densities (Pratt & Pastan, 1978). In addition, environmental conditions such as administration of retinoids can lead to increased EGFR levels whereas phorbol esters to decreased EGF affinity (Jetten, 1980; Shoyab, De Larco, & Todaro, 1979). A study by Jaspers and colleagues also determined significant differences in CD22 levels depending on the day of quantification (Jasper et al., 2011). Together with my initial results for cMET quantitation (table 6.1.4) these results demonstrate how dynamic receptor numbers can be and how essential standardized conditions are (e.g. duration of the assay, environmental parameters). Based on the time-course experiments (Figure 6.1.8) but also on the highly reproducible Snu-5 quantitation experiments it is likely that variations in cMET receptor numbers are, to a certain degree, cell line dependent.

The outcome of the time-course experiments (Figure 6.1.8) might partially explain the high STD which were encountered in other A431 EGFR quantitation studies (table 6.1.11), besides the inherent low assay sensitivity of the radio ligand binding assay. In conclusion, I suggest a change in the nomenclature of receptor numbers besides the use of standardized quantitation protocols. In the case of highly dynamic receptor amounts it would be advantageous to either determine exact assay termination conditions or to provide quantitation results at different culturing time-points to facilitate comparison. For example, cMET receptor levels in A549 could be described as A549 ($8{,}500^{\mathbf{lowest}}$/$66{,}600^{\mathbf{highest}}$/$37{,}000^{\mathbf{quantitation}}$) according to Figure 6.1.8 underlining the dynamic nature of cMET in A549. The assay termination point at day 3 would determine 37,000 cMET receptors whereas the minimum receptor population is at approximately 8,500 and maximum at approximately 66,600. Such precise quantitation could be used for modelling and simulation studies and the evaluation of pharmacokinetics.

Receptor quantitation techniques in relation to Dig-Cy5 BsAb

Out of the twelve listed studies in table 6.1.11 two used a FACS based technique to determine EGFR receptor numbers in A431 (Brotherick et al., 1994; Lopez et al., 1992). Both studies determined significantly lower receptor amounts (approx. 500,000 and 335,000) in comparison to the remaining quantitation studies (approx. 1.5 – 3 x 10^6). Lopez and Brotherick used custom labelled antibodies and determined the F/P ratio of their detection antibodies via SCB. Under the assumption that their experiments suffered the same degree of error as the performed ABC and custom labelling experiments of this study (table 6.1.2, 6.1.3 and Figure 6.1.5), their results are coherent. Systematic error in F/P determination together with the downsides of custom fluorophore labelling, the authors obtained reproducible but yet significantly lower EGFR amounts for A431, T47D, BT20 and MDA in comparison to studies which were conducted by radio ligand binding assays (Brotherick et al., 1994; Fabbro, Kung, Roos, Regazzi, & Eppenberger, 1986; Imai, Leung, Friesen, & Shiu, 1982) or by our quantitation technique. Lopez and Brotherick suggested this constant discrepancy to other quantitation studies may be based on culturing conditions, cell culture passages, machine sensitivities, fluorochrome diversity and the respective method of calibration (Brotherick et al., 1994; Lopez et al., 1992). However, with the recently generated data I can conclude that previous flow cytometry based receptor quantitation experiments most likely suffered under several varying parameters such as (i) non-standardized assay parameters, (ii) an error-prone F/P determination of detection antibodies or (iii) the downsides of custom fluorophore labelling as our experiments showed. The introduction of the novel BsAb coupled Dig-Cy5 detection antibodies does not only circumvent the discussed issues but also leads to a more reliable, reproducible and accurate receptor quantitation tool which operates with a minimum amount of cells and avoids the use of potentially hazardous radio-isotopes (E.g. radio ligand binding assay).

The use of flow cytometric quantitation to detect for instance small tumors in breast screenings is clearly favored over radio ligand binding assays which lack accuracy (see table 6.1.11), require large quantities of tumor tissue and is not able to determine receptor levels of individual cells (Brotherick et al., 1994; Jasper et al., 2011). However, the application of quantitative flow cytometric measurements in the clinic can lead to technical problems such as the specimen age, non-standardized sample processing (lysis, fixation, staining), properties of monoclonal antibodies and the antigen itself (location on the membrane surface) (Barnett, Storie, Wilson, Granger, & Reilly, 1998; Rossmann, Lenkei, Lundin, Mellstedt, & Osterborg, 2007; Davis, Abrams, Iyer,

Hoffman, & Bishop, 1998b; Arun et al., 2010). Jasper (Arun et al., 2010)and colleagues investigated these variables with the QuantiBRITE system together with an anti-CD22 antibody consisting of a 1:1 PE to antibody ratio (F/P ratio = 1:1). The QuantiBRITE system and its PE detection antibodies are similar to the MESF based calibration system and was compared to our quantitation antibodies (Figure 6.1.13) (Jasper et al., 2011). In the work of Jasper and colleagues, CD22 of neoplastic B cells were quantified under varying conditions. Abnormal CD22 levels are characteristic in chronic lymphocytic leukemia (CLL) and several studies underline the importance of antigen quantification for diagnosis, prognosis and in monitoring the therapy in leukemias and lymphomas (Atra, Abboudi, Farahat, & Catovsky, 1997; D'Arena et al., 2000; Ginaldi et al., 1998a; Ginaldi et al., 1998b; Hsi et al., 2003; Jasper et al., 2011; Jiang et al., 2009). In comparison to other FACS based CD22 quantitation studies (Atra et al., 1997; D'Arena et al., 2000). Jasper and colleagues determined a significantly lower STD based on the 1:1 antibody to PE conjugate format. Also the QuantiBRITE beads were analyzed and showed great stability and reproducibility over time similar to MESF beads (Data not shown). The authors concluded that the QuantiBRITE system is a very precise method to determine cell surface receptor numbers under defined environmental conditions (Atra et al., 1997; Jasper et al., 2011). The differences that were observed (Figure 6.1.13) upon direct comparison between both systems, which use defined F/P ratio detection antibodies, can be understood by considering the respective antibody formats.

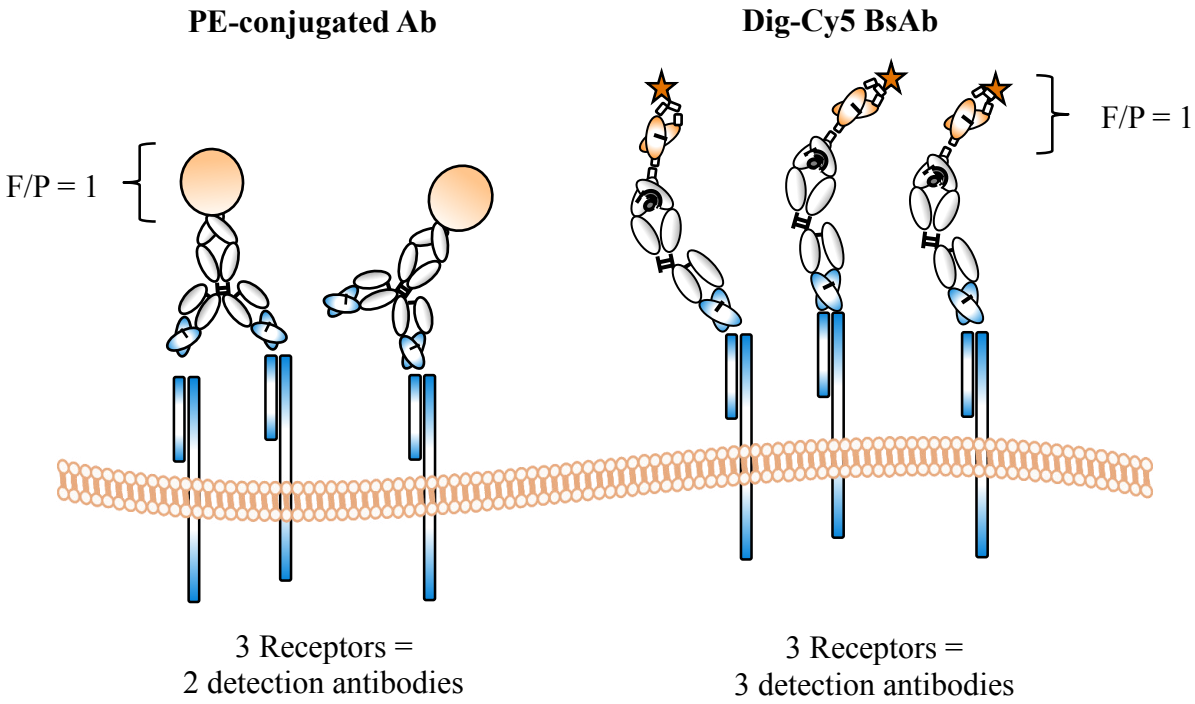

Figure 7.1. Binding possibilities of mono- and bivalent detection antibodies. Comparison between a PE-conjugated mAb (2+1 format) and the Dig-Cy5 BsAb (1+1 format) for the QuantiBRITE and MESF system, respectively. The Figure illustrates that the PE-conjugated mAb might bind to only one target receptor and thereby introduce an error in the quantitation experiment although both antibody formats exhibit an F/P ratio of 1.

Figure 7.1 exemplifies the binding difference between a PE conjugated mAb and the 1+1 Dig-Cy5 BsAb format of our study. Considering binding possibilities and therefore the introduced error, the observed factors (approximately 1.4 – 1.6) in A549-B34, H441 and MDA-MB175 for HER3 levels can be explained. In summary, the QuantiBRITE system together with its PE conjugated detection antibodies represents a highly reproducible and sensitive system and clearly favored over radio ligand binding assays. However, PE conjugation eliminates the option to switch between fluorophores by individual coupling and the use of bivalent detection antibodies may introduce error.

Quantitative confocal microscopy

With quantitative confocal immunofluorescence I could confirm the flow cytometry findings. Indeed, it was also possible to successfully employ bispecific antibodies to quantify the amount of BsAb which was internalized at 37°C in individual cellular organelles. This additional information on subcellular locations complements the FACS analysis. Precise quantitation of antibody content

in organelles may for instance help to infer the rate of internalization in a quantitative manner. Although not a focus in this work, the presented BsAb approach can be easily adopted for confocal microscopy as well.

Summary

Overall, I could successfully and reproducibly quantify the amount of cell surface protein for four different antigens. I confirmed our findings by comparison to existing technologies like lysine-linker chemistry and QuantiBRITE but also to non FACS based methods such as radio ligand binding assays and matched findings to literature known data. As the data indicates, the generated quantitation tool shows so far the highest reproducibility and sensitivity among the different technologies. It can be expected that this concept has broad applicability and could also be expanded for analysis of antigen internalization. FACS-based antigen quantitation experiments can benefit in my opinion from using bispecific antibodies and 1+1 formats for various aforementioned reasons and significantly improve the value of this technique. The confocal microscopy findings support that the approach can be broadly applied for imaging techniques as well. Furthermore flow cytometry decreases the use of potentially hazardous radio-isotopes while offering at the same time multi-parametric analysis of gated cell populations.

7.2 Tetraspanin screen

An siRNA based screen was performed to determine possible anti-proliferative effects upon mRNA downregulation of all 33 Tspan TM proteins. Initially a panel of different cell lines of varying tissue origin was investigated via proliferation assays. In order to assess the quality of mRNA silencing, RT-PCR experiments were performed and a set of possible “hits” defined. Due to this target reduction, comprehensive studies were feasible such as siRNA quality experiments, 3D proliferation assays and cell morphological ACEA analysis. Four potential therapeutic targets were determined in this study: Tspan4, Tspan8, Tspan13 and Tspan15 whereas Tspan4 and Tspan15 remain the most promising targets based on first validation experiments (immunoblot analysis) and data consistency throughout all screening steps.

Performing the Tetraspanin screen: Intensive optimization rounds

The main challenge of this study was the optimization of the different assay set-ups. The bulk of experiments were used to establish suitable readout and assay conditions for the different cell lines in 2D and 3D set-ups. Overall, the optimization led to high siRNA transfection efficiencies for all cell lines (approximately 75-99%) and thus reliable siRNA read-outs. Although these optimizations led to satisfying results the assay conditions for immunoblot analysis were more difficult. Via immunoblot analysis I sought to verify successful mRNA downregulation on protein level. However, a range of factors hindered this commonly "straight-forward" approach. On molecular bases, Tspans protrude only 4-5 nm of the plasma membrane and based on their ability to organize laterally into TEMs their interaction partner remain associated under non-stringent detergent conditions (Hemler, 2008; Hemler, 2005; Kitadokoro et al., 2001; Min, Wang, Sun, & Kong, 2006; Odintsova et al., 2006). Within TEMs, a high level of gangliosides and cholesterol can be found which in turn results into solubilisation resistance by detergents (Charrin et al., 2003b; Odintsova et al., 2006; Ono et al., 2001). With respect to material, only a limited amount of different Tspan detecting immunoblot antibodies were available. This is due to the fact, that most of the 33 mammalian Tspans remain minimally studied (Hemler, 2008). I tested all commercially available immunoblot antibodies (Tspan4, 8, 13 and 15) in combination with a number of different assay conditions suitable for TM protein analysis in six different cell lines. The cell lines were chosen according to Affymetrix data and siRNA transfection efficiencies over 90% (Data not shown).

How to approach a Tetraspanin screen: mAbs vs RNAi

In the emerging field of Tspan research, two major ways in investigation of these TM proteins as potential therapeutic targets are currently discussed (Hemler, 2008; Lazo, 2007; Richardson et al., 2011; Wang, Li, Sharma, Knoblich, & Hemler, 2011):

i) mAb approach
ii) RNA interference (RNAi)

Promising *in vivo* results have already been obtained by the first approach. For instance, targeting Tspan26 and Tspan29 by mAbs have shown to inhibit *in vivo* colon carcinoma cell growth (Ovalle et al., 2007) and led to the depletion of B-cell chronic lymphocytic leukemia (B-CLL) cells (Zhao et al., 2007). The main drawback however, for most Tspan targeting mAbs the underlying biological mechanism and thus the accompanied alterations in cell functions are not understood. It

is assumed that mAbs are likely to inhibit lateral binding to interaction partners whereas multivalent mAbs may lead to the formation of aggregates of TEMs which in turn results in their disruption (Hemler, 2008). Thus, mAb approaches involve a range of unknown Tspan interaction partners. This circumstance could explain why mAb treatment often exceeds the effect which was initially determined by individual Tspan knockdown, as in various studies observed (Boismenu, Rhein, Fischer, & Havran, 1996; Levy, Todd, & Maecker, 1998; Miyazaki, Muller, & Campbell, 1997; Oren, Takahashi, Doss, Levy, & Levy, 1990; Ruiz-Mateos, Pelchen-Matthews, Deneka, & Marsh, 2008; Tsitsikov, Gutierrez-Ramos, & Geha, 1997; von Lindern et al., 2003).

In addition, it has been shown that mAbs directed against Tspans can also lead to agonistic effects. For instance mAbs against Tspan24 increased inherent functions such as cell adhesion and thus immobilization of tumor cells (Zijlstra et al., 2008). Tspan28 and Tspan29 targeting mAbs stimulate cell to cell fusion via agonistic effects or by hampering anti-fusion properties of those Tspans (Gordon-Alonso et al., 2006; Hemler, 2008; Takeda et al., 2003). It is likely that I have observed a similar effect in HT29 cells that were treated with Tspan8 and Tspan15 siRNA. Figure 6.2.6 shows that these cells lacked clear cell to cell borders in contrast to mock controls or Tspan4 and Tspan13 treated cells. Subsequent ACEA analysis (Figure 6.2.8) further indicated a morphological change comparable to the findings of Tspan28 and Tspan29.

RNAi focuses on individual Tetraspanins

Based on these studies, I focused on the alternative approach to evaluate anti-proliferative effects upon Tspan inhibition, namely an RNAi based screening. Via this technique it was possible to concentrate on single Tspans and not unknown interaction partners. The field of RNAi has led to a potent tool consisting of highly effective and chemically stable siRNAs exhibiting minimized off-target effects by enhancing specificity (de, Vornlocher, Maraganore, & Lieberman, 2007; Hemler, 2008). For instance, knockdown of Tspan24, 28 and Tspan29 mRNA by siRNA, has led to these promising targets in cancer therapy as seen in several studies (Barreiro et al., 2005; Kovalenko, Yang, & Hemler, 2007; Winterwood et al., 2006). siRNA mediated mRNA downregulation has revealed that Tspan24 and Tspan29 enhance transendothelial lymphocyte migration (Barreiro et al., 2005) and in the case of Tspan29, integrin dependent cell adhesion and reduced expansion in ovarian carcinoma cells (Furuya et al., 2005).

Tetraspanin screen determines Tspan4 and Tspan15 as potential targets for future studies

Beside Tspan8 and Tspan13, the Tspan screen determined Tspan4 and Tspan15 as the most promising targets. 2D proliferation assays as well as 3D culturing conditions revealed significant and reproducible anti-proliferative effects upon knockdown of these Tspans. To minimize possible siRNA off-target effects it was necessary to validate the determined data. A first step represented single siRNA transfections as shown in Figure 6.2.12 together with RT-PCR analysis. Although alternative siRNA species (Ambion), targeting Tspan4 and Tspan15, did not succeed in mRNA downregulation (RT-PCR and proliferation data not shown), it was possible to demonstrate successful knockdown on protein level with the initial siRNAs (Thermo). Here, a reduction in Tspan4 and Tspan15 protein for A549 and HCT116 cells after siRNA treatment (Figure 6.2.13) was proven. Together with the results shown in Figure 6.2.8 (ACEA), 6.2.11 (PolyHema), 6.2.12 (RT-PCR) and 6.2.13 (Immunoblot) I believe to have found significant evidence for anti-proliferative effects of Tspan4 and Tspan15 upon mRNA silencing while excluding off-target related effects. Out of initially 33 Tspans these two TM proteins were determined as most promising potential targets for future studies.

Tspan4 and Tspan15 are still unknown to be involved in tumor progression

No literature was available for Tspan4 and Tspan15, correlating these TM proteins to tumor progression, at the time this work was conducted. In fact, Tspan15 was investigated in a very limited amount of studies (>5) of which none investigated tumor related properties. The same is true for Tspan4 where none of the performed studies (>15) examined a possible correlation to tumor progression.

Tspan8 and Tspan13 correlate with tumor progression as observed in several studies

Together with Tspan4 and Tspan15, the Tetraspanins Tspan8 and Tspan13 were identified as promising hits in the performed Tspan screen (except for PolyHema analysis which led to inconsistencies, Figure 6.2.11). According to literature, siRNA experiments have initially shown that osteoclastogenesis is inhibited upon Tspan13 mRNA knockdown which led to further studies. Since then, at least three studies correlate Tspan13 with tumor progression in prostate cancer (Arencibia et al., 2009; Huang et al., 2005a; Iwai, Ishii, Ohshima, Miyatake, & Saeki, 2007). Similar results were observed for Tspan8 downregulation. Three studies correlate Tspan8 with tumor progression (Kanetaka et al., 2001; Kuhn et al., 2007; Zhou et al., 2008).

Tspan8 downregulation in HT29 leads to the loss of differentiated cell borders in 3D cultures

Of special interest is the work of Kanetaka and colleagues who observed reduced cell migratory abilities in HT29 after Tspan8 knockdown. Beside the loss of cell migration, an upregulation of integrin-dependent cell-matrix adhesion for laminin and calcium dependent adhesion was observed. Here, laminin binding integrin α3β1 and fibronectin-integrin α5β1 were upregulated whereas CD44 downregulated after Tspan8 knockdown (Kanetaka et al., 2001). These deregulated cell to cell adhesion properties could also lead to our observations shown in Figure 6.2.6 where Tspan8 siRNA treated HT29 led to a loss of differentiated cell boarders. The authors concluded that Tspan8 promotes cancer cell migration by the deregulation of cell adhesion properties (Kanetaka et al., 2001). Table 7.2 summarizes all available and relevant studies of Tspan4, 8, 13 and Tspan15 in the field of cancer research.

Table 7.2. Tetraspanin "hits" in correlation to tumor progression. The table highlights the determined hits of the Tspan screen and the available studies correlating these Tspans to tumor progression.

Tetraspanin "hits" of this study	Tumor progression	Known literature (tumor related)
Tspan4	n.d.	none
Tspan8	correlates	(Kanetaka et al., 2001; Kuhn et al., 2007; Zhou et al., 2008)
Tspan13	correlates	(Arencibia et al., 2009; Huang et al., 2005a)
Tspan15	n.d.	none

Tetraspanin screen evaluation

The literature examples for Tspan8 and Tspan13 underline the positive outcome of the performed Tspan siRNA screen as start to identify reasonable tumor targets for further analyses. Having these examples in mind, I am confident that the Tspan screen provided a set of interesting and highly potential targets which should be further evaluated. Several studies determined a correlation in tumor progression by RNAi experiments and came to the same results as this work i.e. Tspan8 and Tspan13. This screen identified, out of initially 33 Tspans, the four most promising targets which have to be further evaluated by overexpression experiments, colony formation and migration assays based on the molecular properties of Tspans and, of special interest, the generation of mAbs. It is likely, as several Tspan studies have shown (Boismenu et al., 1996; Levy et al., 1998; Miyazaki et al., 1997; Oren et al., 1990; Ruiz-Mateos et al., 2008; Tsitsikov et al., 1997; von Lindern et al., 2003) that the observed mAb treatment will exceed the initial anti-proliferative effects due to the

inhibition of possible interaction partners and TEM formation (Figure 2.7). Based on the fact that the inhibition of the so far determined, tumor related Tspans is caused by the prevention of protein partner interaction and because Tspans are expressed in nearly all cell and tissue types (Helmer, 2008), a co-targeting approach by the development of a bispecific Ab is feasible and might be promising. The data suggest to further investigate Tspan4, Tspan8, Tspan13 and Tspan15.

8 Acknowledgements

I would like to thank Prof. Dr. Johannes Buchner for being my doctoral thesis supervisor at the TU Munich and who enabled the possibility of graduation. I would also like to thank my direct supervisor at Roche Diagnostics Dr. Claudio Sustmann for giving me the opportunity to work in his lab and for his support, guidance and encouragement. The work would not have been possible without his support.

I would like to thank Gerhard Niederfellner and Dr. Christian Klein, as former heads of the oncological department, for their support and professional discussions about my projects. Many thanks goes to Dr. Rita Mateus Seidl, Dr. Raffaella Castoldi and Dr. Florian Schelter who supported me at various steps during my graduation and had always time when I needed help and advice.

I would like to thank my cousin Dr. Björn Willige who invested countless hours into my graduation and who supported me not only during my time at Roche Diagnostics but also during my Bachelor and Masters studies. His professional expertise, patience and endurance were essential for the success of my work. Thank you cousin(e).

I would like to thank Rosa-Maria Busl-Schuller for her constant support in all areas during my entire time at Roche Diagnostics and especially for her encouragement in difficult times. Many thanks goes also to my Ph.D. fellow Leon Pradl who demonstrated great expertise and who was always fun to discuss science with.

Two of my projects would not have been able to succeed without the great help and commitment of my interns Sabrina Fehrenbach and Martin Falke.

I would like to thank Diana Weininger for her help and work in the receptor quantitation project and the establishment of the initial protocols as well as the entire lab of Dr. Claudio Sustmann for their kind support. I would also like to thank Ioannis Ioannidis for his reliable help and prioritization of protein purifications for my projects. Many thanks goes to Wilma Ganslmeier and Gitta Reger for their incredible positivity and the creation of a great working atmosphere.

Special thanks to all those I had the opportunity to perform collaborations with. Especially I would like to mention here the project leaders Dr. Silke Metz, Dr. Alexander Haas, Dr. Olaf Mundigl, Dr. Ulrich Brinkmann, Dr. Rita Mateus Seidl and Dr. Birgit Bossenmaier.

I would also like to thank my chairperson and co-corrector Prof. Dr. K. Lang and Prof. Dr. MJ Feige for investing their time into my Ph.D. defense and the discussion of my work.

Finally I have to thank Dr. Kristina Ludigs for her constant belief in me and in my work, my dear stepfather Dr. Jochen Hellmann for his great support during many years and in all areas, Debora Wolf for her unbelievable patience, unlimited support and unique personality, Dr. Annette Zellmer for her overwhelming positivity, unchallenged pep talks and expertise, and the future scientist Tasja Vennemann for always finding kind and encouraging words.

9 Literature

Abes, R., Dutertre, C. A., & Teillaud, J. L. (2009). [Antibodies: better knowledge for a better use]. *Med.Sci.(Paris), 25,* 1011-1019.

Adachi, M., Taki, T., Ieki, Y., Huang, C. L., Higashiyama, M., & Miyake, M. (1996). Correlation of KAI1/CD82 gene expression with good prognosis in patients with non-small cell lung cancer. *Cancer Res., 56,* 1751-1755.

Adams, G. P. & Weiner, L. M. (2005). Monoclonal antibody therapy of cancer. *Nat.Biotechnol., 23,* 1147-1157.

Adamson, E. D. & Rees, A. R. (1981). Epidermal growth factor receptors. *Mol.Cell Biochem., 34,* 129-152.

Adlersberg, J. B. (1976). The immunoglobulin hinge (interdomain) region. *Ric.Clin.Lab, 6,* 191-205.

Ang, J., Lijovic, M., Ashman, L. K., Kan, K., & Frauman, A. G. (2004). CD151 protein expression predicts the clinical outcome of low-grade primary prostate cancer better than histologic grading: a new prognostic indicator? *Cancer Epidemiol.Biomarkers Prev., 13,* 1717-1721.

Arata, Y., Honzawa, M., & Shimizu, A. (1980). Proton nuclear magnetic resonance studies of human immunoglobulins: conformation of the hinge region of the IgG1 immunoglobulin. *Biochemistry, 19,* 5130-5135.

Arencibia, J. M., Martin, S., Perez-Rodriguez, F. J., & Bonnin, A. (2009). Gene expression profiling reveals overexpression of TSPAN13 in prostate cancer. *Int.J.Oncol., 34,* 457-463.

Arnold, J. N., Wormald, M. R., Sim, R. B., Rudd, P. M., & Dwek, R. A. (2007). The impact of glycosylation on the biological function and structure of human immunoglobulins. *Annu.Rev.Immunol., 25,* 21-50.

Arun, I., Wulu, J. A., Janik, J. E., Jasper, G. A., Yuan, C. M., Venzon, D. et al. (2010a). Visual inspection versus quantitative flow cytometry to detect aberrant CD2 expression in malignant T cells. *Cytometry B Clin.Cytom., 78,* 169-175.

Asaoka, Y., Tada, M., Ikenoue, T., Seto, M., Imai, M., Miyabayashi, K. et al. (2010). Gastric cancer cell line Hs746T harbors a splice site mutation of c-Met causing juxtamembrane domain deletion. *Biochem.Biophys.Res.Commun., 394,* 1042-1046.

Ashman, L. K., Aylett, G. W., Mehrabani, P. A., Bendall, L. J., Niutta, S., Cambareri, A. C. et al. (1991). The murine monoclonal antibody, 14A2.H1, identifies a novel platelet surface antigen. *Br.J Haematol., 79,* 263-270.

Atra, A., Abboudi, Z., Farahat, N., & Catovsky, D. (1997). Quantitative flow cytometry can predict childhood acute lymphoblastic leukaemia presenting with aplasia. *Leuk.Lymphoma, 27,* 173-177.

Atwell, S., Ridgway, J. B., Wells, J. A., & Carter, P. (1997). Stable heterodimers from remodeling the domain interface of a homodimer using a phage display library. *J.Mol.Biol., 270,* 26-35.

Auf der, M. A., Escher, D., & Barberis, A. (2001). Antigen-independent selection of stable intracellular single-chain antibodies. *FEBS Lett., 508,* 407-412.

Baeuerle, P. A., Kufer, P., & Bargou, R. (2009). BiTE: Teaching antibodies to engage T-cells for cancer therapy. *Curr.Opin.Mol.Ther., 11,* 22-30.

Baeuerle, P. A. & Reinhardt, C. (2009). Bispecific T-cell engaging antibodies for cancer therapy. *Cancer Res., 69,* 4941-4944.

Barb, A. W. & Prestegard, J. H. (2011). NMR analysis demonstrates immunoglobulin G N-glycans are accessible and dynamic. *Nat.Chem.Biol., 7,* 147-153.

Barcia, R., Garcia-Vargas, S., Bosca, L., & Lazo, P. A. (1996). CD53 antigen and epidermal growth factor induce similar changes in the pattern of phorbol ester binding in a B cell lymphoma. *Cell Immunol, 169,* 107-112.

Barnett, D., Storie, I., Wilson, G. A., Granger, V., & Reilly, J. T. (1998). Determination of leucocyte antibody binding capacity (ABC): the need for standardization. *Clin.Lab Haematol., 20,* 155-164.

Barreiro, O., Yanez-Mo, M., Sala-Valdes, M., Gutierrez-Lopez, M. D., Ovalle, S., Higginbottom, A. et al. (2005). Endothelial tetraspanin microdomains regulate leukocyte firm adhesion during extravasation. *Blood, 105,* 2852-2861.

Barta, P., Bjorkelund, H., & Andersson, K. (2011). Circumventing the requirement of binding saturation for receptor quantification using interaction kinetic extrapolation. *Nucl.Med.Commun., 32,* 863-867.

Beck, A., Wurch, T., Bailly, C., & Corvaia, N. (2010). Strategies and challenges for the next generation of therapeutic antibodies. *Nat.Rev.Immunol., 10,* 345-352.

Benhar, I. (2007). Design of synthetic antibody libraries. *Expert.Opin.Biol.Ther., 7,* 763-779.

Bepler, G., Bading, H., Heimann, B., Kiefer, P., Havemann, K., & Moelling, K. (1989). Expression of p64c-myc and neuroendocrine properties define three subclasses of small cell lung cancer. *Oncogene, 4,* 45-50.

Berditchevski, F. (2001). Complexes of tetraspanins with integrins: more than meets the eye. *J.Cell Sci., 114,* 4143-4151.

Berditchevski, F., Gilbert, E., Griffiths, M. R., Fitter, S., Ashman, L., & Jenner, S. J. (2001). Analysis of the CD151-alpha3beta1 integrin and CD151-tetraspanin interactions by mutagenesis. *J.Biol.Chem., 276,* 41165-41174.

Berditchevski, F. & Odintsova, E. (1999). Characterization of integrin-tetraspanin adhesion complexes: role of tetraspanins in integrin signaling. *J.Cell Biol., 146,* 477-492.

Berditchevski, F., Odintsova, E., Sawada, S., & Gilbert, E. (2002). Expression of the palmitoylation-deficient CD151 weakens the association of alpha 3 beta 1 integrin with the tetraspanin-enriched microdomains and affects integrin-dependent signaling. *J.Biol.Chem., 277,* 36991-37000.

Beroukhim, R., Mermel, C. H., Porter, D., Wei, G., Raychaudhuri, S., Donovan, J. et al. (2010). The landscape of somatic copy-number alteration across human cancers. *Nature, 463,* 899-905.

Bhargava, M., Joseph, A., Knesel, J., Halaban, R., Li, Y., Pang, S. et al. (1992). Scatter factor and hepatocyte growth factor: activities, properties, and mechanism. *Cell Growth Differ., 3,* 11-20.

Biocca, S., Ruberti, F., Tafani, M., Pierandrei-Amaldi, P., & Cattaneo, A. (1995). Redox state of single chain Fv fragments targeted to the endoplasmic reticulum, cytosol and mitochondria. *Biotechnology (N.Y.), 13,* 1110-1115.

Birchmeier, C., Birchmeier, W., Gherardi, E., & Vande Woude, G. F. (2003). Met, metastasis, motility and more. *Nat.Rev.Mol.Cell Biol., 4,* 915-925.

Birnboim, H. C. & Doly, J. (1979). A rapid alkaline extraction procedure for screening recombinant plasmid DNA. *Nucleic Acids Res, 7,* 1513-1523.

Boismenu, R., Rhein, M., Fischer, W. H., & Havran, W. L. (1996). A role for CD81 in early T cell development. *Science, 271,* 198-200.

Borvak, J., Richardson, J., Medesan, C., Antohe, F., Radu, C., Simionescu, M. et al. (1998). Functional expression of the MHC class I-related receptor, FcRn, in endothelial cells of mice. *Int.Immunol., 10,* 1289-1298.

Bosca, L. & Lazo, P. A. (1994). Induction of nitric oxide release by MRC OX-44 (anti-CD53) through a protein kinase C-dependent pathway in rat macrophages. *J.Exp.Med., 179,* 1119-1126.

Bostrom, J., Yu, S. F., Kan, D., Appleton, B. A., Lee, C. V., Billeci, K. et al. (2009). Variants of the antibody herceptin that interact with HER2 and VEGF at the antigen binding site. *Science, 323,* 1610-1614.

Boucheix, C., Duc, G. H., Jasmin, C., & Rubinstein, E. (2001). Tetraspanins and malignancy. *Expert.Rev.Mol.Med., 2001,* 1-17.

Boucheix, C. & Rubinstein, E. (2001). Tetraspanins. *Cell Mol.Life Sci., 58,* 1189-1205.

Boyiadzis, M. & Foon, K. A. (2008). Approved monoclonal antibodies for cancer therapy. *Expert.Opin.Biol.Ther., 8,* 1151-1158.

Brakebusch, C. & Fassler, R. (2003). The integrin-actin connection, an eternal love affair. *EMBO J., 22,* 2324-2333.

Brambell, F. W. (1966). The transmission of immunity from mother to young and the catabolism of immunoglobulins. *Lancet, 2,* 1087-1093.

Brotherick, I., Lennard, T. W., Wilkinson, S. E., Cook, S., Angus, B., & Shenton, B. K. (1994). Flow cytometric method for the measurement of epidermal growth factor receptor and comparison with the radio-ligand binding assay. *Cytometry, 16,* 262-269.

Bu, Y., Yang, Z., Li, Q., & Song, F. (2008). Silencing of polo-like kinase (Plk) 1 via siRNA causes inhibition of growth and induction of apoptosis in human esophageal cancer cells. *Oncology, 74,* 198-206.

Buranda, T., Wu, Y., & Sklar, L. A. (2011). Quantum dots for quantitative flow cytometry. *Methods Mol.Biol., 699,* 67-84.

Buss, J. E., Kudlow, J. E., Lazar, C. S., & Gill, G. N. (1982). Altered epidermal growth factor (EGF)-stimulated protein kinase activity in variant A431 cells with altered growth responses to EGF. *Proc.Natl.Acad.Sci.U.S.A, 79,* 2574-2578.

Buss, N. A., Henderson, S. J., McFarlane, M., Shenton, J. M., & de, H. L. (2012). Monoclonal antibody therapeutics: history and future. *Curr.Opin.Pharmacol., 12,* 615-622.

Carpenter, G., Lembach, K. J., Morrison, M. M., & Cohen, S. (1975). Characterization of the binding of 125-I-labeled epidermal growth factor to human fibroblasts. *J.Biol.Chem., 250,* 4297-4304.

Carragher, N. O. & Frame, M. C. (2004). Focal adhesion and actin dynamics: a place where kinases and proteases meet to promote invasion. *Trends Cell Biol., 14,* 241-249.

Carragher, N. O., Westhoff, M. A., Fincham, V. J., Schaller, M. D., & Frame, M. C. (2003). A novel role for FAK as a protease-targeting adaptor protein: regulation by p42 ERK and Src. *Curr.Biol., 13,* 1442-1450.

Carter, P. (2001a). Bispecific human IgG by design. *J.Immunol.Methods, 248,* 7-15.

Carter, P. (2001b). Improving the efficacy of antibody-based cancer therapies. *Nat.Rev.Cancer, 1,* 118-129.

Carter, P. J. (2006). Potent antibody therapeutics by design. *Nat.Rev.Immunol., 6,* 343-357.

Cartron, G., Dacheux, L., Salles, G., Solal-Celigny, P., Bardos, P., Colombat, P. et al. (2002). Therapeutic activity of humanized anti-CD20 monoclonal antibody and polymorphism in IgG Fc receptor FcgammaRIIIa gene. *Blood, 99,* 754-758.

Castoldi, R., Jucknischke, U., Pradel, L. P., Arnold, E., Klein, C., Scheiblich, S. et al. (2012). Molecular characterization of novel trispecific ErbB-cMet-IGF1R antibodies and their antigen-binding properties. *Protein Eng Des Sel, 25,* 551-559.

Chan, A. C. & Carter, P. J. (2010). Therapeutic antibodies for autoimmunity and inflammation. *Nat.Rev.Immunol., 10,* 301-316.

Chantler, S. & Batty, I. (1983). Quality control of fluorescein isothiocyanate-labeled reagents. *Ann.N.Y.Acad.Sci., 420,* 68-73.

Chapman, A. P., Antoniw, P., Spitali, M., West, S., Stephens, S., & King, D. J. (1999). Therapeutic antibody fragments with prolonged in vivo half-lives. *Nat.Biotechnol., 17,* 780-783.

Chapple, M. R., Johnson, G. D., & Davidson, R. S. (1990). Fluorescence quenching; a practical problem in flow cytometry. *J Microsc., 159,* 245-253.

Chari, R. V. (2008). Targeted cancer therapy: conferring specificity to cytotoxic drugs. *Acc.Chem.Res., 41,* 98-107.

Charrin, S., Le, N. F., Oualid, M., Billard, M., Faure, G., Hanash, S. M. et al. (2001). The major CD9 and CD81 molecular partner. Identification and characterization of the complexes. *J Biol.Chem., 276,* 14329-14337.

Charrin, S., Le, N. F., Silvie, O., Milhiet, P. E., Boucheix, C., & Rubinstein, E. (2009). Lateral organization of membrane proteins: tetraspanins spin their web. *Biochem.J., 420,* 133-154.

Charrin, S., Manie, S., Billard, M., Ashman, L., Gerlier, D., Boucheix, C. et al. (2003a). Multiple levels of interactions within the tetraspanin web. *Biochem.Biophys.Res.Commun., 304,* 107-112.

Charrin, S., Manie, S., Oualid, M., Billard, M., Boucheix, C., & Rubinstein, E. (2002). Differential stability of tetraspanin/tetraspanin interactions: role of palmitoylation. *FEBS Lett., 516,* 139-144.

Charrin, S., Manie, S., Thiele, C., Billard, M., Gerlier, D., Boucheix, C. et al. (2003b). A physical and functional link between cholesterol and tetraspanins. *Eur.J.Immunol, 33,* 2479-2489.

Chatelier, R. C., Ashcroft, R. G., Lloyd, C. J., Nice, E. C., Whitehead, R. H., Sawyer, W. H. et al. (1986). Binding of fluoresceinated epidermal growth factor to A431 cell sub-populations studied using a model-independent analysis of flow cytometric fluorescence data. *EMBO J., 5,* 1181-1186.

Chatenoud, L. (2004). Anti-CD3 antibodies: towards clinical antigen-specific immunomodulation. *Curr.Opin.Pharmacol., 4,* 403-407.

Chen, L., Wang, Z., Zhan, X., Li, D. C., Zhu, Y. Y., & Zhu, J. (2007). Association of NET-1 gene expression with human hepatocellular carcinoma. *Int.J.Surg.Pathol., 15,* 346-353.

Chen, Q. & Massague, J. (2012). Molecular pathways: VCAM-1 as a potential therapeutic target in metastasis. *Clin.Cancer Res., 18,* 5520-5525.

Chen, Y., Peng, W., Lu, Y., Chen, J., Zhu, Y. Y., & Xi, T. (2013). MiR-200a enhances the migrations of A549 and SK-MES-1 cells by regulating the expression of TSPAN1. *J.Biosci., 38,* 523-532.

Cheng, L., Zhang, S., Alexander, R., Yao, Y., MacLennan, G. T., Pan, C. X. et al. (2011). The landscape of EGFR pathways and personalized management of non-small-cell lung cancer. *Future.Oncol., 7,* 519-541.

Chess, P. R., Ryan, R. M., & Finkelstein, J. N. (1998). H441 pulmonary epithelial cell mitogenic effects and signaling pathways in response to HGF and TGF-alpha. *Exp.Lung Res., 24,* 27-39.

Chirino, A. J., Ary, M. L., & Marshall, S. A. (2004). Minimizing the immunogenicity of protein therapeutics. *Drug Discov.Today, 9,* 82-90.

Chowdhury, P. S. & Wu, H. (2005). Tailor-made antibody therapeutics. *Methods, 36,* 11-24.

Christensen, J. G., Schreck, R., Burrows, J., Kuruganti, P., Chan, E., Le, P. et al. (2003). A selective small molecule inhibitor of c-Met kinase inhibits c-Met-dependent phenotypes in vitro and exhibits cytoreductive antitumor activity in vivo. *Cancer Res., 63,* 7345-7355.

Claas, C., Seiter, S., Claas, A., Savelyeva, L., Schwab, M., & Zoller, M. (1998). Association between the rat homologue of CO-029, a metastasis-associated tetraspanin molecule and consumption coagulopathy. *J.Cell Biol., 141,* 267-280.

Claas, C., Stipp, C. S., & Hemler, M. E. (2001). Evaluation of prototype transmembrane 4 superfamily protein complexes and their relation to lipid rafts. *J.Biol.Chem., 276,* 7974-7984.

Claas, C., Wahl, J., Orlicky, D. J., Karaduman, H., Schnolzer, M., Kempf, T. et al. (2005). The tetraspanin D6.1A and its molecular partners on rat carcinoma cells. *Biochem.J., 389,* 99-110.

Clark, M. (2000). Antibody humanization: a case of the 'Emperor's new clothes'? *Immunol.Today, 21,* 397-402.

Clark, M. R. (1997). IgG effector mechanisms. *Chem.Immunol., 65,* 88-110.

Clynes, R. A., Towers, T. L., Presta, L. G., & Ravetch, J. V. (2000). Inhibitory Fc receptors modulate in vivo cytotoxicity against tumor targets. *Nat.Med., 6,* 443-446.

Cohen, S., Carpenter, G., & King, L., Jr. (1980). Epidermal growth factor-receptor-protein kinase interactions. Co-purification of receptor and epidermal growth factor-enhanced phosphorylation activity. *J.Biol.Chem., 255,* 4834-4842.

Coloma, M. J. & Morrison, S. L. (1997). Design and production of novel tetravalent bispecific antibodies. *Nat.Biotechnol., 15,* 159-163.

Comoglio, P. M., Giordano, S., & Trusolino, L. (2008). Drug development of MET inhibitors: targeting oncogene addiction and expedience. *Nat.Rev.Drug Discov., 7,* 504-516.

Coons, H., Creech, R., Norman Jones, R., & Berliner, R. (1942). The Demonstration of Pneumococcal Antigen in Tissues by the Use of Fluorescent Antibody. *J.Immunol., 45,* 159-170.

Coons, H. & Kaplan, H. (1950). Localization of antigen in tissue cells; improvements in a method for the detection of antigen by means of fluorescent antibody. *J.Exp.Med., 91,* 1-13.

Croasdale, R., Wartha, K., Schanzer, J. M., Kuenkele, K. P., Ries, C., Mayer, K. et al. (2012). Development of tetravalent IgG1 dual targeting IGF-1R-EGFR antibodies with potent tumor inhibition. *Arch.Biochem.Biophys., 526,* 206-218.

D'Arena, G., Musto, P., Cascavilla, N., Dell'Olio, M., Di, R. N., & Carotenuto, M. (2000). Quantitative flow cytometry for the differential diagnosis of leukemic B-cell chronic lymphoproliferative disorders. *Am.J.Hematol., 64,* 275-281.

D'hautcourt, J. L. (2002). Quantitative Flow Cytometric Analysis of Membrane Antigen Expression. *Curr.Protoc.Cytom.,* 6.12.1-6.12.22.

Davis, K. A., Abrams, B., Iyer, S. B., Hoffman, R. A., & Bishop, J. E. (1998). Determination of CD4 antigen density on cells: role of antibody valency, avidity, clones, and conjugation. *Cytometry, 33,* 197-205.

de, F. A., Vornlocher, H. P., Maraganore, J., & Lieberman, J. (2007). Interfering with disease: a progress report on siRNA-based therapeutics. *Nat.Rev.Drug Discov., 6,* 443-453.

Dedhar, S. (2000). Cell-substrate interactions and signaling through ILK. *Curr.Opin.Cell Biol., 12,* 250-256.

Deka, C., Lehnert, B. E., Lehnert, N. M., Jones, G. M., Sklar, L. A., & Steinkamp, J. A. (1996). Analysis of fluorescence lifetime and quenching of FITC-conjugated antibodies on cells by phase-sensitive flow cytometry. *Cytometry, 25,* 271-279.

Dennis, M. S., Zhang, M., Meng, Y. G., Kadkhodayan, M., Kirchhofer, D., Combs, D. et al. (2002). Albumin binding as a general strategy for improving the pharmacokinetics of proteins. *J.Biol.Chem., 277,* 35035-35043.

Der-Balian, G. P., Kameda, N., & Rowley, G. L. (1988). Fluorescein labeling of Fab' while preserving single thiol. *Anal.Biochem., 173,* 59-63.

Didier, E. S., Rogers, L. B., Orenstein, J. M., Baker, M. D., Vossbrinck, C. R., Van, G. T. et al. (1996). Characterization of Encephalitozoon (Septata) intestinalis isolates cultured from nasal mucosa and bronchoalveolar lavage fluids of two AIDS patients. *J Eukaryot.Microbiol., 43,* 34-43.

Digman, M. A., Dalal, R., Horwitz, A. F., & Gratton, E. (2008). Mapping the number of molecules and brightness in the laser scanning microscope. *Biophys.J., 94,* 2320-2332.

Dong, J. T., Lamb, P. W., Rinker-Schaeffer, C. W., Vukanovic, J., Ichikawa, T., Isaacs, J. T. et al. (1995). KAI1, a metastasis suppressor gene for prostate cancer on human chromosome 11p11.2. *Science, 268,* 884-886.

Dong, J. T., Suzuki, H., Pin, S. S., Bova, G. S., Schalken, J. A., Isaacs, W. B. et al. (1996). Down-regulation of the KAI1 metastasis suppressor gene during the progression of human prostatic cancer infrequently involves gene mutation or allelic loss. *Cancer Res., 56,* 4387-4390.

Dua, R., Zhang, J., Parry, G., & Penuel, E. (2011). Detection of hepatocyte growth factor (HGF) ligand-c-MET receptor activation in formalin-fixed paraffin embedded specimens by a novel proximity assay. *PLoS.One., 6,* -e15932.

Eisel, D., Grünewald-Janho, S., & Krushen, B. (2002). *DIG Application Manual for Nonradioactive In Situ Hybridization*. (3 ed.) Penzberg: Roche Diagnostics GmbH.

Ely, K. R., Colman, P. M., Abola, E. E., Hess, A. C., Peabody, D. S., Parr, D. M. et al. (1978). Mobile Fc region in the Zie IgG2 cryoglobulin: comparison of crystals of the F(ab')2 fragment and the intact immunoglobulin. *Biochemistry, 17,* 820-823.

Engelman, J. A., Zejnullahu, K., Mitsudomi, T., Song, Y., Hyland, C., Park, J. O. et al. (2007). MET amplification leads to gefitinib resistance in lung cancer by activating ERBB3 signaling. *Science, 316,* 1039-1043.

Erickson, H. K., Park, P. U., Widdison, W. C., Kovtun, Y. V., Garrett, L. M., Hoffman, K. et al. (2006). Antibody-maytansinoid conjugates are activated in targeted cancer cells by lysosomal degradation and linker-dependent intracellular processing. *Cancer Res., 66,* 4426-4433.

Esteva, F. J., Valero, V., Booser, D., Guerra, L. T., Murray, J. L., Pusztai, L. et al. (2002). Phase II study of weekly docetaxel and trastuzumab for patients with HER-2-overexpressing metastatic breast cancer. *J.Clin.Oncol., 20,* 1800-1808.

Fabbro, D., Kung, W., Roos, W., Regazzi, R., & Eppenberger, U. (1986). Epidermal growth factor binding and protein kinase C activities in human breast cancer cell lines: possible quantitative relationship. *Cancer Res, 46,* 2720-2725.

Fabricant, R. N., De Larco, J. E., & Todaro, G. J. (1977). Nerve growth factor receptors on human melanoma cells in culture. *Proc.Natl.Acad.Sci.U.S.A, 74,* 565-569.

Faust, J. B. & Meeker, T. C. (1992). Amplification and expression of the bcl-1 gene in human solid tumor cell lines. *Cancer Res, 52,* 2460-2463.

Ferenz, N. P., Gable, A., & Wadsworth, P. (2010). Mitotic functions of kinesin-5. *Semin.Cell Dev.Biol., 21,* 255-259.

Filpula, D. (2007). Antibody engineering and modification technologies. *Biomol.Eng, 24,* 201-215.

Fitter, S., Sincock, P. M., Jolliffe, C. N., & Ashman, L. K. (1999). Transmembrane 4 superfamily protein CD151 (PETA-3) associates with beta 1 and alpha IIb beta 3 integrins in haemopoietic cell lines and modulates cell-cell adhesion. *Biochem.J, 338 (Pt 1),* 61-70.

Freeman, W. M., Walker, S. J., & Vrana, K. E. (1999). Quantitative RT-PCR: pitfalls and potential. *Biotechniques, 26,* 112-22, 124.

Furuya, M., Kato, H., Nishimura, N., Ishiwata, I., Ikeda, H., Ito, R. et al. (2005). Down-regulation of CD9 in human ovarian carcinoma cell might contribute to peritoneal dissemination: morphologic alteration and reduced expression of beta1 integrin subsets. *Cancer Res, 65,* 2617-2625.

Gaigalas, A. K., Li, Li., Henderson, O., Vogt, R., Barr, J., Marti, G. et al. (2001). The development of fluorescence intensity standards. *JRes Natl Inst Stand Technol, 106,* 381-389.

Gao, T. Y. & Yu, Y. H. (2008). [Expression of TM4SF9 in human trophoblasts]. *Nan.Fang Yi.Ke.Da.Xue.Xue.Bao., 28,* 1080-1082.

Gazdar, A. F., Linnoila, R. I., Kurita, Y., Oie, H. K., Mulshine, J. L., Clark, J. C. et al. (1990). Peripheral airway cell differentiation in human lung cancer cell lines. *Cancer Res, 50,* 5481-5487.

Geary, S. M., Cambareri, A. C., Sincock, P. M., Fitter, S., & Ashman, L. K. (2001). Differential tissue expression of epitopes of the tetraspanin CD151 recognised by monoclonal antibodies. *Tissue Antigens, 58,* 141-153.

Geisberger, R., Lamers, M., & Achatz, G. (2006). The riddle of the dual expression of IgM and IgD. *Immunology, 118,* 429-437.

Gennari, R., Menard, S., Fagnoni, F., Ponchio, L., Scelsi, M., Tagliabue, E. et al. (2004). Pilot study of the mechanism of action of preoperative trastuzumab in patients with primary operable breast tumors overexpressing HER2. *Clin.Cancer Res., 10,* 5650-5655.

Gesierich, S., Berezovskiy, I., Ryschich, E., & Zoller, M. (2006). Systemic induction of the angiogenesis switch by the tetraspanin D6.1A/CO-029. *Cancer Res., 66,* 7083-7094.

Gesierich, S., Paret, C., Hildebrand, D., Weitz, J., Zgraggen, K., Schmitz-Winnenthal, F. H. et al. (2005). Colocalization of the tetraspanins, CO-029 and CD151, with integrins in human pancreatic adenocarcinoma: impact on cell motility. *Clin.Cancer Res., 11,* 2840-2852.

Gherardi, E., Birchmeier, W., Birchmeier, C., & Vande, W. G. (2012). Targeting MET in cancer: rationale and progress. *Nat.Rev.Cancer, 12,* 89-103.

Giard, D. J., Aaronson, S. A., Todaro, G. J., Arnstein, P., Kersey, J. H., Dosik, H. et al. (1973). In vitro cultivation of human tumors: establishment of cell lines derived from a series of solid tumors. *J Natl Cancer Inst, 51,* 1417-1423.

Gill, G. N. & Lazar, C. S. (1981). Increased phosphotyrosine content and inhibition of proliferation in EGF-treated A431 cells. *Nature, 293,* 305-307.

Ginaldi, L., De, M. M., Matutes, E., Farahat, N., Morilla, R., & Catovsky, D. (1998a). Levels of expression of CD19 and CD20 in chronic B cell leukaemias. *J.Clin.Pathol., 51,* 364-369.

Ginaldi, L., De, M. M., Matutes, E., Farahat, N., Morilla, R., Dyer, M. J. et al. (1998b). Levels of expression of CD52 in normal and leukemic B and T cells: correlation with in vivo therapeutic responses to Campath-1H. *Leuk.Res., 22,* 185-191.

Glover, D. M., Hagan, I. M., & Tavares, A. A. (1998). Polo-like kinases: a team that plays throughout mitosis. *Genes Dev., 12,* 3777-3787.

Goding, J. W. (1976). Conjugation of antibodies with fluorochromes: modifications to the standard methods. *J Immunol Methods, 13,* 215-226.

Gordon-Alonso, M., Yanez-Mo, M., Barreiro, O., Alvarez, S., Munoz-Fernandez, M. A., Valenzuela-Fernandez, A. et al. (2006). Tetraspanins CD9 and CD81 modulate HIV-1-induced membrane fusion. *J Immunol, 177,* 5129-5137.

Gow, J. & Wardlaw, A. C. (1975). Iodination of a mixture of soluble proteins by the (125I)-lactoperoxidase technique. *Biochem.Biophys.Res.Commun., 67,* 43-49.

Graham, F. L., Smiley, J., Russell, W. C., & Nairn, R. (1977). Characteristics of a human cell line transformed by DNA from human adenovirus type 5. *J Gen.Virol., 36,* 59-74.

Green, L. L. (1999). Antibody engineering via genetic engineering of the mouse: XenoMouse strains are a vehicle for the facile generation of therapeutic human monoclonal antibodies. *J.Immunol.Methods, 231,* 11-23.

Greenbaum, D., Colangelo, C., Williams, K., & Gerstein, M. (2003). Comparing protein abundance and mRNA expression levels on a genomic scale. *Genome Biol., 4,* 117.

Gruber, H. J., Hahn, C. D., Kada, G., Riener, C. K., Harms, G. S., Ahrer, W. et al. (2000). Anomalous fluorescence enhancement of Cy3 and cy3.5 versus anomalous fluorescence loss of Cy5 and Cy7 upon covalent linking to IgG and noncovalent binding to avidin. *Bioconjug.Chem., 11,* 696-704.

Guy, P. M., Platko, J. V., Cantley, L. C., Cerione, R. A., & Carraway, K. L., III (1994). Insect cell-expressed p180erbB3 possesses an impaired tyrosine kinase activity. *Proc.Natl.Acad.Sci.U.S.A, 91,* 8132-8136.

Hacker, G. (2000). The morphology of apoptosis. *Cell Tissue Res., 301,* 5-17.

Haeuw, J. F., Goetsch, L., Bailly, C., & Corvaia, N. (2011). Tetraspanin CD151 as a target for antibody-based cancer immunotherapy. *Biochem.Soc.Trans., 39,* 553-558.

Haigler, H., Ash, J. F., Singer, S. J., & Cohen, S. (1978). Visualization by fluorescence of the binding and internalization of epidermal growth factor in human carcinoma cells A-431. *Proc.Natl.Acad.Sci.U.S.A, 75,* 3317-3321.

Hardy, R. R. (1986). *Purification and coupling of fluorescent proteins for use in flow cytometry*. (4 ed.) Boston: Blackwell Scientific Publications.

Hashida, H., Takabayashi, A., Tokuhara, T., Hattori, N., Taki, T., Hasegawa, H. et al. (2003). Clinical significance of transmembrane 4 superfamily in colon cancer. *Br.J.Cancer, 89,* 158-167.

Hashira, S., Okitsu-Negishi, S., & Yoshino, K. (2000). Placental transfer of IgG subclasses in a Japanese population. *Pediatr.Int., 42,* 337-342.

Haugland, R. P. (1995). Coupling of monoclonal antibodies with fluorophores. *Methods Mol.Biol., 45,* 205-221.

Heiss, M. M., Strohlein, M. A., Jager, M., Kimmig, R., Burges, A., Schoberth, A. et al. (2005). Immunotherapy of malignant ascites with trifunctional antibodies. *Int.J.Cancer, 117,* 435-443.

Hemler, M. E. (2001). Specific tetraspanin functions. *J.Cell Biol., 155,* 1103-1107.

Hemler, M. E. (2008). Targeting of tetraspanin proteins--potential benefits and strategies. *Nat.Rev.Drug Discov., 7,* 747-758.

Hemler, M. E. & Lobb, R. R. (1995). The leukocyte beta 1 integrins. *Curr.Opin.Hematol., 2,* 61-67.

Hemler, M. E., Mannion, B. A., & Berditchevski, F. (1996). Association of TM4SF proteins with integrins: relevance to cancer. *Biochim.Biophys.Acta, 1287,* 67-71.

Hemler, M. E. (2003). Tetraspanin proteins mediate cellular penetration, invasion, and fusion events and define a novel type of membrane microdomain. *Annu.Rev.Cell Dev.Biol., 19,* 397-422.

Hemler, M. E. (2005). Tetraspanin functions and associated microdomains. *Nat.Rev.Mol.Cell Biol., 6,* 801-811.

Hirano, C., Nagata, M., Noman, A. A., Kitamura, N., Ohnishi, M., Ohyama, T. et al. (2009). Tetraspanin gene expression levels as potential biomarkers for malignancy of gingival squamous cell carcinoma. *Int.J.Cancer, 124,* 2911-2916.

Hirsch, F. R., Varella-Garcia, M., & Cappuzzo, F. (2009). Predictive value of EGFR and HER2 overexpression in advanced non-small-cell lung cancer. *Oncogene, 28 Suppl 1,* S32-S37.

Holliger, P. & Hudson, P. J. (2005). Engineered antibody fragments and the rise of single domains. *Nat.Biotechnol., 23,* 1126-1136.

Holliger, P., Wing, M., Pound, J. D., Bohlen, H., & Winter, G. (1997). Retargeting serum immunoglobulin with bispecific diabodies. *Nat.Biotechnol., 15,* 632-636.

Holmes, K. L. & Lantz, L. M. (2001). Protein labeling with fluorescent probes. *Methods Cell Biol., 63,* 185-204.

Holtke, H. J., Ankenbauer, W., Muhlegger, K., Rein, R., Sagner, G., Seibl, R. et al. (1995). The digoxigenin (DIG) system for non-radioactive labelling and detection of nucleic acids--an overview. *Cell Mol.Biol.(Noisy.-le-grand), 41,* 883-905.

Holtke, H. J., Seibl, R., Burg, J., Muhlegger, K., & Kessler, C. (1990). Non-radioactive labeling and detection of nucleic acids. II. Optimization of the digoxigenin system. *Biol.Chem.Hoppe Seyler, 371,* 929-938.

Hong, I. K., Jin, Y. J., Byun, H. J., Jeoung, D. I., Kim, Y. M., & Lee, H. (2006). Homophilic interactions of Tetraspanin CD151 up-regulate motility and matrix metalloproteinase-9 expression of human melanoma cells through adhesion-dependent c-Jun activation signaling pathways. *J.Biol.Chem., 281,* 24279-24292.

Hood, J. D. & Cheresh, D. A. (2002). Role of integrins in cell invasion and migration. *Nat.Rev.Cancer, 2,* 91-100.

Hoogenboom, H. R. (2005). Selecting and screening recombinant antibody libraries. *Nat.Biotechnol., 23,* 1105-1116.

Hsi, E. D., Kopecky, K. J., Appelbaum, F. R., Boldt, D., Frey, T., Loftus, M. et al. (2003). Prognostic significance of CD38 and CD20 expression as assessed by quantitative flow cytometry in chronic lymphocytic leukaemia. *Br.J Haematol., 120,* 1017-1025.

Huang, C. I., Kohno, N., Ogawa, E., Adachi, M., Taki, T., & Miyake, M. (1998). Correlation of reduction in MRP-1/CD9 and KAI1/CD82 expression with recurrences in breast cancer patients. *Am.J.Pathol., 153,* 973-983.

Huang, H., Groth, J., Sossey-Alaoui, K., Hawthorn, L., Beall, S., & Geradts, J. (2005a). Aberrant expression of novel and previously described cell membrane markers in human breast cancer cell lines and tumors. *Clin.Cancer Res., 11,* 4357-4364.

Huang, S., Yuan, S., Dong, M., Su, J., Yu, C., Shen, Y. et al. (2005b). The phylogenetic analysis of tetraspanins projects the evolution of cell-cell interactions from unicellular to multicellular organisms. *Genomics, 86,* 674-684.

Hudis, C. A. (2007). Trastuzumab--mechanism of action and use in clinical practice. *N.Engl.J.Med., 357,* 39-51.

Hwang, W. Y. & Foote, J. (2005). Immunogenicity of engineered antibodies. *Methods, 36,* 3-10.

Idusogie, E. E., Presta, L. G., Gazzano-Santoro, H., Totpal, K., Wong, P. Y., Ultsch, M. et al. (2000). Mapping of the C1q binding site on rituxan, a chimeric antibody with a human IgG1 Fc. *J.Immunol., 164,* 4178-4184.

Imai, Y., Leung, C. K., Friesen, H. G., & Shiu, R. P. (1982). Epidermal growth factor receptors and effect of epidermal growth factor on growth of human breast cancer cells in long-term tissue culture. *Cancer Res, 42,* 4394-4398.

Iwai, K., Ishii, M., Ohshima, S., Miyatake, K., & Saeki, Y. (2007). Expression and function of transmembrane-4 superfamily (tetraspanin) proteins in osteoclasts: reciprocal roles of Tspan-5 and NET-6 during osteoclastogenesis. *Allergol.Int., 56,* 457-463.

Iyer, S. B., Hultin, L. E., Zawadzki, J. A., Davis, K. A., & Giorgi, J. V. (1998). Quantitation of CD38 expression using QuantiBRITE beads. *Cytometry, 33,* 206-212.

Jackson, P., Marreiros, A., & Russell, P. J. (2005). KAI1 tetraspanin and metastasis suppressor. *Int.J.Biochem.Cell Biol., 37,* 530-534.

Janes, S. M. & Watt, F. M. (2006). New roles for integrins in squamous-cell carcinoma. *Nat.Rev.Cancer, 6,* 175-183.

Janeway, CA., Travers, P., Walport, M., & Shlomchik, MJ. (2001). *Immunobiology: The Immune System in Health and Disease.* (5 ed.) New York: Garland Science.

Jaracz, S., Chen, J., Kuznetsova, L. V., & Ojima, I. (2005). Recent advances in tumor-targeting anticancer drug conjugates. *Bioorg.Med.Chem., 13,* 5043-5054.

Jasper, G. A., Arun, I., Venzon, D., Kreitman, R. J., Wayne, A. S., Yuan, C. M. et al. (2011). Variables affecting the quantitation of CD22 in neoplastic B cells. *Cytometry B Clin.Cytom., 80,* 83-90.

Jefferis, R. (2007). Antibody therapeutics: isotype and glycoform selection. *Expert.Opin.Biol.Ther., 7,* 1401-1413.

Jetten, A. M. (1980). Retinoids specifically enhance the number of epidermal growth factor receptors. *Nature, 284,* 626-629.

Jiang, L., Yuan, C. M., Hubacheck, J., Janik, J. E., Wilson, W., Morris, J. C. et al. (2009). Variable CD52 expression in mature T cell and NK cell malignancies: implications for alemtuzumab therapy. *Br.J.Haematol., 145,* 173-179.

Johnson, J. L., Winterwood, N., DeMali, K. A., & Stipp, C. S. (2009). Tetraspanin CD151 regulates RhoA activation and the dynamic stability of carcinoma cell-cell contacts. *J Cell Sci., 122,* 2263-2273.

Jones, E. A. & Waldmann, T. A. (1972). The mechanism of intestinal uptake and transcellular transport of IgG in the neonatal rat. *J.Clin.Invest, 51,* 2916-2927.

Joosten, L. A., Helsen, M. M., van de Loo, F. A., & van den Berg, W. B. (2008). Anticytokine treatment of established type II collagen-induced arthritis in DBA/1 mice: a comparative study using anti-TNFalpha, anti-IL-1alpha/beta and IL-1Ra. *Arthritis Rheum., 58,* S110-S122.

Judge, S. M. & Chatterton, R. T., Jr. (1983). Progesterone-specific stimulation of triglyceride biosynthesis in a breast cancer cell line (T-47D). *Cancer Res, 43,* 4407-4412.

Juliano, R. L., Reddig, P., Alahari, S., Edin, M., Howe, A., & Aplin, A. (2004). Integrin regulation of cell signalling and motility. *Biochem.Soc.Trans., 32,* 443-446.

Jung, S. H., Pastan, I., & Lee, B. (1994). Design of interchain disulfide bonds in the framework region of the Fv fragment of the monoclonal antibody B3. *Proteins, 19,* 35-47.

Junutula, J. R., Raab, H., Clark, S., Bhakta, S., Leipold, D. D., Weir, S. et al. (2008). Site-specific conjugation of a cytotoxic drug to an antibody improves the therapeutic index. *Nat.Biotechnol., 26,* 925-932.

Kageyama, S., Yoshiki, T., Isono, T., Tanaka, T., Kim, C. J., Yuasa, T. et al. (2002). High expression of human uroplakin Ia in urinary bladder transitional cell carcinoma. *Jpn.J.Cancer Res., 93,* 523-531.

Kamata, N., Chida, K., Rikimaru, K., Horikoshi, M., Enomoto, S., & Kuroki, T. (1986). Growth-inhibitory effects of epidermal growth factor and overexpression of its receptors on human squamous cell carcinomas in culture. *Cancer Res., 46,* 1648-1653.

Kanetaka, K., Sakamoto, M., Yamamoto, Y., Takamura, M., Kanematsu, T., & Hirohashi, S. (2003). Possible involvement of tetraspanin CO-029 in hematogenous intrahepatic metastasis of liver cancer cells. *J.Gastroenterol.Hepatol., 18,* 1309-1314.

Kanetaka, K., Sakamoto, M., Yamamoto, Y., Yamasaki, S., Lanza, F., Kanematsu, T. et al. (2001). Overexpression of tetraspanin CO-029 in hepatocellular carcinoma. *J.Hepatol., 35,* 637-642.

Karlen, Y., McNair, A., Perseguers, S., Mazza, C., & Mermod, N. (2007). Statistical significance of quantitative PCR. *BMC.Bioinformatics., 8,* 131.

Kashina, A. S., Scholey, J. M., Leszyk, J. D., & Saxton, W. M. (1996). An essential bipolar mitotic motor. *Nature, 384,* -225.

Ke, A. W., Shi, G. M., Zhou, J., Wu, F. Z., Ding, Z. B., Hu, M. Y. et al. (2009). Role of overexpression of CD151 and/or c-Met in predicting prognosis of hepatocellular carcinoma. *Hepatology, 49,* 491-503.

Kessler, C. (1991). The digoxigenin:anti-digoxigenin (DIG) technology--a survey on the concept and realization of a novel bioanalytical indicator system. *Mol.Cell Probes, 5,* 161-205.

Kessler, C., Holtke, H. J., Seibl, R., Burg, J., & Muhlegger, K. (1990). Non-radioactive labeling and detection of nucleic acids. I. A novel DNA labeling and detection system based on digoxigenin: anti-digoxigenin ELISA principle (digoxigenin system). *Biol.Chem.Hoppe Seyler, 371,* 917-927.

King, D., Yeomanson, D., & Bryant, H. E. (2015). PI3King the Lock: Targeting the PI3K/Akt/mTOR Pathway as a Novel Therapeutic Strategy in Neuroblastoma. *J Pediatr.Hematol.Oncol., 37,* 245-251.

Kipriyanov, S. M. & Le, G. F. (2004). Generation and production of engineered antibodies. *Mol.Biotechnol., 26,* 39-60.

Kitadokoro, K., Bordo, D., Galli, G., Petracca, R., Falugi, F., Abrignani, S. et al. (2001). CD81 extracellular domain 3D structure: insight into the tetraspanin superfamily structural motifs. *EMBO J., 20,* 12-18.

Klein, C., Sustmann, C., Thomas, M., Stubenrauch, K., Croasdale, R., Schanzer, J. et al. (2012). Progress in overcoming the chain association issue in bispecific heterodimeric IgG antibodies. *MAbs., 4,* 653-663.

Klosek, S. K., Nakashiro, K., Hara, S., Shintani, S., Hasegawa, H., & Hamakawa, H. (2005). CD151 forms a functional complex with c-Met in human salivary gland cancer cells. *Biochem.Biophys.Res.Commun., 336,* 408-416.

Knoblich, K., Wang, H. X., Sharma, C., Fletcher, A. L., Turley, S. J., & Hemler, M. E. (2013). Tetraspanin TSPAN12 regulates tumor growth and metastasis and inhibits beta-catenin degradation. *Cell Mol.Life Sci.*.

Kobayashi, M., Iwamatsu, A., Shinohara-Kanda, A., Ihara, S., & Fukui, Y. (2003). Activation of ErbB3-PI3-kinase pathway is correlated with malignant phenotypes of adenocarcinomas. *Oncogene, 22,* 1294-1301.

Koga, A., Aoyagi, K., Imaizumi, T., Miyagi, M., & Shirouzu, K. (2011). Comparison between the gastric cancer cell line MKN-45 and the high-potential peritoneal dissemination gastric cancer cell line MKN-45P. *Kurume Med.J, 58,* 73-79.

Kohno, M., Hasegawa, H., Miyake, M., Yamamoto, T., & Fujita, S. (2002). CD151 enhances cell motility and metastasis of cancer cells in the presence of focal adhesion kinase. *Int.J.Cancer, 97,* 336-343.

Kontermann, R. (2012). Dual targeting strategies with bispecific antibodies. *MAbs., 4*.

Kontermann, R. E. (2010). Alternative antibody formats. *Curr.Opin.Mol.Ther., 12,* 176-183.

Kornilova, E. S., Taverna, D., Hoeck, W., & Hynes, N. E. (1992). Surface expression of erbB-2 protein is post-transcriptionally regulated in mammary epithelial cells by epidermal growth factor and by the culture density. *Oncogene, 7,* 511-519.

Kovalenko, O. V., Yang, X., Kolesnikova, T. V., & Hemler, M. E. (2004). Evidence for specific tetraspanin homodimers: inhibition of palmitoylation makes cysteine residues available for cross-linking. *Biochem.J., 377,* 407-417.

Kovalenko, O. V., Yang, X. H., & Hemler, M. E. (2007). A novel cysteine cross-linking method reveals a direct association between claudin-1 and tetraspanin CD9. *Mol.Cell Proteomics., 6,* 1855-1867.

Kristoffersen, E. K. (1996). Human placental Fc gamma-binding proteins in the maternofetal transfer of IgG. *APMIS Suppl, 64,* 5-36.

Krop, I. E., Beeram, M., Modi, S., Jones, S. F., Holden, S. N., Yu, W. et al. (2010). Phase I study of trastuzumab-DM1, an HER2 antibody-drug conjugate, given every 3 weeks to patients with HER2-positive metastatic breast cancer. *J.Clin.Oncol., 28,* 2698-2704.

Kuhn, S., Koch, M., Nubel, T., Ladwein, M., Antolovic, D., Klingbeil, P. et al. (2007). A complex of EpCAM, claudin-7, CD44 variant isoforms, and tetraspanins promotes colorectal cancer progression. *Mol.Cancer Res., 5,* 553-567.

Labrijn, A. F., Aalberse, R. C., & Schuurman, J. (2008). When binding is enough: nonactivating antibody formats. *Curr.Opin.Immunol., 20,* 479-485.

Lazo, P. A. (2007). Functional implications of tetraspanin proteins in cancer biology. *Cancer Sci., 98,* 1666-1677.

Lazo, P. A., Cuevas, L., Gutierrez del, A. A., & Orue, E. (1997). Ligation of CD53/OX44, a tetraspan antigen, induces homotypic adhesion mediated by specific cell-cell interactions. *Cell Immunol, 178,* 132-140.

Le, N. F., Andre, M., Greco, C., Billard, M., Sordat, B., Emile, J. F. et al. (2006). Profiling of the tetraspanin web of human colon cancer cells. *Mol.Cell Proteomics., 5,* 845-857.

Leach, J. L., Sedmak, D. D., Osborne, J. M., Rahill, B., Lairmore, M. D., & Anderson, C. L. (1996). Isolation from human placenta of the IgG transporter, FcRn, and localization to the syncytiotrophoblast: implications for maternal-fetal antibody transport. *J.Immunol., 157,* 3317-3322.

Lee, G. Y., Kenny, P. A., Lee, E. H., & Bissell, M. J. (2007). Three-dimensional culture models of normal and malignant breast epithelial cells. *Nat.Methods, 4,* 359-365.

Lee, J. W. & Juliano, R. (2004). Mitogenic signal transduction by integrin- and growth factor receptor-mediated pathways. *Mol.Cells, 17,* 188-202.

Lee, K. S., Yuan, Y. L., Kuriyama, R., & Erikson, R. L. (1995). Plk is an M-phase-specific protein kinase and interacts with a kinesin-like protein, CHO1/MKLP-1. *Mol.Cell Biol., 15,* 7143-7151.

Lenkei, R., Gratama, J. W., Rothe, G., Schmitz, G., D'hautcourt, J. L., Arekrans, A. et al. (1998). Performance of calibration standards for antigen quantitation with flow cytometry. *Cytometry, 33,* 188-196.

Levy, S. & Shoham, T. (2005). Protein-protein interactions in the tetraspanin web. *Physiology.(Bethesda.), 20,* 218-224.

Levy, S., Todd, S. C., & Maecker, H. T. (1998). CD81 (TAPA-1): a molecule involved in signal transduction and cell adhesion in the immune system. *Annu.Rev.Immunol, 16,* 89-109.

Li, Y., Wang, L., Qiu, J., Da, L., Tiollais, P., Li, Z. et al. (2012). Human tetraspanin transmembrane 4 superfamily member 4 or intestinal and liver tetraspan membrane protein is overexpressed in hepatocellular carcinoma and accelerates tumor cell growth. *Acta Biochim.Biophys.Sin.(Shanghai), 44,* 224-232.

Linke, R., Klein, A., & Seimetz, D. (2010). Catumaxomab: clinical development and future directions. *MAbs., 2,* 129-136.

Litman, G. W., Rast, J. P., Shamblott, M. J., Haire, R. N., Hulst, M., Roess, W. et al. (1993). Phylogenetic diversification of immunoglobulin genes and the antibody repertoire. *Mol.Biol.Evol., 10,* 60-72.

Liu, W. M. & Zhang, X. A. (2006). KAI1/CD82, a tumor metastasis suppressor. *Cancer Lett., 240,* 183-194.

Liu, X., Wang, Q., Yang, G., Marando, C., Koblish, H. K., Hall, L. M. et al. (2011). A novel kinase inhibitor, INCB28060, blocks c-MET-dependent signaling, neoplastic activities, and cross-talk with EGFR and HER-3. *Clin.Cancer Res., 17,* 7127-7138.

Lobo, E. D., Hansen, R. J., & Balthasar, J. P. (2004). Antibody pharmacokinetics and pharmacodynamics. *J.Pharm.Sci., 93,* 2645-2668.

Lonberg, N. (2005). Human antibodies from transgenic animals. *Nat.Biotechnol., 23,* 1117-1125.

Lonberg, N. (2008). Fully human antibodies from transgenic mouse and phage display platforms. *Curr.Opin.Immunol., 20,* 450-459.

Loor, R., Nowak, N. J., Manzo, M. L., Douglass, H. O., & Chu, T. M. (1982). Use of pancreas-specific antigen in immunodiagnosis of pancreatic cancer. *Clin.Lab Med., 2,* 567-578.

Lopez, J. G., Chew, S. J., Thompson, H. W., Malter, J. S., Insler, M. S., & Beuerman, R. W. (1992). EGF cell surface receptor quantitation on ocular cells by an immunocytochemical flow cytometry technique. *Invest Ophthalmol.Vis.Sci., 33,* 2053-2062.

Lu, D., Jimenez, X., Zhang, H., Bohlen, P., Witte, L., & Zhu, Z. (2002). Fab-scFv fusion protein: an efficient approach to production of bispecific antibody fragments. *J.Immunol.Methods, 267,* 213-226.

Lutterbach, B., Zeng, Q., Davis, L. J., Hatch, H., Hang, G., Kohl, N. E. et al. (2007). Lung cancer cell lines harboring MET gene amplification are dependent on Met for growth and survival. *Cancer Res., 67,* 2081-2088.

Lutterbuese, R., Raum, T., Kischel, R., Hoffmann, P., Mangold, S., Rattel, B. et al. (2010). T cell-engaging BiTE antibodies specific for EGFR potently eliminate. *Proc.Natl.Acad.Sci.U.S.A, 107,* 12605-12610.

Luu, V. P., Hevezi, P., Vences-Catalan, F., Maravillas-Montero, J. L., White, C. A., Casali, P. et al. (2013). TSPAN33 is a novel marker of activated and malignant B cells. *Clin.Immunol, 149,* 388-399.

Ma, P. C., Jagadeeswaran, R., Jagadeesh, S., Tretiakova, M. S., Nallasura, V., Fox, E. A. et al. (2005). Functional expression and mutations of c-Met and its therapeutic inhibition with SU11274 and small interfering RNA in non-small cell lung cancer. *Cancer Res., 65,* 1479-1488.

Maecker, H. T., Todd, S. C., & Levy, S. (1997). The tetraspanin superfamily: molecular facilitators. *FASEB J., 11,* 428-442.

Maher, K. J. & Fletcher, M. A. (2005). Quantitative flow cytometry in the clinical laboratory. *Clin.Appl Immunol Rev., 5,* 353-372.

Man, H. Y., Wang, Q., Lu, W. Y., Ju, W., Ahmadian, G., Liu, L. et al. (2003). Activation of PI3-kinase is required for AMPA receptor insertion during LTP of mEPSCs in cultured hippocampal neurons. *Neuron, 38,* 611-624.

Market, E. & Papavasiliou, F. N. (2003). V(D)J recombination and the evolution of the adaptive immune system. *PLoS.Biol., 1,* E16.

Marks, J. D., Hoogenboom, H. R., Bonnert, T. P., McCafferty, J., Griffiths, A. D., & Winter, G. (1991). By-passing immunization. Human antibodies from V-gene libraries displayed on phage. *J.Mol.Biol., 222,* 581-597.

Maulik, G., Shrikhande, A., Kijima, T., Ma, P. C., Morrison, P. T., & Salgia, R. (2002). Role of the hepatocyte growth factor receptor, c-Met, in oncogenesis and potential for therapeutic inhibition. *Cytokine Growth Factor Rev., 13,* 41-59.

McAuley, A., Jacob, J., Kolvenbach, C. G., Westland, K., Lee, H. J., Brych, S. R. et al. (2008). Contributions of a disulfide bond to the structure, stability, and dimerization of human IgG1 antibody CH3 domain. *Protein Sci., 17,* 95-106.

McCormack, T., O'Keeffe, G., MacCraith, B., & O'Kennedy, R. (1996). Assessment of the Effect of Increased Fluorophore Labelling on the Binding Ability of an Antibody. *Anal.Letters, 29,* 953-968.

McKay, I. C., Forman, D., & White, R. G. (1981). A comparison of fluorescein isothiocyanate and lissamine rhodamine (RB 200) as labels for antibody in the fluorescent antibody technique. *Immunology, 43,* 591-602.

Merchant, A. M., Zhu, Z., Yuan, J. Q., Goddard, A., Adams, C. W., Presta, L. G. et al. (1998). An efficient route to human bispecific IgG. *Nat.Biotechnol., 16,* 677-681.

Metz, S., Haas, A. K., Daub, K., Croasdale, R., Stracke, J., Lau, W. et al. (2011). Bispecific digoxigenin-binding antibodies for targeted payload delivery. *Proc.Natl.Acad.Sci.U.S.A, 108,* 8194-8199.

Metz, S., Panke, C., Haas, A. K., Schanzer, J., Lau, W., Croasdale, R. et al. (2012). Bispecific antibody derivatives with restricted binding functionalities that are activated by proteolytic processing. *Protein Eng Des Sel, 25,* 571-580.

Mimori, K., Kataoka, A., Yoshinaga, K., Ohta, M., Sagara, Y., Yoshikawa, Y. et al. (2005). Identification of molecular markers for metastasis-related genes in primary breast cancer cells. *Clin.Exp.Metastasis, 22,* 59-67.

Min, G., Wang, H., Sun, T. T., & Kong, X. P. (2006). Structural basis for tetraspanin functions as revealed by the cryo-EM structure of uroplakin complexes at 6-A resolution. *J Cell Biol., 173,* 975-983.

Mirschberger, C., Schiller, C. B., Schraml, M., Dimoudis, N., Friess, T., Gerdes, C. A. et al. (2013). RG7116, a therapeutic antibody that binds the inactive HER3 receptor and is optimized for immune effector activation. *Cancer Res, 73,* 5183-5194.

Mittag, A. & Tarnok, A. (2009). Basics of standardization and calibration in cytometry--a review. *J.Biophotonics., 2,* 470-481.

Miyake, M., Nakano, K., Ieki, Y., Adachi, M., Huang, C. L., Itoi, S. et al. (1995). Motility related protein 1 (MRP-1/CD9) expression: inverse correlation with metastases in breast cancer. *Cancer Res., 55,* 4127-4131.

Miyamoto, S., Maruyama, A., Okugawa, K., Akazawa, K., Baba, H., Maehara, Y. et al. (2001). Loss of motility-related protein 1 (MRP1/CD9) and integrin alpha3 expression in endometrial cancers. *Cancer, 92,* 542-548.

Miyazaki, T., Muller, U., & Campbell, K. S. (1997). Normal development but differentially altered proliferative responses of lymphocytes in mice lacking CD81. *EMBO J, 16,* 4217-4225.

Moroni, M., Veronese, S., Benvenuti, S., Marrapese, G., Sartore-Bianchi, A., Di, N. F. et al. (2005). Gene copy number for epidermal growth factor receptor (EGFR) and clinical response to antiEGFR treatment in colorectal cancer: a cohort study. *Lancet Oncol., 6,* 279-286.

Morphis, L. G. & Gitlin, D. (1970). Maturation of the maternofoetal transport system for human gamma-globulin in the mouse. *Nature, 228,* -573.

Nazarenko, I., Rana, S., Baumann, A., McAlear, J., Hellwig, A., Trendelenburg, M. et al. (2010). Cell surface tetraspanin Tspan8 contributes to molecular pathways of exosome-induced endothelial cell activation. *Cancer Res., 70,* 1668-1678.

Nelson, A. L., Dhimolea, E., & Reichert, J. M. (2010). Development trends for human monoclonal antibody therapeutics. *Nat.Rev.Drug Discov., 9,* 767-774.

Nieri, P., Donadio, E., Rossi, S., Adinolfi, B., & Podesta, A. (2009). Antibodies for therapeutic uses and the evolution of biotechniques. *Curr.Med.Chem., 16,* 753-779.

Nishiuchi, R., Sanzen, N., Nada, S., Sumida, Y., Wada, Y., Okada, M. et al. (2005). Potentiation of the ligand-binding activity of integrin alpha3beta1 via association with tetraspanin CD151. *Proc.Natl.Acad.Sci.U.S.A, 102,* 1939-1944.

Normanno, N., De, L. A., Bianco, C., Strizzi, L., Mancino, M., Maiello, M. R. et al. (2006). Epidermal growth factor receptor (EGFR) signaling in cancer. *Gene, 366,* 2-16.

Novitskaya, V., Romanska, H., Dawoud, M., Jones, J. L., & Berditchevski, F. (2010). Tetraspanin CD151 regulates growth of mammary epithelial cells in three-dimensional extracellular matrix: implication for mammary ductal carcinoma in situ. *Cancer Res., 70,* 4698-4708.

Novy, Z., Barta, P., Mandikova, J., Laznicek, M., & Trejtnar, F. (2012). A comparison of in vitro methods for determining the membrane receptor expression in cell lines. *Nucl.Med.Biol., 39,* 893-896.

Ober, R. J., Martinez, C., Lai, X., Zhou, J., & Ward, E. S. (2004). Exocytosis of IgG as mediated by the receptor, FcRn: an analysis at the single-molecule level. *Proc.Natl.Acad.Sci.U.S.A, 101,* 11076-11081.

Ober, R. J., Martinez, C., Vaccaro, C., Zhou, J., & Ward, E. S. (2004). Visualizing the site and dynamics of IgG salvage by the MHC class I-related receptor, FcRn. *J.Immunol., 172,* 2021-2029.

Odintsova, E., Butters, T. D., Monti, E., Sprong, H., van, M. G., & Berditchevski, F. (2006). Gangliosides play an important role in the organization of CD82-enriched microdomains. *Biochem.J, 400,* 315-325.

Olayioye, M. A. (2001). Update on HER-2 as a target for cancer therapy: intracellular signaling pathways of ErbB2/HER-2 and family members. *Breast Cancer Res., 3,* 385-389.

Olsburgh, J., Harnden, P., Weeks, R., Smith, B., Joyce, A., Hall, G. et al. (2003). Uroplakin gene expression in normal human tissues and locally advanced bladder cancer. *J.Pathol., 199,* 41-49.

Ono, M., Handa, K., Sonnino, S., Withers, D. A., Nagai, H., & Hakomori, S. (2001). GM3 ganglioside inhibits CD9-facilitated haptotactic cell motility: coexpression of GM3 and CD9 is essential in the downregulation of tumor cell motility and malignancy. *Biochemistry, 40,* 6414-6421.

Oren, R., Takahashi, S., Doss, C., Levy, R., & Levy, S. (1990). TAPA-1, the target of an antiproliferative antibody, defines a new family of transmembrane proteins. *Mol.Cell Biol., 10,* 4007-4015.

Orlandi, R., Gussow, D. H., Jones, P. T., & Winter, G. (1989). Cloning immunoglobulin variable domains for expression by the polymerase chain reaction. *Proc.Natl.Acad.Sci.U.S.A, 86,* 3833-3837.

Ovalle, S., Gutierrez-Lopez, M. D., Olmo, N., Turnay, J., Lizarbe, M. A., Majano, P. et al. (2007). The tetraspanin CD9 inhibits the proliferation and tumorigenicity of human colon carcinoma cells. *Int.J Cancer, 121,* 2140-2152.

Pace, C. N., Vajdos, F., Fee, L., Grimsley, G., & Gray, T. (1995). How to measure and predict the molar absorption coefficient of a protein. *Protein Sci., 4,* 2411-2423.

Panchuk-Voloshina, N., Haugland, R. P., Bishop-Stewart, J., Bhalgat, M. K., Millard, P. J., Mao, F. et al. (1999). Alexa dyes, a series of new fluorescent dyes that yield exceptionally bright, photostable conjugates. *J Histochem.Cytochem., 47,* 1179-1188.

Panke, C., Weininger, D., Haas, A., Schelter, F., Schlothauer, T., Bader, S. et al. (2013). Quantification of cell surface proteins with bispecific antibodies. *Protein Eng Des Sel, 26,* 645-654.

Pannu, K. K., Joe, E. T., & Iyer, S. B. (2001). Performance evaluation of QuantiBRITE phycoerythrin beads. *Cytometry, 45,* 250-258.

Papsidero, L. D., Kuriyama, M., Wang, M. C., Horoszewicz, J., Leong, S. S., Valenzuela, L. et al. (1981). Prostate antigen: a marker for human prostate epithelial cells. *J Natl Cancer Inst, 66,* 37-42.

Park, J. G., Oie, H. K., Sugarbaker, P. H., Henslee, J. G., Chen, T. R., Johnson, B. E. et al. (1987). Characteristics of cell lines established from human colorectal carcinoma. *Cancer Res, 47,* 6710-6718.

Parker, D. C. (1993). The functions of antigen recognition in T cell-dependent B cell activation. *Semin.Immunol., 5,* 413-420.

Peltier, J., O'Neill, A., & Schaffer, D. V. (2007). PI3K/Akt and CREB regulate adult neural hippocampal progenitor proliferation and differentiation. *Dev.Neurobiol., 67,* 1348-1361.

Petrou, P. S., Mastichiadis, C., Christofidis, I., & Kakabakos, S. E. (2007). Glycerin suppression of fluorescence self-quenching and improvement of heterogeneous fluoroimmunoassay sensitivity. *Anal.Chem., 79,* 647-653.

Phelps, R. M., Johnson, B. E., Ihde, D. C., Gazdar, A. F., Carbone, D. P., McClintock, P. R. et al. (1996). NCI-Navy Medical Oncology Branch cell line data base. *J Cell Biochem.Suppl, 24,* 32-91.

Pickl, M. & Ries, C. H. (2009). Comparison of 3D and 2D tumor models reveals enhanced HER2 activation in 3D associated with an increased response to trastuzumab. *Oncogene, 28,* 461-468.

Pier, GB., Lyczak, JB., & Wetzler, LM. (2004). *Immunology, Infection and Immunity.* (1 ed.) Washington: ASM Press.

Pitt, J. C., Lindemeier, J., Habbes, H. W., & Veh, R. W. (1998). Haptenylation of antibodies during affinity purification: a novel and convenient procedure to obtain labeled antibodies for quantification and double labeling. *Histochem.Cell Biol., 110,* 311-322.

Polya, G. (2003). *Biochemical Targets of Plant Bioactive Compounds*. (1 ed.) New York: Taylor & Francis Ltd.

Pratt, R. M. & Pastan, I. (1978). Decreased binding of epidermal growth factor to BALB/c 3T3 mutant cells defective in glycoprotein synthesis. *Nature, 272,* 68-70.

Presta, L. G. (2002). Engineering antibodies for therapy. *Curr.Pharm.Biotechnol., 3,* 237-256.

Putnam, F. W., Liu, Y. S., & Low, T. L. (1979). Primary structure of a human IgA1 immunoglobulin. IV. Streptococcal IgA1 protease, digestion, Fab and Fc fragments, and the complete amino acid sequence of the alpha 1 heavy chain. *J.Biol.Chem., 254,* 2865-2874.

Ravetch, J. V. & Bolland, S. (2001). IgG Fc receptors. *Annu.Rev.Immunol., 19,* 275-290.

Reagan-Shaw, S. & Ahmad, N. (2005). Silencing of polo-like kinase (Plk) 1 via siRNA causes induction of apoptosis and impairment of mitosis machinery in human prostate cancer cells: implications for the treatment of prostate cancer. *FASEB J., 19,* 611-613.

Reichert, J. M. (2008). Monoclonal antibodies as innovative therapeutics. *Curr.Pharm.Biotechnol., 9,* 423-430.

Reiter, Y., Brinkmann, U., Jung, S. H., Pastan, I., & Lee, B. (1995). Disulfide stabilization of antibody Fv: computer predictions and experimental evaluation. *Protein Eng, 8,* 1323-1331.

Reiter, Y., Brinkmann, U., Lee, B., & Pastan, I. (1996). Engineering antibody Fv fragments for cancer detection and therapy: disulfide-stabilized Fv fragments. *Nat.Biotechnol., 14,* 1239-1245.

Richardson, M. M., Jennings, L. K., & Zhang, X. A. (2011). Tetraspanins and tumor progression. *Clin.Exp.Metastasis, 28,* 261-270.

Ridgway, J. B., Presta, L. G., & Carter, P. (1996). 'Knobs-into-holes' engineering of antibody CH3 domains for heavy chain heterodimerization. *Protein Eng, 9,* 617-621.

Ridley, A. J., Schwartz, M. A., Burridge, K., Firtel, R. A., Ginsberg, M. H., Borisy, G. et al. (2003). Cell migration: integrating signals from front to back. *Science, 302,* 1704-1709.

Ritter, G., Cohen, L. S., Williams, C., Jr., Richards, E. C., Old, L. J., & Welt, S. (2001). Serological analysis of human anti-human antibody responses in colon cancer patients treated with repeated doses of humanized monoclonal antibody A33. *Cancer Res., 61,* 6851-6859.

Roberts, J. J., Rodgers, S. E., Drury, J., Ashman, L. K., & Lloyd, J. V. (1995). Platelet activation induced by a murine monoclonal antibody directed against a novel tetra-span antigen. *Br.J Haematol., 89,* 853-860.

Rodewald, R. (1976). pH-dependent binding of immunoglobulins to intestinal cells of the neonatal rat. *J.Cell Biol., 71,* 666-669.

Romanska, H. M. & Berditchevski, F. (2011). Tetraspanins in human epithelial malignancies. *J.Pathol., 223,* 4-14.

Romanska, H. M., Potemski, P., Collins, S. I., Williams, H., Parmar, S., & Berditchevski, F. (2013). Loss of CD151/Tspan24 from the complex with integrin alpha3beta1 in invasive front of the tumour is a negative predictor of disease-free survival in oral squamous cell carcinoma. *Oral Oncol., 49,* 224-229.

Roskos, L., Klakamp, S., Liang, M., Arends, R., & Green, L. (2007). *Handbook of Therapeutic Antibodies*. (1 ed.) Weinheim: Wiley-VCH Verlag GmbH.

Rossmann, E. D., Lenkei, R., Lundin, J., Mellstedt, H., & Osterborg, A. (2007). Performance of calibration standards for antigen quantitation with flow cytometry in chronic lymphocytic leukemia. *Cytometry B Clin.Cytom., 72,* 450-457.

Ruiz-Mateos, E., Pelchen-Matthews, A., Deneka, M., & Marsh, M. (2008). CD63 is not required for production of infectious human immunodeficiency virus type 1 in human macrophages. *J Virol., 82,* 4751-4761.

Sadej, R., Romanska, H., Baldwin, G., Gkirtzimanaki, K., Novitskaya, V., Filer, A. D. et al. (2009). CD151 regulates tumorigenesis by modulating the communication between tumor cells and endothelium. *Mol.Cancer Res., 7,* 787-798.

Salfeld, J. G. (2007). Isotype selection in antibody engineering. *Nat.Biotechnol., 25,* 1369-1372.

Sanderson, R. J., Hering, M. A., James, S. F., Sun, M. M., Doronina, S. O., Siadak, A. W. et al. (2005). In vivo drug-linker stability of an anti-CD30 dipeptide-linked auristatin immunoconjugate. *Clin.Cancer Res., 11,* 843-852.

Sauer, G., Kurzeder, C., Grundmann, R., Kreienberg, R., Zeillinger, R., & Deissler, H. (2003). Expression of tetraspanin adaptor proteins below defined threshold values is associated with in vitro invasiveness of mammary carcinoma cells. *Oncol.Rep., 10,* 405-410.

Sawin, K. E., LeGuellec, K., Philippe, M., & Mitchison, T. J. (1992). Mitotic spindle organization by a plus-end-directed microtubule motor. *Nature, 359,* 540-543.

Schaefer, G., Haber, L., Crocker, L. M., Shia, S., Shao, L., Dowbenko, D. et al. (2011a). A two-in-one antibody against HER3 and EGFR has superior inhibitory activity compared with monospecific antibodies. *Cancer Cell, 20,* 472-486.

Schaefer, W., Regula, J. T., Bahner, M., Schanzer, J., Croasdale, R., Durr, H. et al. (2011b). Immunoglobulin domain crossover as a generic approach for the production of bispecific IgG antibodies. *Proc.Natl.Acad.Sci.U.S.A, 108,* 11187-11192.

Schanzer, J., Jekle, A., Nezu, J., Lochner, A., Croasdale, R., Dioszegi, M. et al. (2011). Development of tetravalent, bispecific CCR5 antibodies with antiviral activity against CCR5 monoclonal antibody-resistant HIV-1 strains. *Antimicrob.Agents Chemother., 55,* 2369-2378.

Schier, R., McCall, A., Adams, G. P., Marshall, K. W., Merritt, H., Yim, M. et al. (1996). Isolation of picomolar affinity anti-c-erbB-2 single-chain Fv by molecular evolution of the complementarity determining regions in the center of the antibody binding site. *J.Mol.Biol., 263,* 551-567.

Schmittgen, T. D., Zakrajsek, B. A., Mills, A. G., Gorn, V., Singer, M. J., & Reed, M. W. (2000). Quantitative reverse transcription-polymerase chain reaction to study mRNA decay: comparison of endpoint and real-time methods. *Anal.Biochem., 285,* 194-204.

Scholz, C. J., Kurzeder, C., Koretz, K., Windisch, J., Kreienberg, R., Sauer, G. et al. (2009). Tspan-1 is a tetraspanin preferentially expressed by mucinous and endometrioid subtypes of human ovarian carcinomas. *Cancer Lett., 275,* 198-203.

Schroy, P. C., III, Brown-Shimer, S., Kim, K., Johnson, K. A., Murnane, M. J., Yang, S. et al. (1995). Detection of p21ras mutations in colorectal adenomas and carcinomas by enzyme-linked immunosorbent assay. *Cancer, 76,* 201-209.

Schwartz, A. & Fernandez-Repollet, E. (2001). Quantitative flow cytometry. *Clin.Lab Med., 21,* 743-761.

Schwartz, A., Gaigalas, A. K., Wang, L., Marti, G. E., Vogt, R. F., & Fernandez-Repollet, E. (2004). Formalization of the MESF unit of fluorescence intensity. *Cytometry B Clin.Cytom., 57,* 1-6.

Schwartz, A., Wang, L., Early, E., Gaigalas, A. K., Zhang, Y., Marti, G. E. et al. (2002). Quantitating fluorescence intensity from fluorophore: the definition of MESF assignment. *J Res Natl Inst Stand Technol, 107,* 83-91.

Seigneuret, M., Delaguillaumie, A., Lagaudriere-Gesbert, C., & Conjeaud, H. (2001). Structure of the tetraspanin main extracellular domain. A partially conserved fold with a structurally variable domain insertion. *J.Biol.Chem., 276,* 40055-40064.

Sergeeva, A., Kolonin, M. G., Molldrem, J. J., Pasqualini, R., & Arap, W. (2006). Display technologies: application for the discovery of drug and gene delivery agents. *Adv.Drug Deliv.Rev., 58,* 1622-1654.

Serke, S., van, L. A., Pardo, I., & Huhn, D. (1998). Selective susceptibility of CD34-expressing cells to acquire flow cytometric features of apoptosis/necrosis on exposure to an ammonium chloride-based red blood cell lysing reagent. *J.Hematother., 7,* 315-318.

Serru, V., Le, N. F., Billard, M., Azorsa, D. O., Lanza, F., Boucheix, C. et al. (1999). Selective tetraspan-integrin complexes (CD81/alpha4beta1, CD151/alpha3beta1, CD151/alpha6beta1) under conditions disrupting tetraspan interactions. *Biochem.J, 340 (Pt 1),* 103-111.

Shaw, K. R. M., Wrobel, C. N., & Brugge, J. S. (2004). Use of three-dimensional basement membrane cultures to model oncogene-induced changes in mammary epithelial morphogenesis. *J.Mammary.Gland.Biol.Neoplasia., 9,* 297-310.

Shi, G. M., Ke, A. W., Zhou, J., Wang, X. Y., Xu, Y., Ding, Z. B. et al. (2010). CD151 modulates expression of matrix metalloproteinase 9 and promotes neoangiogenesis and progression of hepatocellular carcinoma. *Hepatology, 52,* 183-196.

Shields, R. L., Lai, J., Keck, R., O'Connell, L. Y., Hong, K., Meng, Y. G. et al. (2002). Lack of fucose on human IgG1 N-linked oligosaccharide improves binding to human Fcgamma RIII and antibody-dependent cellular toxicity. *J.Biol.Chem., 277,* 26733-26740.

Shields, R. L., Namenuk, A. K., Hong, K., Meng, Y. G., Rae, J., Briggs, J. et al. (2001). High resolution mapping of the binding site on human IgG1 for Fc gamma RI, Fc gamma RII, Fc gamma RIII, and FcRn and design of IgG1 variants with improved binding to the Fc gamma R. *J.Biol.Chem., 276,* 6591-6604.

Shigeta, M., Sanzen, N., Ozawa, M., Gu, J., Hasegawa, H., & Sekiguchi, K. (2003). CD151 regulates epithelial cell-cell adhesion through PKC- and Cdc42-dependent actin cytoskeletal reorganization. *J.Cell Biol., 163,* 165-176.

Shire, S. J. (2009). Formulation and manufacturability of biologics. *Curr.Opin.Biotechnol., 20,* 708-714.

Sho, M., Adachi, M., Taki, T., Hashida, H., Konishi, T., Huang, C. L. et al. (1998). Transmembrane 4 superfamily as a prognostic factor in pancreatic cancer. *Int.J.Cancer, 79,* 509-516.

Shoham, T., Rajapaksa, R., Kuo, C. C., Haimovich, J., & Levy, S. (2006). Building of the tetraspanin web: distinct structural domains of CD81 function in different cellular compartments. *Mol.Cell Biol., 26,* 1373-1385.

Shoyab, M., De Larco, J. E., & Todaro, G. J. (1979). Biologically active phorbol esters specifically alter affinity of epidermal growth factor membrane receptors. *Nature, 279,* 387-391.

Shuptrine, C. W., Surana, R., & Weiner, L. M. (2012). Monoclonal antibodies for the treatment of cancer. *Semin.Cancer Biol., 22,* 3-13.

Si, Z. & Hersey, P. (1993). Expression of the neuroglandular antigen and analogues in melanoma. CD9 expression appears inversely related to metastatic potential of melanoma. *Int.J.Cancer, 54,* 37-43.

Siciliano, M. J., Barker, P. E., & Cailleau, R. (1979). Mutually exclusive genetic signatures of human breast tumor cell lines with a common chromosomal marker. *Cancer Res, 39,* 919-922.

Silverton, E. W., Navia, M. A., & Davies, D. R. (1977). Three-dimensional structure of an intact human immunoglobulin. *Proc.Natl.Acad.Sci.U.S.A, 74,* 5140-5144.

Simister, N. E. & Mostov, K. E. (1989). An Fc receptor structurally related to MHC class I antigens. *Nature, 337,* 184-187.

Simister, N. E. & Rees, A. R. (1985). Isolation and characterization of an Fc receptor from neonatal rat small intestine. *Eur.J.Immunol., 15,* 733-738.

Simister, N. E., Story, C. M., Chen, H. L., & Hunt, J. S. (1996). An IgG-transporting Fc receptor expressed in the syncytiotrophoblast of human placenta. *Eur.J.Immunol., 26,* 1527-1531.

Sincock, P. M., Mayrhofer, G., & Ashman, L. K. (1997). Localization of the transmembrane 4 superfamily (TM4SF) member PETA-3 (CD151) in normal human tissues: comparison with CD9, CD63, and alpha5beta1 integrin. *J.Histochem.Cytochem., 45,* 515-525.

Sithanandam, G., Smith, G. T., Masuda, A., Takahashi, T., Anderson, L. M., & Fornwald, L. W. (2003). Cell cycle activation in lung adenocarcinoma cells by the ErbB3/phosphatidylinositol 3-kinase/Akt pathway. *Carcinogenesis, 24,* 1581-1592.

Skerra, A. & Pluckthun, A. (1988). Assembly of a functional immunoglobulin Fv fragment in Escherichia coli. *Science, 240,* 1038-1041.

Sliwkowski, M. X. & Mellman, I. (2013). Antibody therapeutics in cancer. *Science, 341,* 1192-1198.

Smith, H. S. (1979). In vitro properties of epithelial cell lines established from human carcinomas and nonmalignant tissue. *J Natl Cancer Inst, 62,* 225-230.

Smith, S. L. (1996). Ten years of Orthoclone OKT3 (muromonab-CD3): a review. *J.Transpl.Coord., 6,* 109-119.

Smolen, G. A., Smolen, G. A., Sordella, R., Sordella, R., Muir, B., Muir, B. et al. (2006). Amplification of MET may identify a subset of cancers with extreme sensitivity to the selective tyrosine kinase inhibitor PHA-665752. *Proc.Natl.Acad.Sci.U.S.A, 103,* 2316-2321.

Stelos, P. & Pressman, D. (1962). Papain digestion of antigenantibody precipitates. *J.Biol.Chem., 237,* 3679-3685.

Stipp, C. S., Kolesnikova, T. V., & Hemler, M. E. (2003). Functional domains in tetraspanin proteins. *Trends Biochem.Sci., 28,* 106-112.

Stuttle, A. W., Powling, M. J., Ritter, J. M., & Hardisty, R. M. (1991). Effects of a monoclonal antibody to glycoprotein IIb/IIIa (P256) and of enzymically derived fragments of P256 on human platelets. *Thromb.Haemost., 65,* 432-437.

Su, H. W., Wang, S. W., Ghishan, F. K., Kiela, P. R., & Tang, M. J. (2009). Cell confluency-induced Stat3 activation regulates NHE3 expression by recruiting Sp1 and Sp3 to the proximal NHE3 promoter region during epithelial dome formation. *Am.J.Physiol Cell Physiol, 296,* C13-C24.

Swann, P. G., Tolnay, M., Muthukkumar, S., Shapiro, M. A., Rellahan, B. L., & Clouse, K. A. (2008). Considerations for the development of therapeutic monoclonal antibodies. *Curr.Opin.Immunol., 20,* 493-499.

Szala, S., Kasai, Y., Steplewski, Z., Rodeck, U., Koprowski, H., & Linnenbach, A. J. (1990). Molecular cloning of cDNA for the human tumor-associated antigen CO-029 and identification of related transmembrane antigens. *Proc.Natl.Acad.Sci.U.S.A, 87,* 6833-6837.

Takahashi, T., Nau, M. M., Chiba, I., Birrer, M. J., Rosenberg, R. K., Vinocour, M. et al. (1989). p53: a frequent target for genetic abnormalities in lung cancer. *Science, 246,* 491-494.

Takeda, Y., Tachibana, I., Miyado, K., Kobayashi, M., Miyazaki, T., Funakoshi, T. et al. (2003). Tetraspanins CD9 and CD81 function to prevent the fusion of mononuclear phagocytes. *J Cell Biol., 161,* 945-956.

Tan, M. & Yu, D. (2007). Molecular mechanisms of erbB2-mediated breast cancer chemoresistance. *Adv.Exp.Med.Biol., 608,* 119-129.

Tarrant, J. M., Robb, L., van Spriel, A. B., & Wright, M. D. (2003). Tetraspanins: molecular organisers of the leukocyte surface. *Trends Immunol, 24,* 610-617.

Testa, J. E., Brooks, P. C., Lin, J. M., & Quigley, J. P. (1999). Eukaryotic expression cloning with an antimetastatic monoclonal antibody identifies a tetraspanin (PETA-3/CD151) as an effector of human tumor cell migration and metastasis. *Cancer Res., 59,* 3812-3820.

Tokuhara, T., Hasegawa, H., Hattori, N., Ishida, H., Taki, T., Tachibana, S. et al. (2001). Clinical significance of CD151 gene expression in non-small cell lung cancer. *Clin.Cancer Res., 7,* 4109-4114.

Trail, P. A. & Bianchi, A. B. (1999). Monoclonal antibody drug conjugates in the treatment of cancer. *Curr.Opin.Immunol., 11,* 584-588.

Tsarfaty, I., Rong, S., Resau, J. H., Rulong, S., da Silva, P. P., & Vande Woude, G. F. (1994). The Met proto-oncogene mesenchymal to epithelial cell conversion. *Science, 263,* 98-101.

Tsitsikov, E. N., Gutierrez-Ramos, J. C., & Geha, R. S. (1997). Impaired CD19 expression and signaling, enhanced antibody response to type II T independent antigen and reduction of B-1 cells in CD81-deficient mice. *Proc.Natl Acad.Sci.U.S.A, 94,* 10844-10849.

Turabelidze, A., Guo, S., & DiPietro, L. A. (2010). Importance of housekeeping gene selection for accurate reverse transcription-quantitative polymerase chain reaction in a wound healing model. *Wound.Repair Regen., 18,* 460-466.

Umana, P., Jean-Mairet, J., Moudry, R., Amstutz, H., & Bailey, J. E. (1999). Engineered glycoforms of an antineuroblastoma IgG1 with optimized antibody-dependent cellular cytotoxic activity. *Nat.Biotechnol., 17,* 176-180.

van den Berg, W. B., Joosten, L. A., Helsen, M., & van de Loo, F. A. (1994). Amelioration of established murine collagen-induced arthritis with anti-IL-1 treatment. *Clin.Exp.Immunol., 95,* 237-243.

van der Weij-De Wit CD, Doust, A. B., van, S., I, Dekker, J. P., Wilk, K. E., Curmi, P. M. et al. (2006). How energy funnels from the phycoerythrin antenna complex to photosystem I and photosystem II in cryptophyte Rhodomonas CS24 cells. *J.Phys.Chem.B, 110,* 25066-25073.

Van Oss, C. J. (1995). Hydrophobic, hydrophilic and other interactions in epitope-paratope binding. *Mol.Immunol., 32,* 199-211.

Vira, S., Mekhedov, E., Humphrey, G., & Blank, P. S. (2010). Fluorescent-labeled antibodies: Balancing functionality and degree of labeling. *Anal.Biochem., 402,* 146-150.

von Lindern, J. J., Rojo, D., Grovit-Ferbas, K., Yeramian, C., Deng, C., Herbein, G. et al. (2003). Potential role for CD63 in CCR5-mediated human immunodeficiency virus type 1 infection of macrophages. *J Virol., 77,* 3624-3633.

Wang, H. X., Li, Q., Sharma, C., Knoblich, K., & Hemler, M. E. (2011). Tetraspanin protein contributions to cancer. *Biochem.Soc.Trans., 39,* 547-552.

Wang, J. C., Begin, L. R., Berube, N. G., Chevalier, S., Aprikian, A. G., Gourdeau, H. et al. (2007a). Down-regulation of CD9 expression during prostate carcinoma progression is associated with CD9 mRNA modifications. *Clin.Cancer Res., 13,* 2354-2361.

Wang, L., Gaigalas, A. K., Abbasi, F., Marti, G. E., Vogt, R. F., & Schwartz, A. (2002). Quantitating Fluorescence intensity from fluorophores: practical use of
MESF Values. *J Res Natl Inst Stand Technol, 107,* 339-353.

Wang, L., Gaigalas, A. K., Marti, G., Abbasi, F., & Hoffman, R. A. (2008). Toward quantitative fluorescence measurements with multicolor flow cytometry. *Cytometry A, 73,* 279-288.

Wang, X., Zhang, S., MacLennan, G. T., Biermann, K., Foster, R. S., Beck, S. D. et al. (2009). Epidermal growth factor receptor protein expression and gene amplification in the chemorefractory metastatic embryonal carcinoma. *Mod.Pathol., 22,* 7-12.

Wang, X., Zhang, S., MacLennan, G. T., Eble, J. N., Lopez-Beltran, A., Yang, X. J. et al. (2007b). Epidermal growth factor receptor protein expression and gene amplification in small cell carcinoma of the urinary bladder. *Clin.Cancer Res., 13,* 953-957.

Ward, E. S., Zhou, J., Ghetie, V., & Ober, R. J. (2003). Evidence to support the cellular mechanism involved in serum IgG homeostasis in humans. *Int.Immunol., 15,* 187-195.

Watson, J. D., Baker, T. A., Bell, S. P., Gann, A., Levine, M., & Losick, R. (2004). *Molecular Biology of the Gene*. (5 ed.) San Francisco: Cold Spring Harbor Laboratory Press.

Watt, F. M. (2002). Role of integrins in regulating epidermal adhesion, growth and differentiation. *EMBO J., 21,* 3919-3926.

Weidle, U. H., Tiefenthaler, G., Weiss, E. H., Georges, G., & Brinkmann, U. (2013). The intriguing options of multispecific antibody formats for treatment of cancer. *Cancer Genomics Proteomics., 10,* 1-18.

Weinberg, W. C., Frazier-Jessen, M. R., Wu, W. J., Weir, A., Hartsough, M., Keegan, P. et al. (2005). Development and regulation of monoclonal antibody products: challenges and opportunities. *Cancer Metastasis Rev., 24,* 569-584.

Weng, W. K. & Levy, R. (2003). Two immunoglobulin G fragment C receptor polymorphisms independently predict response to rituximab in patients with follicular lymphoma. *J.Clin.Oncol., 21,* 3940-3947.

Werthen, M. & Nygren, H. (1988). Effect of antibody affinity on the isotherm of antibody binding to surface-immobilized antigen. *J.Immunol.Methods, 115,* 71-78.

Winterwood, N. E., Varzavand, A., Meland, M. N., Ashman, L. K., & Stipp, C. S. (2006). A critical role for tetraspanin CD151 in alpha3beta1 and alpha6beta4 integrin-dependent tumor cell functions on laminin-5. *Mol.Biol.Cell, 17,* 2707-2721.

Woegerbauer, M., Thurnher, D., Houben, R., Pammer, J., Kloimstein, P., Heiduschka, G. et al. (2010). Expression of the tetraspanins CD9, CD37, CD63, and CD151 in Merkel cell carcinoma: strong evidence for a posttranscriptional fine-tuning of CD9 gene expression. *Mod.Pathol., 23,* 751-762.

Wolf, E., Hofmeister, R., Kufer, P., Schlereth, B., & Baeuerle, P. A. (2005). BiTEs: bispecific antibody constructs with unique anti-tumor activity. *Drug Discov.Today, 10,* 1237-1244.

Wong, M. L. & Medrano, J. F. (2005). Real-time PCR for mRNA quantitation. *Biotechniques, 39,* 75-85.

Woof, J. M. & Burton, D. R. (2004). Human antibody-Fc receptor interactions illuminated by crystal structures. *Nat.Rev.Immunol., 4,* 89-99.

Wrann, M. M. & Fox, C. F. (1979). Identification of epidermal growth factor receptors in a hyperproducing human epidermoid carcinoma cell line. *J Biol.Chem., 254,* 8083-8086.

Wright, M. D., Moseley, G. W., & van Spriel, A. B. (2004). Tetraspanin microdomains in immune cell signalling and malignant disease. *Tissue Antigens, 64,* 533-542.

Wu, A. M. & Senter, P. D. (2005). Arming antibodies: prospects and challenges for immunoconjugates. *Nat.Biotechnol., 23,* 1137-1146.

Wuttig, D., Zastrow, S., Fussel, S., Toma, M. I., Meinhardt, M., Kalman, K. et al. (2012). CD31, EDNRB and TSPAN7 are promising prognostic markers in clear-cell renal cell carcinoma revealed by genome-wide expression analyses of primary tumors and metastases. *Int.J.Cancer, 131,* E693-E704.

Yamada, M., Tamura, Y., Sanzen, N., Sato-Nishiuchi, R., Hasegawa, H., Ashman, L. K. et al. (2008). Probing the interaction of tetraspanin CD151 with integrin alpha 3 beta 1 using a panel of monoclonal antibodies with distinct reactivities toward the CD151-integrin alpha 3 beta 1 complex. *Biochem.J, 415,* 417-427.

Yanez-Mo, M., Barreiro, O., Gordon-Alonso, M., Sala-Valdes, M., & Sanchez-Madrid, F. (2009). Tetraspanin-enriched microdomains: a functional unit in cell plasma membranes. *Trends Cell Biol., 19,* 434-446.

Yang, X., Claas, C., Kraeft, S. K., Chen, L. B., Wang, Z., Kreidberg, J. A. et al. (2002). Palmitoylation of tetraspanin proteins: modulation of CD151 lateral interactions, subcellular distribution, and integrin-dependent cell morphology. *Mol.Biol.Cell, 13,* 767-781.

Yang, X., Kovalenko, O. V., Tang, W., Claas, C., Stipp, C. S., & Hemler, M. E. (2004). Palmitoylation supports assembly and function of integrin-tetraspanin complexes. *J.Cell Biol., 167,* 1231-1240.

Yang, X., Wei, L., Tang, C., Slack, R., Montgomery, E., & Lippman, M. (2000). KAI1 protein is down-regulated during the progression of human breast cancer. *Clin.Cancer Res., 6,* 3424-3429.

Yang, X., Wei, L. L., Tang, C., Slack, R., Mueller, S., & Lippman, M. E. (2001). Overexpression of KAI1 suppresses in vitro invasiveness and in vivo metastasis in breast cancer cells. *Cancer Res., 61,* 5284-5288.

Yang, X. H., Flores, L. M., Li, Q., Zhou, P., Xu, F., Krop, I. E. et al. (2010). Disruption of laminin-integrin-CD151-focal adhesion kinase axis sensitizes breast cancer cells to ErbB2 antagonists. *Cancer Res., 70,* 2256-2263.

Yang, X. H., Richardson, A. L., Torres-Arzayus, M. I., Zhou, P., Sharma, C., Kazarov, A. R. et al. (2008). CD151 accelerates breast cancer by regulating alpha 6 integrin function, signaling, and molecular organization. *Cancer Res., 68,* 3204-3213.

Yarden, Y. & Sliwkowski, M. X. (2001). Untangling the ErbB signalling network. *Nat.Rev.Mol.Cell Biol., 2,* 127-137.

Yau, J. C., Dabbagh, L. K., Formenti, K. S., Coupland, R. W., Burns, B. F., & Shaw, A. R. (1998). Expression of transmembrane 4 superfamily member, CD9, is related to improved progression-free survival in patients with diffuse non-Hodgkin's lymphoma. *Oncol.Rep., 5,* 1507-1511.

Yoon, S. O., Zhang, X., Freedman, A. S., Zahrieh, D., Lossos, I. S., Li, L. et al. (2010). Down-regulation of CD9 expression and its correlation to tumor progression in B lymphomas. *Am.J.Pathol., 177,* 377-386.

Yue, S., Mu, W., & Zoller, M. (2013). Tspan8 and CD151 promote metastasis by distinct mechanisms. *Eur.J.Cancer, 49,* 2934-2948.

Yunta, M. & Lazo, P. A. (2003a). Apoptosis protection and survival signal by the CD53 tetraspanin antigen. *Oncogene, 22,* 1219-1224.

Yunta, M. & Lazo, P. A. (2003b). Tetraspanin proteins as organisers of membrane microdomains and signalling complexes. *Cell Signal., 15,* 559-564.

Zenger, V. E., Vogt, R., Mandy, F., Schwartz, A., & Marti, G. E. (1998). Quantitative flow cytometry: inter-laboratory variation. *Cytometry, 33,* 138-145.

Zhang, X. A., Bontrager, A. L., & Hemler, M. E. (2001). Transmembrane-4 superfamily proteins associate with activated protein kinase C (PKC) and link PKC to specific beta(1) integrins. *J.Biol.Chem., 276,* 25005-25013.

Zhao, X., Lapalombella, R., Joshi, T., Cheney, C., Gowda, A., Hayden-Ledbetter, M. S. et al. (2007). Targeting CD37-positive lymphoid malignancies with a novel engineered small modular immunopharmaceutical. *Blood, 110,* 2569-2577.

Zhong, Y. Q., Wei, J., Fu, Y. R., Shao, J., Liang, Y. W., Lin, Y. H. et al. (2008). [Toxicity of cationic liposome Lipofectamine 2000 in human pancreatic cancer Capan-2 cells]. *Nan.Fang Yi.Ke.Da.Xue.Xue.Bao., 28,* 1981-1984.

Zhou, Z., Ran, Y. L., Hu, H., Pan, J., Li, Z. F., Chen, L. Z. et al. (2008). TM4SF3 promotes esophageal carcinoma metastasis via upregulating ADAM12m expression. *Clin.Exp.Metastasis, 25,* 537-548.

Zhu, Z., Presta, L. G., Zapata, G., & Carter, P. (1997). Remodeling domain interfaces to enhance heterodimer formation. *Protein Sci., 6,* 781-788.

Zijlstra, A., Lewis, J., Degryse, B., Stuhlmann, H., & Quigley, J. P. (2008). The inhibition of tumor cell intravasation and subsequent metastasis via regulation of in vivo tumor cell motility by the tetraspanin CD151. *Cancer Cell, 13,* 221-234.

Zoller, M. (2009). Tetraspanins: push and pull in suppressing and promoting metastasis. *Nat.Rev.Cancer, 9,* 40-55.